Loughborough University

Fatigue and Creep
-of-
Adhesively Bonded Joints

by

Abdulhakeem H. Al-Ghamdi

A Doctoral Thesis
Submitted in Partial Fulfilment of the Requirements
for the Award of Doctor of Philosophy of
Loughborough University

Wolfson School of Mechanical and Manufacturing Engineering

October 2004

ABSTRACT

Adhesives are extensively used in modern structural engineering as they can deliver specific benefits over other joining methods. For example, adhesives allow more flexibility in component design and eliminate the weight and space penalties of other joining methods such as riveting and bolting. The removal of the requirement to drill the structure for joining improves the stress distribution in the joint and thereby increase fatigue resistance and service life. Adhesives are extensively used in the manufacture of high strength to weight ratio components such as the honeycomb structures used in aerospace applications. Even in some miniature components, adhesives have been employed to increase reliability and performance and reduce the number of assembly components. In order to ensure reliable in-service performance, it is vital that the long term behaviour of bonded joints should be understood. In terms of loading the two distinct, but related, features of a joint that determine its long-term performance are its fatigue and creep behaviour. Recent work [1.1-1.8] has shown that creep can be significant in adhesive materials, even at ambient temperatures, and the accumulation of creep strain under normal service loading conditions can lead to premature failure in adhesively bonded structures. Creep-fatigue interaction is an important problem that must be addressed in the design of many bonded structures. It is generally believed that when there is creep-fatigue interaction, such as under low frequency fatigue or high frequency fatigue combined with extended hold periods, a crack will grow faster than under either fatigue or creep loading alone. This is a practical consideration in many industrial areas such as the aerospace and automotive sectors. The aims of the current project were therefore to investigate the creep and fatigue performance of adhesively bonded joints and to evaluate any creep-fatigue interactions.

An extensive range of experimental data has been generated in this work to provide the information required for the development and assessment of creep and fatigue failure criteria. A creep rig has been designed to collect creep data and tensile tests have been conducted to obtain the mechanical properties of the adhesive.

Adhesively bonded double-cantilever beam (DCB) samples have been tested in fatigue at various frequencies (0.1-10 Hz) and temperatures (22 ±1 -120°C). The adhesive used in this work was a toughened epoxy (FM300-2M) and the substrates used were a carbon fibre reinforced polymer (CFRP) and mild steel. Results showed that the crack growth per cycle increases and the fatigue threshold decreases as the test frequency decreases. The locus of failure with the CFRP adherends was predominantly in the adhesive layer whereas the locus of failure with the steel adherends was in the interfacial region between the steel and the adhesive. The crack growth was faster, for a given strain energy release rate, and the fatigue thresholds lower for the samples with steel adherends. Increasing the temperature to 120°C drastically reduced the threshold fatigue value. Tests with variable frequency loading were also carried out at a range of temperatures.

The effects of creep, fatigue and creep-fatigue were investigated through a series of experiments using steel-epoxy DCB samples. This entailed testing under quasi-static, fatigue and creep loading and an investigation of the effects of test frequency and temperature on the fatigue life and the crack growth rate. The experimental work was supported by linear and non-linear finite element analysis of the joints and an investigation of elastic, elastic-plastic and time dependent fracture mechanics parameters. Various correlations between the fracture parameters and crack growth for time and frequency dependent fracture have been explored.

Four methods to predict crack growth under creep-fatigue conditions have been investigated. The first method assumed that crack growth can be described by an empirical

crack growth law and the crack growth law constants can be determined experimentally as functions of frequency and temperature. The Second method assumed creep and fatigue crack growth are competing mechanisms and the crack growth rate is determined by whichever is dominant. The third method assumed that crack growth can be partitioned into cyclic dependent (fatigue) and time dependent (creep) components. The fourth method was used to treat the effect of creep/fatigue interaction. The predicted crack growth using these methods agreed well with the experimental results. Each of these methods was shown to be useful in predicting crack growth and the selection of the most appropriate method is dependent on the data available and the loading /environmental conditions.

ACKNOWLEDGEMENTS

LIST OF CONTENTS

CHAPTER 1

INTRODUCTION

CHAPTER 2
ADHESIVES IN ENGINEERING

CHAPTER 3

FRACTURE AND FATIGUE IN ADHESIVE JOINTS

CHAPTER 4

ANALYSIS OF CRACKS IN CREEPING MATERIALS

CHAPTER 5
CREEP-FATIGUE CRACK GROWTH

CHAPTER 6

DETERMINATION OF FRACTURE PARAMETERS FOR DCB JOINTS

CHAPTER 7

QUASI-STATIC AND CREEP PROPERTIES OF FM300-2M ADHESIVE

CHAPTER 10

PREDICTION OF CREEP AND FATIGUE CRACK GROWTH IN ADHESIVELY BONDED JOINTS

NOMENCLATURE

ENGLISH ALPHABET

A	Paris law constant.
a	Crack length, also with subscripts o (initial length), f (final length) , c (critical length) and eff (effective length).
b	The width of the sample.
C	Compliance.
C^*	Time dependent fracture parameter calculated at steady state.
C_t	Time dependent fracture parameter for conditions ranging from small-scale to extensive creep.
$C(t)$	C^* determined close to the crack tip.
$(C_t)_{avg}$	Time dependent fracture parameter for fatigue creep loading.
d	Elastic foundation length for beam on elastic foundation model.
dA	The incremental change in crack area.
da	The incremental change in crack length.
ds	Incremental distance.
E	Young's modulus of elasticity.
E_a	The adhesive modulus.
EI	The flexural stiffness of the beam (where I is the second moment of area).
F	With subscripts x,y,z indicate the components of nodal forces.
F_L	The external work of the load.
f	Fatigue test frequency.
f_{ij}	Dimensionless function of θ used in stress field approach to calculate the stress intensity factor.
G	Strain energy release rate, also with subscripts I,II or III to indicate mode of failure.
G_c	The critical strain energy release rate.
G_{max}	Maximum applied strain energy release rate in a fatigue spectrum.
G_{min}	Minimum applied strain energy release rate in a fatigue spectrum.
G_{th}	The strain energy release rate at fatigue threshold.

ΔG	Strain energy release rate range ($\Delta G = G_{max} - G_{min}$).
h	Thickness of substrate arms.
h_l	A non-dimensional function of crack length used in reference method to calculate C^*.
I_n	Normalizing factor function of the plasticity exponent used in stress strain field equations.
J	J-integral.
K	Stress intensity factor, also with subscripts I,II or III.
K_c	Critical stress intensity factor.
K_{max}	Maximum Applied stress intensity factor in a fatigue spectrum.
K_{min}	Minimum Applied stress intensity factor in a fatigue spectrum.
ΔK	Stress intensity factor range ($\Delta K = K_{max} - K_{min}$).
K_c	Critical stress intensity factor.
L_p	The plastic zone size ahead of a crack.
N_f	The number of cycles to failure.
P	Load.
P_c	The load at the onset of crack propagation.
P_{max}	The maximum load in a fatigue spectrum.
P_{min}	The minimum load in a fatigue spectrum.
ΔP	The load range ($\Delta P = (P_{max} - P_{min})$.
R	The crack resistance.
r	The radius at the tip of crack.
r_c	The creep zone size.
r_d	Dugdale plastic zone radius.
r_p	The plastic zone radius.
T_i	The components of the traction vector.
t	Time.

t_T	Transition time from small scale creep to extensive creep.
t_r	Rise time in trapezoidal loading form.
t_h	Hold time in trapezoidal loading form.
t_d	Decay time in trapezoidal loading form.
U	The strain energy.
u	Displacement, or displacement vector components also with subscripts 1,2 or 3.
u_o	Instantaneous deflections.
$\dot{u}_c$	The displacement rate.
Up	The potential energy of the load system.
U^*	The stress-power input into cracked bodies.
ΔU^*	The stress- power difference between two bodies.
Δu_c	Deflection accumulation during a hold time.
$\Delta \bar{u}$	The relative displacement between mating crack surfaces.
w	The width of un-cracked part of DCB joints.
W	The strain energy density (energy of new crack surfaces).
w_c	The opening of a crack at the start of the stress free zone.
Z	Scaling factor used in Saxena model for estimating C_t for small scale creep.

GREEK ALPHABET

σ	The remotely applied stress.
σ_a	The stress amplitude ($\sigma_{max} - \sigma_{min}$).
σ_f	Stress at failure.
σ_{max}	The maximum stress in fatigue cycle.
σ_{min}	The minimum stress in fatigue cycle .

σ_{ref}	The reference stress.
$\bar{\sigma}$	The surface stress distribution.
σ_{Y}	The yield stress.
σ_{y}	The vertical stress.
ε_{max}	The maximum strain in a fatigue cycle.
ε_{min}	The minimum strain in a fatigue cycle.
$\dot{\varepsilon}_{o}$	Initial strain rate.
ε_{ref}	The reference strain.
ε_{ij}	The strain tensors.
$\dot{\varepsilon}_{ss}$	The steady- state strain rate.
$\dot{\varepsilon}_{ij}$	The strain rate tensor.
$\hat{\varepsilon}_{ij}(\theta,n)$	various strain, function of θ and n.
ε_{o}	The strain at time equal zero.
θ	Polar coordinate. (angle).
γ	The surface energy of material (Specific surface energy).
δ	The specimen deformation.
ν	Poisson's ratio.
w	Characteristic length dimension of crack body.
η	Constant depend end on the geometry of the specimen.
Γ	Clockwise contour in J-integral and C*-integral.
Π	Total energy associated with cracked body.

MAIN ABBREVIATIONS

ASTM	American Society for testing and materials.
BEF	Beam on elastic foundation model.
BEPF	Beam on elastic/plastic foundation model.
CFRP	Carbon fibre reinforced polymer.
CTOD	Crack tip opening displacement.
(CTOD)$_c$	Critical crack tip opening displacement.

DCB	Double-cantilever beam.
EPFM	Elastic-Plastic Fracture Mechanics.
FCP	Fatigue crack propagation.
EC	Extensive creep.
FCPR	Fatigue crack propagation rate.
LEFM	Linear elastic fracture mechanics.
PTFE	PolyTetraFluoroEthylene.
TDFM	Time-Dependent Fracture Mechanics.
SBT	Simple beam theory.
SEM	Scanning electron microscopy.
SSC	Small-scale creep.
TDCB	Tapered double cantilever beam.
TC	Transition creep.

CHAPTER 1

INTRODUCTION

1.1 Background

The use of structural adhesives in the construction, aerospace, marine and automotive industries has increased significantly over the last 40 years. Adhesive bonding can offer substantial benefits in comparison to traditional joining techniques, such as mechanical fastening and welding. Operational benefits which can result from the use of adhesive bonding include improved structural performance, resulting largely from the significant weight reduction adhesive bonding can provide, together with substantial reductions in both procurement and life-cycle maintenance costs. With the ever increasing role of structural adhesives in modern engineering comes a need for a greater understanding of the fracture and failure of bonded joints. Fracture mechanics is widely applied to the characterisation of adhesive failure. Fatigue loading is generally considered to be the most damaging form of structural loading. For adhesives to have wider application, within the aerospace and automotive industries in particular, it is vital that their long term properties be understood. One of the important features of an adhesive which determines its long-term performance is its creep behaviour. Adhesives, unlike metals, often exhibit significant rate dependent material behaviour at ambient temperatures. Thus it is not surprising that previous workers [1.1-1.8] have reported that the fatigue response of bonded joints is affected by the creep strain developed during fatigue cycling. This interaction between creep and fatigue becomes increasingly important as the joint is subjected to cyclic loading at high temperature, high mean stress level or low frequency. Xu et al. [1.9-1.10] studied the fatigue crack growth behaviour of bonded joints experimentally under opening mode I and mixed mode I and II. They concluded that creep plays a significant role in the crack

propagation process. Harris and Fay [1.11] measured the fatigue life of single lap joints over a range of test temperature. They found that creep plays a major role in determining the fatigue life. Although many experimental works have been carried out to study fatigue crack growth in adhesive joints, very few have been devoted to the study of creep or creep / fatigue crack growth behaviour. Gledhill and Kinloch [1.12] showed experimentally that for a double cantilever beam, the crack growth life is an exponential function of the strain energy release rate. The recent work of Crocombe and Wang [1.13] showed that the creep crack growth rate could be formulated as a power function of K or C*, where C* is the creep fracture parameter equivalent to J in a time dependent elastoplastic analysis.

Creep-fatigue interaction is an important problem that must be addressed in the design of many bonded structures. It is generally believed that when there is creep-fatigue interaction, such as under low frequency fatigue or high frequency fatigue combined with extended hold periods, a crack will grow faster than under either fatigue or creep loading alone. This is a practical consideration in many industrial areas such as the aerospace and automotive sectors. The aims of the current project were therefore to investigate the creep and fatigue performance of adhesively bonded joints and to evaluate any creep-fatigue interactions.

1.2 Aims of the present research

The overall aim of this research project is to study creep and fatigue crack growth in adhesively bonded joints and to develop a numerical approach in order to predict crack propagation in adhesively bonded joints. The general aim can be expanded to include the following objectives:

1) Generate static, fatigue and creep data using fracture mechanics principles.

2)   Investigate the effect of temperature and frequency in adhesively bonded joints.

3)   Investigate the effect of variable frequency fatigue loading in adhesively bonded joints.

4)   Investigate the effect of loading rate at ambient and elevated temperature for adhesively bonded joints and bulk adhesive samples.

5)   Design a creep rig to test the bulk adhesive properties at different temperatures.

6)   Identify the locus of failure using optical and scanning electron microscopy (SEM).

7)   Determine numerically and analytically the relevant fracture mechanics parameters, namely, the strain energy release rate, G, J-integral and creep parameters C^* and C_t.

8)   Develop methods to predict the crack growth rate, da/dN under fatigue, variable frequency loading and creep-fatigue loading.

1.3 Thesis outline

This thesis incorporates eleven further chapters. These chapters will now be briefly summarised.

Chapter 2 "Adhesive in engineering". This chapter will state the basic principles of adhesive bonding. Topics that will be discussed include; the advantages and disadvantages of adhesively bonded joints, basic concepts in adhesion, types of adhesive, types of adhesive test specimen, surface preparation, surface treatment and test methods.

Chapter 3 *"Fracture and fatigue behaviour in adhesive joints".* This chapter will investigate the application of fracture mechanics problems to fatigue and fracture in bonded joints. Topics discussed include the energy and stress approaches used in LEFM, crack tip plasticity, R-curve, J-integral, the S-N curve, the effect of frequency, the effect of temperature, rate effects and fatigue crack propagation.

Chapter 4 *"Analysis of cracks in creeping materials".* This chapter focuses on the analytical framework for considering time-dependent creep deformation and cracking under conditions of sustained loading. Topics discussed include the analysis of cracks propagating under steady-state creep, the analysis of cracks under small-scale and transition creep, the C^*-integral, the energy rate interpretation of C^*, methods of determining C^*, the C_t parameter and creep crack growth rate.

Chapter 5 *"Creep-Fatigue crack growth".* This chapter focuses on the analytical framework for considering creep-fatigue interactions. Topics discussed include the creep-fatigue interaction loading form, early approaches for characterizing creep-fatigue crack growth behaviour, TDFM parameters for creep-fatigue crack growth, crack tip parameters during creep-fatigue, methods of determining $(C_t)_{avg.}$, experimental methods for characterizing creep crack growth, creep-fatigue crack correlations and creep-fatigue crack growth rate.

Chapter 6 *"Determination of fracture parameters for DCB joints".* This chapter will investigate the different methods used in this work to calculate the parameters of fracture. Topics discussed include simple beam theory (SBT), the beam on elastic foundation model

(*BEF*), the beam on elastic/plastic model (BEPF), the crack closure method, the J-integral method and the creep parameter (C*-integral) method.

Chapter 7 *"Quasi-static and creep properties of FM300-2M adhesive"*. This chapter will present the material properties of FM300-2M bulk adhesive. Topics discussed include bulk adhesive sample manufacture, test procedures (quasi-static and creep testing), test results and conclusions.

Chapter 8 *"DCB tests -experimental details"*. This chapter will present the experimental apparatus and procedures used in testing the bonded DCB samples. Topics discussed include the experimental materials, sample manufacture, test set up and test types.

Chapter 9 *"DCB tests -Experimental results"*. This chapter will present the experimental results from DCB tests. Topics discussed include the quasi static test results, rate effects, fatigue test results and surface treatment effects.

Chapter 10 *"Prediction of Creep and Fatigue Crack Growth in Adhesively Bonded Joints"*. This chapter will present various methods of predicting crack growth in bonded joints under creep-fatigue conditions. Topics discussed include prediction of crack growth rate based on an empirical method; a dominate damage method, and a damage partitioning method.

Chapter 11 *"Discussion"*. This chapter will present a discussion of the experimental and theoretical results. Topics discussed include quasi- static and rate effects, frequency effects,

temperature effects, surface treatment effects, creep crack growth, failure locus and fatigue-creep prediction methods.

Chapter 12, *"Conclusions and future work"*. This chapter will present the main conclusions drawn from the work and suggested areas for future work.

1.4 References

[1.1] Xu, X.X., Crocombe, A.D., and Smith, P.A., "Creep Crack Growth in a filled and Toughened Adhesive", Proc. EuroMat 95, Padua, Italy, 1995, pp. 82-85.

[1.2] Xu, X.X., Crocombe, A.D., and Smith, P.A., "Fatigue Crack Growth rates in Adhesive Joints Tested at different frequencies", Journal of Adhesion, Vol.58, No.3-4, 1996, pp.191-204.

[1.3] Crocombe, A.D., and Gwenael, A.P, "Experimental and Numerical Studies of the Response of Adhesives and Bonded Joints to Creep Loads", Adhesion 99, 7th Conference, 1999, pp. 84-89.

[1.4] Ashcroft, I.A., Hughes, D.J., Shaw, S.J., Abdel-Wahab, M.M and Crocombe, A.D., "Effect of Temperature on the Quasi-Static Strength and Fatigue Resistance of Bonded Composite Double Lap Joints", Journal of Adhesion, Vol. 75, 2001, pp.61-88.

[1.5] Ashcroft, I.A., Hughes, D.J. and Shaw, S.J., "Mode I Fracture of Epoxy Bonded Composite Joints (Quasi-Static Loading)", International Journal of Adhesion & Adhesives, Vol. 21, 2001, pp.87-99.

[1.6] Knox, E.M., Cowling, M.J. and Hashim, S.A., "Creep Analysis of Adhesive Joints for Composite Components", Proceeding of the SAEV, Bristol, UK, Institute of Materials, 1998, pp.104-112.

[1.7] Knox, E.M., Cowling, M.J. and Hashim, S.A., "Creep Analysis of Adhesively Bonded Connections in GRE Pipes Including the effect of Defects", J. of Composite: Part A, Vol. 31, 2000, pp.583-590.

[1.8] Cowling, M.J., Knox, E.M., Lafferty, S. and Hashim, S.A., "Structural Integrity of Adhesively Bonded Pipe work Systems Including the Effects of Temperature and Time" Proceedings Workshop on "The cost Effective Use of Fibre Composites Offshore", Manchester, September, 1999.

[1.9] Xu, X.X., Crocombe, A.D., and Smith, P.A., "Fatigue Behaviour of Joints with either Filled or Filled and Toughened Adhesive", Int. J. of Fatigue, Vol. 16, 1994, pp.469-477.

[1.10] Xu, X.X., Crocombe, A.D., and Smith, P.A., "Mixed Mode Fatigue and Fracture Behaviour of Joints Bonded with either Filled or Filled and Toughened Adhesive", Int. J. of Fatigue, Vol. 17, 1995, pp.276-286.

[1.11] Harris, J.A. and Fay, P.A., "Fatigue Life Evaluation of Structural Adhesives for Automotive Application", Int. J. Adhesion and Adhesives, Vol. 12, No.1, 1992, pp.9-18.

[1.12] Gledhill, R.A., Kinloch, A.J., "Failure Criterion for the Fracture of Structural Adhesive Joints", Polymer, Vol. 17, 1976, pp.727-731.

[1.13] Crocombe, A.D. and Wang G., "Modelling Crack Propagation in Structural Adhesives under External Creep Loading", Journal of Adhesion Science and Technology, Vol. 12, 1988, pp.655-675.

CHAPTER 2

ADHESIVES IN ENGINEERING

2.1 Introduction

According to the ASTM definition; *"an adhesive is a substance capable of holding materials together by surface attachment"* [2.1]. In an adhesively bonded structure, the bond is the location at which two materials, called the adherends, are held together with a layer of adhesive. The interactions of interest are those between the adherends and the adhesive. The forces of attraction acting across the adhesive/ adherend interface are, therefore, those responsible for holding the materials together. They may arise because of the formation of chemical bonds or physical interactions.

The use of adhesives in structural applications has been developing over the last fifty years. The main reason for this is that the adhesives employed in nearly all technically demanding application are based upon synthetic polymers, and such polymers have only been available for about the last fifty years. At the present time adhesive are used in wide-ranging structural applications, including bonding of both metallic and non-metallic substrates, in the automotive, marine, and aerospace and construction industries.

There are a lot of studies in this field ranging from the chemistry of adhesives to the mechanical properties of adhesives and bonded structures. Work reviewed in this chapter will focus on the mechanisms and concepts of adhesion, the advantages & disadvantages of adhesive bonding, surface preparations and treatments, types of adhesives and test methods.

2.2 Types of adhesive joint

The nature of an adhesive joint is largely determined by the circumstances in which it is to be used. Joints can be subdivided into the four basic types shown in Figure (2.1) [2.2]. The strength of a given type of joint depends, for a given type of load, on the stress distribution within the joint and the mechanical properties of the adhesive and adherends. In particular the following parameter can be significant: length of overlap; adherend thickness; adhesive thickness; surface area: adherend strength and elastic modulus and adhesive stress/ strain characteristics.

Single lap

Double lab

Scarf

Stepped lap
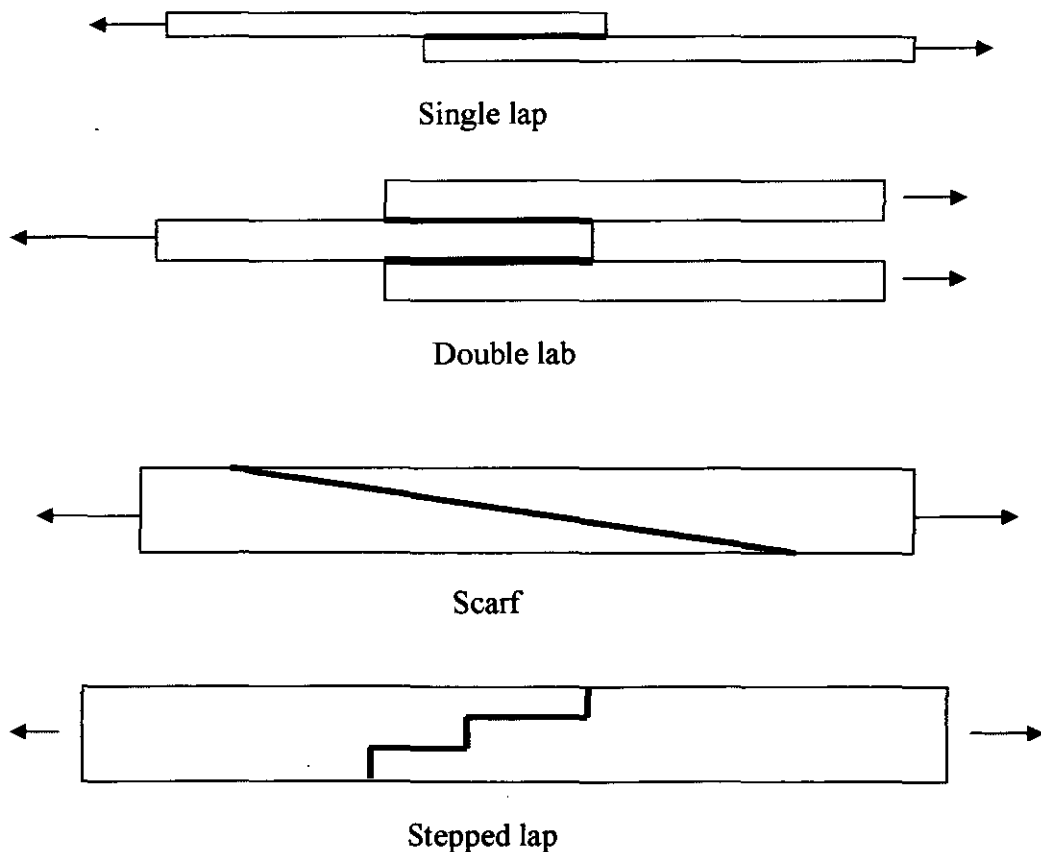
Fig. 2.1 Basic types of joint.

2.3 Advantages and disadvantages of adhesively bonded joints

The advantages that engineering adhesives can offer, compared to more traditional methods of joining such as bolting, brazing, welding, mechanical fasteners, etc., include [2.2-2.3]:

a) The ability to join dissimilar materials to give light-weight, but strong and stiff, structures, e.g. the joining of metals, plastics, rubbers, fibre-composites, wood, paper products, etc.

b) The ability to join thin-sheet material efficiently. This is a major use of adhesives for joining both metallic and non-metallic materials. Compared to metallic substrates, adhesives, being based largely upon organic polymers, do not possess anywhere near the level of tensile fracture strengths exhibited by most metals. However, when bonded lap joints are used to join relatively thin sheets of metal the strength of the joint can be as high as that of the metallic adherends.

c) An improved stress distribution in the joint which imparts, for example, a very good fatigue resistance to the bonded component. This is one of the main reasons that engineering adhesives are widely used in the construction of helicopter blades.

d) The fact that they frequently represent the most convenient and cost-effective joining technique. The bonding operation can often be automated. This removes the necessity for any human operator to mix together the various components of an adhesive formulation, apply the adhesive to the correct location and repeat the procedure correctly many hundred of times a day. Also, as demonstrated by the vehicle manufacturing industries, adhesives may be readily adapted to robotic-assembly techniques.

e) An increase in design flexibility that enables novel design concepts to be implemented and allows a wider choice of materials to be available to the designer.

f) An improvement in the appearance of the joined structure; for example, if adhesives are used instead of spot-welding or riveting then the smooth, blemish-free, appearance of the bonded structure is more appealing to the consumer.

g) An improvement in corrosion resistance. The above comparison to the spot-welded component serves as a good example where the use of a well-selected adhesive system will inherently result in far less corrosion.

h) Join structures where there is access to only one side.

However, as with any technology, there are some disadvantages:

a) To attain long service-life from adhesive joints in hostile environments elaborate surface pre-treatment processes may be necessary.

b) Compared to other fastening techniques such as welding, riveting, etc. the upper-service temperatures that polymeric adhesives can withstand are limited.

c) The strength and toughness of adhesives in tension or shear is relatively low compared to many metals.

d) Non-destructive test methods for adhesive joints are relatively limited compared to those used with other fastening methods.

e) Process sensitivity, which includes curing temperature, environmental condition, etc.

f) Curing the adhesive may be a lengthy process, requiring an additional stage in the manufacturing process.

g) Limited gap-filling properties may present tolerance problems when joining large substrates.

h) Adhesive are not recommended where periodic disassembly is required.

2.4 Principles of Structural bonding

An understanding of adhesion and adhesive bonding requires consideration of concepts from a number of scientific disciplines including: chemistry, physics, material science, surface science, mechanics, and thermodynamics. Some of these concepts will be discussed in the following sections:

2.4.1 Surface and interfacial phenomena

The role of interfacial contact is extremely important in obtaining strong adhesive joints. To achieve strong joints, the adhesive needs to be able to spread over the surface of the material, displace air and other contaminants, and establish intimate molecular contact. Kinloch [2.3] suggests three criteria to which an adhesive should ideally conform to:

a) The adhesive should exhibit a zero or near zero contact angle on the adherend surface.

b) The adhesive should have a low viscosity at some time during the bonding process.

c) The joint should be assembled in a manner that assists in the displacement of any trapped air.

In the assessment of an adhesive/substrate combination, it is necessary to consider not only the kinetics of the wetting process and the wetting equilibrium, but also the value of the surface free energies of the adhesive and substrate, and details of the bonding process.

2.4.2 Design of adhesive joints

The basic design criteria of adhesive joints can be summarized into the following points:

1. The maximum bonded area should be used.

2. The bond should be stressed in its strongest direction, such as shear or compression.

3. Stresses in the weakest bond direction should be minimized, i.e., in peel and cleavage.

4. Residual stresses due to differential thermal expansion should be allowed for.

Initial design considerations require knowledge of the chemical and physical properties of both adhesive and adherends. Furthermore, an adhesive joint is expected to perform satisfactorily under the expected service conditions for the planned lifetime of the structure. Thus changes in the properties of the adhesive as a function of environment, fatigue, temperature, loading rate, and age must also be known, or be predicted [2.3, 2.18].

2.4.3 Mechanisms of adhesion

The generation of strong intrinsic adhesion forces is a key requirement to obtain good performance from adhesive systems. There are four widely accepted mechanisms by which intrinsic adhesion forces are generated over the adhesive/ substrate interface [2.3-2.4].

2.4.3.1 Mechanical interlocking

This theory states that adhesion is promoted within a bond by the amount of keying-in of the adhesive into the surface of the substrate. The literature contains several references [2.5-2.6] concerning the effect of surface roughness on adhesive bond strength. It is a common practice to roughen a wood surface with glass paper so that the glue may penetrate into the surface layers of the wood and provide a bond by interlocking. Another example of this sort of interlocking is the traditional dental technique of filling restorations which involves drilling a cavity with an "ink-well" configuration, i.e. with an opening narrower than the main part of the cavity. This is then packed with metal amalgam, which expands on setting to form a strong mechanical bond. This type of bond involves a structure in which separation requires a mechanical force great enough to break one of the components. Packham [2.7] provided further evidence for the importance of substrate surface topography. In his studies on the adhesion of polyethylene to metallic substrates, he found that high peel strengths were obtained when a very rough, fibrous type, oxide surface was formed on the substrate.

Using scanning electron microscopy, Venables [2.8] revealed that, apparently smooth, oxide films, particularly those on aluminium, had both pores and protruding whiskers on an Angstrom scale. An adhesive both penetrated into these pores and enclosed the whiskers to give an interphase which was both strong and durable. Extension of this work [2.9] has demonstrated that good adhesion to a metal surface requires a surface which is irregular in structure, with both crevices and protruding features.

2.4.3.2 Diffusion theory

This theory, put forward by Voyutskii [2.10], states that intrinsic adhesion of polymers to themselves is due to mutual diffusion of polymer molecules across the interface. This requires that the macromolecules or chain segments of polymers (adhesive and substrate) possess sufficient mobility and are mutually soluble, i.e. they possess similar values of the solubility parameter. This theory is most applicable to the bonding of polymeric materials of the same chemical type.

2.4.3.3 Electronic theory

This theory was advanced by Deryaguin et al. [2.11]. They considered the adhesion and separation of a pressure-sensitive tape from a rigid substrate. When these two substances of different electro-negativity are in intimate contact, an electric double layer will be formed at the interface. In order to separate the two layers, the electrostatic attraction of the double layer has to be overcome, and this produces a potential difference between the two which will increase until there is an electric discharge. Deryaguin's theory essentially treats the adhesive-substrate system as a capacitor which is charged due to the contact of the two different materials. Separation of the parts of the capacitor, as during interface rupture, leads to a separation of change and to a potential difference which increases until a discharge occurs. Some attempts to repeat Deryaguin's measurements have not been successful. Thus, this theory has been largely discredited. Also it assumes failure in an adhesive joint to be at the adhesive-substrate interface and not cohesive in the adhesive as is commonly the case.

2.4.3.4 Adsorption theory

The adsorption theory of adhesion is the most generally accepted theory and has been discussed by many researchers [2.12-2.15]. This theory proposes that the cohesive strength of any solid depends upon the various forces of attraction that exist between the ultimate particles of which it is composed. These include those of chemical origin, covalent, ionic and metallic bonding, hydrogen bonding, as well as those considered to be of physical origin –secondary or van der Waals forces, provide a source of adhesive strength. In any particular instance, which of these are present and their relative significance will depend upon the chemical nature of the material, but the dispersion forces will always be present and effective to a greater or lesser extent. A quantitative consideration of these forces enables the ideal strength of the material to be calculated.

One important feature which is common to all these forces is that they are only significant over short distances. Most of them are quite negligible beyond a few Angstroms. This means that if they are to have any significant effect in holding two surfaces together, they must be in very close contact.

2.4.3.5 Summary

Various basic explanations and developments in adhesion science have been reviewed in this section. Various mechanism of adhesion have been proposed, however, it may well be that more than one mechanism is contributing in an adhesive bond, and debate continues on this issue. Current thinking seems to be that the adsorption theory is the most applicable to a wide range of cases.

The establishment of a strong joint is concerned with attaining intimate interfacial contact between the adhesive and substrates, and then establishing strong and stable intrinsic

adhesion across the adhesive/substrate interfaces. In order to achieve these requirements during manufacture of samples in this work, the substrates will be subjected to some form of surface treatment before the adhesive is applied. This has the primary objective of cleaning the surfaces and providing a suitable surface morphology for adhesive bonding. In some cases the surface treatment is also considered to enhance chemical bonding in the interface region.

2.5 Surface preparation

One of the few disadvantages of adhesive bonding as a method of fastening is that the surfaces need to be clean and, whatever their chemical nature, must be coherent in the sense that they must not be powdery or friable.

Surface treatment of an adherend prior to adhesive bonding can bring about one or a combination of the following effects [2.16]:

a) Remove material

b) Modify the chemistry of the surface

c) Change the surface topography

The effect of such treatments may be to increase the strength of the newly made joint, but perhaps more importantly to improve joint durability on exposure to water or water vapour. Metals have high energy surfaces because of the very polar oxide layer they carry. There is therefore little difficulty in getting almost any adhesive to bond to them provided they are clean and free from loose or incoherent oxide.

Compared with metals, all plastics have relatively low energy surfaces and some, such as polyethylene, polypropylene, and politetrafluoroethylene (PTFE), have surfaces of very

low free surface energy and are difficult to bond. Mostly the surfaces can be treated to render them capable of being bonded.

2.5.1 Removal of material

Material on the surface of an adherend which is cohesively weak, or which will not adhere to the substrate or adhesive with sufficient strength, may constitute a weak boundary layer. Materials that may need to be removed from a surface prior to bonding include [2.16]:

1) Lubricating oils and greases on metals

2) Weak oxide layers on metals

3) Dust and other particulate contamination

4) Additives and low molecular weight material on the surfaces of plastics

5) Mould release agents such as silicones, fluorocarbons and waxes.

All the metals in common engineering practice possess an oxide surface, but not all are coherent. Some tend to flake (e.g. copper oxide) or powder (e.g. rust). The purpose of surface preparation is to remove these loose layers and then possibly to etch away the existing oxide and to replace it with one which gives good performance, both in the form of high initial joint strength and resistance to high humidity.

2.5.2 Modification of surface chemistry

The physical adsorption theory of adhesion takes the view that adhesive bonds depend upon the weaker dispersion forces and the somewhat stronger polar forces. For the latter to operate, surfaces of both the substrate and the adhesive need to contain polar chemical groups. Some plastics lack such groups (e.g. polyethylene and polypropylene) but they can be introduced by treatments such as corona-discharge.

2.5.3 Modification of surface topography

The mechanical interlocking theory of adhesion can clearly be exploited by creating a rough surface. Some surfaces such as that of wood are naturally rough, and abrasion is a simple means of roughening others. The physical effect of etching and anodizing aluminium and its alloys is to create a honeycomb structure made of the oxide, which is receptive to mechanical interlocking.

2.6 General methods of surface treatment

2.6.1 Abrasive methods

Abrasive methods include the use of abrasive papers or cloths, which are acceptable for small-scale work, and shot- and grit-blasting. All these methods remove material and can in fact remove tens of μm from the surface. For ferrous metals, shot-blasting can be used whilst for other metals, grit-blasting with alumina or carborundum is preferable. These methods are unsuitable for accurately machined parts, but wet-blasting with fine alumina powder, which gives a polishing- cleaning action, may be used within the required tolerances. Proprietary machines are available for wet-blasting which are used for cleaning precision moulds for rubber and plastics mouldings and may be trusted to remove the minimum of metal.

It is important to keep the grit or shot clean, and to prevent contamination of the compressed air by oil. Any products of abrasion should be removed by brushing or air-blasting and the substrate should then be degreased. Abrasive methods usually combined with a subsequent degrease stage.

2.6.2 Use of solvents

Solvents are very effective at removing oils and greases from metals, and additives from the surfaces of polymers. They can be used in the liquid form or in vapour degreasing.

There are five considerations which govern the choice of a solvent: toxicity, flammability, efficiency for degreasing, the environment and cost. There is also the factor of convenience, in that it is desirable to have only one or perhaps two different solvents available for degreasing, whereas the optimum efficiency, if this were the sole criterion, might require a number to be available.

Ingestion of solvents by humans is most likely to be by inhaling, and with this assumption, occupational exposure limits (OELs) have been recommended for the solvents in most common use [2.17]. All solvents which are efficient for cleaning surfaces will also remove the natural body greases from hands. Whilst direct handling and wiping of components with solvent-soaked cloths or tissues is to be discouraged, there are occasions when it will be done. Barrier creams will themselves contaminate the surfaces to be cleaned; the hands are best protected with cheap, disposable polyethylene gloves, but compounds in their surface can also contaminate other surfaces.

2.6.3 Use of detergents

The following is a procedure involving the use of a detergent, to treat metal surfaces for adhesive bonding [2.16].

1) Brush to remove loose oxide, dust and dirt.

2) Degrease by solvent vapour or wipe.

3) Shot-, sand – or grit –blast, wet or dry.

4) Wash in detergent solution followed by clean water. A suitable detergent solution is

   5 ml with 25g trisodium orthophosphate in 1 litre of water.

This procedure has been selected to be one of the methods used to treat the mild steel substrates in this project.

2.7 Surface treatment of mild steel

A recommended procedure for treating the surfaces of mild steel is as follows [2.16]:

a) Any obvious rust or mill scale on mild steel should be removed by brushing prior to vapour degreasing.

b) The mild steel should then be grit-blasted.

c) Etch, for a time measured from the beginning of the reaction, for 10 min at 71-77° C in a solution consisting of:

    a. Sodium dichromate   (4 parts by wt.)

    b. Sulphuric acid   (10 parts by wt.)

    c. Water   (30 parts by wt.)

d) Rinse in running water. Brush off carbon residue with nylon brush while washing in running water.

e) Rinse with distilled water followed by bath in acetone.

f) Dry at 93°C.

g) Store in a desiccator until needed or apply a primer coating at once.

2.8 Primers

Primers may be applied to adherend surfaces for one or more of the following reasons:

1) A coating of primer applied immediately to a freshly prepared surface protects it until the bonding operation is carried out.

2) It wets the surface more easily and thoroughly than the adhesive itself. This may be achieved by using as the primer the adhesive dissolved in a solvent to give a solution of much lower viscosity. Alternatively the primer may be a solution of a polymer other than the adhesive which wets the substrate and which, after drying, is easily wetted by the adhesive.

3) It may serve to block the pores of porous surface. This is probably only important for structural adhesive bonds to concrete or wood. However, some penetration of the adhesive into the substrate may be very desirable and the viscosity can be adjusted to give optimum penetration whilst avoiding the possibility of a starved joint.

4) It can act as the vehicle for corrosion inhibitors, keeping them near to the surface where they are needed. The reagents most commonly employed are strontium and zinc chromates. As only those particles in direct contact with the steel or aluminium surface are effective inhibitors, it is reasonable to apply them in a suitable binder in as thin a layer as possible.

5) The primer may be a coupling agent capable of forming chemical bonds both with adherend surface and the adhesive. This does not necessarily add to bond strength when dry but can enhance strength in wet conditions.

Examples of some commercially available primers are as follows:

a) *Cyanamid BR 127* is particularly recommended for use with FM73 and FM300 toughened epoxy film adhesives. The primer is a modified epoxy-phenolic which can be applied by brush or spray to give a dry coating of thickness 2.5-5 μm. After drying in air for 30 min the primed surface is

cured for 30 min at 120 ±6°C; it then has an indefinite shelf-life, but wrapping in Kraft paper is recommended. BR 127 has corrosion inhibiting properties and protects the metal oxide layer from hydrolysis.

b) **Hysol EA 2989** has the advantage of being water-based and not containing chromium, even though it is corrosion inhibiting. It is formulated for use with Hysol EA 9689 film adhesive. Recommended coating thickness is 5-10μm. The primer is dried in air for at least 1 hr and is then cured for 1 hr at 175°C.

c) **3M EC-2320** is particularly recommended for AF-111, AF-126 and AF-126-2 film adhesives; it improve shear and peel strengths and environmental resistance. This primer is supplied as a solution in organic solvents and recommended coating thicknesses are 1.3-5.1 μm. It can be dried at temperatures up to 120°C and primed surfaces have a 90 day shelf life.

2.9 Types of Adhesive

There are many types of adhesives and understanding the difference between them and selecting the right one for a particular application can be difficult. Many different attributes are used to describe adhesive types [2.18].

a) Physical form (liquid, two-part, paste, film).

b) Chemical form (epoxy, acrylic, cyanoacrylate, polyurethane)

c) Type of material bonded (metal to metal, wood, paper)

d) End use (automotive, dental, surgical)

e) Bonding or curing method (pressure sensitive, high temperature, room temperature anaerobic, contact)

f) Brand names (Superglue, Sellotape, Araldite, Loctite).

There are some major family groups of adhesives likely to be of value to the design engineer and these will be briefly discussed. The main adhesive types used in industry are:

a) Orthophthalic Polyester (general purpose, undemanding applications)

b) Isophthalic Polyester (general purpose, improved chemical and mechanical performance).

c) Urethane Methacrylate (general purpose, low smoke and toxicity)

d) Vinyl Ester (good chemical resistance)

e) Epoxy (high mechanical performance)

f) Phenolic (excellent fire resistance, low smoke)

The main types of structural adhesive used in industry are described in the following sections:

2.9.1 Epoxy adhesives

Epoxy adhesives are thermosetting structural adhesives. They consist of an epoxy resin, often based upon the diglycidyl ether of bisphenol A (DGEBA), and harden to give a thermosetting polymer by step-growth polymerisation or addition polymerisation, and are then capable of supporting sustained loads. Epoxies are either two-part systems (resin and hardener) which require mixing or single-part systems which require heat to start the cure process.

Epoxies produce joints with high shear strength but have limited peel and impact strength unless toughened. This brittleness has limited the use of un-toughened epoxies in automotive applications but they are used for some non-structural applications such as bonding of electronic components.

2.9.2 Toughened epoxy adhesives

The toughening of adhesives is a method of increasing their peel, fatigue and impact performance without sacrificing static shear strength or durability. A common method of toughening epoxies works by dispersing a 'rubbery' phase within the harder adhesive matrix. These rubber particles increase the toughness by blunting the cracks. Toughened epoxy adhesives offer a very good balance of mechanical properties and are widely used in structural applications. They represent a significant improvement over the traditionally brittle un-toughened epoxy adhesives and are extensively used in automotive applications.

In this project a modified epoxy resin, FM300-2M, is used for bonding the composite and mild steel substrates. It is widely used in bonding aircraft structures. It has excellent moisture and corrosion resistance in high humidity environments with no significant reduction in mechanical properties. The curing temperature is 120 C°. It meets the requirements of military and aerospace specifications.

2. 10 Types of adhesive test specimen

Many types of test specimen can be used to determine the strength and durability of bonded joints. In this research project the double-cantilever beam (DCB) specimen will be used to investigate mode I crack propagation in adhesive joints. This is a popular test because of the ease of sample manufacture and testing, coupled with simple analysis

methods. Ripling et al. [2.19-2.21] first adapted the DCB test for testing structural adhesive and suggested a theory based on a built-in beam. They suggested that rotation at the assumed built-in end could be corrected for by using an empirically derived rotation factor that was added to the measured crack length. Later workers modelled the DCB as a beam on an elastic foundation in order to theoretically account for the contribution of the adhesive to the compliance [2.22-2.25].

The DCB has been used to generate fracture data for composites [2.26-2.29], bonded composites [2.30-2.40] and bonded metal joints [2.41-2.44]. The DCB is frequently used to generate fatigue data as well as quasi-static fracture data.

2.11 Test methods

A wide variety of standard test procedures are listed by the International Standards Organization (ISO), European Standards (EN), American society for testing and materials (ASTM), British Standards Institution (BSI) and other organizations. These standards bring together the knowledge and experience of general interest groups, producers, and consumers to write test methods and specifications on a non-partisan basis so that they represent the best balance of all interest involved.

One of the technical committees involved in this far-reaching process of standardization is the ASTM committee D-14 on adhesives. D-14 was organized in 1944 and has been instrumental in writing more than 60 test methods, specifications, and recommended practices as will as a set of definition of terms relating to adhesives. This review will only touch on some of the basic test methods relevant to this research project.

2.11.1 Tensile tests

Pure tensile adhesion tests are those in which the load is applied normal to the plane of the bond and in line with the centre of the bond area. D897, "Tensile properties of adhesives", is one of the oldest methods. The specimens and grips require considerable machining and, because of the design, tend to develop edge stresses during the test. Because of these limitations, D897 is being replaced as by D2095, "Tensile strength of adhesives, rod and bar specimens". The rod and bar specimens, prepared per D2094, are simpler to align and, when correctly prepared and tested, more properly measure tensile adhesion.

2.11.2 Peel tests

Peel tests are designed to measure the resistance of adhesive bonds to highly localized tensile stresses. Peel forces are therefore considered as being applied to linear fronts. The more flexible the adherend and the higher the adhesive modulus, the more nearly the stressed area is reduced to linearity. The stress then approaches infinity. Since the area over which the stress is applied is dependent on the thickness and modulus of the adherend and the adhesive, and therefore very difficult to evaluate exactly, the applied stress and failing stress are reported as linear values. Probably the most widely used peel test for thin-gauge metal adherends is the so called T-peel test. The designation of the ASTM version is D1876.

2.11.3 Creep tests

When a bonded structure is subjected to a permanent load in service, the adhesive's resistance to creep is an important characteristic. Two ASTM methods are available for evaluating this property: D2293, "Creep properties of adhesives in shear by compression

loading (metal to metal)", and D2294, "Creep properties of adhesives in shear by tension loading (metal to metal)". These two methods use lap-shear specimens with springs to apply the compression or tension load.

2.11.4 Fatigue tests

Fatigue testing refers to the repeated application of a specified load or deformation on a bonded specimen. Tests are conducted under dynamic conditions according to the data required to evaluate an adhesive under service conditions.

Fatigue tests perform a necessary function in that they make it possible to screen and select adhesives for most bonded applications with a fair degree of accuracy. When they are combined with representative environments, they diminish even more the uncertainties involved in selecting adhesives for critical applications.

For fatigue loading, ASTM D3166 specifies a specimen similar to the single-lap shear specimen of D1002 but with a shorter free length to resist buckling.

2.12 Summary

This chapter covers the basic fundamentals of adhesive bonding. The advantages of using adhesives are discussed as is the bonding requirements of the surfaces to be bonded and the surface treatment procedures. Through this review a suitable primer for epoxy adhesive FM300-2M was selected and two methods for pre-treating mild steel substrates were selected.

2.13 References

[2.1]   Annual Book of ASTM Standards, Part 22, American Society for Testing and Materials, Philadelphia, Pennsylvania, ISBN: 0803117469, 1982.

[2.2]   Bruyne, N.A., "Fundamentals of adhesion. Proceedings of Conference on Bonded Aircraft Structures", Bonded Structures Limited, Cambridge, Uk, 1957, pp. 1-9.

[2.3]   Kinloch, A.J., "Adhesion and Adhesives: Science and Technology", Chapman and Hall, London and New York, ISBN: 041227440, 1987, pp.302-306,

[2.4]   Allen, K.W., "A review of Some Basics of Adhesion over the Past Four Decades", Int. Journal of Adhesion, Vol. 23, 2003, pp.87-93.

[2.5]   Boroff, E.M and Wake, W.C., Trans Inst Rubber Ind, Vol.25, 1949, pp199-210.

[2.6]   Haines, B.M. In: Alner, D.J., Editor, "Aspects of adhesion", University of London Press, Vol.3, ISBN: 00668656, 1967, P.40.

[2.7]   Packham, D.E., "Adhesion of Polyethylene to High Energy Substrates", Ph.D. Thesis, London: City University, 1970.

[2.8]   Venables, J.D., In: Allen, K.W., Editor, "Adhesion", Applied Science Publishers, Vol. 7, London, ISBN: 02604450, 1983, P.87.

[2.9]   Aleen, K.W., Alsalim, H.S. and Wake, W.C., "Faraday Special Discussions of the Chemical Society of London", No.2, 1972.

[2.10] Voyutskii, S.S., "Autohesion and Adhesion of High Polymers", Wiley Interscience, New York, 1963, pp.117-140.

[2.11] Deryaguin, B.V., and Smilga, V.P., "Adhesion, Fundamentals and Practice", McLaren and Son, London, 1969, pp.152-153.

[2.12] Huntsberger, J.R., "In Treatise on Adhesion and Adhesives", Mercel Dekker, New York, ISBN: 0824770374, 1967, pp.119-149.

[2.13] Wake, W.C., "Royal Institute of Chemistry Lecture Series 4", 1965.

[2.14] Kinloch, A.J., "Adhesives in Engineering", Eighty-Fourth Thomas Hawksley Memorial Lecture, 1996.

[2.15] Bikerman, J.J., "The Science of Adhesive Joints", 2nd edition, London: Academic Press, 1968.

[2.16] Adams, R. D., Comyn, J., and Wake, W.C., "Structural Adhesive Joints in Engineering", Published by Chapman and Hall, London, UK, ISBN: 0412709201, 1997, pp.7-9.

[2.17] Royal Society of Chemistry, "Solvent in Common Use", 1988.

[2.18] Hartshorn S.R., "Structural Adhesives Chemistry and Technology", Plenum Press, New York, ISBN: 03064216, 1986.

[2.19] Ripling, E.J., Mostovoy, S. and Patrick, R.L., "Measuring Fracture Toughness of Adhesive Joints", Mater Res Stands, Vol. 4, 1964, pp.129-134.

[2.20] Mostovoy, S., Crosley, P.B. and Ripling, E.J., "Use of Crack-Line-Loaded Specimens for Measuring Plane strain Fracture Toughness", Journal of Material, Vol. 2, 1967, pp.661-681.

[2.21] Ripling, E.J., Corten, M.T. and Mostovoy, S., "Fracture Mechanics: A Tool for Evaluating Structural Adhesives", J. of Adhesion, Vol. 3, 1971, pp.107-123.

[2.22] Chow, C.L., Woo, C.W. and Sykes, J.L., "On the Determination and Application of COD to Epoxy-Bonded Aluminium Joints", Journal of Strain Analysis, Vol. 14, 1979, pp.37-42.

[2.23] Ben Ouezdou, M. and Chudnovsky, A., "Stress and Energy Analysis of Toughness Measurements of Adhesive Bonds", Engineering Fracture Mechanics, Vol. 29, 1988, pp.253-261.

[2.24] Penado, F.E., "A Closed Form Solution for the Energy Release rate of the Double Cantilever Beam Specimen with an Adhesive Layer", Journal of Composite Material, Vol. 27, 1993, pp.383-407.

[2.25] Olsson, R., "A Simplified Improved Beam Analysis of the DCB Specimen", Computing Science Technology, Vol. 43, 1992, pp.329-338.

[2.26] Ben Ouezdou, M. and Chudnovsky, A. and Abdelsamie, M., "Re-Evaluation of Adhesive Fracture Energy", Journal of Adhesion, Vol. 25, 1988, pp.169-183.

[2.27] Rybicki, E.F., Hernandez, T.D., Deibler, J.E., Knight, R.C. and Vinson, S., "Mode I and Mixed mode Energy Release Rates Values For Delaminating of graphite/Epoxy test Spec.", J. of Composite Mat., Vol. 21, 1987, pp.105-123.

[2.28] Prel, Y.J., Davies, P., Benzeggah, M.L. and de Charentenay, F. "Mode I and Mode II Delaminating of Thermosetting and thermoplastic Composites" In: Composite Materials: Fatigue and Fracture, Vol. ASTM STP 1012, Philadelphia: American Society for Testing and Materials, 1989, pp.251-269

[2.29] Ducept, F., Davies, P. and Gamby D. "An Experimental Study to Validate Tests Used to Determine Mixed Mode Failure Criteria of Glass/ Epoxy Composites" Composites A, Vol. 28, 1997, pp.19-29.

[2.30] Truss, R.W., Hine, P.J. and Duckett, R.A., Interlaminar and Intralaminar Fracture Toughness of Uniaxial Continuous Carbon Fibre/Epoxy Composites", Composite A, Vol. 28, 1997, pp.627-636.

[2.31] Mall, S., Johnson, W.S. and Everett Jr, R.A., "Cyclic Debonding of Adhesively Bonded Composite", In: Mittal KL Editor, Adhesive Joints: Their Formation, Characteristics and Testing, New York: Plenum Press, 1984, pp.639-658.

[2.32] Mall, S., Johnson W.S., "Characterisation of Mode 1 and Mixed Mode Debond Failure of Adhesive bonds Between Composite Adherends", In: Composite

Materials: Testing and Design, Vol. ASTM STP 893, Philadelphia: American Society for Testing and Materials, Philadelphia, 1986, pp.332-334.

[2.33] Mall, S., Rezaizdeh, M.A. and Ramamurthy, G., "Interaction of Mixed Mode Loading on Cyclic Debonding in Adhesively bonded composite Joints", ASME Paper No. 85-WA/Mats-1, Presented at ASME Winter Annual Meeting, Miami Beach, Florida, November, 1985.

[2.34] Kinloch, A.J. and Osiyemi, S.O., "Prediction The Fatigue Life of Adhesively Bonded Joints", Journal of Adhesion, Vol. 43, 1993, pp.79-90.

[2.35] Charalambides, M.N., Kinloch, A.J. and Mathews, F.L., "Strength Prediction of bonded Joints", 83rd Meeting of the AGARD Structures and Materials Panel, Florence, Italy: NATO, 1996.

[2.36] Ripling, E.J., Santner, J.S., Crosley, P.B., "Fracture Toughness of Composite Adherend Adhesive Joints Under Mixed Mode I and III Loading", Journal of Material Science, Vol. 18, 1983, pp. 74-82.

[2.37] Chai, H., "On the Correlation between the Mode I Failure of Adhesive Joints and Laminated Composites", Eng. Fracture Mech., VOl. 24, 1986, pp. 413-431.

[2.38] Mangalgiri, P.D., Johnson, W.S., and Everett Jr, R.A., "Effect of Bond Thickness on Fracture, Fatigue Strength of Adhesively Bonded Composite Joints", Journal of Adhesion, Vol. 9, 1987, pp. 263-288.

[2.39] Ashcroft, I.A., Hughes, D.J. and Shaw, S.J., "Mode I Fracture of Epoxy Bonded Composite Joints: 1. Quasi-Static Loading", Int. Journal of Adhesion and Adhesive, Vol. 21, 2001, pp. 87-99.

[2.40] Ashcroft, I.A., Hughes, D.J. and Shaw, S.J., "Mixed Mode Fatigue Testing of Bonded Composite Joints" Proceeding of the Fifth International conference on

Structural Adhesives in Engineering, Bristol: Institute of Materials, 1998, pp.422-426.

[2.41] Gledhill, R.A. and Kinloch, A.J., "Failure Criterion for the Fracture of Structural Adhesive Joints", Polymer, Vol. 17, 1976, pp.727-731.

[2.42] Kinloch, A.J., Shaw, S.J., "The Fracture Resistance of a toughened Epoxy Adhesive", Journal of Adhesion, Vol. 12, 1981, pp.59-77.

[2.43] Dillard, D.A., Wang, J.Z. and Parvatareddy, H., "A Simple Constant Strain Energy Release Rate Loading Method For Double Cantilever Beam Specimens", Journal of Adhesion, Vol. 41, 1993, pp.33-50.

[2.44] Little, M.S.G., "The Durability of Structural Adhesive Joints", Ph.D Thesis, Imperial College, London, 1999.

CHAPTER 3

FRACTURE AND FATIGUE IN ADHESIVE JOINTS

3.1 Introduction

The use of adhesively bonded joints that are subjected to cyclic loading has increased significantly during the last three decades, not only in the aerospace industry but also in the automotive, marine, medical and constructions sectors. Since 1970, a considerable amount of research work has been devoted to the study of the fatigue of adhesively bonded joints using stress analyses and fracture mechanics. The field of fracture mechanics is highly multidisciplinary and is studied and used by engineers from several disciplines. For example, engineers in basic materials industries such as steel, aluminium, plastics, and composites use fracture mechanics based test methods to evaluate and characterize materials. Researchers, in aerospace, automotive, marine equipment, power generation, petrochemical, and construction industries use fracture mechanics based methods for design and life prediction, for remaining life prediction, for establishment of safe inspection intervals, for developing inspection criteria and understanding field failure of structural components. Thus, it is also an engineering tool used by design and maintenance engineers in a variety of industries.

The fatigue behaviour of a material can be characterised in terms of resistance to crack propagation using fracture mechanics parameters, such as the stress intensity factor, or the strain energy release rate, G. This approach is based on the measurement of the incremental crack growth, from a sharp crack, through a material. The fundamental concept of fatigue design is based on plotting the stress amplitude versus the fatigue life in cycles using experimental data. For some metals such as steel, there exists a stress value below which the material can undergo a large number of cycles. This stress value is usually

referred to as the endurance limit. In adhesively bonded joint, the presence of an endurance limit indicates a threshold stress value below which cracks will not propagate in the adhesive layer or along the adhesive/adherend interface exists. Sancaktar et al. [3.1] have reported the presence of two thresholds in bonded joints. These two thresholds are the onset threshold level before the steady crack propagation and the catastrophic threshold level before the fast crack propagation.

The high stress level arising at the overlap edge of an adhesive joint has attracted a lot of research. The early work of Goland and Reissner [3.2] based on elastic stress analysis showed that high peel and shear stresses occur at the adhesive edge in a single-lap joint. Geometric parameters such as overlap length and adhesive thickness affect the value of this stress concentration. Many attempts have been made to reduce these stress concentrations. Sancaktar and Lawry [3.3] have used pre-bent adherends to increase the load carrying capacity of single lap joints, while Hart-Smith and Bunin [3.4] have used tapered overlap edges. Adams et al. [3.5] have concentrated on using fillet geometry at the overlap edge. Due to the stress singularity discussed above, many researchers have used fracture mechanics to predict the fatigue service life of adhesive joints. It was found that considering the fracture process significantly enhanced prediction of the bonded adhesive behaviour [3.6, 3.7]. In order to characterize the crack growth behaviour, fracture parameters such as the stress intensity factor (K) and the strain energy release rate (G) can be used [3.7]. In this chapter the concepts of fracture and fatigue mechanics will be discussed and how these concepts can be applied to bonded joints.

3.2 Griffith Theory

3.2.1 Stress concentrations

In a classic paper by Inglis [3.8], a solution is presented for the stresses occurring around an elliptical hole in a plate subjected to uniaxial tension, as illustrated in Figure (3.1). The greatest concentration of stress occurs at point p, and is defined by:

$$\sigma_y = \sigma\left[1 + 2\sqrt{\frac{a}{\rho}}\right] \qquad\qquad (3.1)$$

where σ_y is the vertical stress at p, σ is the stress far from the hole, a is half the major axis of the hole, and ρ is the radius at the tip. Inspection of Equation (3.1) shows that the magnitude of the stress at the tip of the hole increases both with the size of the hole and with the sharpness of the tip. The relevance of this solution for strength of materials problems is that even small cracks or other discontinuities in a material can have tremendous impact on local stresses. Indeed, a small crack with a sub-micron tip radius can amplify stresses several hundred times, causing a structural member to fail by fracture under relatively low average stress.
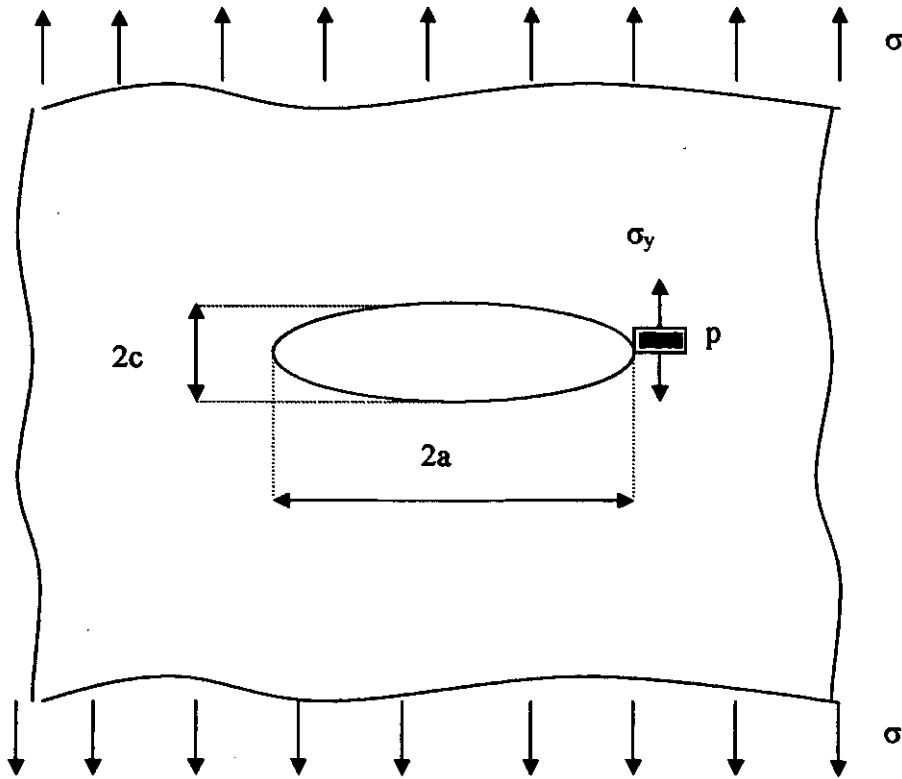
Fig. 3.1 Illustration of elliptical hole in Inglis solution.

3.2.2 Conditions for crack growth

While the stress concentrations provided by cracks present a mechanism for fracture at low stresses, it dose not provide a quantitative criterion for crack growth. Griffth's approach [3.9] was to consider the thermodynamic equilibrium of a crack system. If an elastic body is deformed by an external load, elastic strain energy is stored in the body and there is a change in the potential energy of the system (equal to the negative work of the load). The presence of a crack is accounted for in the energy balance by the surface energy of the crack surfaces. The total energy of the system, Π, may be written as the sum of these components:

$$\Pi = U + Up + W$$

$$= U - F_L + W \qquad (3.2)$$

where U is the strain energy, Up is the potential energy of the load system, F_L is the external work of the load, and W is the surface energy associated with crack formation. According to Griffith, if the crack is to grow, the total energy must be either reduced or unchanged. This may be written in term of system equilibrium:

$$\frac{d\Pi}{dA} = \frac{d}{dA}(U - F_L + W) = 0 \qquad (3.3)$$

or

$$\frac{d}{dA}(F_L - U) = \frac{dW}{dA} \qquad (3.4)$$

where *dA* is the incremental change in crack area. Equation (3.4) represents the Griffith criterion for crack growth, which may be illustrated by a consideration of the cracked body shown in Figure (3.1).

In this case, the crack may be represented by an ellipse with a minor axis that approaches zero (dimension c in Figure 3.1). Then Inglis's solution can be applied to evaluate the strain energy:

$$U = \frac{\pi \sigma^2 a^2 b}{E} \qquad (3.5)$$

where b is the thickness of the plate and E is the material's modulus of elasticity. For an elastic body with a crack that grows under a state of constant stress, the external work of the load can be shown to be twice the internal strain energy.

$$F_L = 2U \qquad (3.6)$$

The surface energy of the crack can be written in terms of the surface energy of material, γ:

$$W = 4ab\gamma \qquad (3.7)$$

where the 4ab term is based on two surfaces of length 2a. The terms of Equation (3.2) can be plotted as shown in Figure 3.2. The plots shows that the total system energy is in equilibrium at a crack length of a=a_0, where the slope of Π is zero. However, this is an unstable equilibrium. If the system is perturbed such that a > a_0 the system will seek a lower energy state, and because Π drops indefinitely, the crack will grow without limits.
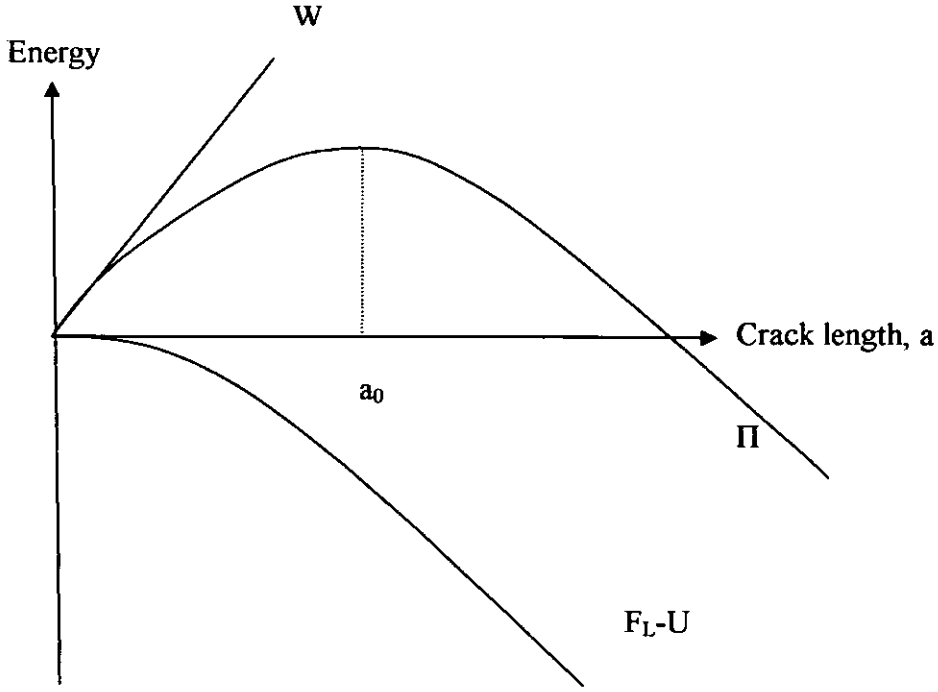
Fig. 3.2 Energetic of crack growth.

The equilibrium state can be determined by substituting Equations (3.5) and (3.7) into (3.4), noting that $dA = b\ da$ for constant thickness b:

$$\frac{2\pi\sigma^2 ab}{E} = 4b\gamma \qquad (3.8)$$

Solving for stress yields:

$$\sigma_f = \sqrt{\frac{2E\gamma}{\pi a}} \qquad (3.9)$$

where σ_f denotes the fracture stress or fracture strength of the material. This equation clearly indicates the relationship between maximum stress and crack length. The fracture

strength decreases with one over the square root of crack size. This equation can alternatively be used to determine the allowable crack size for a given stress.

3.3 Linear Elastic Fracture Mechanics (LEFM)

The failures of load bearing materials and structures tend to fall into two categories, those of yield-dominant failure and those of crack-dominant failure. Fracture mechanics is associated with crack-dominant failure. In this case, failure is concerned with the initiation and propagation of flaws, or cracks, until a critical crack length is reached when the load cannot be sustained, and the material fails. The advent of unstable, catastrophic fracture in welded structures, such as ships lead to research into the concept of brittle fracture. This resulted in the evolution of the theory of linear elastic fracture mechanics (LEFM). The development of LEFM has led to a greater understanding of the fracture mechanisms of materials, and to the establishment of tests to evaluate the fracture resistance of materials. Two main approaches have been developed in the study of the fracture of materials, and are described below as the energy-balance approach and stress-field approach.

3.3.1 Strain energy release rate

Referring to the energy balance and equilibrium Equations (3.2) and (3.4) respectively, the left- hand side of Equation (3.4) is commonly referred to as the strain energy release rate G, while the right-hand side of Equation (3.4) is commonly referred to as the crack resistance R. Equation (3.4) can then be written as:

$$G = \frac{d}{dA}(F_L - U) \qquad (3.10)$$

and

$$R = \frac{dW}{dA} \qquad\qquad (3.11)$$

Thus, the critical condition for crack growth of Equation (3.4) may be rewritten as:

$$G = R \qquad\qquad (3.12)$$

G and R have units of energy per unit area. Therefore, G is often interpreted as the energy available to grow a crack of unit area, while R is interpreted as the energy required for propagation of a crack of unit area. Frequently, the crack growth condition is written in terms of a critical strain energy release rate G_c. The condition for crack growth in this case is:

$$G = G_c \qquad\qquad (3.13)$$

G can be calculated for an elastic body subjected to a load that may be classified as either a load or a displacement control loading condition. Figure 3.3 illustrates these two conditions and their respective load-displacement curves for a crack of length a, that has grown an amount *da* in a specimen of thickness *b*. In load control, a known load is applied to the structure, and the corresponding displacement is measured. Conversely, in displacement control, the structure is forced to undergo a prescribed displacement, and the corresponding load is measured.

a)   Load constant   b) Displacement constant
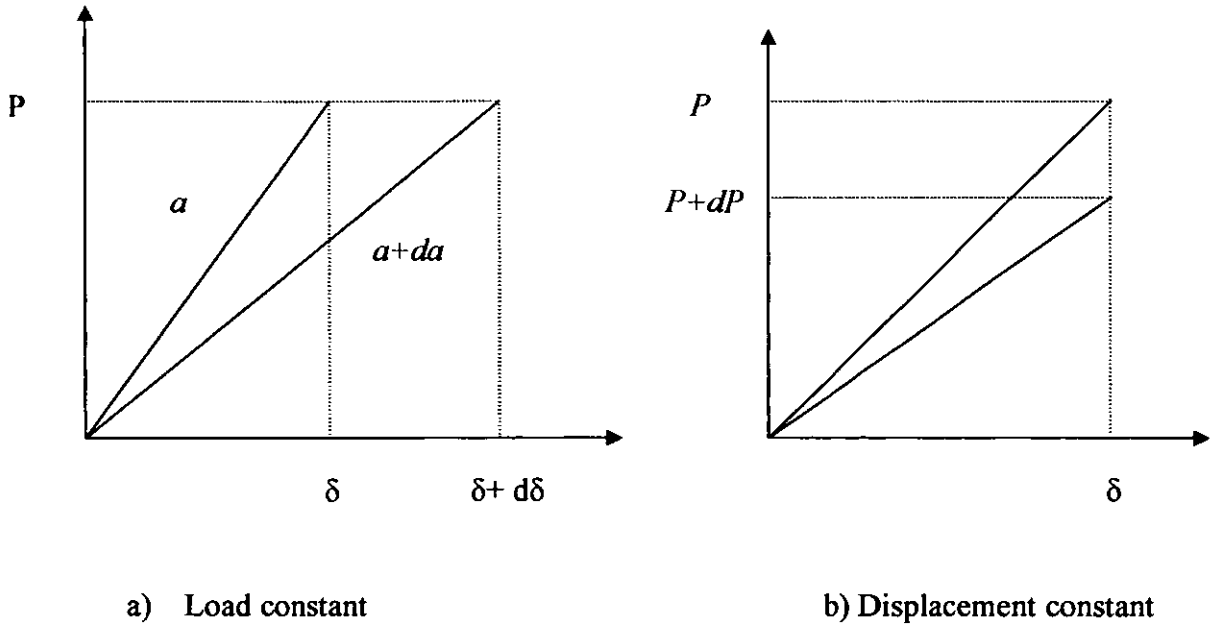
Fig. 3.3 Crack growth under load control and displacement control.

In the case of constant load (Figure 3.3a), the strain energy in the body at crack length a may be given by:

$$U_1 = \frac{1}{2}P\delta \qquad\qquad (3.14)$$

For the same body with crack length $a+da$, the strain energy becomes:

$$U_2 = \frac{1}{2}P(\delta + d\delta) \qquad\qquad (3.15)$$

So the incremental change in strain energy during this time is:

$$dU = U2 - U1 = \frac{1}{2}P(\delta + d\delta) - \frac{1}{2}Pd\delta \qquad\qquad (3.16)$$

The incremental work, dF_L, done by the load during this crack growth is simply Pdδ. Substituting this result and those of Equation (3.16) into Equation (3.10) yields:

$$G = \frac{1}{b}\left[\frac{dF_L}{da} - \frac{dU}{da}\right] = \frac{1}{b}\left[P\frac{d\delta}{da} - \frac{1}{2}P\frac{d\delta}{da}\right] = \frac{1}{2b}P\frac{d\delta}{da} \qquad (3.17)$$

A similar analysis for a constant displacement yields:

$$G = -\frac{1}{2b}\delta\frac{dP}{da} \qquad (3.18)$$

It may appear that the value of G is dependent on whether the loading condition is displacement or load controlled, by virtue of the different signs in the two results. However, it can be shown that the results are in fact identical by writing Equations (3.17) and (3.18) in terms of the change in specimen compliance that accompanies crack growth. Specifically, if the compliance C is defined as the reciprocal of the slope of the load-displacement curve, i.e. $C = \delta/P$, then G becomes:

$$G = \frac{P^2}{2b}\frac{dC}{da} \qquad (3.19)$$

which is valid for both load control and displacement control.

Ripling et al [3.10] were the first to apply fracture mechanics to adhesive joints. From LEFM the value of the adhesive fracture energy, G_c, may be calculated from a test conducted at a constant rate of displacement using the relationship:

$$G_c = \frac{P_c^2}{2b}\frac{dC}{da}$$

(3.20)

where P_c is the load at the onset of crack propagation, C is the compliance of the specimen, a is the crack length and b is the width of the specimen.

3.3.2 Stress-field approach

For certain cracked configurations subjected to external forces, it is possible to derive closed-form expressions for the stresses in the body, assuming isotropic linear elastic material behaviour. Westergaard [3.11], Irwin [3.12], Sneddon [3.13] and Williams [3.14] were among the first to publish such solutions. If we define a polar coordinate axis with the origin at the crack tip as shown in Figure (3.4), it can be shown that the stress field in any linear elastic cracked body is given by:

$$\sigma_{ij} = \left[\frac{K}{\sqrt{r}}\right] f_{ij}(\theta) + \sum_{m=0}^{\infty} A_m r^{\frac{m}{2}} g_{ij}^m(\theta)$$

(3.21)

44
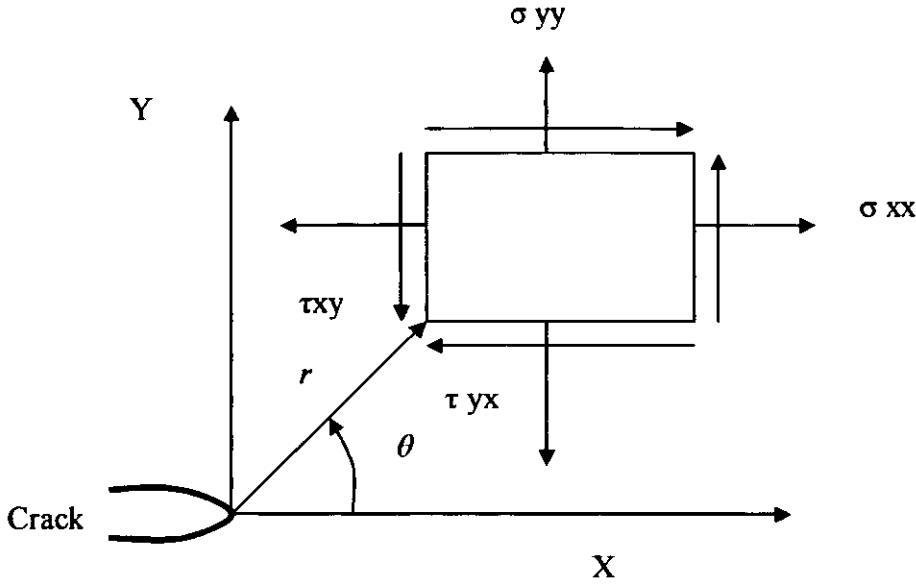
Fig. 3.4 Definition of the coordinate axis ahead of a crack tip.

where σ_{ij} is the stress tensor, r and θ are as defined in Figure (3.4), K is the stress intensity factor, and $f_{ij}(\theta)$, $g_{ij}(\theta)$ are angular functions. The higher order terms in equation (3.21) depend on geometry, but the solution for any given configuration contains a leading term that is proportional to $1/\sqrt{r}$. As $r \rightarrow o$, the leading term approaches infinity, but the other terms remain finite or approach zero. Thus stress near the crack tip varies with $1/\sqrt{r}$, regardless of the configuration of the cracked body. It can also be shown that displacement near the crack tip varies with $\sqrt{r}$.

The stress fields and displacement modes at the crack tip can be classified into three types as shown in Figure (3.5) [3.12]:

a) The opening mode (Mode I) is characterized by displacement of the two crack surfaces moving directly apart from each other. In this case, the applied load and

displacement are perpendicular to the crack surfaces. The stress intensity factor corresponding to this mode is denoted by K_I.

b) The shear or sliding mode (Mode II) occurs when the two crack surfaces are displaced by sliding over each other. The direction of the applied load and displacement, u, is parallel to the crack surfaces.

c) The tearing mode (Mode III) occurs when the crack surfaces slide over each other in a direction parallel to the leading edge of the crack.

The tensile opening mode, or Mode I, type of failure represents the most frequent type of separation that engineers design against and must be prevented. Failure of structure parts by Mode II or Mode III, where fracture is induced by shear stresses, is also possible. Throughout this project, attention will be given to the opening mode, Mode I, However, in bonded joints, fracture may be restricted to the plane of the bond line and may have both mode I and mode II components.

Mode I   Mode II   Mode III
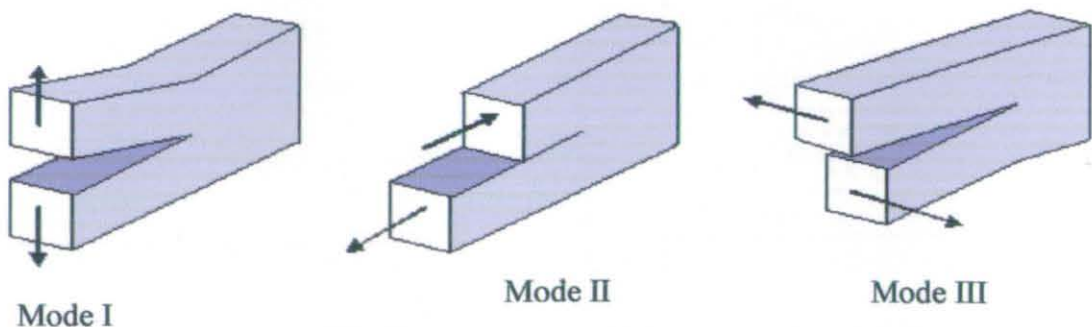
Fig. 3.5 The three modes of crack loading.

The stress intensity factor is usually given a subscript to denote the mode of loading; i.e.,

K_I, K_{II}, K_{III}. Thus the stress fields ahead of a crack tip in an isotropic linear elastic

material can be written as:

$$\underset{r \to 0}{Lim}\, \sigma_{ij}^{(I)} = \frac{K_I}{\sqrt{2\pi r}} f_{ij}^{(I)}(\theta) \qquad (3.22)$$

$$\underset{r \to 0}{Lim}\, \sigma_{ij}^{(II)} = \frac{K_{II}}{\sqrt{2\pi r}} f_{ij}^{(II)}(\theta) \qquad (3.23)$$

$$\underset{r \to 0}{Lim}\, \sigma_{ij}^{(III)} = \frac{K_{III}}{\sqrt{2\pi r}} f_{ij}^{(III)}(\theta) \qquad (3.24)$$

for modes I, II, and III, respectively. In a mixed-mode problem, the individual

contributions to a given stress component are additive:

$$\sigma_{ij} = \sigma_{ij}^{(I)} + \sigma_{ij}^{(II)} + \sigma_{ij}^{(III)} \qquad (3.25)$$

Equation (3.25) stems from the principle of linear superposition.

3.3.3 Reconciliation of *K* and *G*

As is demonstrated in the preceding sections, both K and G can be used to predict the

fracture strength of a particular structure, even though the development of these two

fracture parameters was quite different. The strain energy release rate was developed using

global energy balance, while the stress intensity factor was developed evaluating the stress field at the tip of a crack. If there are they are accurate predictors, there should be some way to reconcile the two parameters.

A simple way to reconcile K and G is to look at their values for a common geometry. For a centre-cracked plate of unit thickness [3.12]:

$$K_I = \sigma\sqrt{\pi a} \quad \text{and} \quad G_I = \frac{\pi\sigma^2 a}{E} \qquad (3.26)$$

If both equations are solved for σ, and set equal to each other, then for the plane stress case:

$$K_i = \sqrt{EG_i} \qquad (3.27)$$

where i= I, II or III.

For a plane-strain condition:

$$K_i = \sqrt{\frac{EG_i}{(1-\nu^2)}} \qquad (3.28)$$

where v is the Poisson's ratio and E is the modulus of elasticity.

The advantages and disadvantages of each parameter in practical applications are apparent. The disadvantage of G is its global nature. A relationship between work of load and strain and strain energy must be known for an impending crack growth. The advantage of this approach, however, is that it is not as sensitive to the precise crack tip geometry. In the

case of the stress intensity factor K, a well defined crack tip geometry is necessary for proper evaluation of the crack tip stress field. However, it is not necessary to evaluate the influence of the individual crack growth on the entire structure. It may be argued that G is a more fundamental quantity in that it is derived directly from first principles, and its units have direct physical meaning: the energy required to create new crack surfaces. K on the other hand is an integration constant whose units do not have a direct physical meaning.

3.4 Fatigue behaviour of adhesive joints

In the previous sections, some basic fracture mechanics concepts were introduced. These concepts are applicable to both static and fatigue test conditions. However, there are additional concepts which are essential in order to understand the fatigue behaviour of adhesives. A brief introduction to these concepts is presented in this section. After this, the effects of fatigue test conditions such as frequency and temperature are reviewed.

3.4.1 Basic concepts

Materials subjected to cyclic loading have often been found to fail at low stresses, well below the tensile strength measured under monotonic loading at a constant displacement rate. This is due to the phenomenon of fatigue. In nearly all engineering applications, fatigue loading is encountered and damage due to this accounts for over 90% of structural and mechanical failures [3.15]. Much work has been undertaken in characterising fatigue failure, focusing on both the initiation of fatigue cracks and their propagation. Two common approaches for characterising the fatigue behaviour of polymers, based on well established methodologies for metals are the use of (i) S-N curves (i.e. plots of stress amplitude verses the number of cycles to failure) and (ii) fatigue crack propagation (FCP) analysis. With both approaches a threshold is often established. For S-N curves, a stress

amplitude may be found below which the material will not undergo fatigue failure, and with FCP curves a threshold fracture parameter can be obtained, below which a crack will not propagate.

A number of parameters can affect the fatigue performance of a given material. These include:

a) Specimen geometry.

b) Environment.

c) Characteristic wave form.

d) Frequency.

f) Stress ratio, $\sigma_{min} / \sigma_{max}$.

g) Strain ratio, $\varepsilon_{min} / \varepsilon_{max}$.

h) Mean stress level.

i) Mean strain level

j) Stress range.

When a material is in service, the fluctuating load exerted on it might not be regular in form. However, in numerous studies the cyclic loading is often assumed to be sinusoidal in nature.

3.4.2 The S-N curve

Characterisation of fatigue performance is usually carried out by applying a constant amplitude cyclic load until failure. This load is usually expressed as the stress amplitude, σ_a, where:

$$\sigma_a = \frac{\sigma_{max} - \sigma_{min}}{2} \qquad (3.29)$$
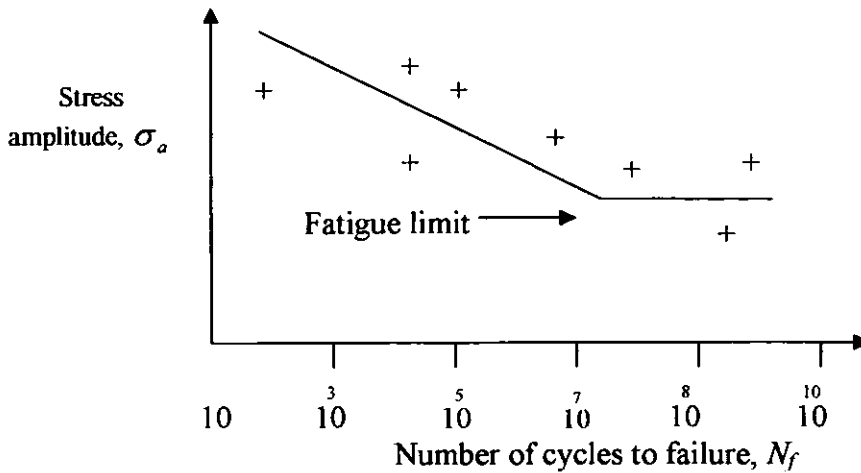
Figure 3.6 A schematic of a typical S-N curve

The stress amplitude is then plotted against the number of cycles of failure, N_f. A wide range of different amplitudes are then chosen to give points on the S-N curve as shown in Figure (3.6). A fatigue limit (or endurance limit) may exist, below which a defect free specimen will not undergo fatigue failure. It is usual to assume a threshold at typically $10^7 - 10^8$ cycles depending on the particular system.

It is possible to divide the whole fatigue process into three consecutive and partly overlapping stages:

1) Fatigue hardening and/or softening, depending mainly on the original state of the material and the stress or strain amplitude. This stage is characterized by the changes of substructure within the whole volume of the loaded structure.

2) Microcrack nucleation, taking place in a small part of the total volume, namely the surface layer. A common denominator of all types of nucleation is the stress concentration in the surface layer.

3) Crack propagation ending in final failure. The controlling factor of crack propagation is the highly concentrated cyclic plastic deformation within the plastic zone at the crack tip.

The sequence of events which occur during cycling is shown schematically in Figure (3.7). The fatigue life curve (S/N curve) represents the end of crack propagation and, simultaneously, the end of the whole fatigue process. The other two curves mark the end of nucleation and of hardening/softening respectively. It is necessary to stress that there is no well defined border between the stages. For example, it is still more or less a matter of convention to choose a minimum crack length to separate nucleation and propagation. The numbers of cycles corresponding to the respective stages depend very strongly on the material, geometry of the loaded body and of the external forces, loading conditions, environment, etc.
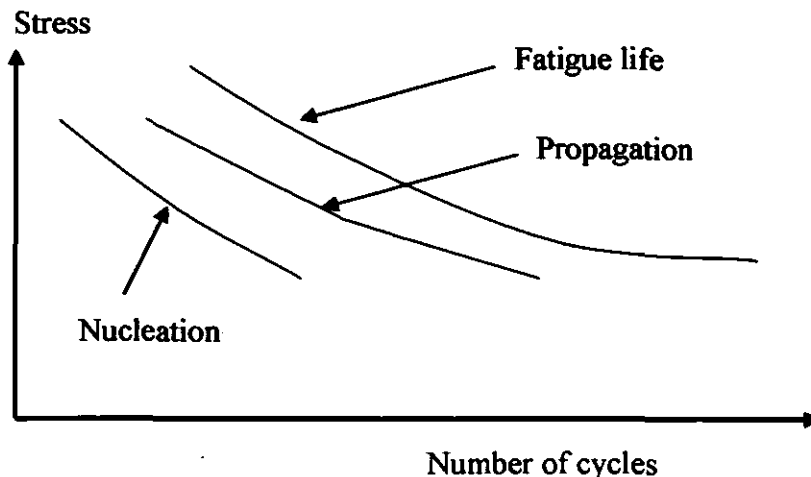
Fig. (3.7) Stages of fatigue process.

3.4.3 Fatigue crack propagation

The fatigue behaviour of a material can be characterised in terms of resistance to crack propagation using fracture mechanics parameters, such as the stress intensity factor, K, or the fracture energy G. This approach is based on measurement of the incremental crack growth, from a sharp crack, through a material. The number of cycles is measured for each increment of growth, hence a rate of crack growth per cycle, *da/dN*, can be obtained which is plotted against the applied stress intensity factor range, *ΔK*, or the applied strain energy release rate range, ΔG. This range may be described as:

$$\Delta K = K_{max} - K_{min} \qquad (3.30)$$

$$\Delta G = G_{max} - G_{min} \qquad (3.31)$$

Three distinct regions may be identified from a typical FCP curve as shown in Figure (3.7).
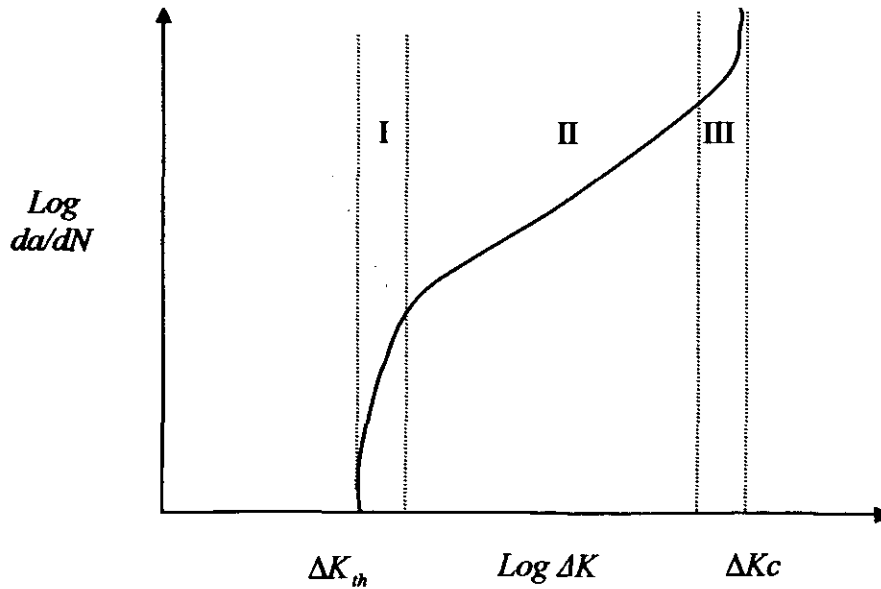
Figure (3.7) Schematic FCP curve.

Region I of the FCP curve is associated with a fatigue threshold ΔK_{th}, below which measurable crack growth does not occur. ΔK_{th} is an important parameter when designing with materials in which fatigue crack growth is to be avoided.

Region II of the FCP curve is essentially linear and in many cases the Paris relationship, given in Equation (3.32), fits the data well.

Region III of the FCP curve signifies unstable crack growth as ΔK approaches the critical stress intensity factor ΔK_c.

There have been a number of equations proposed to relate the crack growth rate, da/dN, to the applied stress intensity factor, ΔK. The most successful has been the Paris law [3.16], which describes the linear region of the logarithmic crack growth curve (Region II):

$$\frac{da}{dN} = D(\Delta K)^n \qquad (3.32)$$

where D and n are experimentally derived constants.

Ewalds [3.17] proposed an equation to describe the complete logarithmic da/dN versus logarithmic ΔK, shown in Figure (3.7), namely:

$$\frac{da}{dN} = D(\Delta K)^n \left\{ \frac{1 - \left(\dfrac{\Delta K_{th}}{\Delta K} \right)^{n1}}{1 - \left(\dfrac{K_{max}}{K_c} \right)^{n2}} \right\}^{n3} \qquad (3.33)$$

where D, n, n_1, n_2 and n_3 are empirically derived constants.

The maximum applied strain energy release rate, G_{max}, is given by the relationship:

$$G_{max} = \frac{P_{max}^2}{2b} \frac{dC}{da}$$

(3.34)

where P_{max} is the maximum load applied during the fatigue cycle. G_{max} has been used as a parameter in describing the relationship between the strain energy release rate and the fatigue crack growth rate. This was suggested by Martin and Murri [3.18], where it was reasoned that because of facial interference effects, such as surface debris and fibre bridging. This scheme has found favour with a number of workers [3.19, 3.20]

If the fatigue data are plotted in the form of G_{max} versus da/dN, using logarithmic axes for both parameters, then a major portion of the relationship so obtained is often linear and a form of the Paris Equation may describe this region, namely:

$$\frac{da}{dN} = DG_{max}^n$$

(3.35)

where D and n are material constants. Alternatively, the complete relationship between $\text{Log}\,G_{max}$ versus Log da/dN is often of a sigmoidal form, which may be described by:

$$\frac{da}{dN} = DG_{max}^n \left\{ \frac{1 - \left(\dfrac{G_{th}}{G_{max}}\right)^{n1}}{1 - \left(\dfrac{G_{max}}{G_c}\right)^{n2}} \right\}^{n3}$$

(3.36)

where G_{th} is the fatigue threshold, G_c is the adhesive fracture energy and D, n_1, n_2 and n_3, are material constants.

3.4.4 Effect of experimental parameters

Fatigue crack propagation is affected by experimental parameters such as the frequency, and temperature. In this section, the effects of these parameters are briefly reviewed.

3.4.4.1 Effect of frequency

The increasing use of adhesives has created a need to evaluate their performance under many different loading and environmental conditions. Many adhesive joints are subject to cyclic loads during service, such as bonded bridge strengthening plates and aircraft fuselages [3.21]. There has been considerable research into various aspects of the fatigue behaviour of adhesive joints [3.22-3.32]. The time span of each fatigue load cycle can vary significantly from one structure to another. It could be, for instance, several seconds in the case of bridge plates to tens of hours in the case of aircraft fuselages and in many applications variable fatigue frequencies are encountered in service. The time taken to generate fatigue data means that most fatigue testing of bonded joints has been undertaken at relatively high frequencies, typically 5-10 Hz. However, the visco-elastic nature of polymeric adhesives means that rate and frequency dependence might be expected and that this would increase at elevated temperatures or when the adhesive has absorbed moisture. There is, therefore a requirement to understand the effect of frequency on the fatigue life of bonded joints and how parameters such as joint geometry, environment and materials affect this behaviour. Ideally, a general method of predicting fatigue life at any given frequency (or combination of frequencies and hold times) should be developed. This is the aim of the current work.

The effect of frequency on fatigue crack propagation (FCP) in metals has been extensively investigated. For instance, James [3.33-3.34] demonstrated the influence of frequency and waveform on fatigue crack growth in a stainless steel. This work showed that the fatigue crack propagation rate (FCPR) increased with decreasing frequency. It should be noted here that FCPR is defined as the crack growth per fatigue cycle, i.e. da/dN where a is crack growth and N is number of cycles. A similar study demonstrated that the FCPR increased with hold time in a trapezoidal loading waveform for a Cr-Mo-V steel [3.35]. Plumtree [3.36] also showed that for a 304 stainless steel the time dependent damage accumulates more rapidly during the loading portion of the cycle than during the hold time. Pre-notched samples of a number of polymers have also been tested in fatigue over a range of frequencies [3.37-3.40]. The FCPR for several of these polymers, such as polymethyl methacrylate, polystyrene, polyviny chloride and a polyphenylene oxide, decreased with increasing frequency. Other polymers such as polycarbonate, polysulfone, nylon, and a polyvinylidene fluoride showed no apparent sensitivity to test frequency [3.37-3.40].

The effect of frequency on the performance of adhesively bonded joints has also been considered previously. Marceau [3.41] studied fatigue crack growth rates in both lap-shear and double cantilever beam (DCB) joints at a range of frequencies and found that low frequency fatigue was more damaging to adhesive joints than high frequency fatigue. Althof [3.42] studied the build up of shear strain in adhesive joints during fatigue loading at a range of frequencies and suggested that fatigue failure is creep controlled at low frequencies. Mostovoy and Ripling [3.43] used bonded tapered double cantilever beam (TDCB) specimens to study the effect of frequency on the FCPR in different adhesive systems. For a standard amine-cured epoxy, there was no discernible effect of frequency between 0.01 and 0.25 Hz, however, at 3 Hz the FCPR decreased significantly. A standard nitrile-phenolic film adhesive exhibited no significant effect of frequency in the range

0.01-3 Hz. With a modified epoxy adhesive, no effect of frequency was observed on increasing the frequency from 0.25-3 Hz, however, at 5 Hz the FCPR decreased. Luckyram and Vardy [3.44] studied the fatigue performance of two structural adhesives and found no effect of frequency on FCPR between 0.5-5 Hz. Likewise, Osiyemi [3.45] found no effect of frequency on the FCPR in composite DCB joints bonded with a 120°C cure epoxy film adhesive in the frequency range 1-5 Hz. Xu et al. [3.46] studied the effect of frequency on FCP using steel DCB joints bonded with two structural epoxy adhesives. Adhesive A was filled with a mixture of magnesium silicate and chalk and tested at frequencies of 2 and 20 Hz. Adhesive B was rubber- toughened and was tested at frequencies of 0.02, 0.2, 2 and 20 Hz. They found that the FCPR for adhesive (A) was relatively independent of frequency whilst the FCPR in joints bonded with adhesive (B) decreased with increasing frequency. Pirondi et al. [3.47] studied the effect of R-ratio and frequency on DCB joints bonded with an elastomer-methacrylate adhesive. They found the influence of frequency is much lower than the influence of R-ratio. It can be seen, therefore, that the sensitivity of FCPR in adhesives is material dependent but that there is a tendency in many systems for the FCPR to increase as frequency decreases. This is a concern as most fatigue data is generated at relatively high frequencies and this will tend to lead to non-conservative predictions of fatigue life if applied to joints subjected to lower frequencies.

In this work the effect of frequency on FCPR and the fatigue threshold for adhesively bonded DCB joints with carbon fibre reinforced polymer (CFRP) and mild steel substrates will be investigated. This work will be presented in section (9.4.1)

3.4.4.2 Effect of temperature

Environmental effects is one of the most important topics in the design of adhesively bonded structures. Joints are more prone to fail under static or cyclic loads in hostile environmental conditions. These types of loading and condition cause deterioration to the adhesive and interface. The temperature effect is one of the most typical environmental factors that have to be taken into account. Parker [3.48-3.49] has investigated the effect of test temperature on bonded joints with 120°C and 175°C curing CFRP. Results showed that the test temperature had a significant effect on the strength of the joints from 50°C to 90°C, and a huge effect on the strength of the joints as the temperature increased from 90°C to 120°C. Marceau et al. [3.50] studied the effect of temperature on an unspecified adhesive for bonding aluminium to aluminium. They reported an increase in the fatigue crack propagation rate (FCPR) at constant ΔG on increasing from 24 to 60°C. A corresponding decrease in fatigue life was also noted in S-N tests. In a study by Chen et al. [3.51] on the fatigue behaviour of adhesively bonded joints under static and dynamic loading, they found an increase in test temperature to greatly reduce the fatigue life. The effect of temperature on the strength of aluminium lap joints bonded with epoxy adhesive has been reported by Brewis et al. [3.52-3.53]. They found that the joint strength significantly decreases as the test temperature increases. At high temperature, the joints become weaker and the mode of failure becomes cohesive. Girifalco and Good [3.54] have shown that the strength of the joint interface decreases with increasing temperature. Although they show results for polymer to polymer interfaces, it is likely that adhesive substrate interface would have the same trend of results. Adams et al. [3.55] studied the effect of temperature on the strength of epoxy/steel lap joints tested from -60° C to 200° C. They found that joints were stronger in the region 0-70° C. At low temperature the adhesive became brittle, leading to lower strength and increased scatter. At higher

temperature the adhesive softened and failed by plastic yielding. Ashcroft et al. [3.56] tested CFRP/epoxy single-lap joints both quasi-statically and in fatigue over a range of temperatures. They found that with CFRP substrates the joints were strongest at room temperature and weakest at -40° C, a significant decrease in strength also being observed at 90°C. Ashcroft et al. [3.57] tested CFRP DCB joints bonded with an epoxy adhesive in the temperature range -50°C to 90°C. They found that the critical strain energy release rate increased with temperature and the failure locus transferred from predominantly in the composite substrate to predominantly in the adhesive. Harris and Fay [3.58] tested steel single lap joints, bonded with modified epoxy and polybutadiene adhesives, quasi-statically and in fatigue over the temperature range -30 to 90°C. They found that the quasi-static strength reduced quickly as T_g was approached.

Ashcroft et al. [3.59] study the fatigue behaviour of CFRP/epoxy lap-strap joints. They showed that, the fatigue resistance of the lap-strap joints did not vary significantly until the glass transition temperature, T_g, was approached, at which point a considerable reduction in the fatigue threshold load was observed. They showed also that, the locus of failure of the joints was highly temperature dependent, transferring from primarily in the composite adherend at low temperatures to primarily in the adhesive at elevated temperatures.

Compared with FCP studies involving test frequency variations, very little information has been gathered to identify the effect of test temperature on FCP behaviour. As such, it is not yet possible to make fatigue crack growth rate predictions at non ambient temperatures using such methods as the time-temperature equivalency concept [3.60]. Furthermore, the limited amount of available data is not self-consistent since test methods differ among the reporting laboratories and different materials were examined that possessed different viscoelastic and deformation characteristics. For example, Kurobe and Wakashima [3.61-3.62] found that the macroscopic FCPR in PMMA increased with decreasing temperature

over a testing range of 50°C to -10°C. Conversely, Radon and Culver [3.63] and Skibo [3.64] found in PMMA that at 1, 5 and 100 Hz, FCPR's decreased monotonically with decreasing temperature from 50°C to -10°C. FCPR's in polystyrene under fixed loading test conditions also have been shown to decrease with decreasing test temperature. Mai and Williams [3.65] reported a 20-fold decrease in FCPR at 0.15 Hz when the test temperature was reduced from 60 to -60°C.

In this work the effect of frequency and temperature on FCPR and the fatigue threshold for adhesively bonded DCB joints with mild steel substrates will be investigated. This work will be presented in section (9.4.2).

3.5 Nonlinear fracture mechanics

In the previous section, concepts are described that apply primarily to materials that exhibit essentially linear elastic stress-strain relationships right up to rupture. The basic assumption of LEFM is that all available strain energy goes into propagating a crack, or in the view of Griffith, the creation of new material surfaces. In nearly all materials, there are numerous other micro-structural mechanisms that are capable of dissipating strain energy: plastic deformation around the crack tip in metals, micro-cracking and fraction in concrete and rock, fibre bridging in wood and fibrous composite. These and other 'toughening mechanisms' are discussed in more detail below, however, they all affect the measured fracture energy to varying degrees. The degree to which the various toughening mechanisms affect fracture behaviour dictates whether LEFM can be applied to a particular material. Generally, if the effects are small, LEFM can be applied without modification. If the effects are large, then modifications to the theory must be made to account for the nonlinearity caused by the toughening mechanisms.

3.5.1 The fracture process zone

Typically, nonlinearities manifest themselves in size effects. Although fracture toughness is considered a material property, measured fracture toughness will vary with specimen size if nonlinearities are significant. Specifically, large specimens are observed to have lower fracture toughness than smaller specimens of the same material. The reason for this 'size effect' is the presence of a 'fracture process zone'. The fracture process zone is the region around the tip of the crack in which various toughening mechanisms are mobilised. Ahead of the crack tip plastic deformation, micro-cracking, or intersection with voids or interfaces might be observed, while behind the crack tip bridging by fibres, friction between crack faces, or crack branching might be observed. Clearly, the degree of heterogeneity in the material strongly influences the characteristics and extent of this region of energy dissipation. The reason for the observed size effect is that the size of a fracture process zone is essentially invariant and its relative influence tends to decrease as the specimen size increases. Thus, larger specimen exhibit behaviour closer to that predicted by LEFM. In smaller specimens the influence of the fracture process zone is greater, and they are observed to have a relatively high toughness. The limit states of these two extremes are traditional ultimate stress theory for small specimens and LEFM for large specimens, as illustrated in Figure (3.9). Nonlinear fracture theories are aimed at bridging the gap between these two theories of failure [3.66].
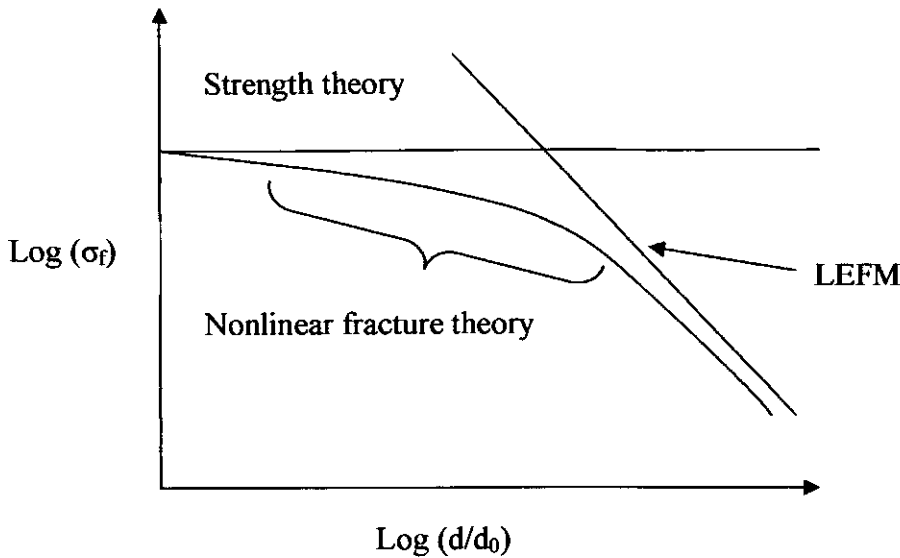
Fig. 3.9 Illustration of transition from strength theory to fracture theory: d/d0 represents the ratio of Specimen size to the process zone size.

3.5.2 *R*-curves

A convenient tool for quantifying the influence of the fracture process zone on various fracture properties is the 'crack growth resistance curve' or *R*-curve. Crack resistance, *R*, has already been defined in Equations (3.10) and (3.11). The R-curve is a plot of R as a function of crack length, and is thus a way to represent crack resistance that is not constant. Rising R-curves are common among materials that exhibit the toughening mechanisms described above. An example of such a curve is shown in Figure (3.10) along with some mechanisms that cause the rising R-curve behaviour. Essentially, rising R-curves reflect the fact that certain toughening mechanisms are not mobilised until the crack grows to a certain size. This is especially true of crack bridging, where bridging fibres require sufficient deformation to produce a closing force. The levelling off of the R-curve at longer crack lengths is an indication that the influence of the toughening mechanisms is not indefinite. At sufficiently large crack sizes, R becomes nominally constant as assumed in

LEFM. Such R-curves reinforce the notion that very large specimens approach a fracture behaviour that follows LEFM.
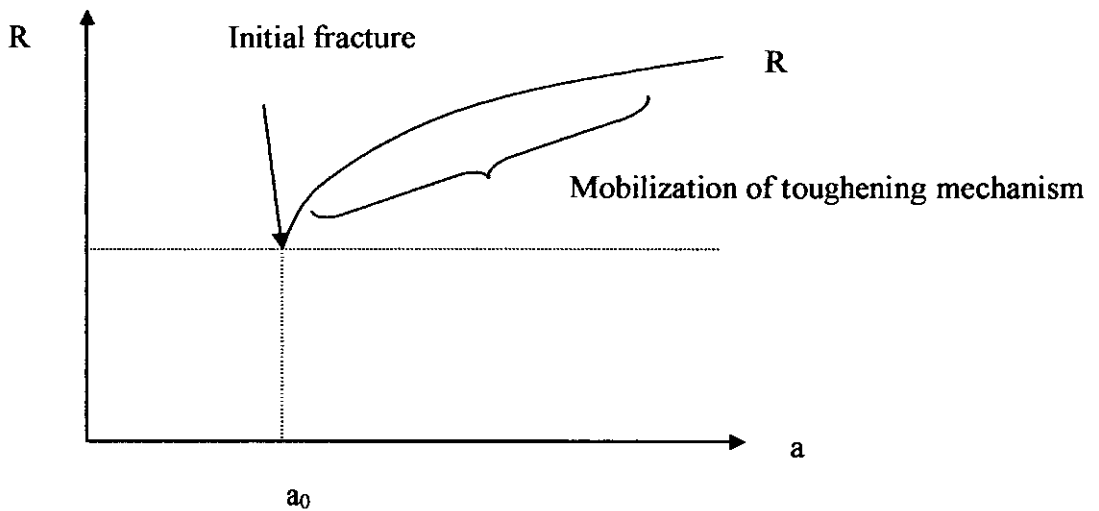
Fig. 3.9 R-curve for material with toughening mechanism.

3.5.3 Fictitious / effective crack models

Linear elastic fracture mechanics assumes a sharp crack tip for which the stress field may be calculated. While the elastic solutions predict infinite stresses at the crack tip, in real materials, yielding and damage prevent this from actually occurring. According to the discussion above, as long as the size of the fracture process zone is small LEFM theory can be applied. A number of different approaches have been used to examine the size of the process zone. These approaches have in turn been used to develop predictive models for non-linear fracture processes.

3.5.3.1 The Irwin Approach

Irwin [3.12] assumed the plastic-zone to be circular with a radius of r_p, as shown in Figure (3.11), where in mode I,

$$r_p = \frac{1}{6\pi}\left(\frac{K_I}{\sigma_Y}\right)^2 , \text{ for plane strain,} \qquad (3.37)$$

and

$$r_p = \frac{1}{2\pi}\left(\frac{K_I}{\sigma_Y}\right)^2 , \text{ for plane stress} \qquad (3.38)$$

The size of plastic zone is smaller under plane strain fracture, since there is a greater constraint at the crack-tip.
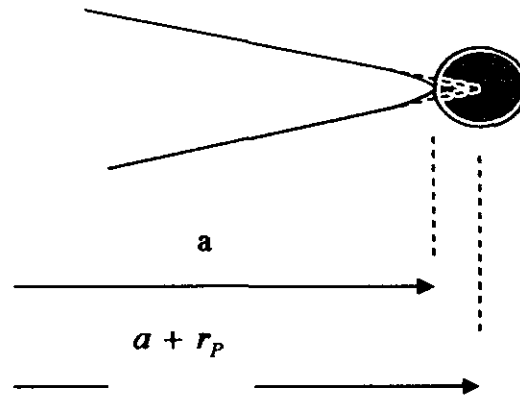
Fig. 3.11 Irwin's model.

3.5.3.2 Dugdale - Barenblatt approach

Dugdale [3.67] and Barenblatt [3.68] separately treated a crack with a plastic zone as a slightly larger fictitious crack with closing stresses applied at the tips. Referring to Figure (3.12), the length of the plastic zone is the difference between the size of the fictitious crack and the real crack, while the closing stress is equal to the yield stress of the material.

This length, r_d, is determined such that the stress intensity factor goes to zero at the tip of the fictitious crack. For this to occur, the two cases (real crack subject to a far field tension stress and fictitious crack subject to closing stresses) are superimposed.

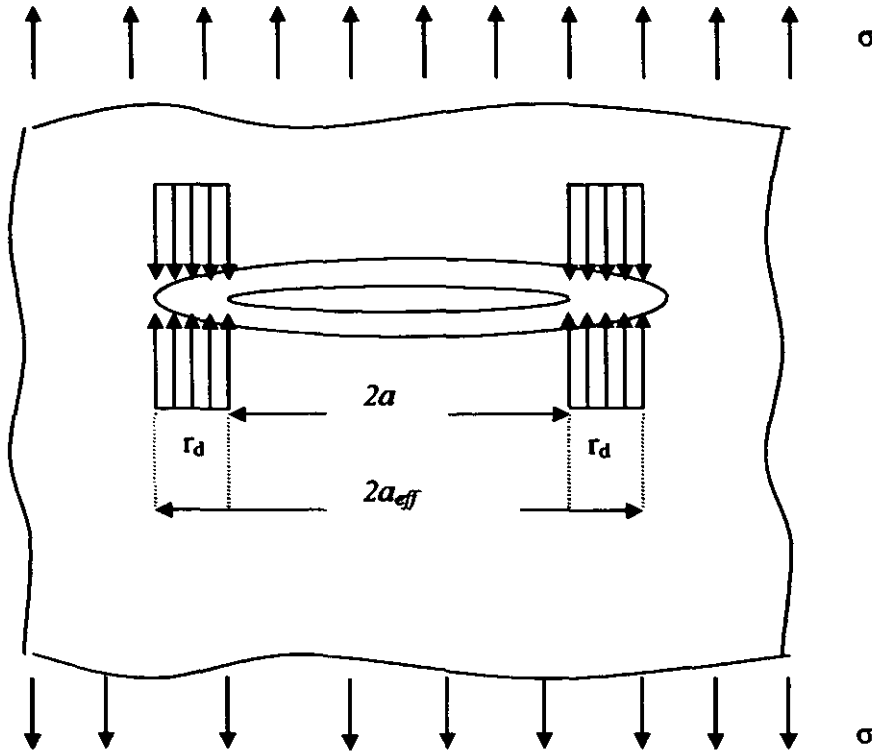Fig. 3.12 Effective crack length for plastic deformation at crack tip.

The stress intensity factor for the fictitious crack subjected to the uniform tension stress is:

$$K_I^{\sigma} = \sigma \sqrt{\pi(a + r_d)} \tag{3.39}$$

While the stress intensity factor due to the closing stress of σ_{YS} can be shown to be:

$$K_I^{P} = 2\sigma_{YS} \sqrt{\frac{a + r_d}{\pi}} Cos^{-1} \frac{a}{a + r_d} \tag{3.40}$$

66

Since the requirement was that the stress intensity factor vanishes, $K_I^\sigma = -K_I^{r_d}$ and the solution for r_d is:

$$r_d = \frac{\pi^2 \sigma^2 a}{8\sigma_Y^2} = \frac{\pi K_I^2}{8\sigma_Y^2}$$
(3.41)

It should be noted that higher order terms are neglected in this solution. The way this result is used is that the plastic zone effectively makes the crack seem slightly longer than it really is. Thus, in fracture calculations an effective crack length is used rather than the actual crack length. This effective length is simply:

$$a_{eff} = a + r_d$$
(3.42)

As long as this zone is small, traditional LEFM assumptions and solutions can be applied using this correction.

3.5.3.3 Crack tip opening displacement

The crack tip in a ductile material has a different character to that in a brittle material. Wells [3.69] observed significant blunting at the tip of existing cracks as shown in Figure (3.13). Furthermore, he found that tougher materials have a larger degree of blunting prior to rupture. He therefore proposed a crack tip opening displacement (CTOD) fracture criterion that better reflects the fracture toughness of these ductile materials. He proposed that a critical crack tip opening displacement (CTOD$_C$) could be considered a material parameter and that fracture would initiate when CTOD= CTOD$_C$ in the specimen.

Conceptually CTOD can be defined as shown in Figure (3.13), however this, is a somewhat ambiguous measurement.

While useful as laboratory tool, the CTOD criterion has not gained wide acceptance due to the difficulty in both defining a unique CTOD for a given crack tip, and measuring it in real structures. Despite its practical shortcomings, CTOD has relevance in a variety of materials and can't be consider as material property.
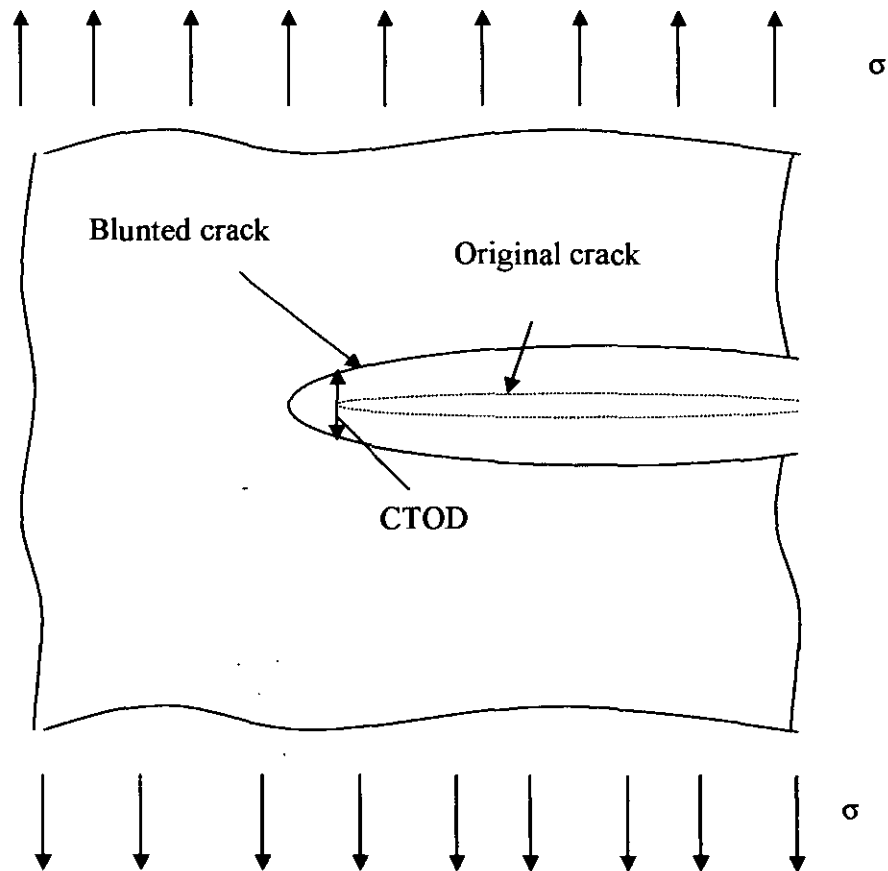

Fig. 3.13 Crack tip opening displacement.

3.5.4 Rice's J-Integral

Fracture under essentially elastic conditions (but where some scale plasticity is allowed) can be described using linear elastic fracture mechanics (LEFM). However, when more ductile materials are considered, analysis of their behaviour cannot be described using LEFM methods. This led to the J-integral concept which is based on an energy balance approach and is concerned with describing fracture under nonlinear elastic conditions. For a linear elastic case, J=G.

In 1968, J.R. Rice [3.70-3.71] published papers in which he discussed the potential of a path-independent integral, J, for characterizing fracture in nonlinear-elastic materials. This integral is identical in form to the elastic component of the energy-momentum tensor for characterizing generalized forces on dislocations and point defects introduced by Eshelby. Cherapnov [3.72] working independently in the former Soviet Union during the same period as Rice, also presented a formulation of an integral similar to Rice's J.

Rice defined the J-integral for a cracked body as follows:

$$J = \int_{\Gamma} \left[\left(W dy - T_i \frac{\partial u_i}{\partial x} ds \right) \right] \qquad (3.43)$$

where W is the strain energy density, T_i are components of the traction vector, u_i are the displacement vector components, and Γ is the counter clockwise contour as shown in Figure (3.14). The strain energy density is defined as:

$$W = \int_{0}^{\varepsilon_{ij}} \sigma_{ij} d\varepsilon_{ij} \qquad (3.44)$$

where σ_{ij} and ε_{ij} are the stress and strain tensors, respectively. The traction is a stress vector normal to the contour. T_i defines the normal stresses acting at the boundaries. The components of the traction vector are given by:

$$T_i = \sigma_{ij} n_j \qquad (3.45)$$

where n_j are the components of the unit vector normal to Γ.

J can be a powerful tool for analysing crack problems and many commercial finite element packages contain routines for calculating J for user-defined contours. The limitation of J is the fact that it is based on an elastic response for the material. While inelastic materials clearly violate this assumption, it can be noted that for monotonic loading an inelastic material will typically exhibit a similar stress-strain response as a nonlinear elastic material. The differences occur when the material is unloaded. Then the inelastic material will have permanent deformation, the non-linear elastic material will not. Thus, J is appropriate for monotonic loading conditions where material unloading is not significant. It should be clear that the size of the process zone relative to the contour is important for an inelastic material. Clearly, there is local unloading as the crack advances due to the creation of stress-free surfaces. Since J cannot handle inelastic unloading, the local unloading around the newly formed crack must be small; otherwise the calculation will not be accurate. If the process zone is large compared to the dimensions of the structure, J is not an appropriate fracture parameter.
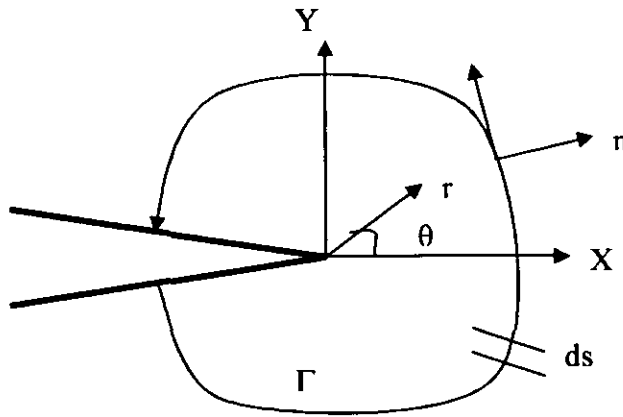
Fig. 3.14 Crack tip coordinate system and arbitrary contour along which J-Integral is evaluated.

3.6 Summary

In this chapter, the basic principles of fatigue and fracture mechanics were reviewed and can be summarised in the following points:

1) The derivation of the strain energy release rate, G, was introduced. In this study G will be used to correlate the crack growth rate (da/dt or da/dN) in adhesively bonded joints.

2) The relationship between the fracture parameters G and K was investigated. The stress intensity factor K, is dependent on a proper evaluation of the crack tip stress field whilst G is not so sensitive to the precise crack tip geometry. It may also be argued that G is a more fundamental quantity and its units have direct physical meaning: the energy required to create the new crack surface.

3) The effect of experimental parameters, such as frequency and temperature were reviewed. This review discuses the influence of frequency and temperature in adhesively bonded joints. This will help in understanding and analysing the experimental work in this study.

4) The concept of nonlinear fracture mechanics and the limitation of LEFM were introduced. This will be discussed further in the next chapter.

3.8 References

[3.1] Sancaktar, E. and Tang, J., "Mixed mode Fracture in Adhesively Bonded Joints under Dynamic Loading", In Proceeding of Adhesion, Plastic and Rubber Institute, 1987, pp.19.1-18.7.

[3.2] Goland, M. and Reissner, E., "The stresses in Cemented Joints", Journal of Applied Mechanics, Vol. 11, 1944, pp.A17-A27.

[3.3] Sancaktar, E. and Lawry, P., "A Photoelastic Study of the Stress Distribution in Adhesively Bonded Joints with Prebent Adherend", Journal of Adhesives, Vol. 11, 1980, pp.233-241.

[3.4] Hart-Smith, L. and Bunin, B., "Selection of Taper Angles for Doubles", Splices and Thickness in Fibrous Composite Structures, Douglas Paper 7299, McDonnell Douglas Corporation, 1983.

[3.5] Adams, R., Atkins, R., Harris and Kinloch, A., "Stress Analysis and Failure Properties of Carbon-Fibre Reinforced-Plastic/Steel Double Lap Joints", Journal of adhesions, Vol. 20, 1986, pp.29-53.

[3.6] Sancaktar, E., "Non-Destructive Examination of Adhesive Bonds with Neutron Radiography", International journal of adhesives, Vol. 1, 1981, pp.329-330.

[3.7] Broek, D., "The Practical use of Fracture Mechanics", Kluwer Academic Publishers, ISBN: 9024737079, 1989.

[3.8]   Inglish, C.E., "Stresses in a Plate due to the Presence of Cracks and Sharp Corners", Transactions of in the Institute of Naval Architects, Vol. 55, 1913, pp.219-241.

[3.9]   Griffith, A.A., "The Phenomena of Rupture and Flow in Solids", Philosophical Transactions of the Royal Society of London, Vol. 221, 1921, pp.163-197.

[3.10] Ripling, E.J., and Mostovoy, S., "Application of Fracture Mechanics" Vol. 6, 1939, pp.49-53.

[3.11] Westergaard, H.M., "Bearing Pressures and Cracks" Journal of Applied Mechanics, Vol. 6, 1939, pp.49-53.

[3.12] Irwin, G.R., "Analysis of Stresses and Strains near the End of a Crack Traversing a Plate" Journal of Applied Mechanics, Vol. 24, 1957, pp.361-364.

[3.13] Sneddon, I.N., "The Distribution of Stress in the Neighbourhood of a Crack in an Elastic Solid" Proceedings, Royal Society of London, Vol. A-187, 1946, pp.229-260.

[3.14] Williams, M.L, "On the Stress Distribution at the Base of a Stationary Crack" Journal of Applied Mechanics, Vol. 24, 1957, pp. 109-114.

[3.15] Anderson, J.C., Leaver, K.D., Rawlings, R.D., and Alexander, J. M., "Materials Science", Chapman and Hall, ISBN: 0470028300, 1990.

[3.16] Paris P., and Erdogan, F., "A critical analysis of crack propagation laws", Trans. ASME, ser. D., Vol. 85, No. 4, 1963, pp.528-534.

[3.17] Ewalds, H.L, "Fracture Mechanics", Edward Arnold, 1984.

[3.18] Martin, R.H. and Murri, G.B., "Characterisation of mode I and mode II Delaminating Growth and Thresholds in Graphite/Peek Composites", In Composite Materials, NASA, Vol. 9, 1988.

[3.19] Osiyemi, S.O.O., "The Fatigue Performance of Adhesively Bonded Fibre Composite Joints", PhD, Univ. of London, 1992.

[3.20] Jethwa, J.K., "The Fatigue Performance of Adhesively-Bonded Metal Joints", PhD, Thesis, Imperial College, London, 1995.

[3.21] Adams, R.D., and Williams, W.C., "Structural Adhesive Joints in Engineering", Elsevier Applied Science Publishers, ISBN: 0412709201, 1984.

[3.22] Mall, S., "Fatigue Behaviour of Adhesively Bonded Joints", NASA-CR-174458, (1983).

[3.23] Mall, S., Ramamurthy, G. and Rezaizdeh, M.A., "Stress Ratio Effect on Cyclic Debonding in Adhesively Bonded Composite Joints", Composite Structures, Vol. 8, 1987, pp.31-45.

[3.24] Ashcroft, A.I., Gilmore, R.B. and Shaw, S.J., AGARD CP-590, NATO,1996, pp.14.1-14.9

[3.25] Dessureault, M. and Spelt, J.K., "Observations of Fatigue Crack Initiation and Propagation in an Epoxy adhesive", Int. J. Adhesion and Adhesives, Vol. 17,1997, pp. 183-195.

[3.26] Ashcroft, I.A., Hughes, D.J., and Shaw, S.J., "Adhesive Bonding of Composite Materials", Assembly Automation, Vol. 20, 2000, pp.150-156.

[3.27] Xu, X.X., Crocombe, A.D. and Smith, P.A., "Creep Crack Growth in A Filled and Toughened Adhesive", J. Adhesion, Vol. 58, 1995, pp. 191-200.

[3.28] Ashcroft, I.A., Hughes, D.J., Shaw, S.J., AbdelWahab, M.M. and Crocombe A.D.," Resistance of Bonded Composite Double Lap Joints" J. Adhesion, Vol. 75, 2001, pp. 61-88.

[3.29] Ashcroft, I.A, AbdelWahab, M.M., Crocombe, A.D., Hughes, D.J., and Shaw, S.J., "The Effect of Environment on the Fatigue of Bonded Composite Joints", Composites Part A, Vol. 32, 2001, pp.45-58, 2001

[3.30] Crocombe, A.D., Ong, A.D., Chan, C.Y., AbdelWahab, M.M. and Ashcroft, I.A., "Fatigue Crack Propagation in Adhesively Bonded Joints", J. Adhesion, Vol. 78, 2002, pp.745-752.

[3.31] Erpolat, S., Ashcroft, I.A., Crocombe, A.D., and AbdelWahab, M.M., "An Investigation of Crack Growth Acceleration in Bonded Joints Subjected to Variable Amplitude Fatigue Loading", Proc. 26th Annual Meeting of the Adhesion Society, Ed. G.L. Anderson, The Adhesion Society, 2003, pp.74-76.

[3.32] Al-Ghamdi, A.H., Ashcroft, I.A., Crocombe, A.D. and AbdelWahab, M.M., "Crack Growth in Adhesively Bonded Carbon Fibre composite Joints Subjected to Fatigue and Creep", Proc. Euradh 2002/Adhesion 02, IOM Communications, 2002, pp.190-194.

[3.33] James, L.A., ASTM STP 513, American Society for Testing and Materials, 1972, pp.218-229.

[3.34] James LA, Nuclear Technology, Vol. 16, 1972, pp.521-526,

[3.35] Saxena, A. and Bassani, J.L., "Interactions of Microstructure Mechanisms and Mechanics", TMS-AIME, 1984, pp.357-383.

[3.36] Plumtree, A. and Yu, M., "Thermal and Environmental Effects in Fatigue: Research-Design Interface", Ed. Jaske C, Hudak S, and Mayfield M, American Society for Mechanical Engineers, Vol. 71, 1983, pp.13-19.

[3.37] Thorkildsen, R.L., "Engineering Design for Plastics", Ed. E. Baer, Van Nostrand-Reinhold, 1964, pp.279-283.

[3.38] Bucknall, C.B., Gotham, K.V., and Vincent, P.I., "Polymer Science" Handbook, Vol.1, Chapter 10, Elsevier, 1972.

[3.39] Skibo, M.D., Manson, J.A., Hertzberg, R.W. and Collins, E.A., "Durability of Macromolecular Materials", ACS Symposium Series No.95; American Chemical Society, 1979, pp.311-315.

[3.40] Hertzberg, R.W. and Menson, J.A., "Fatigue of Engineering Plastics", Academic Press, ISBN: 0123435501, 1980, pp.83-96.

[3.41] Marceau, J.A., McMillan, J.C. and Scardino, W.M., "Cyclic Stress Testing of Adhesive Bonds", Adhesive Age, 1978, pp.37-41.

[3.42] W. Althof " Effect on Low Cycle Fatigue on Shear Stressed Adhesive Bondlines", Adhesive Joints: Formation, Characteristics and Testing, Kansas city, Missouri, USA, 12-17 Sept., 1982, Plenum Press, New York, 1984, pp.659-677.

[3.43] Mostovoy, S., and Ripling, E.J., "Flow Tolerance of a Number of Commercial and Experimental adhesives", Polym. Sci. Technology, Vol.9B, 1975, pp. 513-562.

[3.44] Luckyram, J. and Vardy, A.E., "Fatigue Performance of two Structural Adhesives", J. Adhesion, Vol. 26, 1988, pp.273-291.

[3.45] Osiyemi, S.O., "The Fatigue Performance of Adhesively Bonded Fibre-Composite Joints", Ph.D thesis, Imperial College, London, 1992.

[3.46] Xu, X.X., Crocombe, A.D., and Smith, P.A., "Frequency Effect on Fatigue Crack Growth Rate in Joints Bonded with either Filled and Toughened Adhesive", EURADH 94, France Adhesion Division, 1994, pp.232-236.

[3.47] Pirondi, A. and Nicoletto, G., J., "The Effect of R-ratio and Frequency in DCB joints", J. of Engineering Frac. Mech. In press, 2003.

[3.48] Parker, B.M., "On the environmental durability of adhesive bonded titanium joints", J. of Adhesion, Vol. 26, 1988, pp. 131-154.

[3.49] Parker, B.M., "Environmental durability of aluminium joints with different pre-treatment", Int. J. Adhesion and Adhesives, Vol. 13, 1993, pp.47-51.

[3.50] Marceau J.A., McMillan J.C. and Scardino, W.M., "Cyclic Stress Testing of Adhesive Bonds", Sci. Adv. Mat. Process Eng., Vol. 22, 1977, pp.64-80.

[3.51] Chen, N.N.S., Niem, P.I.F. and Lee, R.C., "Fatigue Behaviour of Adhesive Bonded Joints", J. Adhesion, Vol. 21, 1987, pp.115-128.

[3.52] Brewis, D., Comyn, J. and Shalash, R., "The Effect of Moisture and Temperature on the Properties of an Epoxide-Polyamide Adhesive in Relation to its Performance in Single Lap Joints" Int. J. Adhesion and Adhesive, Vol. 2, 1982, pp.215-222.

[3.53] Brewis, D., Comyn, J. and Shalash, R., "The Effect of Water and Heat on the Properties of an epoxide adhesive in relation to its performance in Single Lap Joints", Polymer, Vol. 24, 1983, pp.67-70.

[3.54] Girifalco, L. and Good, R., "A Theory for the Estimation of Surface and Interfacial Energies: Part I. Derivation and Application to Interface Tension" J. Phys. Chem., Vol. 61, 1957, pp.904-909.

[3.55] Adams, R. D., Coppendal, J., Mallick, V. and Al-Hamdan, H., "The Effect of Temperature on Strength of Adhesive Joints", Int. J. Adhesion and Adhesives, Vol. 12, 1992, pp.185-190.

[3.56] Ashcroft, I.A., Digby, R.P. and Shaw, S.J. "The Effect of Environment on the Performance of Bonded Composite Joints" I. Mech. E. Conf. Trans., Joining and Repair of Plastics and Composites (Professional Engineering Publishing, London), 1999, pp.73-85.

[3.57] Ashcroft, I.A., Hughes, D.J. and Shaw, S.J., "Mode I Fracture of Epoxy Bonded Composite Joints: 1. Quasi-Static Loading" Int. J. Adhesion and Adhesives, Vol. 21, 2001, pp.87-99.

[3.58] Harris, J.A. and Fay, P.A. "Fatigue Life Evaluation of Structural Adhesives for Automotive Applications", Int. J. Adhesion and Adhesives, Vol. 12, 1992, pp.9-18.

[3.59] Ashcroft, I.A., Hughes, D.J., Shaw, S.J., Abdelwahab, M.M, "Effect of Temperature on the Quasi-Static Strength and Fatigue Resistance of Bonded Composite Double Lap Joints", J. of Adhesion, Vol. 75, 2001, pp.61-88.

[3.60] Williams, M.L., Landel, R.F. and Ferry, J.D. "The Temperature Dependence of Relaxation Mechanisms in Amorphous Polymers and other Glass-Forming Liquids" J.Chem. Soc. 77, 1955.

[3.61] Kurobe, T. and Wakashima, H., Jpn. Congr. Mater. Res., Non Metall. Mater., 13th 192, 1970.

[3.62] Kurobe, T. and Wakashima, H., Jpn. Congr. Mater. Res., Non Metall. Mater., 15th 137, 1972

[3.63] Radon, J.C. and Culver, L.E., "Growth of Fatigue Cracks in Polycarbonate", Polym. Eng. Sci. Vol. 15, 1975, pp. 500.

[3.64]   Skibo, M.D., Ph.d. Dissertation, Lehigh Univ., 1977.

[3.65]   Mai, Y.M. and Williams, J.G., J. Mater. Sci. Vol. 14, 1979, pp.1933.

[3.66]   Bazant, Z.P., "Size Effect on Structural Strength", a review of applied Mechanics, Vol. 69, 1999, pp.703-725.

[3.67]   Dugdale, D.S., "Yielding of Steel Sheets Containing Slits", Journal of the Mechanics and Physics of Solids, Vol. 8, 1960, pp.100-108.

[3.68]   Barenblatt, G.I., "The Mathematical Theory of Equilibrium of Cracks in Brittle Fracture", Advances in Applied Mechanics, Vol.7, 1962, pp. 55-129.

[3.69]   Wells, A.A., "Application of Fracture Mechanics at and Beyond General Yielding" British welding Research Association Report M13, 1963.

[3.70]   Rice, J.R.,"A Path-Independent Integral and the Approximate Analysis of Strain Concentration by Notches and Cracks", Journal of Applied Mechanics, Trans. ASME, Vol. 35, 1968, pp.379-386.

[3.71]   Rice, J.R., "Mathematical Analysis in the Mechanics of Fracture", Fracture-An Advanced Treatise, Vol. II, H. Liebowitz, editor, Academic Press, N.Y., 1968, pp.191-308.

[3.72]   Cherapnov, G.P, "Crack Propagation in Continuous Media", Applied Mathematics and Mechanics, (trans.P.M.M.), Vol. 31, 1967, pp.476-488.

CHAPTER 4

ANYLYSIS OF CRACKS IN CREEPING MATERIALS

4.1 Introduction

Creep is an important area of material research and a major threat to the safety of structures and components working at elevated temperature (relative to their melting temperatures for metals and ceramics or their glass transition temperatures for polymers). Most structural adhesives are of a viscoelastic nature and are able to creep at ambient room temperatures. Extensive work has been done to investigate creep in metals, especially in high temperature structural steels. However, considerably less literature is available on creep in viscoelastic materials, let alone in adhesives and adhesive joints.

Creep has been defined by ASTM (D2293) on adhesives as "the dimensional change with time of a material under load, following the initial instantaneous elastic or rapid deformation". Failures due to creep can be classified either as resulting from widespread creep damage, or resulting from localized creep damage. Structural components that can be damaged by widespread creep are those that are typically subjected to uniform temperatures and stress during service, such as thin-wall pipes. The life of these components can be estimated from creep rupture data, an approach that has been used in engineering analyses for several decades. However, frequently high temperature components, especially those containing thick sections, are subjected to stress and temperature gradients and do not fail by creep rupture. It is more likely that at the end of the predicted creep rupture life, a crack develops at a high stress location which propagates and ultimately causes failure. The discrepancy between the actual life and that predicted from the rupture data can be the crack propagation period which was not considered.

Therefore, it is important to develop the capability to predict crack propagation at elevated temperatures in the presence of creep deformation.

Figure (4.1) shows a typical creep curve. At constant stress and temperature, strain develops as shown by the curve. At $t=0$ the curve shows an instantaneous response ε_o, which, depending on the magnitude of the stress, could be elastic or elastic-plastic. The creep curve generally arranges itself into three regimes, classified as: primary, secondary, and tertiary creep. Creep rupture occurs at the end of the tertiary zone. Materials differ in the arrangement of the three regimes. Some have hardly any secondary creep, whilst others have hardly any tertiary creep, and so on. In the first region (the primary creep region) the strain rate continuously decreases with time until it reaches a steady- state value, in the second region. In the tertiary region, the creep strain rates begin to rise with time as necking develops and this is followed by rupture. Since the object of engineering design is to avoid rupture, the tertiary creep regime is not significant in practical applications. Primary creep in several materials is short-lived, thus, making the steady-state creep region the most important in design considerations. The strain rates in this region remain constant with time; however, they change significantly with stress and this relationship is often described by a power-law,

$$\dot{\varepsilon}_{ss} = A\sigma^n \qquad\qquad (4.1)$$

where $\dot{\varepsilon}_{ss}$ is the steady- state strain rate and σ is the applied stress. Equation (4.1) can be used to describe the creep deformation kinetics.
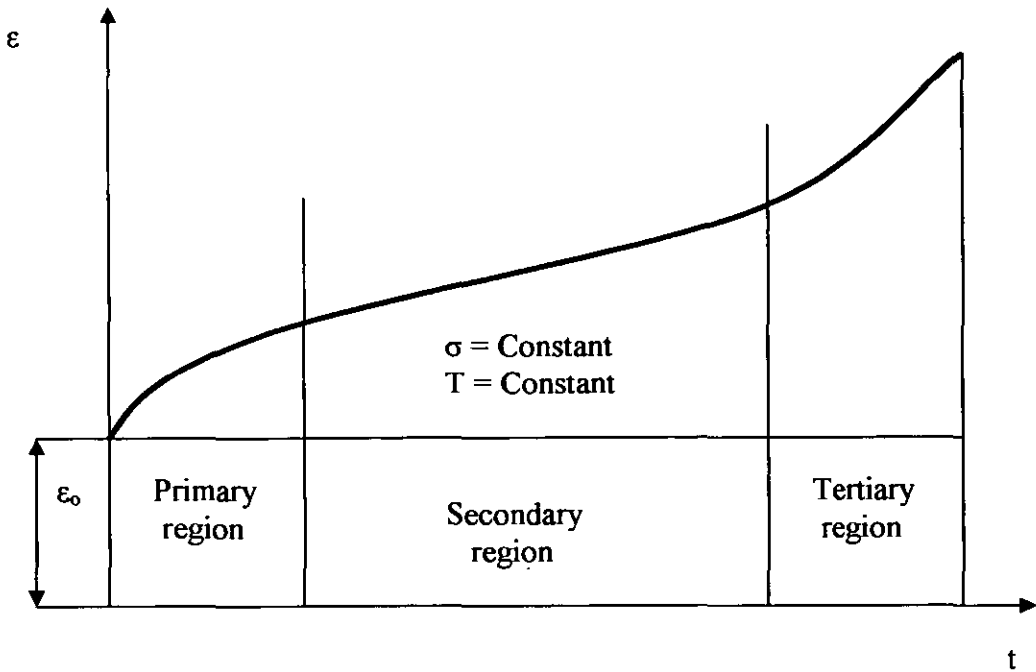
Fig. 4.1 Creep deformation behaviour

As described above, the creep strain of most conventional materials develops in three stages. However, things may be different for adhesives and adhesive joints. For example, Mays [4.1] conducted creep tests on double lap joints bonded with four industrial adhesive and found that most of the log-log plots of strain vs. time were linear from start to end. Only one plot showed the three stage creep behaviour. Allen and Shanahan [4.2] presented a three-stage diagram of shear creep strain against logarithmic time for a structural adhesive lap joint; they found that, the strain develops through a primary stage, a constant gradient stage and an accelerating stage. This viewpoint was shared by Adams and Wake [4.3].

Another indication of creep is the change of elastic modulus or (creep modulus, defined as the ratio of initial applied stress to creep strain) with time. Lark and Mays [4.4] determined the creep modulus as a function of time for an epoxy adhesive. They found that the modulus fell substantially as testing time elapsed.

Creep rate in terms of creep strain/deformation per unit time, varies with stress level. The higher the stress level, the greater the creep rate. This is also reflected by the rapid decrease in creep modulus at high stresses [4.5]. There is evidence that when the applied stress is below a certain threshold, there is no apparent creep deformation [4.6].

The linear elastic fracture mechanics (LEFM) concept discussed in the previous chapter is unable to predict crack growth in the presence of significant creep strains. Thus, this chapter will focus on developing the concepts of time-dependent fracture mechanics (TDFM), which possesses such capabilities.

4.2 Stress analysis of cracks under steady-state creep

To identify the relevant field parameters for characterizing crack growth at elevated temperature, the following process should be considered [4.7]. Figure (4.2) shows a schematic of the deformation zones ahead of a stationary crack tip subjected to loading in the creep regime. A load, P, is assumed to be applied instantaneously and is sustained indefinitely. Upon loading, a plastic zone is formed at the crack tip. The size of the plastic zone depends on the applied K level and the yield strength of the material. Also shown in the figure is a K-zone in which the K-controlled elastic stress and deformation fields hold, if small-scale yielding conditions are maintained during the initial loading. If extensive plastic deformation occurs during initial loading, K loses its significance as the dominating crack tip parameter. Under such conditions, the crack tip stresses and strains are characterized by the J-integral. With time, in either case, the stresses in the vicinity of the crack begin to relax due to creep deformation and the size of the creep (or relaxation) zone increases with time if the crack is assumed to remain stationary. Neither K nor J is expected to uniquely characterize the crack tip stress relaxation behaviour within the creep zone because creep deformation is not admitted in their formulation. However, if the creep

zone is small, K or J will continue to characterize the crack tip stresses outside the creep zone. When the creep zone becomes comparable to the dimensions of the cracked body, K and J completely lose their significance as crack tip parameters. Therefore, when creep is present we have to look for new crack tip parameters.

Figure (4.3) schematically shows the regimes of small-scale creep (SSC), transition creep (TC), and extensive creep (EC). Under SSC, the creep zone size is small in comparison to the crack length and pertinent dimensions of the body. On the other hand, under EC conditions the creep zone completely engulfs the uncracked ligament. The TC condition represents an intermediate regime. SSC and TC are transient conditions characterized by the crack tip stresses, which vary with time as the stress redistributes within the uncracked ligament. On the other hand, The EC condition is a steady-state condition because the crack tip stresses remain constant with time.
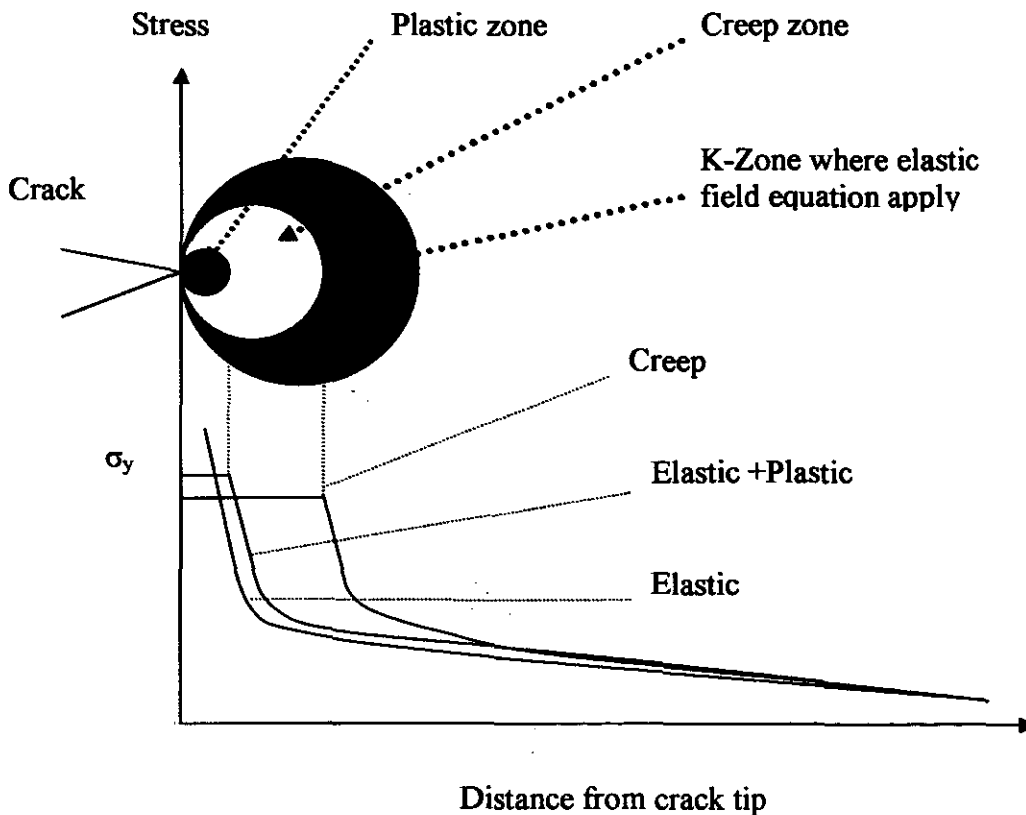

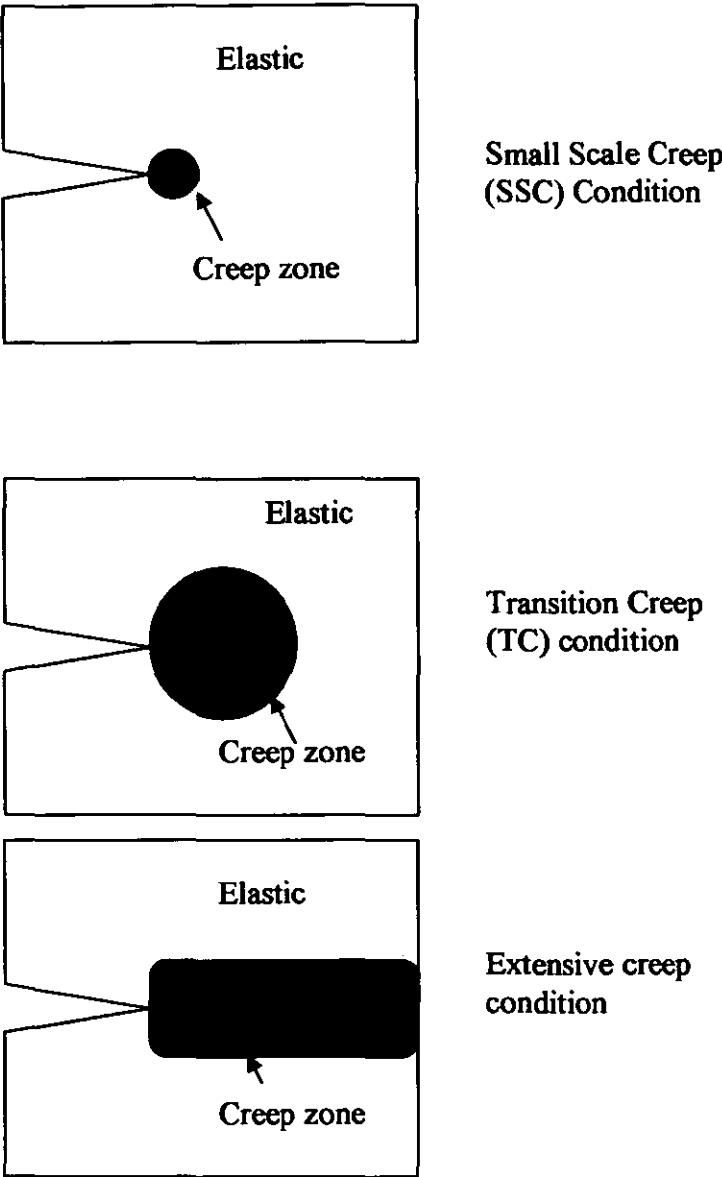Fig. 4.2 Schematic of the deformation zone ahead of the crack tip.

Fig. 4.3 Schematic representation of the levels of creep deformation during crack growth.

4.2.1 The C*-Integral

Landes and Begley [4.8] and Nikbin, Webster, and Turner [4.9] independently defined an integral analogous to Rice's J-integral. Landes and Begley called this new integral C* and defined it in the following manner:

$$C^* = \int_\Gamma W^* dy - T_i \left\{ \frac{\partial \dot{u}_i}{\partial x} \right\} ds \qquad (4.2)$$

85

Where

$$W^* = \int_0^{\dot{\varepsilon}_{ij}} \sigma_{ij} d\dot{\varepsilon}_{ij} \qquad\qquad (4.3)$$

Γ is a line contour shown in Figure (4.4) taken counter clockwise from the lower crack surface to the upper crack surface, W^* is the strain energy rate density associated with the point stress, σ_{ij} and strain rate $\dot{\varepsilon}_{ij}$, T_i is the traction vector defined by the outward normal, n along Γ, $\dot{u}_i$ is the displacement rate vector and s is the arc length along the contour.
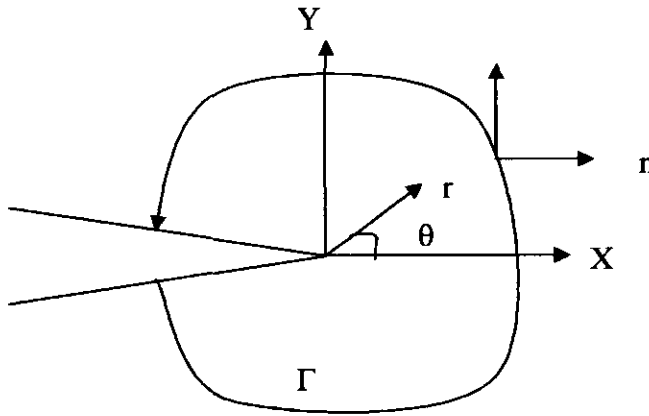

Fig. 4.4 Crack tip coordinate system and arbitrary contour along which C*-integral is evaluated.

4.2.1.1 Energy rate interpretation of C*

The energy rate definition of C* was given by Landes and Begley [4.8]. They considered two cracked bodies which are identical in all respects but one. The crack length of one body is a and the crack length of the other is incrementally longer, i.e. $a + \Delta a$. Both bodies are subjected to an identical static load, P_1; their load deflection rates $\dot{u}_c$ are monitored after sufficient time has been allowed for steady-state conditions to develop in the

86

specimens. Next, they considered several other similar pairs of cracked bodies loaded them to different levels of loads. They then plotted the relationship between the load (P) and the displacement rate $\dot{u}_c$ for all specimens of crack size a and for those with crack size $a +$ Δa. The area under the load-displacement rate diagrams will be $U^*(a)$ and $U^*(a + \Delta a)$ as shown in Figure (4.5). The difference between the two areas is ΔU^*. U^* is the energy rate or the stress-power input into the cracked bodies and ΔU^* is the stress- power difference between the two bodies. The C^*-integral can be shown to be equal to [4.8]:

$$C^* = -\frac{1}{b}\frac{dU^*}{da} \qquad (4.4)$$
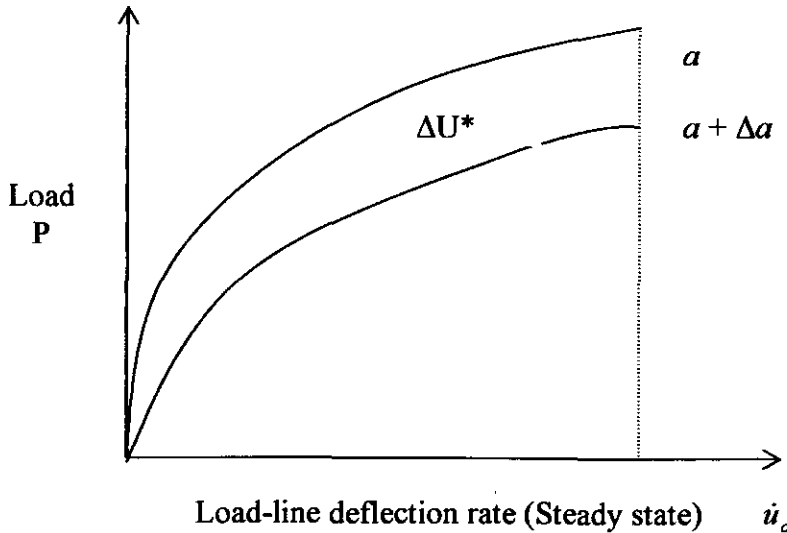
where b is the thickness of the specimen.

Fig. 4.5 Schematic illustration of the energy rate interpretation of the C^*-integral.

4.2.1.2 Relationship between C*-Integral and crack tip stress fields

Goldman and Hutchinson [4.10] used the analogy with the HRR (Hutchinson, Rice and Rosengren) crack tip stress fields for elastic- plastic and fully-plastic conditions, and derived the following relationships between crack tip stress and strain rate and the C*-integral for extensive steady state creep:

$$\sigma_{ij} = \left[\frac{C^*}{I_n A r} \right]^{\frac{1}{1+n}} \hat{\sigma}_{ij}(\theta, n) \qquad (4.5)$$

$$\dot{\varepsilon}_{ij} = A \left[\frac{C^*}{I_n A r} \right]^{\frac{n}{1+n}} \hat{\varepsilon}_{ij}(\theta, n) \qquad (4.6)$$

where A is a constant dependent on the stress and strain at the yield point, r is the distance from the crack tip, n is the creep exponent, $\hat{\sigma}_{ij}$ and $\hat{\varepsilon}_{ij}$ are angular functions and I_n is a normalizing factor which depends on n. The above equations establish the unique relationship between the crack tip stress and C*. It is an attractive parameter for characterizing the creep crack growth rate under condition of extensive steady-state creep.

4.2.2 Methods of determining C*

C* can be obtained analytically for some limited geometries, such as centre crack tension (CCT) and compact tension (CT) specimens. The methods that can be applied to complex geometries and loading conditions include (1) experimental methods, (2) semi-empirical methods, (3) numerical methods. These methods are discussed further in the following sections.

4.2.2.1 Experimental Method for Determining C*

This method is based on the energy rate (or stress-power) interpretation of C* given by Equation (4.4). The method requires several sets of identical specimens. The crack size is varied between different sets of specimens. If five sets are used and five specimens in each set, the crack sizes of specimens in the various sets are a_1, a_2, a_3, a_4, a_5. Thus, a total of 25 specimens are machined, 5 specimens each of the 5 crack sizes. Five load levels, P1, P2... P5 are selected and each load applied to one specimen from each set and the steady state deflection rates measured. Next the P-$\dot{u}_c$ relationship for each crack size can be plotted and the area under the curve for different values of $\dot{u}_c$ can be obtained to determine U*. Then U* can be expressed as a function of crack size for fixed values of $\dot{u}_c$. The slope of the U* vs. *a* curve can be related to C*. This method of determining C* is not usually a practical method due to the extensive amount of testing that is required. Although this method was used for determining C* in the early studies of creep crack growth [4.8], it was quickly abandoned in favour of more direct methods. These are the semi-empirical methods described next.

4.2.2.2 Semi-empirical methods of determining C*

C* can be estimated using the load-displacement record from a single specimen. Recalling the definition of potential energy, U, it is possible to estimate C* based on the following relationship [4.11]:

$$C^* = \frac{P\dot{u}}{bW}F \qquad (4.7)$$

Where F is a non-dimensional function given by:

$$F = -\frac{n}{n+1}\frac{W}{P_L}\frac{d\,P_L}{da} = -\frac{n}{n+1}\frac{1}{m}\frac{dm}{d(a/W)} \qquad (4.8)$$

Hence, C* can be re-expressed as:

$$C^* = \frac{P\dot{u}}{b(W-a)}\left(1-\frac{a}{W}\right)\frac{n}{n+1}\eta \qquad (4.9)$$

where a is crack length, W is the width, b is the thickness, P is load, $\dot{u}$ is the creep load-line displacement rate and n is material constant. The Eta function (η) for DCB joint shown in Figure (4.6) is given by [4.12]:
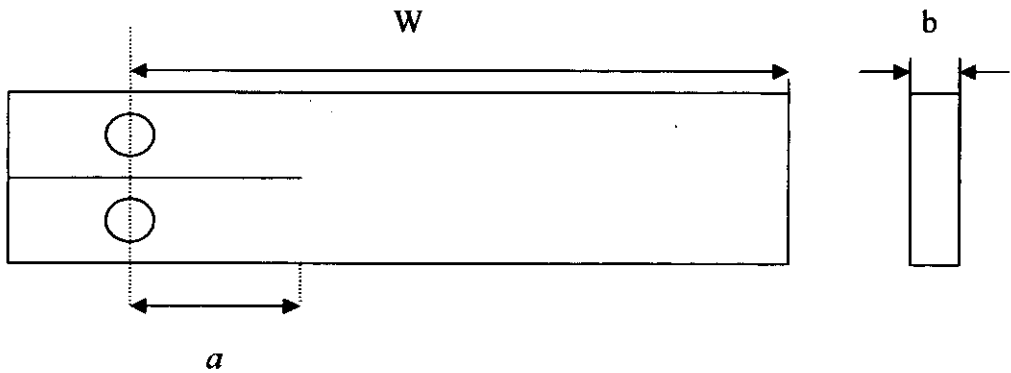
$$\eta = \frac{1-a/W}{a/W} \qquad (4.10)$$

Fig. 4.6 DCB joint dimensions.

4.2.2.3 C* based on numerical solutions

Numerical solutions are necessary to estimate the C*-integral values, where no measurements of load-line deflection rate are available. These solutions are restricted to either plane stress or plane strain conditions [4.7]. This method has been derived for well known geometries such as CT and CCT specimens [4.7, 4.13]. In this work a finite element method was used to evaluate C* for DCB specimen as a function of crack length. This will be described in section (6.4.5).

4.2.3 Correlation between creep crack growth rates and C*

The early attempts by Landes and Begley [4.8] to correlate da/dt with C* under creep conditions met with only limited success. These experiments were conducted on A286 alloy in which it was difficult to obtain the conditions of extensive steady-state creep within the time period of the experiment. Similar experiments were then conducted by Saxena [4.7] on 304 stainless steel at 594°C to promote extensive steady-state creep in the specimens; these experiments were conducted using CT and CCT specimen geometries, the results of this study demonstrated the validity of C* for correlating creep crack growth rates. Similar correlations have been obtained by several other investigators since these early experiments and the validity of C* for characterizing creep crack growth rates is now widely accepted. However, little work has been done on the application of C* to creep in polymeric materials.

4.3 Analysis of cracks under small-Scale and Transition creep

The validity of the C*-integral presented in the previous section is limited to extensive steady-state creep condition. In practice, this condition may not always be realized because components contain stress and temperature gradients and are designed to resist widespread

creep deformation. Therefore, in this section, we will illustrate the crack tip stress fields for the conditions of small-scale creep (SSC) and transition creep (TC).

4.3.1 Crack tip stress fields in small scale creep

Riedel and Rice [4.13] and Ohji, Ogura, and Kubo [4.14] independently derived expressions describing the crack tip stress fields for the conditions of small-scale creep (SSC) and transition creep (TC). The results can be written as follows:

$$\sigma_{ij} = \left[\frac{K^2(1-v^2)}{I_n EA(n+1)t\ r} \right]^{\frac{1}{1+n}} \hat{\sigma}_{ij}(\theta, n) \qquad (4.11)$$

$$\dot{\varepsilon}_{ij} = A \left[\frac{K^2(1-v^2)}{I_n EA(n+1)t\ r} \right]^{\frac{n}{1+n}} \hat{\varepsilon}_{ij}(\theta, n) \qquad (4.12)$$

In the above equations, the time-dependence of the crack tip stress, strain, and strain rate fields is quite evident. The above analysis lends itself to the estimation of the creep zone size and transition time, t_T which is the time needed for extensive creep conditions to develop from SSC conditions. These are discussed in subsequent sections.

4.3.2 Estimation of creep zone size

Riedel and Rice [4.13] defined the creep zone boundary as the locus of points where time dependent effective creep strains equal the instantaneous effective elastic strains in the cracked body. This leads to:

$$r_c(\theta, t) = \frac{1}{2\pi} \left[\frac{(n+1)^2}{2n\alpha_n^{n+1}} \right]^{\frac{2}{n+1}} k^2 (EAt)^{\frac{2}{n-1}} F_{cr}(\theta, n) \qquad (4.13)$$

where r_c is the creep zone size, α_n^{n+1} is a constant that has an approximate value of 0.69 for $3 \leq n \leq 13$ and F_{cr} is a function dependent on (θ, n) and the state of stress. Various values of F_{cr} (n, θ) for plane stress and plane strain as functions of n and θ are shown in Riedel and Rice's [4.13] work. The creep zone size is dependent on time as $t^{\frac{2}{(n+1)}}$ and K as the second power.

4.3.3 Transition time (t_T)

Riedel and Rice [4.13] defined the transition time, t_T as the time when the small-scale-creep stress field equal the extensive steady-state creep field characterized by C^*.

$$t_T = \frac{K^2(1-\nu^2)}{E(n+1)C^*} \qquad (4.14)$$

We can then state that if $t \ll t_T$, equations (4.11, 4.12) describe the crack tip conditions and for $t \gg t_T$, Equation (4.5, 4.6) describe the crack tip conditions. The crack tip stress fields for $t \approx t_T$ will be described on the next section.

4.3.4 C(t)-integral in the transition creep region

Bassani and McClintock [4.15] recognized that the crack tip stress field under SSC can also be characterized by a time-dependent C-integral, whose value is determined along a contour taken very close to the crack tip:

$$C(t) = \int_{\Gamma} W^* \, dy - T_i \left\{ \frac{\partial \dot{u}_i}{\partial x} \right\} ds \qquad (4.15)$$

C(t) is the same as C* but its value is determined close to the crack tip within a region where the creep strains dominate over the elastic strains. Recall that the value of C* could be determined along any contour which originated at the lower crack surface, ended on the upper crack surface, and enclosed the crack tip. Bassani and McClintock [4.15] further related the value of C (t) to K for the condition of small-scale creep:

$$C(t) = \frac{K^2(1 - v^2)}{E(n+1)t} \qquad (4.16)$$

Ehlers and Riedel [4.16] and Bassani and McClintock [4.15] independently proposed the same interpolation formula for approximating the HRR stress fields in the transition creep region:

$$C(t) = \frac{K^2(1 - v^2)}{E(n+1)t} + C^* \qquad (4.17)$$

Equation (4.17) can be combined with Equation (4.14) to develop an alternate expression for *C(t)*:

$$C(t) = (1 + t_T / t) C^* \qquad (4.18)$$

The accuracy of Equation (4.17) has been proven in several finite element studies by Bassani, Hawk, and Saxena [4.17] and Leung, McDowell, and Saxena [4.18-4.19].

The *C(t)*- integral, by virtue of its ability to characterize the HRR fields from small-creep to extensive steady- state creep, is an attractive parameter for correlating creep crack growth rate data. However, it has a major drawback in that it cannot be measured at the loading pins under small-scale and transition creep conditions. Its value must be calculated from Equation (4.17).

4.4 The C_t parameter

Unlike K, and C*, direct experimental measurement of C (t) under transient conditions is usually not possible. Consequently Saxena [4.18] defined an alternate parameter that can be measured relatively easily. This will be discussed in the following sections.

4.4.1 Estimation of C_t for small scale creep

For small scale creep (SSC) condition, Saxena defined an effective crack length, analogous to the Irwin concept [4.20] as follows:

$$a_{\textit{eff}} = a_o + Z r_c \qquad (4.19)$$

where r_c is the creep zone size as defined in Equation (4.13) and Z is a scaling factor. Since the creep zone can sustain stresses, the entire creep zone does not act as a crack. Therefore, the value of Z is less than one. If we choose the value of r_c corresponding to

$\theta=90°$, it has been shown by finite element analysis [4.17] that Z=1/3. The additional load-line displacement due to creep, u_c at any time, t, is given by:

$$u_c = u - u_o = P \frac{dC}{da} Z r_c \qquad (4.20)$$

Where P is the applied load, u is the total displacement, u_o is the instantaneous deflection and C is the elastic compliance of the cracked body. Saxena showed that the small scale creep limit for C_t can be expressed as follows:

$$(C_t)_{SSC} = \frac{P\dot{u}_c}{bW} \frac{F'}{F} \qquad (4.21)$$

where

$$F(a/w) = (K/P)bW^{1/2} \qquad (4.22)$$

$$F' = \frac{dF}{d(a/w)} \qquad (4.23)$$

Or

$$(C_t)_{SSC} = \frac{4\alpha(1-v^{2})}{E(n-1)} BF_{cr}(\theta,n) \frac{K^4}{w} (EA)^{\frac{2}{n-1}} (F'/F) t^{\frac{-n-3}{n-1}} \qquad (4.24)$$

and

$$\alpha = \frac{1}{2\pi} \left[\frac{(n+1)2}{2n\alpha_n^{n+1}} \right]^{\frac{2}{n-1}} \qquad (4.25)$$

Equation (4.24) relates $(C_t)_{SSC}$ to the creep zone expansion rate which is a crack tip quantity. This relationship qualifies $(C_t)_{SSC}$ as a crack tip parameter and it is a method by

which $(C_t)_{ssc}$ can be computed for any geometry and loading configuration provided the K-calibration expression is available and also the creep constants A and n are known. Thus; Equation (4.21) is suitable for determining $(C_t)_{ssc}$ in test specimens where the load is applied and $\dot{u}_c$ is measured. Conversely, Equation (4.24) is more suitable for estimating $(C_t)_{ssc}$ in components where load-line deflection cannot be measured.

4.4.2 Determining C_t for a wide range of conditions

It is convenient to have a single expression for estimating C_t for conditions ranging from small-scale to extensive creep. An approach similar to the one used for estimating the elastic and plastic parts of the J-integral has also been used successfully for C_t. Thus C_t can be expressed as [4.17, 4.20]:

$$C_t = (C_t)_{ssc} + C^*$$
(4.26)

Another approximate expression for estimating C_t over a wide range was proposed by Bassani et al. [4.17] as follows:

$$C_t = \left[1 + \left(\frac{t_T}{t}\right)^{\frac{n-3}{n-1}}\right] C^*$$
(4.27)

Equation (4.26) can be implemented for test specimens where the load-line displacement is available and given by [4.21]:

$$C_t = \frac{P\dot{u}_c}{bw}\frac{F'}{F} - C*\left(\frac{F'}{\eta F} - 1\right)$$

(4.28)

where η is a geometry constant.

4.5 Creep crack growth

Creep crack growth is an important design consideration for several high temperature components. In the previous sections, $C*$, $C(t)$ and C_t were identified as crack tip parameters suitable for characterizing creep crack growth.

Several sources [4.22-4.24] show that the creep crack growth rate can be related to C_t by the following relationship:

$$\frac{da}{dt} = mC_t^q$$

(4.29)

where m and q are material constants obtained from regression of the data and are related to the intercept and slope, respectively, of the da/dt vs. C_t relationship on a log-log plot. Such a relationship between da/dt and C_t is now widely accepted. The crack growth rate, *da/dt* in Equation (4.29) can also be related to the $C*$ and $C(t)$ parameters. The values of *m* and *q* can change from material to material. Ridel [4.23] demonstrated that there is remarkable consistency between the measurements of creep crack growth from a variety of laboratories. Thus, the correlation between da/dt and C_t must be robust enough to withstand minor variation in experimental procedures that may have been present in the test techniques used by the various laboratories.

A detailed test procedure for characterizing creep crack growth is described in ASTM standard E-1457-92 [4.25]. In this procedure, pre-cracked specimens are heated to the desired test temperature and then subjected to a constant load. The crack length and the load-line deflection are both recorded as a function of time for the duration of the test. The crack length is determined by the dc potential drop method, compliance change or the crack gauge method. The test is continued until either the specimen fails by rapid fracture or until sufficient crack growth has occurred. Interrupting the test prior to failure allows the opportunity for the final visually measured crack length to be compared with the non-visual techniques. If the specimen fails, the terminal point of creep crack growth may not be discernable from the fast fracture surface and this comparison may not be possible.

In the present study, the crack length and deflection vs. time data will be numerically processed to obtain rates. Two techniques that can used for calculating rates are the secant method and the seven-point incremental polynomial method recommended in ASTM standard E-647 [4.26] for calculating rates from fatigue crack growth data. In the secant method, the crack growth rate, da/dt and the deflection rate, du/dt are calculated as follows:

$$\left[\frac{da}{dt} \right]_i = \frac{a_{i+1} - a_{i-1}}{t_{i+1} - t_{i-1}} \tag{4.30}$$

$$\left[\frac{du}{dt} \right]_i = \frac{u_{i+1} - u_{i-1}}{t_{i+1} - t_{i-1}} \tag{4.31}$$

The seven- point incremental polynomial method involves fitting a second order polynomial through a group of seven successive data points. The rates are then obtained by differentiating the fitted equation. The characteristic equations for this procedure are given below:

$$\hat{a}_i = b_o + b_1 \left[\frac{t_i - C_1}{C_2} \right] + b_2 \left[\frac{t_i - C_1}{C_2} \right]^2 \qquad (4.32)$$

Where $\hat{a}_i$ is the fitted value of a_i corresponding to time t_i. b_o, b_1 and b_2 are regression parameters which are determined by the least-squares method (that is the minimization of the square of the deviations between the observed and the fitted values of crack length) over the range, $a_{i-3} < a < a_{i+3}$. The parameters $C_1 = 1/2(t_{i-3} + t_{i+3})$ and $C_2 = 1/2(t_{i-3} - t_{i+3})$, are used to scale the input data, thus avoiding numerical difficulties in determining the regression parameters. The crack growth rate at time t_1 is obtained from the derivative of the above equation which is given by the following expression:

$$\frac{da_i}{dt} = \frac{b_1}{C_2} + \frac{2b_2(t_i - C_1)}{C_2^2} \qquad (4.33)$$

A similar set of equations can also be written to obtain the deflection rates. The du/dt data obtained from the above step is further processed to calculate du_c/dt, the deflection rate due to creep deformation, using the following equation [4.27- 4.28]:

$$\dot{u}_c = \dot{u} - \frac{\dot{a}b}{P} \left[\frac{2K^2}{E} + (m+1)J_p \right] \qquad (4.34)$$

m is the plasticity exponent defined by Equation (4.35).

$$\frac{\varepsilon}{\varepsilon_o} = \alpha \left[\frac{\sigma}{\sigma_o} \right]^m$$

(4.35)

where ε_o and σ_o are the strain and stress, respectively, at the yield point.

If the instantaneous loading results in considerable plasticity, Equation (4.34) must be used. However, Equation (4.34) reduces to Equation (4.35) when the plastic part of J, J_p, is negligible.

$$\dot{u}_e = \frac{2b\dot{a}}{P} \left[\frac{K^2}{E} + (1 + v^2) \right]$$

(4.35)

where $\dot{u}_e$ is the elastic rate deflection

4.6 Summary

In this chapter, crack tip stress field derivation in the presence of creep deformation has been reviewed. Initially, the deformation has been modelled with a power-law relationship between strain-rate and stress, ignoring elastic stress redistribution near the crack tip, primary creep, and also effects due to crack growth. The C*-integral has been identified for such conditions as the relevant crack tip parameter for characterizing creep crack growth rates. Methods for estimating C* in test specimens and in components were described. However, C* cannot be measured at the loading pins under small-scale creep and transition creep conditions. Therefore, an alternative crack tip parameter, C_t, was introduced.

Methods for estimating the transition time and the transition creep parameter, $C(t)$ were also described. Finally, detailed test methods for conducting creep crack growth tests were described.

4.7 Reference

[4.1]   Mays, G.C. "Fatigue and Creep Performance of Epoxy Resin Adhesive Joints", Contractor Report 224, Transport and Road Research Laboratory, Department of Transport, 1990.

[4.2]   Allen, K.W. and Shanahan M. "The Creep Behaviour of Structural Adhesive Joints II", *Int. J. of Adhesion*, Vol.8, 1976, pp.43-56.

[4.3]   Adams, R.D. and W.C., "Structural Adhesive Joints in Engineering", Elsevier Applied Science Publishers", ISBN: 0412709201, 1985.

[4.4]   Lark, R.J. and Mays, G.C., "Epoxy Adhesive Formulation: it's Influence on Civil Engineering Performance", Editor K. W. Allen, Elsevier Applied Science Publisher, London, 1984, pp.95-110.

[4.5]   Gledhill, R. and Kinloch, A., "Polymer", Vol.17, 1976, p.727.

[4.6]   Hughes, E. and Rutherford, J.L., "Stress dependence of Creep in Bonded Adhesive", *Material since and Engineering*, Vol.44, 1980, pp.57-62.

[4.7]   Saxena, A., "Evaluation of C* for Characterization of Creep Crack Growth behaviour of 304 Stainless-Steel", in Fracture Mechanics: Twelfth Conference, ASTM STP 700, American Society for Testing and materials, Philadelphia, 1980, pp.131-151.

[4.8]   Landes, J.D., and Begley, J.A., "A Fracture Mechanics Approach to Creep Crack Growth", in Mechanics of Crack Growth, ASTM STP 590, American Society for Testing and Materials,1976, pp.128-148.

[4.9] Nikbin, K.M., Webster, G.A., and Turner, C.E., "Relevance of Nonlinear Fracture Mechanics to Creep Crack Growth", Crack and Fracture, ASTM STP 601, American Society for Testing and Materials, 1976, pp.47-62.

[4.10] Goldman, N.L., and Hutchinson, J.W., "Fully Plastic Crack Problems: the Centre Cracked Strip under Plain Strain", International Journal Solids and Structures, Vol.11, 1975, pp.575-591.

[4.11] Webster, G.A., "Fracture Mechanics in Creep Range", *Journal of Strain Analysis*, Vol.3, 1994, pp.215-223.

[4.12] Webster, G.A. and Ainsworth, R.A., "High Temperature Component Life Assessment", Chapman and Hall, ISBN: 0412585200, 1994.

[4.13] Riedel, H. and. Rice, J.R., "Tensile Cracks in Creeping Solids", Fracture Mechanics: Twelfth conference, ASTM STP 700, American Society for Testing and Materials, Philadlphia, 1980, pp.112-130.

[4.14] Ohji, K., Ogura, K., and Kubo, S., "Stress-Strain Fields and Modified J-Integral in the Vicinity of the Crack Tip under Transient Creep Conditions", Japan Society of Mechanical Engineering, No.790-13, 1979.pp.18-20(in Japanese).

[4.15] Bassani, J.L., and McClintock, F.L., "Creep Relaxation of Stress around a Crack Tip", International Journal of Solids and Structures, Vol. 17, 1981, pp.79-89.

[4.16] Ehlers, R., and Riedel, H., " A Finite Element analysis of Creep Deformation in a Specimen Containing a Macroscopic Crack", Advances in fracture Research, Vol.2, ECF-5, Pergamon Press, 1991,pp.691-698.

[4.17] Bassani, J.L., Hawk, D.E., and Saxena, A., "Evaluation of C(t) Parameter for Characterizing Creep Crack Growth Rate in the Transient Regime", Nonlinear Fracture Mechanics: Time –Dependent Fracture Mechanics, Vol. I, ASTM STP 995, American Society for Testing and Materials, Philadelphia, 1989, pp.7-29.

[4.18] Saxena, A., "Creep Crack Growth under Non-Steady-State conditions", in Fracture Mechanics: Seventeenth Volume, ASTM STP 905, American Society for Testing and Materials, 1986, pp.185-201.

[4.19] Leung, C., McDowell, D.L., and Saxena, A., "A Numerical Study of Non-Steady-State Creep at Stationary Crack Tips", Nonlinear Fracture Mechanics: Time-Dependent Fracture Mechanics, Vol. I, ASTM STP 995, American Society for testing and materials, Philadelphia, 1989, pp.141, 158.

[4.20] Saxena, A., "Creep Crack Growth in Ductile Materials", Engineering Fracture Mechanics, Vol. 40, 1991, pp.721-736.

[4.21] Saxena, A., "Mechanics and Mechanisms of Creep Crack Growth", in Fracture Mechanics: Microstructure and Micromechanics S. V. Nair et al., editors, ASM International, Metals Park, Ohio, 1989, pp.283-334.

[4.22] Saxena, A., Han, J., and Banerji, K., " Creep crack Growth Behaviour in Power Plant Boiler and Steam Pipe Steels", Journal of pressure Vessel Technology, ASME, Vol.110, 1988, pp.137-146.

[4.23] Riedel, H., and Detampel, V., "Creep Crack Growth in Ductile, Creep Resistant Steel", International Journal of Fracture, Vol. 33, 1987, pp.239-262.

[4.24] Kino, H., "Electric Potential Technique for monitoring crack Growth and Creep Crack Growth Behaviour in Various Steels", unpublished data, Mitsibushi Heavy Industries, Ltd, Dec.1985.

[4.25] Johnson, H.H., Materials Research and Standards, Vol. 5, N. 9, 1965, pp.442-445.

[4.26] "Standard Test Method for Measurement of Fatigue Crack Growth Rates", ASTM Standard E647-91, ASTM Book of Standards, Vol. 03.01, 1992, pp.674-701.

[4.27] Saxena, A., Ernst, H.A., and Landes, J.D., "Creep Crack Growth Behaviour in 316 Stainless Steel at 594°C", International Journal of Fracture, Vol. 23, 1983, pp.245-257.

[4.28] Saxena, A. and Landes, J.D., "Characterization of creep Crack Growth in Metals", Advances in Fracture Research, S.R. Valluri et al., editors, Pergamon Press, 1985, pp.3977-3988.

CHAPTER 5

CREEP-FATIGUE CRACK GROWTH

5.1 Introduction

Creep-fatigue interaction is an important problem that often must be addressed in the design of high temperature metallic structures [5.1]. There are two types of creep-fatigue interaction, namely, sequential and simultaneous interaction. Sequential interaction occurs when a fatigue load (or a static load) and static load (or fatigue load) are applied sequentially. Simultaneous interaction is due to the simultaneous creeping during fatigue loading. It is generally believed that when there is creep-fatigue interaction, a crack will grow faster than under either fatigue or creep loading alone. However, there are cases that creep-fatigue interaction reduces the crack growth rate. For example, Sun and Chim [5.2] conducted fatigue-creep tests by applying combinations of fatigue and creep loads to a graphite/ epoxy laminated composite. It was found that creep increased the fatigue life in term of number of cycles to failure, or retarded the fatigue crack growth rate. The retardation was thought to be caused by the permanent strain build up at the fatigue crack tip as a result of creep in the matrix.

In the previous chapter, the analytical frameworks for considering time-dependent creep deformation under conditions of sustained loading were investigated. Cyclic or fatigue loading is prominent in many components that are operated at elevated temperature, making crack growth behaviour under creep-fatigue conditions important. This will be the main subject of this chapter.

5.2 Creep-fatigue interaction

Some of the common loading waveforms used in the study of creep-fatigue crack growth behaviour are shown in Figure (5.1). The important time parameters characterizing the wave forms are, t_r = rise time, t_h = hold time, t_d = decay time. The amplitude of the loading waveform

(ΔP) can be characterized by the difference between the maximum and minimum

loads, $(P_{max} - P_{min})$ and the load ratio, $R=P_{min}/P_{max}$. The loading frequency is termed f.
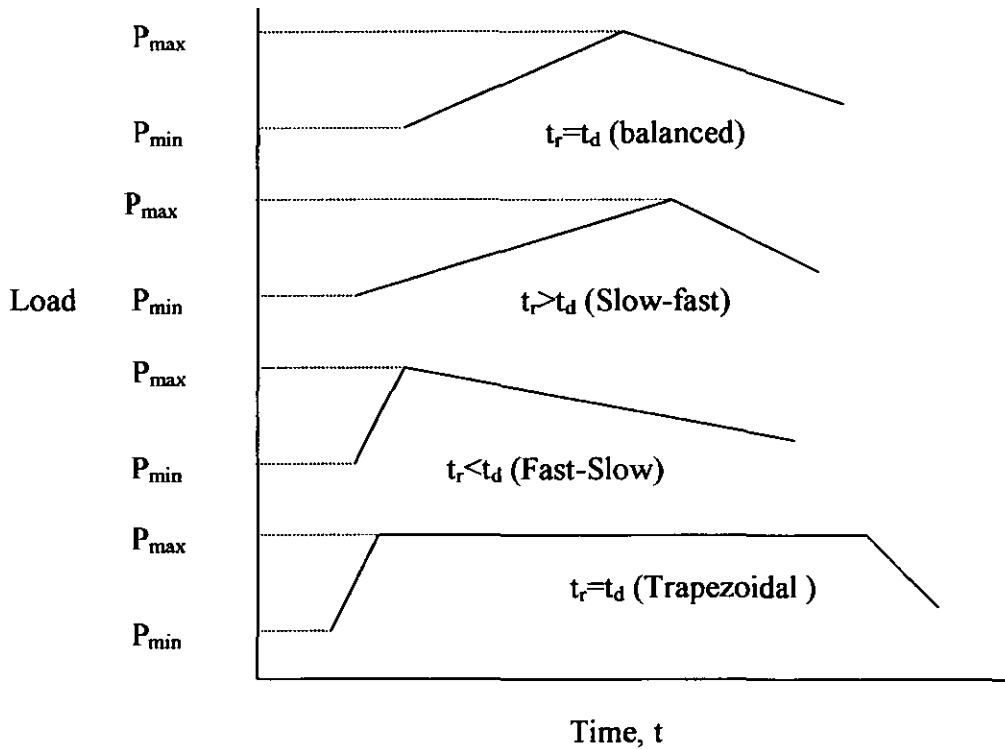

Fig. 5.1 Loading waveforms typically employed in creep-fatigue experiments.

5.3 Early approaches for characterizing creep-fatigue crack growth behaviour

Early approaches for characterizing creep-fatigue crack growth behaviour were based entirely on

LEFM and met with some degree of success. In the subsequent discussion, some of these

approaches will be reviewed as well as the limitations of these approaches. This will set the stage

for a discussion of the more recent nonlinear fracture mechanics approaches.

5.3.1 LEFM approach

The LEFM approach for characterizing creep-fatigue crack growth behaviour used ΔK to

characterize the crack growth rate per cycle, da/dN, while keeping the loading frequency and

loading waveform constant. The experimental work of James [5.3-5.4] demonstrated the

influence of loading frequency and waveform on da/dN verses ΔK. This work showed that the

crack growth rate increases with decreasing frequency. Similar data demonstrated the influence

of hold time in a trapezoidal loading waveform on the da/dN verses ΔK plots for a Cr-Mo-V

steel at 538 °C [5.5]. This study showed that da/dN increases with hold time for a constant ΔK.

These results established the importance of time-dependent damage on fatigue crack growth

behaviour at elevated temperature. Such phenomena can be attributed to creep damage at the

crack tip, the influence of environment, or possibly microstructural changes such as the

formation of cavities which occur due to loading at elevated temperature, or a combination of the

above factors. The separation of contributions to damage due to environment (oxidation) and

creep has been attempted by several researchers [5.6-5.8] by performing elevated temperature

crack growth tests at various loading frequencies and waveforms in air and in inert

environments. These studies show that the time dependent effects, at least in some materials, are

significantly enhanced by oxidation. Therefore, environmental effects must be considered in any

model for predicting the fatigue crack growth behaviour. The microstructural changes near the

crack tip due to creep cavitations are quite often constrained by the deformation behaviour in the

surrounding grains. Therefore, their contribution to damage development is implicitly included

when the crack growth response is correlated with the magnitude of the crack tip parameter for a

given loading waveform and frequency.

5.3.2 Limitations of the LEFM approaches

There are several questions about the validity of the linear elastic parameter ΔK in the presence of significant creep deformation at the crack tip [5.9-5.10]. For example, it is unlikely that ΔK remains valid for uniquely determining the fatigue crack growth behaviour at low loading frequencies. There is an additional concern about the use of ΔK at elevated temperature because for a large number of high temperature ductile material, the 0.2% yield strength decreases significantly with temperature and the influence of instantaneous plasticity becomes important. When instantaneous plasticity becomes significant, one can use ΔJ instead of ΔK, to correlate crack growth rates. The validity of ΔJ for characterizing high temperature crack growth under plasticity conditions has been shown in several studies [5.9-5.10]. However, the validity of ΔJ is limited to cyclic plastic deformation and cannot be extended to include time-dependent creep deformation which occurs if the loading frequencies are low or there are hold times involved in the loading cycles. For these conditions, time-dependent fracture mechanics (TDFM) parameters are needed. An extensive discussion of time dependent fracture mechanics crack tip parameters was included in the previous chapter. In the subsequent sections, this concept will be extended to include cyclic loading.

5.4 TDFM parameters for creep-fatigue crack growth

During a trapezoidal loading waveform, creep deformation can occur at the crack tip during the hold time as well as during the loading and unloading portions of the cycle. During loading, creep deformation at the crack tip will also be accompanied by elastic and possibility plastic deformation and the relative amount of creep and instantaneous deformation depends on the loading rate. For fast loading rates, creep will be negligible whereas for very slow loading rates, creep can be dominant. During the hold period, creep deformation will occur, causing the crack tip stresses to redistribute. If the hold period is sufficiently long, extensive creep (EC) conditions

will ultimately prevail. Therefore, to gain a complete understanding of the creep-fatigue crack tip mechanics, solutions must be obtained for a wide range of loading and material deformations. However, analytical solutions for crack tip stresses are not possible for such complex conditions, thus, one must depend on a numerical approach [5.9-5.10].

As a first step toward understanding crack tip conditions under creep-fatigue loading, Riedel [5.11] assumed that the material deformed elastically and by power-law creep. He considered triangular and trapezoidal loading waveforms. For a triangular waveform without hold time, the load was increased linearly with time. The peak stress in the crack tip region was shown to depend on the loading rate. The higher the loading rate, the higher the peak stress because less time was available for creep strains to develop and redistribute the stresses. Riedel also showed that for a linearly increasing load, the transition from small-scale creep conditions to extensive creep conditions will occur at a time t_{TC} given by:

$$t_{TC} = \frac{1+2n}{n+1} \frac{K^2(t_{TC})(1-v^2)}{C^*(t_{TC})E}$$
(5.1)

In the above equation, $K(t_{TC})$ and $C^*(t_{TC})$ are the values of K and C* at $t = t_{TC}$, respectively. In order to develop a clearer picture of creep-fatigue interaction, it is necessary to include the effects of cyclic deformation and also the effects of repeated cycling. A study by Yoon, Saxena, and McDowell [5.12] and another by Adefris, Saxena, and McDowell [5.13] considered such effects for trapezoidal loading waveforms with a 1.25 Cr-0.5Mo steel and a 1Cr-1Mo-0.25V steel, respectively. These studies were carried out with the purpose of investigating the applicability of C_t for creep-fatigue crack growth.

The value of t_{TC} can be used to select loading frequencies during fatigue crack growth testing at high temperature to maintain predominantly elastic conditions. We can also see that if the

loading rate is slow enough, there is little justification for using ΔK for characterizing fatigue crack growth rates at elevated temperature.

Most successful correlations of time-dependent crack growth during trapezoidal loading at elevated temperature are with time-dependent fracture mechanics parameters. These parameters are based on estimating a C^* value using the measured load-line deflection rate. The first available evidence of this approach is in the work of Jaske and Begley [5.14] and Taira, Ohtani and co-workers [5.15]. These proposals were for extensive creep conditions. A similar approach based on the C(t)-integral was proposed by Saxena et al. [5.16] during the same period. The latter approach also included the small-scale and transition creep conditions, which are quite commonly encountered in creep-fatigue. This approach was later modified and the time-dependent crack growth rate during the hold time of a fatigue cycle was characterized by the average value of the C_t parameter, $(C_t)_{avg}$ during the hold time in a given cycle [5.17]:

$$(C_t)_{avg} = \frac{1}{t_h} \int_{t(N)}^{t(N)+t_h} C_t \, dt \qquad (5.2)$$

where $t(N)$ is a function of the number of fatigue cycles, N. For materials in which the crack tip stresses are completely re-instated and insignificant creep deformation accumulates from cycle to cycle, $t(N)$ can be chosen as 0, when negligible creep reversal due to cyclic plasticity occurs, $t(N)$ is a simple linear function of N which for the Nth cycle will be $(N-1)t_h$. Thus, for materials which exhibit complete stress reversal each cycle:

$$(C_t)_{avg} = \frac{1}{t_h} \int_0^{t_h} C_t \, dt \qquad (5.3)$$

and for materials that do not exhibit any stress reversal:

$$(C_t)_{avg} = \frac{1}{t_h} \int_{(N-1)t_h}^{Nt_h} C_t dt \qquad (5.4)$$

The $(C_t)_{avg}$ approach is able to capture the essence of all other parameters. Therefore, in the subsequent discussion, it will be used more frequently to address creep-fatigue crack growth. In the next section, the methods of determining $(C_t)_{avg}$ will be illustrated.

5.5 Methods of determining $(C_t)_{avg}$

Methods of determining $(C_t)_{avg}$ include those that are more suitable for test specimens in which both load and load-line deflection behaviour with time are measured. In this case $(C_t)_{avg}$ can be obtained from the following equation [5.9]:

$$(C_t)_{avg} = \frac{\Delta P \Delta u_c}{bwt_h} \frac{F'}{F} - C * \{(F'/F)/\eta - 1\} \qquad (5.5)$$

where Δu_c is the amount of deflection accumulation during the hold time, ΔP corresponds to the amplitude of the applied load, given by $P_{max} - P_{min}$, C* is calculated using the load during the hold time, P_{max} and the value of F for DCB joints obtained from the following equation [5.18]

$$F = \sqrt{4w\left(\frac{3a^2}{h^3} + \frac{1}{h}\right)} \qquad (5.6)$$

Thus, the value calculated represents the average value of C_t during the hold time. Since the deflection change is measured, the influence of instantaneous plasticity, primary and secondary creep are included in the measurement.

5.6 Experimental methods for characterizing creep crack growth

Primarily, two methods have been used to obtain creep-fatigue crack growth rate data. The first is a traditional fracture mechanics method based on testing compact type specimens subjected to cyclic loading under load-control. In this method, specimens are subjected to cyclic loading of a prescribed loading waveform and frequency and a positive load ratio. The load-line displacement during the entire loading cycle is measured and the crack size is measured by the electric potential method. This method yields satisfactory results provided linear-elastic conditions can be maintained in the specimens. Incremental creep and plastic deformation can accumulate during each cycle and eventually the dominance of linear elasticity conditions cannot be assured. It has been observed [5.9,5.19-5.20] that if the initial a/w values in test specimens of about 0.3 are chosen, sufficient crack growth data in Cr-Mo steels and Cr-Mo-V steels can be obtained in the temperature range of interest before LEFM conditions are violated.

The second method used for generating creep-fatigue crack growth data has been largely through the efforts of Japanese researchers [5.21-5.22]. In this method, hollow cylindrical specimens containing a small crack along the circumference are loaded under axial conditions. The loading is imposed in the form of prescribed displacement or stress. Crack size is monitored using the electric potential method as previously described.

5.7 Creep-fatigue crack growth correlations

The total crack growth rate during the cycle can be partitioned into a cycle dependent part and a time dependent part. Such partitioning is given by [5.23]:

$$\frac{da}{dN} = \left[\frac{da}{dN}\right]_{Cycle} + \left[\frac{da}{dN}\right]_{Time} \qquad (5.7)$$

The cyclic portion of the crack growth rate is determined from a high frequency fatigue test with no hold period.

Another approach of considering the cycle-dependent and time-dependent crack growth rates during creep-fatigue is to assume that those mechanisms are competing mechanisms and the crack growth rate is determined by whichever of the two is greater [5.24]:

$$\frac{da}{dN} = \max\left[\frac{da}{dN}\right]_{Cycle}, \left[\frac{da}{dN}\right]_{Time} \qquad (5.8)$$

The above approach is known as the dominant damage hypothesis. The $(da/dt)_{avg}$ by the partitioning approach is given by:

$$\left[\frac{da}{dt}\right]_{avg} = \frac{1}{t_h}\left[\frac{da}{dN} - \left(\frac{da}{dN}\right)_0\right] \qquad (5.9)$$

and by the dominant damage hypothesis:

$$\left[\frac{da}{dt}\right]_{avg} = \frac{1}{t_h}\left[\frac{da}{dN}\right] \qquad (5.10)$$

5.8 Models for creep-fatigue crack growth

The following equation can be used to represent the creep-fatigue crack growth rate [5.25]:

$$\frac{da}{dN} = C_0(\Delta K)^{n_0} + C_1\big[(C_t)_{avg}\big]^q \qquad\qquad (5.11)$$

where C_0 and n_0 are regression constants which represent the fast-frequency (or cycle-dependent) part of the crack growth rate and the second term has C_1 and q as regression constants, which represent the time-dependent part of the overall crack growth rate. The above equation assumes damage partitioning analysis, which is generally preferred for applications because it is conservative.

5.9 Summary

When linear-elastic fracture mechanics (LEFM) conditions can be maintained, such as during high loading frequencies, ΔK has been shown to be an appropriate crack tip parameter for characterizing creep-fatigue crack growth rates for a constant loading frequency and waveform. As the temperature rises and the loading frequencies decrease, the validity of ΔK becomes questionable and nonlinear fracture mechanics parameters are needed. The ΔJ-integral and parameters such as $(C_t)_{avg}$ are more appropriate where ΔK becomes invalid. It has been shown that $(C_t)_{avg}$ emerges as the most widely applicable crack tip parameter for representing hold-time effects during creep-fatigue crack growth. Methods for estimating $(C_t)_{avg}$ in specimens and components are described in this chapter as are the test methods for characterizing creep-fatigue crack growth rates.

5.10 Reference

[5.1] Jaske, C.E., "Fatigue of Engineering Materials and Structures", Vol.6, No.2, 1983, pp.159-166.

[5.2] Sun, C.T., and Chim, E.S., "Fatigue Retardation due to Creep in a Fibrous Composite", American Society for Testing and Materials, ASTM STP 723, 1981, pp.233-242.

[5.3] James, L.A., "The Effect of Frequency Upon the Fatigue-Crack Growth of Type 304 Stainless Steel at 1000F", in Stress Analysis of Growth of Cracks, ASTM STP 513, American Society for Testing and Materials, Philadelphia, 1972, pp.218-229.

[5.4] James, L.A., "Hold-Time Effects on the Elevated Temperature Fatigue-Crack Propagation of 304 Stainless Steel", Nuclear Technology, Vol.16, 1972, pp.521-526.

[5.5] Saxena, A., and Bassani, J.L., "Time-Dependent Fatigue Crack Growth Behaviour of Elevated Temperature", in Fracture: Interactions of Microstructure, Mechanisms and Mechanics, TMSAIME, Warrendale, 1984, pp.357-383.

[5.6] Pelloux, R.M., Huang, J.S., "Creep-Fatigue Environment Interaction in Astrolloy", in Creep-Fatigue Environment Interactions, R. Pelloux and N. Stollogg, Editors, TMS-AIME, 1980, pp.151-164.

[5.7] Floreen, S. and Kane, R.H., "An Investigation of Creep-Fatigue-Environment Interactions in Ni Base Super Alloy", Fatigue of Engineering Materials and Structures, Vol.2, 1980, pp.401-412.

[5.8] Saxena, A., "A Model for Predicting Environment Enhanced Fatigue Crack Growth Behaviour at High Temperatures", in Thermal and Environmental Effects in Fatigue: Research Design Interface, PVP-Vol.71, American Society for mechanical Engineers, 1983, pp.171-184.

[5.9] Yoon, K.B., Saxena, A., and Liaw, P.K., "Characterization of Creep-Fatigue Crack Growth Behaviour under Trapezoidal Wave shape Using C (t) parameter", International Journal of Fracture, Vol.59.1993, pp.95-114.

[5.10] Saxena, A., Shih, T.T., and Williams, R.S., "A Model for Representing the Influence of Hold Time on Fatigue Crack Growth Behaviour at Elevated Temperature", in Fracture Mechanics: Thirteenth Conference, ASTM STO 743,1981,pp.86-99.

[5.11] Riedel, H., "Crack-Tip Stress Fields and Crack Growth under Creep-Fatigue Conditions", in Elastic-Plastic Fracture: Second Symposium Vol. I-Inelastic Crack Analysis, ASTM STP 803, American Society for testing and Materials Philadelphia,1983,pp.I/505-I/520.

[5.12] Yoon, K.B., Saxena, A. and McDowell, D.L., "Influence of Crack Tip Plasticity on Creep-Fatigue Crack Growth", in Fracture Mechanics: Twenty Second Symposium (Vol.I) ASTM STP 1131, American Society for Testing and Materials, Philadelphia, 1992,pp.367-392.

[5.13] Adefris, N., Saxena, A., and McDowell, D.L., "Creep-Fatigue Crack Growth Behaviour in 1 Cr-1Mo-0.25V steel. Part I: Estimation of Crack Tip Parameters", Fatigue and Fracture of Engineering Materials and Structures, Vol. 19, 1996, pp.387-399.

[5.14] Jaske, C.E., and Begley, J.A., "An Approach to Assessing Creep/ Fatigue Crack Growth: in Ductibility and Toughness Considerations in Elevated Temperature Service", MPC-ASME-8, American Society for Mechanical Engineers, 1978, pp.391-409.

[5.15] Taira, S., Ohtani, R., and Komatsu, T., "Application of J-integral to High Temperature Crack propagation Part II-Fatigue Crack Propagation", Transactions of ASME, Journal of Engineering Materials Technology, Vol.101,1979, pp.163-167.

[5.16] Saxena, A., and Bassani, J.L., "Time-Dependent Fatigue Crack Growth Behaviour of elevated Temperature", in Fracture: Interaction of Microstructure, Mechanisms and Mechanics, TMSAIME, Warrendale, 1984, pp.357-383.

[5.17] Saxena, A., and Gieseke, B., "Transients in Elevated Temperature Crack Growth", Proceedings of MECAMAT, International Seminar on high Temperature Fracture Mechanisms and Mechanics III, EGF-6,1987,pp.19-36.

[5.18] Webster, G.A. and Ainsworth, R.A., "High Temperature Component Life Assessment", Chapman and Hall, 1994.

[5.19] Grover, P. S., "Creep-Fatigue Crack Growth in Cr-Mo-V Base Material and Weldments", Ph.D. Thesis, Georgia Institute of Technology, May 1996.

[5.20] Saxena, A., "Limits of Linear Elastic Fracture Mechanics in the Characterization of high Temperature Fatigue Crack Growth", ASTM STP 924, American Society for Testing and Materials, 1988.pp.27-42.

[5.21] Ohtani, R., Kitamura, T., Nitta, A., and Kuwabara, K., "High Temperature Low Cycle Fatigue Crack propagation of Life Laws of Smooth Specimens Derived from the Crack Propagation Laws", ASTM STP 942, American Society for Testing and Materials, 1988, pp.163-169.

[5.22] Kuwabara, K., Nitta, A., Kitamura, T., and Ogala, T., "Effect of Small-Scale Creep on Crack Initiation and Propagation Under Cyclic Loading", ASTM STP 942, American Society for testing and materials, 1988, pp.41-59.

[5.23] Adefris, N., Saxena, A., and McDowell, D.L., "Creep-Fatigue Crack Growth Behaviour in 1 Cr-1Mo-0.25V Steel. Part II—Crack Growth Behaviour and Models", Fatigue and Fracture of Engineering Materials and Structures, Vol. 19, 1996, pp.401-441.

[5.24] Ohji, K., and Kubo, S., "Fracture Mechanics Evaluation of Crack Growth Behaviour Under Creep and Creep-Fatigue Condition", in High Temperature Fracture and Fatigue, Current Japanese Materials Research, Vol.3, Elsevier Applied Science, Tokyo, 1988,pp.99-113.

[5.25] Saxena, A., "Fracture Mechanics Approaches for Characterizing Creep-Fatigue Crack Growth", JSME International Journal, Series A, Vol.36, No.1, 1993, pp.1-20.

CHAPTER 6

DETERMINATION OF FRACTURE PARAMETERS FOR DCB JOINTS

6.1 Introduction

Fracture mechanics problems have been classified, as described in the previous chapters, into linear-elastic fracture mechanics (LEFM), elastic-plastic fracture mechanics (EPFM), and time-dependent fracture mechanics (TDFM) regimes. These classifications are based on the dominant deformation mode in the cracked bodies. When the stress-strain behaviour and the load-displacement behaviour are linear, LEFM can be used and the relevant parameter is the strain energy release rate, G or stress intensity factor, K. In this regime, the plastic zone is small in comparison to the crack size and other pertinent dimensions of the cracked body. When linear conditions can no longer be ensured, e.g., due to large-scale plasticity, EPFM is used and the relevant crack tip parameter is the J-integral. Finally, when the stress-strain behaviour and the load-displacement behaviour is time-dependent due to either fatigue loading or to time-dependent creep, the concept of TDFM must be used and the relevant crack tip parameters in such cases are the C^*-integral, used for extensive creep conditions, $C(t)$, used for transition creep conditions, C_t used for conditions ranging from small-scale to extensive creep and $(C_t)_{avg}$ used for creep-fatigue loading conditions. This chapter is mainly concerned with the analytical and numerical methods used to calculate the values of these parameters in bonded DCB joint.

6.2 Determination of the strain energy release rate, G

The strain energy release rate, G, is commonly selected as the governing fracture parameter in the analysis of bonded joints. Several methods can be used to calculate the strain energy release rate, including those based on experimental compliance

measurements, those based on beam theory and finite element based methods. The experimental compliance method is attractive as variation in the mechanical properties of the samples can be accounted for. This method requires the monitoring of load, displacement and crack length to determine the variation of compliance with crack growth. However, for practical reasons, there is still a need for analytical methods. One of them is that the load value in a bonded joint, particularly in the case of composite joints, can be as low as 50 N. Therefore the load values are susceptible to error. Since the experimental compliance method requires an accurate monitoring of load in order to determine the compliance variation; the load cell should be very well calibrated and the temperature in the testing laboratory carefully controlled. If an analytical method is used to determine G from the test it is sufficient to monitor either load or displacement. It can also be seen from Equation (3.19) that in the experimental compliance method, sufficient data points must be collected to determine the change in compliance as a function of crack length. This can be difficult to achieve for a fast moving crack. Finally, even if you are using the experimental compliance methods to determine G from tests, analytical methods are useful in predicting behaviour prior to testing. In the following sub-sections, the various methods used to calculate G in DCB joint will be presented.

6.2.1 Simple beam theory (SBT)

Ripling and Mostovoy [6.1] determined the strain energy release rate, G, for a DCB joint with an adhesive layer in Figure (6.1) by considering bending and shear deflection of the cantilever arms as:

$$G_c = \frac{4P^2}{Eb^2}\left(\frac{3a^2}{h^3} + \frac{1}{h}\right)$$

(6.1)
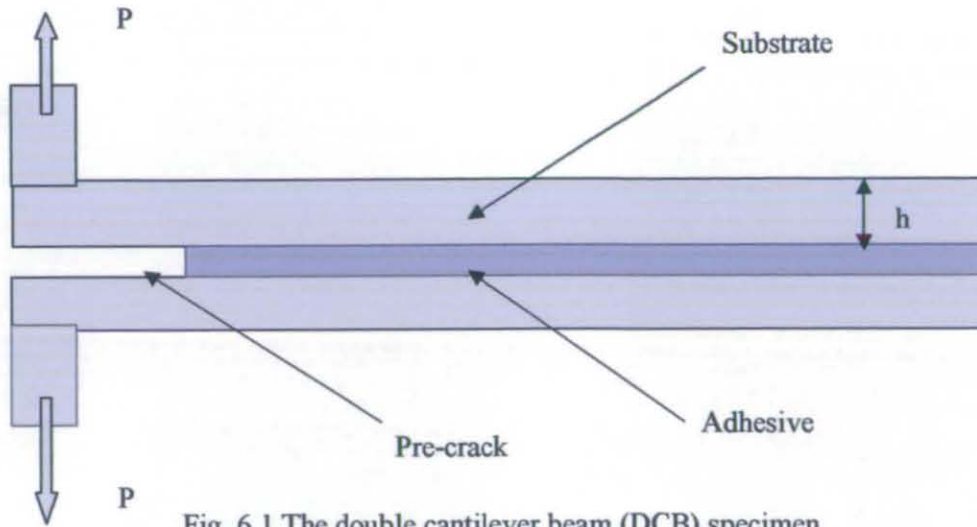
Fig. 6.1 The double cantilever beam (DCB) specimen

where P is the applied load acting perpendicular to the bond line, a is the crack length, h is the substrate thickness, b is the specimen width and E is the elastic modulus of the adherend. This simple beam theory, SBT, approach treats each arm of the specimen as a linear cantilever-beam with a rigidly supported built-in end. Although Equation (6.1) is recommended in ASTM D5041-98-"Standerd Test Method for Fracture Strength in Cleavage of Adhesive in Bonded Joints", it neglects the contribution of the adhesive and rotation at the assumed built-in end, which can be considerable sources of error. Therefore the SBT method usually underestimates the strain energy release rate for specimens tested under load control and overestimates it when the testing is carried out under displacement control. An empirical correction to the simple beam theory has been suggested to correct this effect [6.2]. The SBT equations can be modified by introducing an increase in crack length (i.e. $a_{corr} = a + \Delta$) which is interpolated from a plot of $C^{1/3}$ vs. a, where C is sample compliance (P/v). However, this is of limited use because if a reliable compliance history is already available, the experimental compliance method can be applied, negating the requirement for an analytical method of computing G.

6.2.2 The beam on elastic foundation (BEF) model

The beam-on-elastic-foundation (BEF) model as developed by Kanninen [6.3] is shown in Figure (6.2). Each half of the beam is considered as a beam partly free, and partly supported by an elastic foundation, which represents the interaction of the two beams along the bonded length.
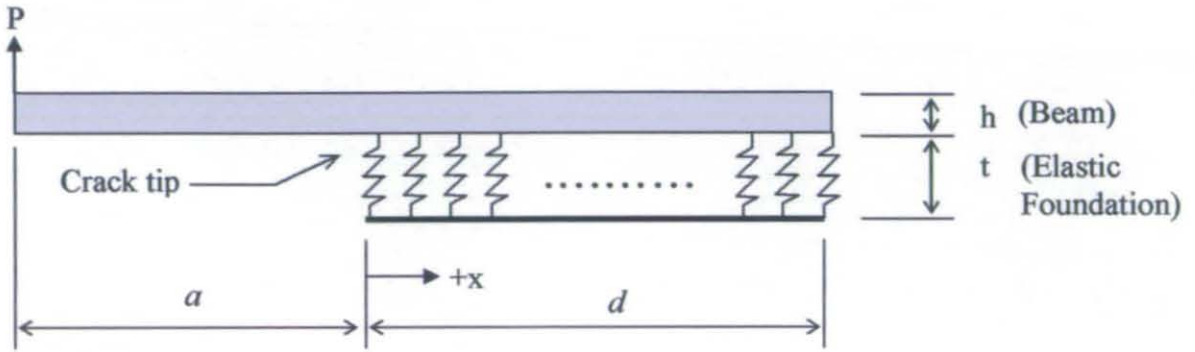
Fig. 6.2 The beam-on-elastic-foundation model

Analytical methods corresponding to a DCB joint tested under displacement control require firstly determining the relationship between load, P, and displacement, v, and then determining the strain energy release rate, G, corresponding to P. For the simple beam theory (SBT) approach [6.1], v can be written as function of P as:

$$v = C.P = \frac{8a}{bEh^3}\left(a^2 + h^2\right)P \qquad (6.2)$$

where E is the Young's modulus of the substrate. A similar procedure can be followed for the models with a compliant crack front. Using the *BEF* model v can be written as function of P [6.3]:

$$v = 2\left(\frac{Pa^3}{3EI} - R_1 a + R_2\right) \qquad (6.3)$$

where

$$R_1 = -\frac{P}{2EI\lambda^2}D_1 \qquad (6.4)$$

$$R_2 = -\frac{P}{2EI\lambda^3}D_2 \qquad (6.5)$$

$$\Delta^4 = \frac{1}{\lambda^4} = \frac{4EIt}{E_a b}\bigg|_1 \qquad (6.6)$$

EI is the flexural stiffness of the beam; E_a is the Young's modulus of the adhesive, t is the thickness of the foundation (i.e. half the thickness of the adhesive) and Δ (λ^{-1}), serves as a length scale [6.4].The equations for D_1 and D_2 are quite complicated, incorporating hyperbolic cosine and sine functions, however, they can be simplified to $D_1 \approx (1+2a\lambda)$ and $D_2 \approx (1+a\lambda)$ by using the assumption that λd is comparable to or larger than 2π. a and d as shown in Figure (6.2), are the lengths of the cracked and uncracked parts of the beam (the crack length and the length of the foundation), respectively.

Since both R_1 and R_3 are directly proportional to P, once v is defined, P can be calculated explicitly from Equation (6.3).

Chang et al. [6.5] and Chow et al. [6.6] independently derived equations for the strain energy release rate in a bonded DCB joint using Kanninen's BEF model. Chow et al. [6.6] made the useful assumption that λd is larger than 2π, and included shear deformation of the beam in their formulation. For a typical DCB joint this is a reasonable assumption. Furthermore, the shear energy in the beam is usually negligible compared with the bending energy and can be ignored. This leads to the following simplified equation for the strain energy release rate [6.7]:

$$G_I = \frac{12P^2}{b^2 h^3 E}(a+\Delta)^2 \qquad (6.7)$$

where h is the thickness of the beam.

6.2.3 Crack closure method

For isotropic materials the distribution of stresses near the crack tip is given in terms of stress intensity factors K_I, K_{II} and K_{III}. Knowing the crack-tip stress field and the dependence of stress intensity factors on the crack size a, the corresponding value of the available strain energy release rate $G_I(a)$ can be represented as:

$$G_I(a) = \frac{K_1^2}{E} \qquad \text{(Plane stress)} \qquad (6.8)$$

$$G_I(a) = \frac{K_1^2}{E}(1-v^2) \qquad \text{(Plane strain)} \qquad (6.9)$$

where E is the Young's modulus and v the Poisson's ratio. For a general case of mixed-mode crack initiation and growth, the total strain energy release rate is given by:

$$G = G_I + G_{II} + G_{III} \qquad (6.10)$$

where G_I, G_{II} and G_{III} denote the mode I, mode II and mode III components, respectively.

Irwin [6.8] showed that the elastic strain energy released during an incremental crack extension is equal to the work done in closing the incremental crack. This crack closure representation provides a direct determination of strain energy release rate (G) from crack-tip stresses and displacements. When the crack is opened as in Figure (6.3b), the work done to close the crack opening is given by:

$$\Delta W = \frac{1}{2} \int_0^{\Delta a} \bar{\sigma} \Delta \bar{u}\, da \qquad (6.11)$$
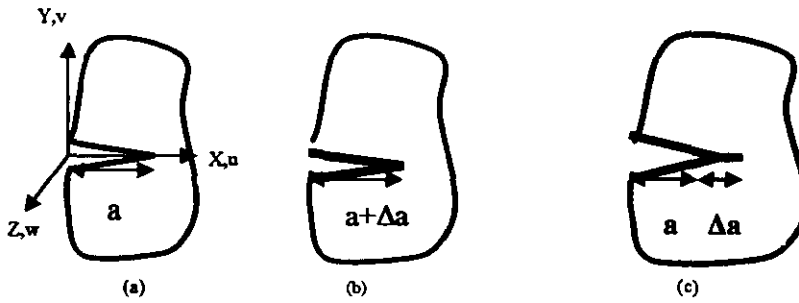
Fig. 6.3 Schematic representation of crack closure technique.

where $\Delta \bar{u}$ is the relative displacement between the mating crack surfaces along Δa. $\bar{\sigma}$ is the surface stress distribution along Δa when the crack is closed as shown in Figure (6.3c). According to Irwin's crack closure equivalence, the available energy release rate G for a crack size a is expressed by the integral:

$$G(a) = \underset{\Delta a \to 0}{Lim} \frac{1}{2\Delta a} \int_0^{\Delta a} \bar{\sigma} \Delta \bar{u}\, da \qquad (6.12)$$

125

Substituting the component of the surface stresses, $\bar{\sigma}$ and the corresponding relative displacements, $\Delta\bar{u}$ into Equation (6.12) yields components of G. The crack closure representation is particularly convenient for adaptation to numerical computation.

A numerical technique to calculate the strain energy release rate using a finite element solution of Irwin's crack closure integral is given by the following equation [6.8-6.9]:

$$\Delta W \cong \frac{1}{2}\left[F_x(u_f - u_g) + F_y(v_f - v_g) + F_z(w_f - w_g)\right] \qquad (6.13)$$

In the finite element representation, the continuous stress and displacement fields of the solid are represented in terms of the nodal forces and nodal displacements respectively. Figure (6.4a) represents the finite element model near the crack tip region. A crack of length a is shown with the crack tip at node c. The finite element solution determines the displacement components (u, v, w) of the crack tip node c. An incremental crack extension Δa is introduced, replacing the crack tip node c with two separate nodes f and g as depicted in Figure (6.4b). For the new crack geometry the finite element solution for the nodal displacements (u, v, w)f and (u, v, w)g are found for nodes f and g respectively. The crack opening is then collapsed by applying equal and opposite forces at nodes f and g such that their common displacements match the displacements found earlier at c. These forces correspond to the internal nodal forces which exist at node c before it opens. The work required to close the crack opening is given by Equation (6.13)
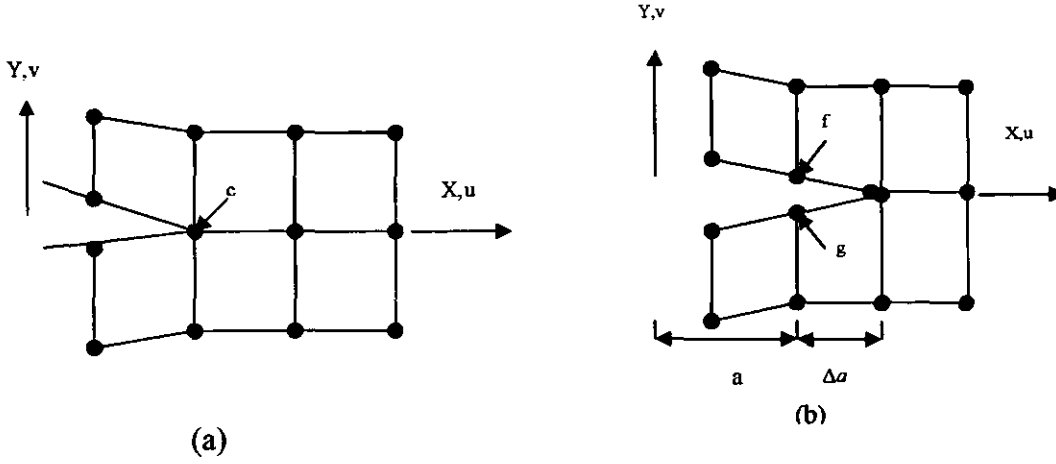
Fig. 6.4 Finite element mesh at crack tip illustrating the crack closure technique.

where Fx, Fy, Fz are components of nodal forces required to close nodes f and g together. The energy release rates for the three crack extension modes are approximated by:

$$G_I \cong \frac{1}{2\Delta a}\left[F_y(v_f - v_g)\right] \tag{6.14}$$

$$G_{II} \cong \frac{1}{2\Delta a}\left[F_x(u_f - u_g)\right] \tag{6.15}$$

$$G_{III} \cong \frac{1}{2\Delta a}\left[F_z(w_f - w_g)\right] \tag{6.16}$$

This method does not require the calculation of the stresses, as stress and strain fields are approximated by nodal forces and displacements respectively.

6.2.3.1 Finite element implementation

In this work, finite element analysis was carried out for the DCB joint shown in Figure

(6.5) using the commercial finite element analysis software LUSAS v.13.4 (FEA Ltd.)
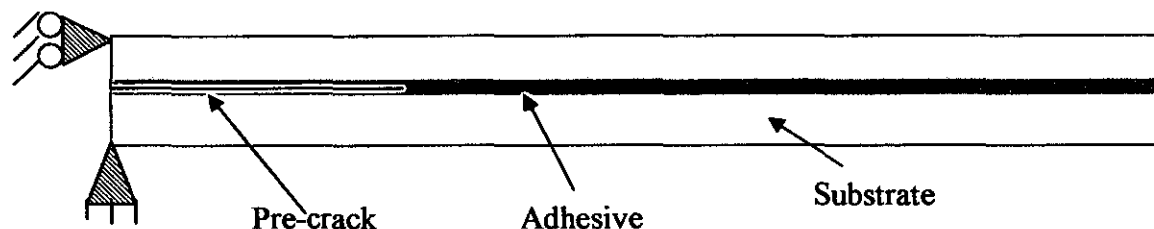
Fig. 6.5 The double cantilever beam joints.

The finite element mesh used in the analysis is shown in Figure (6.6). Mesh refinement

was applied around the crack tip, where stress concentrations were assumed. The

calculated value of G was used to establish the degree of finite element mesh refinement.

A starter crack was introduced at one end of the double cantilever beam (DCB) specimen.

A tensile (Mode I) displacement was applied to the cracked end of the sample. The

displacement of the lower left hand side of the specimen was fixed in the X and Y

directions while on the upper lift hand side it was fixed only in the X direction. These

boundary conditions simulate the situation during the experimental test. A quadrilateral 4

noded plane strain element (QPN4M) was used to model both the adhesive and substrates.

The material properties used in the finite element model for substrates and adhesive are

presented in section (7:3.2) and section (8.2).

Deform mesh
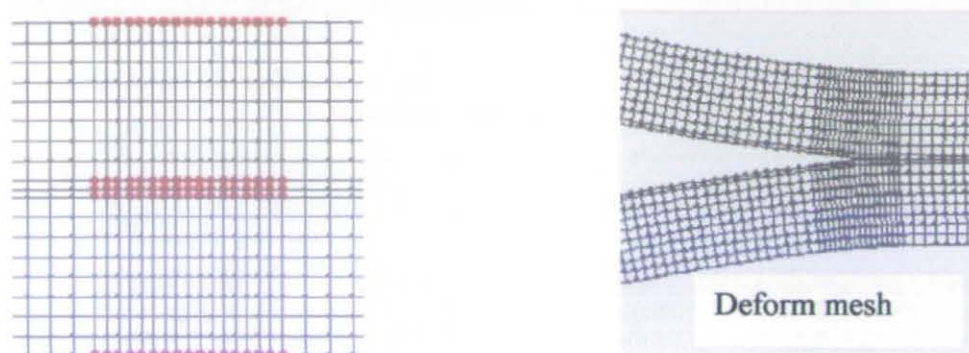
Fig. 6.6 Finite element mesh for the double cantilever beam (DCB) joints.

Linear and geometric non-linear analyses were carried out to calculate the forces and displacements along the DCB joints. Stiff spring elements were used to obtain the nodal forces. A command file (Appendix *C*) was used to find the forces and displacement at nodes around the crack tip as shown in Figure (6.7). Various crack lengths were introduced in the model in order to determine G value as a function of the crack length. The calculated G values from geometric linear and non-linear analyses were almost the same over a range of crack lengths.

Substrate

Spring Joint

Adhesive layer
FM300-2M
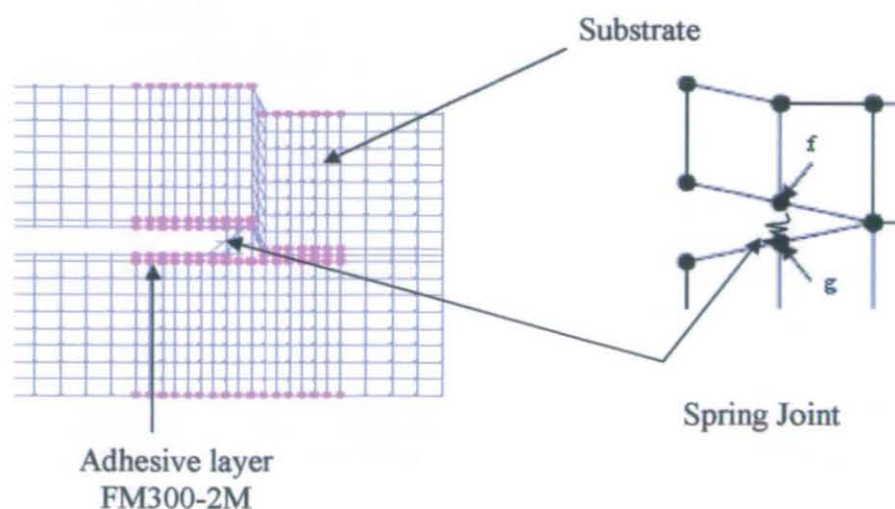
Fig. 6.7 Finite element mesh at crack tip illustrating the crack closure technique

6.2.4 Strain energy release rate results

Based on the analytical methods (SBT and BEF) and numerical method (crack closure method) presented above, the strain energy release rate (G) was calculated at different crack lengths. The analyses were carried out at constant displacement for all methods, namely, 1.8 mm and 0.6 mm for IM7/8552 and mild steel joints respectively. Plot of the analytical and numerical G against the crack length are shown in Figure (6.8) and Figure (6.9) for IM7/8552 and mild steel respectively.
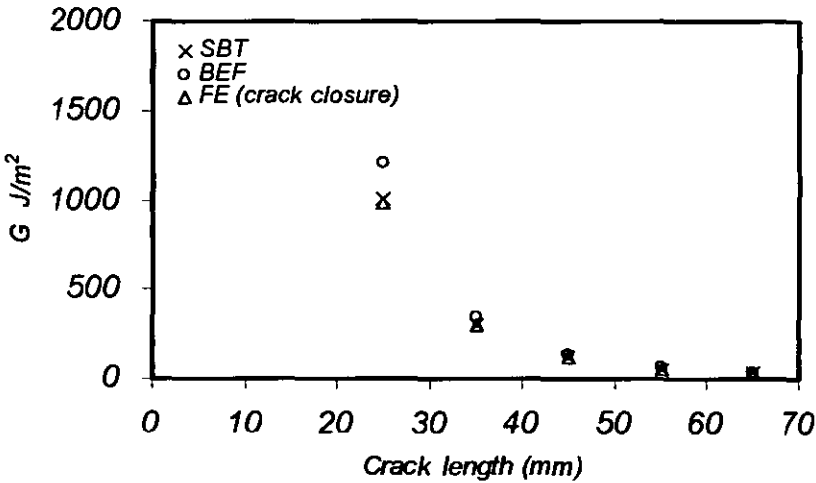
Fig. 6.8 Strain energy release rate, G against the crack length for CFRP joints.
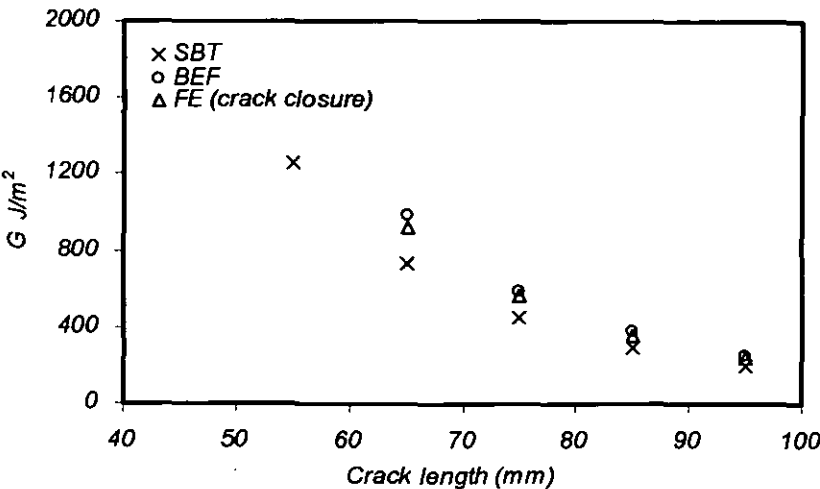
Fig. 6.9 Strain energy release rate, G against the crack length for mild steel joints.

It is clear that all the analytical methods show the same trend. It can also be seen that as the crack length increases the difference between these methods diminishes. The BEF model was found to agree more closely with the FE results than the SBT model. The BEF model has hence been used during this work to analyse the experimental data in term of the maximum strain energy release rate, G_{max}.

6.3 Determination of J-integral

In section (3.5.4), the J-integral was defined and shown to characterize cracking under elastic-plastic and fully plastic conditions. The usefulness of a fracture parameter in engineering applications is dependent upon how readily it can be calculated for cracked components of different geometries and loading. In the following sub-section, we will discuss methods for calculating the value of the J-integral for DCB joints.

6.3.1 The beam on elastic/plastic foundation (BEPF) model

Yamada [6.10] extended Kanninen's method [6.3] to consider plasticity effects at the crack tip. He developed an elastic-plastic foundation model, as shown in Figure (6.10). The bonding material was assumed to be elastic/perfectly plastic whereas the cantilever beams remained elastic. This idealized behaviour of the adhesive is shown in Figure (6.11). Therefore, within the yield zone, a uniform uniaxial stress was assumed, and the springs reaching the elastic limit around the crack tip were replaced by a uniform stress equal to the yield strength of the adhesive, σ_Y.
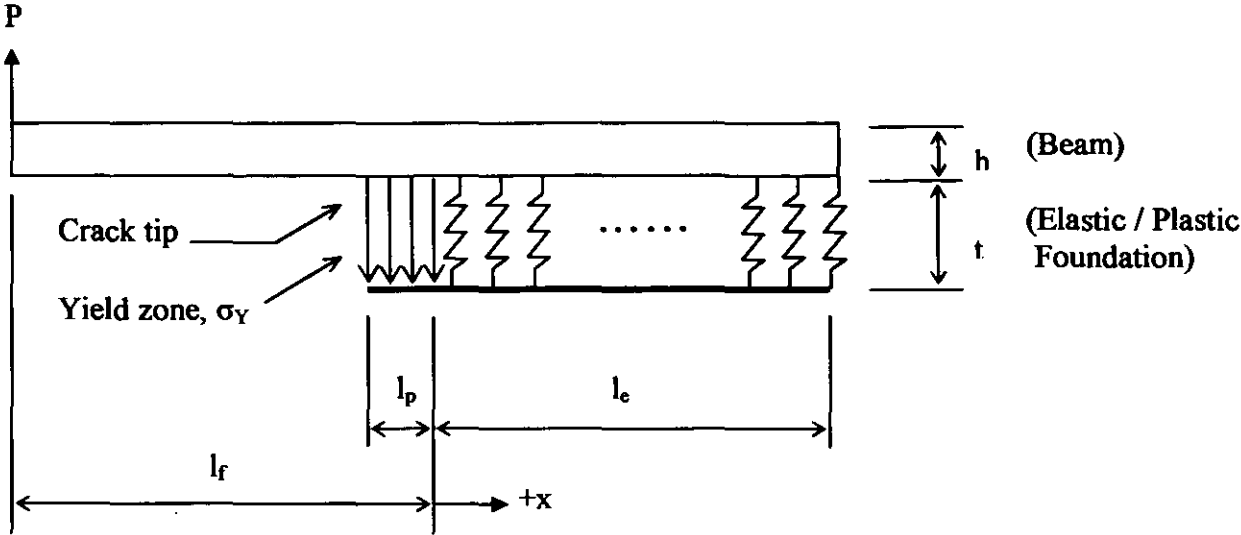
Fig. 6.10 The beam-on-elastic/plastic- foundation model.
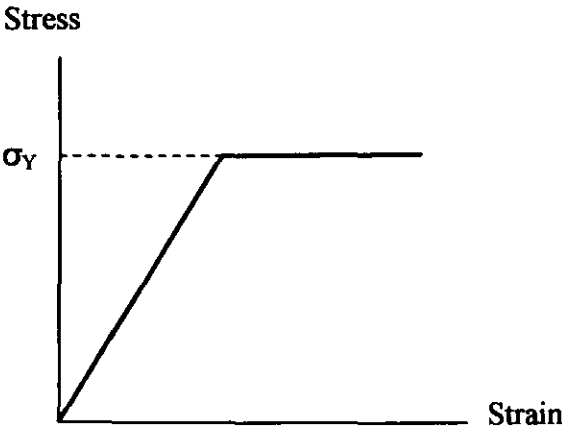
Fig. 6.11 Elastic/perfectly plastic stress-strain behaviour

Yamada calculated the plastic zone size, l_p as:

$$l_p = \frac{1}{\lambda}\left(\alpha_1 - 1 + \sqrt{\alpha_1^2 + 2\alpha_2}\right) \qquad (6.17)$$

where:

$$\alpha_1 = \frac{P\lambda}{\sigma_y b} \qquad (6.18)$$

$$\alpha_2 = \frac{Pa\lambda^2}{\sigma_y b} \qquad\qquad (6.19)$$

$$\alpha_3 = \frac{\sigma_y b}{EI\lambda^3} \qquad\qquad (6.20)$$

and EI is the flexural stiffness of the beam.

For elastic-plastic fracture problems, the path independent J-integral is the most widely recognized fracture parameter. The use of this parameter is not simple due to the difficulty in analytical manipulation. Yamada [6.10] expressed this integral for the double cantilever specimen, including plastic deformation in the adhesive as:

$$J = -2\frac{P}{b}\left[\frac{-Pl_f^2}{2EI} + R_1\right] \qquad\qquad (6.21)$$

where

$$l_f = a + l_p \qquad\qquad (6.22)$$

$$R_1 = \frac{\alpha_3}{6}\left(\lambda l_p\right)^3 + C_1 \qquad\qquad (6.23)$$

$$C_1 = -\left(C_2 + \frac{C_3}{2\lambda^2}\right)\lambda \qquad\qquad (6.24)$$

$$C_2 = \frac{1}{4\lambda}\alpha_3 \qquad\qquad (6.25)$$

$$C_3 = \alpha_3\lambda\left(\alpha_2 - \frac{1}{2}\lambda^2 l_p^2 + \alpha_1\lambda l_p\right) \qquad\qquad (6.26)$$

6.3.2 Determination of the J-integral based on finite element analysis

The path-independent J-integral is given by:

$$J = \int_\Gamma \left[(W\,dy - T_i\frac{\partial u_i}{\partial x}\,ds) \right] \qquad\qquad (3.43)$$

where W is the strain energy density, T_i are components of the traction vector, u_i are the displacement vector components, Γ is the contour clockwise around the crack tip and ds is the increment of arc length along the contour Γ.

The J contour was applied around the crack tip of the double cantilever beam (DCB) specimen as shown in Figure (6.12).

Non-linear analyses including plastic behaviour of the adhesive, were carried out to compute the stresses and displacements in the DCB joints. Then a command file (Appendix D) was used to compute the stresses, strains and displacements along the path Γ. The differentiation in the second term in Equation (3.43) was calculated numerically by shifting the path a small amount in the X-direction. Various crack lengths were used to determine the J value as a function of the crack length.
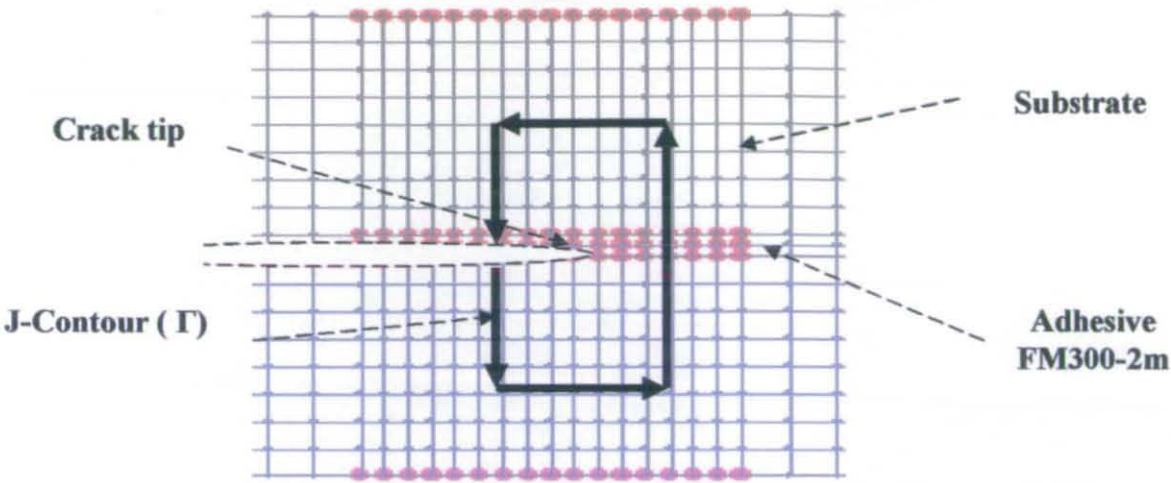
Fig. 6.12 J-Contour around the crack tip in the DCB joints model.

6.3.3 J-integral results

Based on the analytical method (BEPF) and numerical method (J-integral) presented above, J was calculated at different crack lengths. A tensile (Mode I) displacement was applied at the cracked end of the sample. The displacement applied was 1.8 mm and 0.6 mm for IM7/8552 and mild steel joints respectively. A plot of these results is shown in Figures (6.13) and (6.14) for IM7/8552 and mild steel joints respectively.
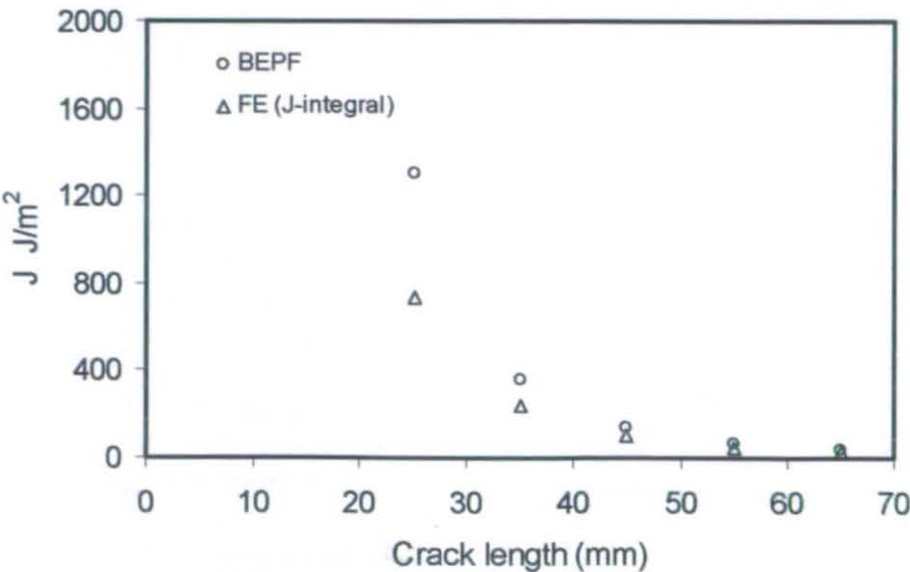
Fig. 6.13 J-integral against the crack length for CFRP joints.

135
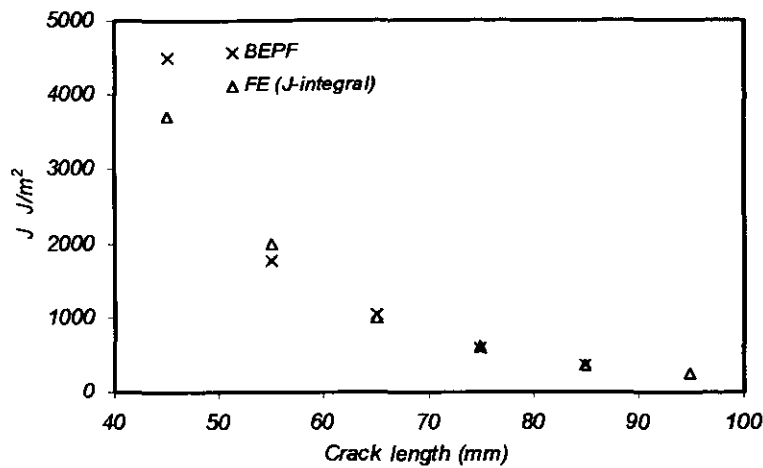
Fig. 6.14 J-integral against the crack length for mild steel joints.

These plots show almost the same trend. Therefore, the BEPF model was found to be in good agreement with the finite element analyses. Throughout this work, the BEPF model will be used to analysis the experimental results in term of J-integral.

Figures (6.15), (6.16) and (6.17) show the parameters of fracture G and J as functions of crack length calculated at RT, 90°C and 120°C respectively. It is seen clearly that; as the crack length increases the values of G and the J-integral converge, this is an indication that the plastic zone size diminishes with crack length. However large variations between G and J are observed as temperature increases. This is due to the increase in plasticity with temperature for a given stress level.
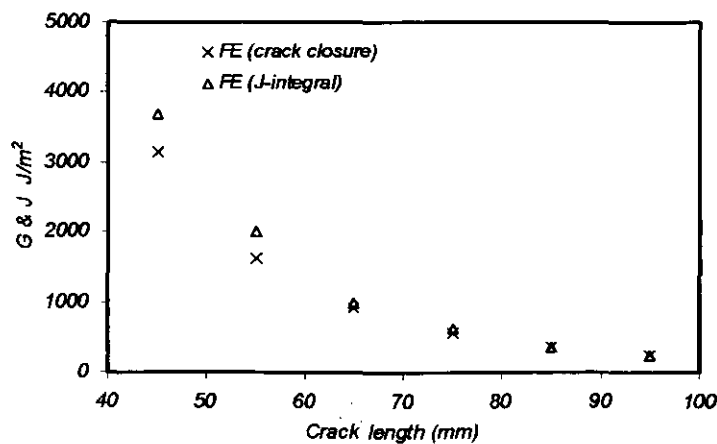
Fig. 6.15 G and J against the crack length for mild steel joints at RT.
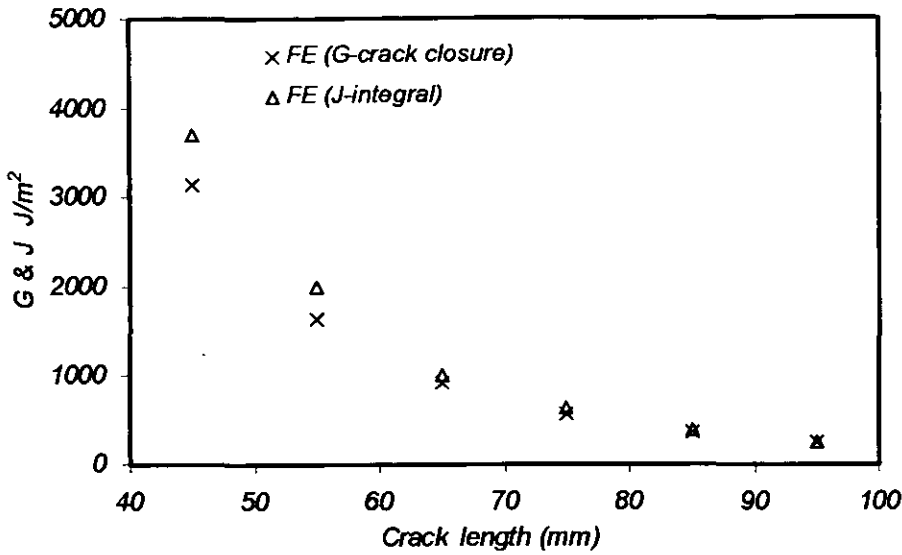
Fig. 6.16 G and J against the crack length for mild steel joints at 90°C.
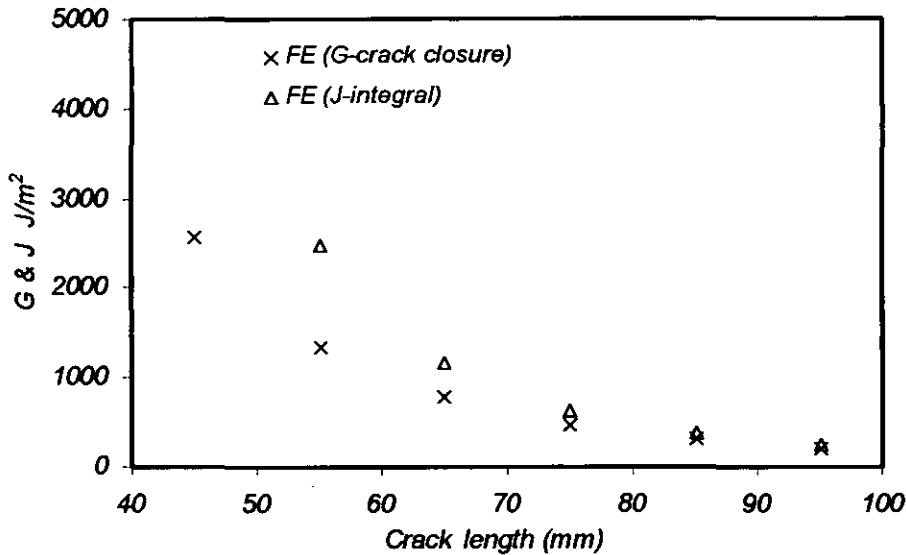
Fig. 6.17 G and J against the crack length for mild steel joints at 120°C.

6.4 Determination of creep parameters

Methods of determining the various parameters have been discussed in chapters (4) and (5). C^*-integral, $C(t)$, C_t and $C(t)_{avg}$ were defined and shown to characterize the fracture process under creep and fatigue conditions. These parameters can be obtained analytically for very limited geometry. In this section, methods used for calculating the value of these creep parameters for DCB joints will be presented.

137

6.4.1 Reference stress method

This method is based on the procedure used to obtain the plastic solution of the J contour integral and results in an expression of the form [6.11]:

$$C^* = \sigma_o \dot{\varepsilon}_o \; b \left[1 - \frac{a}{b} \right] h_1 \left(a / b, n \right) \left[\frac{P}{P_o} \right]^{n+1} \tag{6.27}$$

where h_1 is a non-dimensional function of crack length, a, specimen width, b, and creep exponent, n. If h_1 functions are not available, C^* can be estimated using the reference stress technique [6.11]:

$$C^* = \mu \sigma_{ref} \dot{\varepsilon}_{ref} \left[\frac{K}{\sigma_{ref}} \right]^2 \tag{6.28}$$

where $\mu = 1$ for plane stress conditions and 0.75 for plane strain conditions. The reference strain rate is calculated either from a creep law or from a stress rupture law of the form:

$$t_{rup} = Z \sigma^{-g} \tag{6.29}$$

where Z and g are material constants. The reference strain rate is then given by:

$$\dot{\varepsilon}_{ref} = \frac{\varepsilon_f}{t_{rup}} \tag{6.30}$$

where ε_f is the uniaxial creep ductility. Once a steady state distribution of damage has developed ahead of the crack tip, creep crack growth rate can be described by a law of the form:

$$\dot{a}_{ss} = D \, \dot{C}^{\phi} \qquad (6.31)$$

where the constants D and ø can be based on experimental crack growth data or can be estimated from uniaxial creep and rupture data using a model of the cracking process [6.12].

Based solely on creep rate data:

$$D = (n+1)\frac{\dot{\varepsilon}_o}{\dot{\varepsilon}_f}\left[\frac{1}{I_n \sigma_o \dot{\varepsilon}_o}\right]^{n/(n+1)} r_c^{\,1/(n+1)} \qquad (6.32)$$

Based on creep rate data given by Equation (6.32) and stress rupture data given by Equation (6.29):

$$D = \frac{(n+1)}{n+1-g}\frac{\dot{\varepsilon}_o}{\dot{\varepsilon}_f}\left[\frac{1}{I_n \sigma_o \dot{\varepsilon}_o}\right]^{g/(n+1)} r_c^{\,1/(n+1)} \qquad (6.33)$$

$$\phi = \frac{g}{n+1} \qquad (6.34)$$

where I_n is a non-dimensional factor which is a function of n and state of stress [6.13], r_c is the size of the creep process zone ahead of the crack tip, which can usually be taken to

equal the material grain size, and ε_f^* is the creep ductility appropriate to the state of stress at the crack tip. For plane stress conditions this is usually taken as the uniaxial creep ductility, ε_f, and for plane strain conditions as $\varepsilon_f/50$ [6.14].

Alternatively, when there is insufficient data to evaluate D and $\emptyset$ from Equations (6.35) and (6.36) and experimental values have not been determined, the following approximate expressions can be employed [6.14]. For plane stress conditions:

$$\dot{a}_{ss} = \frac{3C^{*0.85}}{\varepsilon_f} \qquad (6.35)$$

and for plane strain loading,

$$\dot{a}_{ss} = \frac{150C^{*0.85}}{\varepsilon_f} \qquad (6.36)$$

where ε_f is inserted as a fraction and C^* has unit MJ/m^2h to give $\dot{a}_{ss}$ in mm/h.

6.4.2 Experimental determination of the creep parameter C^*

As discussed in section (4.2), experimentally we are measuring the crack length and displacement as function of time. The next step is the calculation of the creep parameter (C^*) as a function of the crack propagation rate and displacement rate based on the following relationship [4.11]:

$$C^* = \frac{P\dot{u}}{B(W-a)}\left(1-\frac{a}{W}\right)\frac{n}{n+1}\eta \qquad (4.9)$$

where a is crack length, W is the width, b is the thickness, P is load, $\dot{u}$ is the creep load-line displacement rate and n is material constant. The Eta function (η) for DCB joint is giving by:

$$\eta = \frac{1 - a/W}{a/W} \qquad (4.10)$$

6.4.3 Determination of the creep parameter C_t

It is convenient to have a single expression for estimating C_t for conditions ranging from small-scale to extensive creep. An approach discussed in section (4.4)) for estimating C_t is through the following equation:

$$C_t = (C_t)_{SSC} + C^* \qquad (6.26)$$

Where:

$$(C_t)_{SSC} = \frac{P\dot{u}_c}{bW}\frac{F'}{F} \qquad (4.21)$$

The value of F given by Equation (5.6) can be expressed as F *(a/W)* for DCB joint, resulting in an equation of the following form:

$$F = 1.6971 + 174.49(\frac{a}{W}) + 13.366(\frac{a}{W})^2 - 12.047(\frac{a}{W})^3 + 4.1151(\frac{a}{W})^4 \qquad (6.37)$$

6.4.4 Determination of the creep parameter $(C_t)_{avg}$

Methods of determining $(C_t)_{avg}$ include those that are more suitable for test specimens in which both load and load-line deflection behaviour with time are measured. This was presented in section (5.8) and given by the following equation:

$$(C_t)_{avg} = \frac{\Delta P \Delta u_c}{BWt_h} \frac{F'}{F} - C * \{(F' / F) / \eta - 1\}$$ (5.5)

6.4.5 Determination of the C*-Integral based on finite element analysis

The path-time independent C*-integral is given by:

$$C^* = \int_\Gamma W^* dy - T_i \left\{ \frac{\partial \dot{u}_i}{\partial x} \right\} ds$$ (4.2)

Where

$$W^* = \int_0^{\dot{\varepsilon}_{ij}} \sigma_{ij} d\dot{\varepsilon}_{ij}$$ (4.3)

Γ is a line contour shown in Figure (6.18) taken counter clockwise from the lower crack surface to upper crack surface, W* is the strain energy rate density associated with the point stress, σ_{ij} and strain rate, $\dot{\varepsilon}_{ij}$. T_i is the traction vector defined by the outward normal, n_j along Γ and $\dot{u}_i$ is the displacement rate vector and s is the arc length along the contour.

Non-linear analysis was carried out to compute the stresses and displacements in the DCB joints. A command file (Appendix *E*) was used to compute the stresses, creep strains and displacements along the path Γ at time t_1. Another command file computed the components in Equation (4.2) that varied with time at t_2. The differentiation in the second term in Equation (4.2) was calculated numerically by shifting the path a small amount in the x-direction. An Excel macro was written using VBA to calculate the creep parameter C*. Various crack lengths were used to determine the C* value as function of the crack length.

142
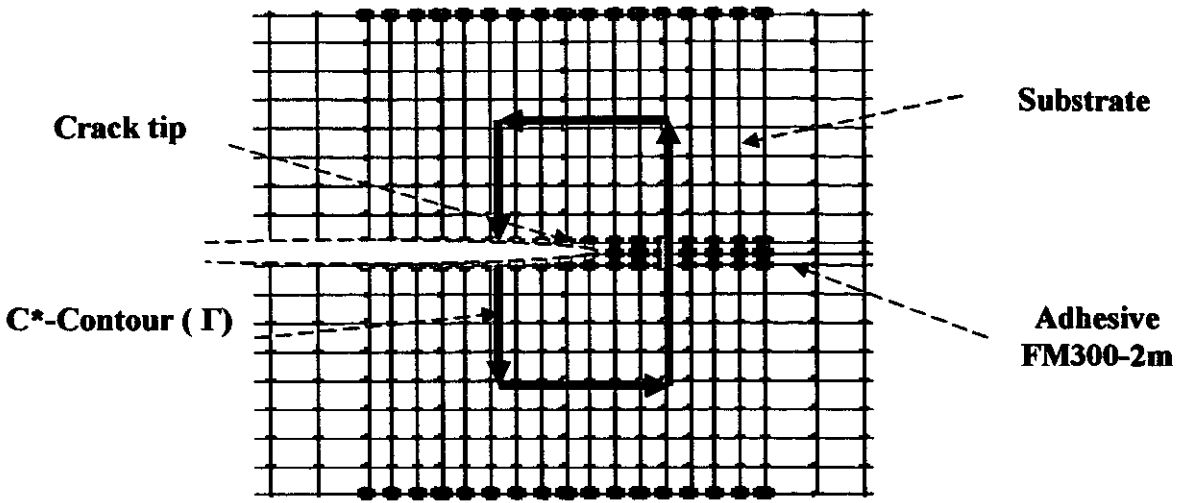
Fig. 6.18 J-Contour around the crack tip in the DCB joints model.

6.4.6 Creep parameters results

The results of the creep parameter, C^* calculated using the finite element and experimental method will be presented and compared. Other parameters such as C_t and $(C_t)_{avg}$ will be shown later during the analysis of the experimental work.

In LUSAS the creep power law is given by:

$$\varepsilon = Cq^{n_1}t^{m_1} \tag{6.38}$$

where ε is the creep strain, q is the von Mises equivalent stress, t is the time and C, n_1 and m_1 are material parameters. A method was required to find the optimum set of model parameters to represent the experimental data. An Excel data sheet was programmed to find the best parameters to correlate the experimental strain and predicted strain, based on Equation (6.38). Results are tabulated in Table (6.1) for joints tested at 90°C subjected to 1200N and joints tested at 120°C subjected to 600 N.

Table (6.1) Power low creep constants optimized for adhesive FM300-2M (stress (MPa) and time(S))

Temperature	C	n_1	m_1
90 °C	2E-6	1.6	0.71
120 °C	8E-8	1.4	1.39

Based on the finite element method the fracture parameter, C* was calculated at different crack lengths. The applied load was the same as the applied load used in the experiments. Figures (6.19) and (6.20) shows the experimental and numerical calculation of the creep parameter, C* against crack length for mild steel joints bonded with FM300-2M adhesive tested at 90°C and 120°C respectively. Finite element has satisfactory agreement with joints tested at 120°C albeit with some scatter, while at 90°C agreement is poor at short crack length but good at longer length. This may possibly be explained by blunting of the crack at the beginning of the tests, but further work is required to confirm this.
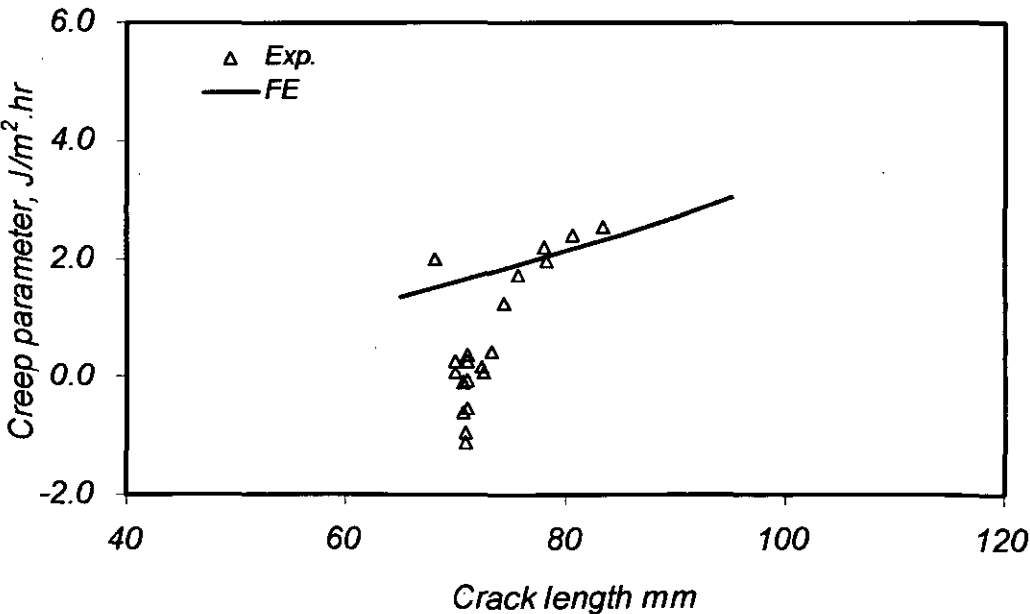
Fig. 6.19 Creep parameter, C* against crack length at 90°C.
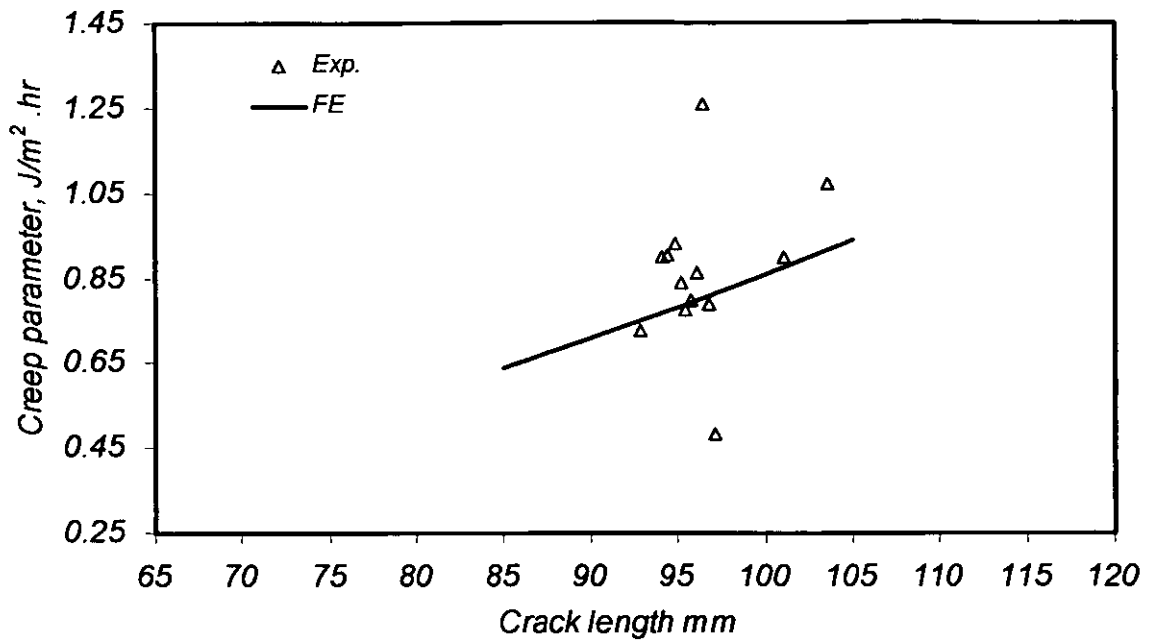
Fig. 6.20 Creep parameter, C* against crack length at 120°C.

6.5 References

[6.1]   Mostovoy, S. and Ripling, E.J., "Flow Tolerance of a Number of Commercial and Experimental Adhesives", In Adhesion Science and Technology, New Plenum Press, Vol. 9B, 1975, pp.64-80.

[6.2]   Davies, P., "Protocols for Interlaminar Fracture Testing of Composites", European Structural Integrity Society: Polymer and Composites Task Group, 1992.

[6.3]   Kanninen, M.F., "An Augmented Double Cantilever Beam Model for Studying Crack Propagation and arrest", International Journal of Fracture, Vol. 9, 1973, pp.83-92.

[6.4]   Abo-Hamda, M.M., Megahed, M.M. and Hammouda M.M., "Fatigue Crack Growth in Double Cantilever Beam Specimen with an Adhesive Layer", Engineering Fracture Mechanics, Vol. 60, 1998, pp.605-614.

[6.5] Chang, D.J., Muki, R. and Westman R.A., "Double Cantilever Beam Models in Adhesive Mechanics", Int. J. Solids Structural, Vol. 12, 1976, pp.13-26.

[6.6] Chow, C.L., Woo, C.W. and Sykes, J.L., "On the Determination and Application of COD to Epoxy-bonded Aluminium Joints", Journal of Strain Analysis, Vol. 14, 1976, pp.37-42.

[6.7] Erpolat, S., Ashcroft, I.A., Crocombe, A.D. and Abdel-Wahab, M.M., "On the Analytical Determination of Strain Energy Release Rate in Bonded DCB Joints", J. Eng. *Fract. Mech.*, Vol. 71, 2003, pp.1393-1401.

[6.8] Irwin, G. R., "Fracture", Handbuch der Physik, Vol. 5, Springer-Verlag, 1958, pp550-551.

[6.9] Sethuraman R. and Maiti S.K, "Finite Element Based Computation of Strain Energy Release Rate by a Modified Crack Closure Integral" J. Eng. Fracture Mechanics, 1988, pp.227-231.

[6.10] Yamada, K., Cao Q. and Okado, N., "Fatigue Crack Growth Measurements under Spectrum Loading", Engineering Fracture Mechanics, Vol. 66, 2000, pp.483-497.

[6.11] Nuclear Electric, "R5 Assessment Procedure for High Temperature Response of Structures", Report R5, Nuclear Electric Ltd, UK, 1990.

[6.12] Nikbin, K.M., Smith, D.J. and Webster, G.A., "Prediction of Creep Crack Growth from Uniaxial Data", Proceeding of the Royal Society of London, A396, 1984, pp.183-197.

[6.13] Hutchinson, J.W., "Singular Behaviour at the End of a Tensile Crack in a Hardening Material", Journal of the Mechanics and Physics of Solids, Vol.16, 1968, pp.13-31.

[6.14] Nikbin, K.M., Smith, D.J. and Webster, G.A., "Modes of Failure under Creep/Fatigue Loading of a Nickel-Based Superalloy", Journal of material science, Vol.20, 1985, pp.2471-2476.

CHAPTER 7

QUASI-STATIC AND CREEP PROPERTIES OF FM300-2M ADHESIVE

7.1 Introduction

The ability to model the mechanical behaviour of adhesively bonded structures using stress analysis techniques, especially finite elements analysis methods, is critical in determining the response of a advanced engineering structure to the loads likely to be experienced in service. The quality and reliability of the results obtained from such analyses are controlled by the quality of the material properties data that can be obtained.

In this project it was necessary to generate an extensive range of experimental data for the adhesive FM300-2M. This chapter presents the experimental work carried out to obtain the material properties of FM300-2M epoxy adhesive. This can be summarized into the following steps:

a) Conducting quasi-static tests to obtain the mechanical properties of FM300-2M adhesive. This was carried out at different test rates, namely 0.1, 1 and 10 mm/min and at different temperatures, namely room temperature (22 ±1°C), 90°C and 120°C.

b) Designing and constructing a creep test in order to generate creep test results that can be used to calculate the creep parameter, C* for adhesively bonded joints. This was carried out at room temperature (22 ±1°C), 90°C and 120°C.

7.2 Sample manufacture

The adhesive used in this work was the toughened epoxy FM300-2M supplied by Cytec. The adhesive is supplied as a 0.2 mm thick film adhesive. The process of manufacturing

148

quasi-static and creep test samples involved layering adhesive sheets, of dimension 120x 120mm, followed by curing and machining of the dumbbell shapes. The equipment used for curing the adhesive was made from three parts as shown in Figure (7.1). Part one is the mould with thickness 3 mm while parts 2 and 3 are the upper and lower plates respectively. The plates were covered with PTFE to prevent adhesion during cure. On the lower plate, 25 layers of the adhesive were added and rolled flat individually. The adhesive was kept at 55°C during this process. This helps to release trapped air and ensure a pore-free sample. The mould was then placed over the adhesive and covered with the upper plate. This sandwich arrangement was then cured for 2.5 hours at 120°C with a pressure of 0.28 MPa.
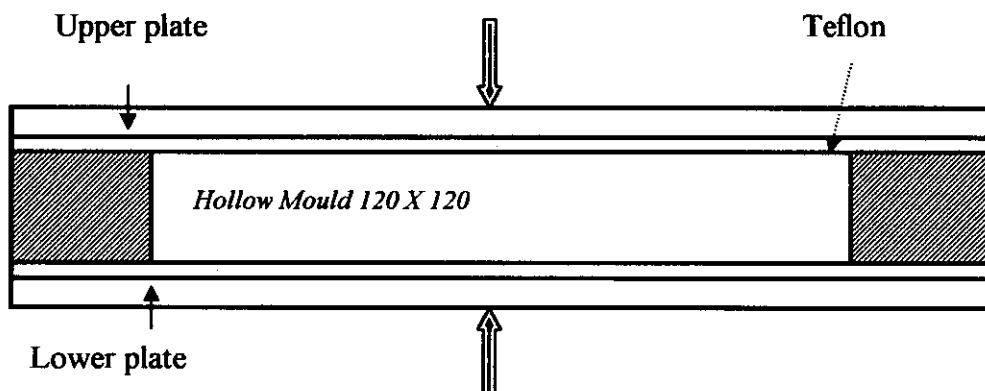
Fig. 7.1 Schematic drawing of mould used in manufacturing bulk adhesive.

The resulting adhesive plate was trimmed to the sizes shown in Figures (7.2) and (7.3). The sample shown in Figure (7.2) was used to find the mechanical properties and investigate rate effects at different temperatures while the sample shown in Figure (7.3) was used to generate the creep data at different temperatures. In the creep samples, shown in Figure (7.3), two 4 mm holes were drilled in the end tabs to enable them to be fixed in the creep rig. The final step was to use fine grade grit to remove any surface defects within the gauge length.

H=20 mm   b=10 mm
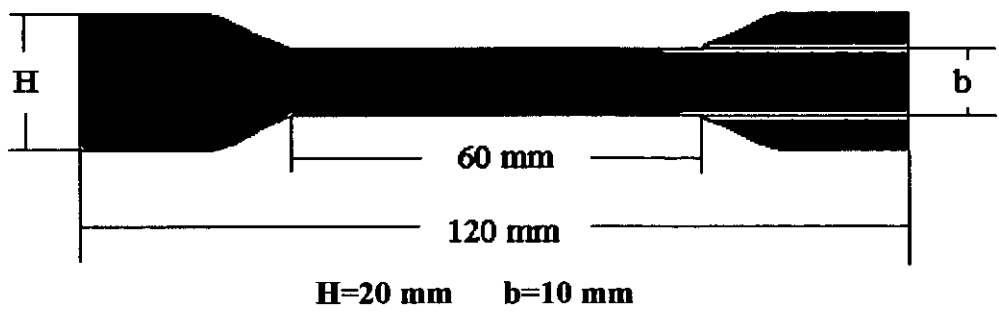
Fig. 7.2 Bulk adhesive sample used for quasi-static tests.

H = 12 mm   b = 3 mm   d = 4 mm
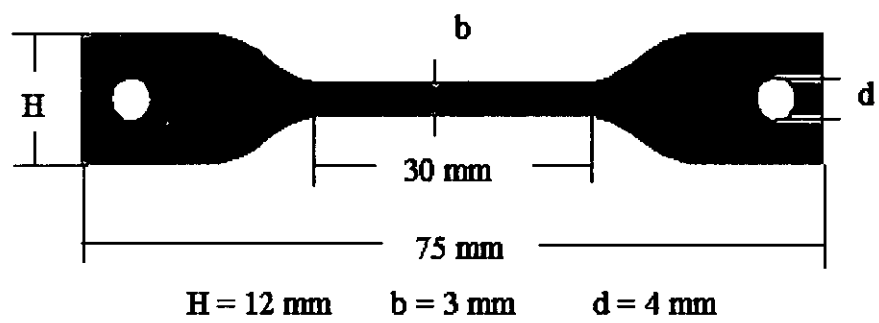
Fig. 7.3 Bulk adhesive sample used for creep tests.

7.3 Test procedures and results

7.3.1 Quasi-static test procedure

All tests were carried out using a servo-mechanical test machine fitted with a 10 KN load cell and temperature cabinet. A calibrated extensometer was used to measure the axial strain in the gauge length of the tensile test specimen shown in Figure (7.2). The

extensometer used had a gauge length of 25 mm and a full scale range of 100% strain. To calculate Poisson's ratio, both axial and transverse strain measurements are required. Care was taken not to affix the extensometer so firmly that the knife edge indented the sample. During testing, load and strain were logged using a computer based system. Data was imported into Microsoft's Excel in order to plot the stress-strain curves.

The dumbbell samples were used to investigate the effect of loading rate and temperature on the mechanical properties of the adhesive. The crosshead rates used were 0.1, 1 and 10 mm/min and the temperatures were RT, 90°C and 120°C. A minimum of three tests were preformed at each condition.

Given below is an outline of the test procedure used for tensile bulk specimen testing:

1) The width, thickness and effective gauge length (the length of the straight section) of the specimens to be tested were measured.

2) The load cell and extensometer were calibrated.

3) Specimens tested at elevated temperature were placed in the temperature cabinet prior to testing to allow them to stabilise at the test temperature.

4) Before each test, the extensometer was fitted to the specimen. The specimen was then placed in the grips and adjusted to obtain good alignment.

5) After the temperature in the temperature cabinet had stabilised, the extensometer was balanced and the test started.

6) Once the test had finished the test data was stored in an Excel spread sheet.

7.3.2 Quasi-static test results

Figures (7.4), (7.5) and (7.6) show the stress strain response of FM300-2M adhesive with different rates tested at room temperature, 90°C and 120°C respectively. For all

151

tests the elastic modulus (E), ultimate tensile stress (UTS) and yield stress (σ_y) were determined. The yield stress was defined [7.1] by constructing two straight lines, one with the same gradient as the Young's modulus and passing through the origin, the second with the same gradient as the plastic region of the curve. A line perpendicular to the stress-strain curve, which passed through the intersect of these two lines, was drawn. The value at which the stress-strain curve was intersected was taken as the yield stress. The average value for each case was determined and a summary of the results can be seen in Table (7.1). The Poisson's ratio (μ) values were determined and had a mean value of (0.38±0.1).
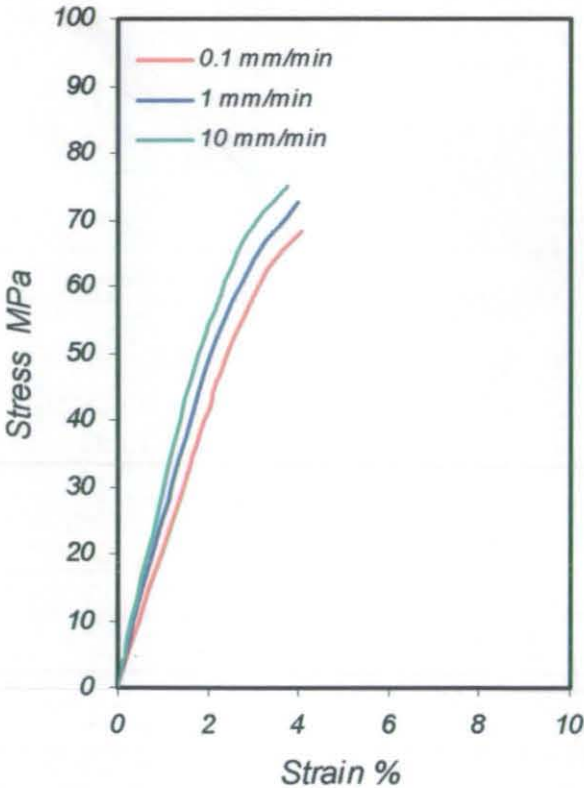
Fig. 7.4 Stress strain response rate test of FM300-2M adhesive tested at RT.
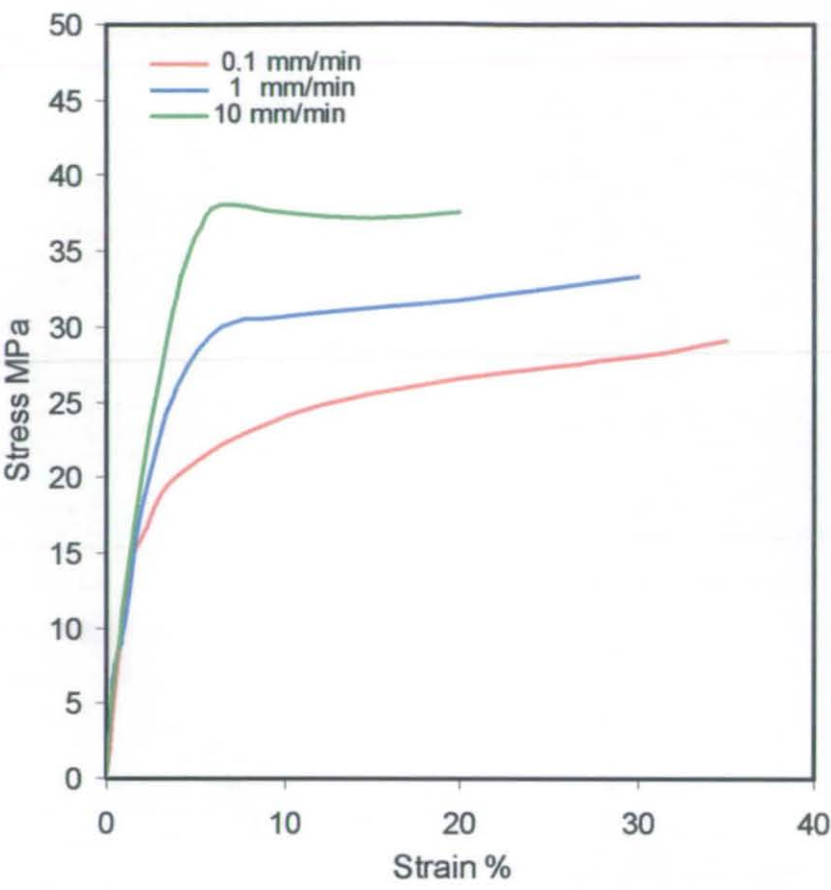
Fig. 7.5 Stress strain response rate test of FM300-2M adhesive tested at 90°C.
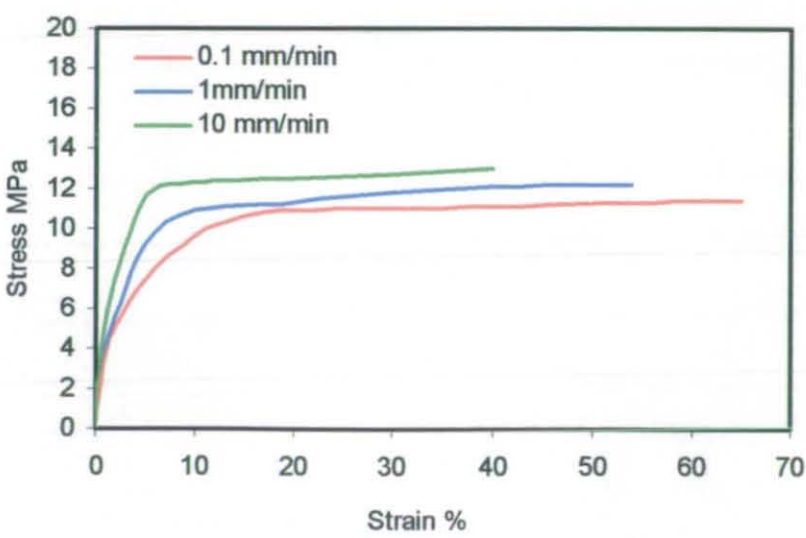
Fig. 7.6 Stress strain response rate test of FM300-2M adhesive tested at 120°C.

Table (7.1) Summary of results from constant crosshead speed tests on FM300-2M adhesive dumbbells

Temperature °C	Test rate mm/min	Elastic modulus GPa	Yield stress MPa	UTS MPa
RT	0.1	2.418 ± 0.06	45 ± 2	68 ±3
RT	1	2.589 ± 0.12	49 ±1.5	72±2.5
RT	10	2.72 ± 0.1	55 ±2.5	75 ±3.2
90	0.1	1.462 ±0.15	19 ±1.6	27.73 ± 3.5
90	1	1.588 ± 0.12	21 ±3.2	32.73 ±2.4
90	10	1.80 ± 0.09	30 ±2.6	37.74 ±2.5
120	0.1	0.592 ± 0.07	6.4 ±2.1	10.63 ±1.1
120	1	0.632 ± 0.05	7.1 ±1.8	11.62 ±1.9
120	10	0.705 ± 0.06	10.2 ±2.3	13.37 ±2.2

Plots of modulus, UTS and yield stress can be seen in Figures (7.7), (7.8) and (7.9) respectively. These figures clearly show that as the loading rate increases the elastic modulus, ultimate tensile stress and yield stress are increases.

154
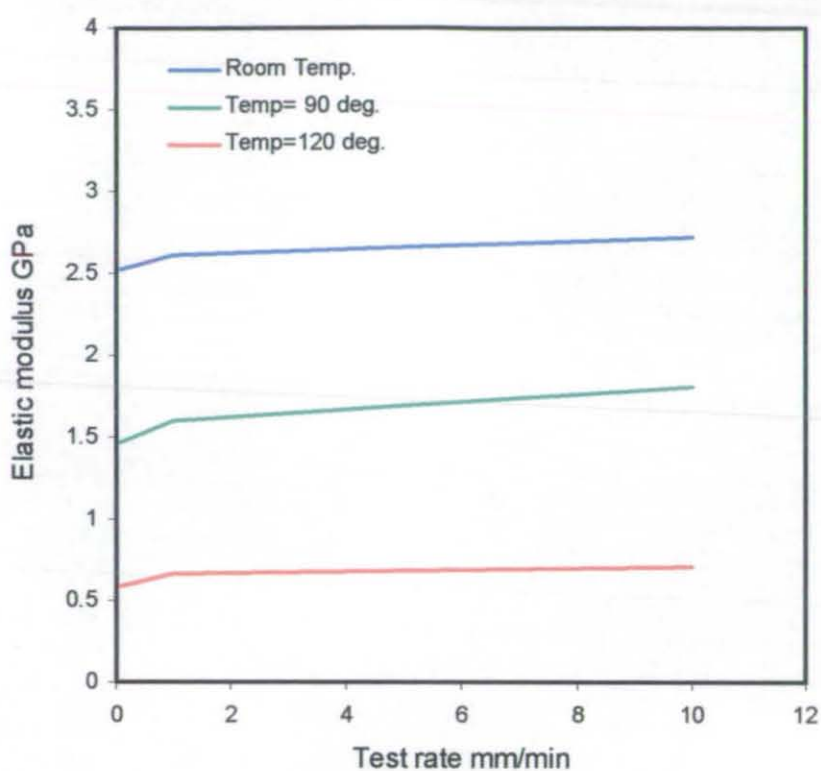
Fig. 7.7 Modulus variation as a function of the loading rate for FM300-2M Adhesive.
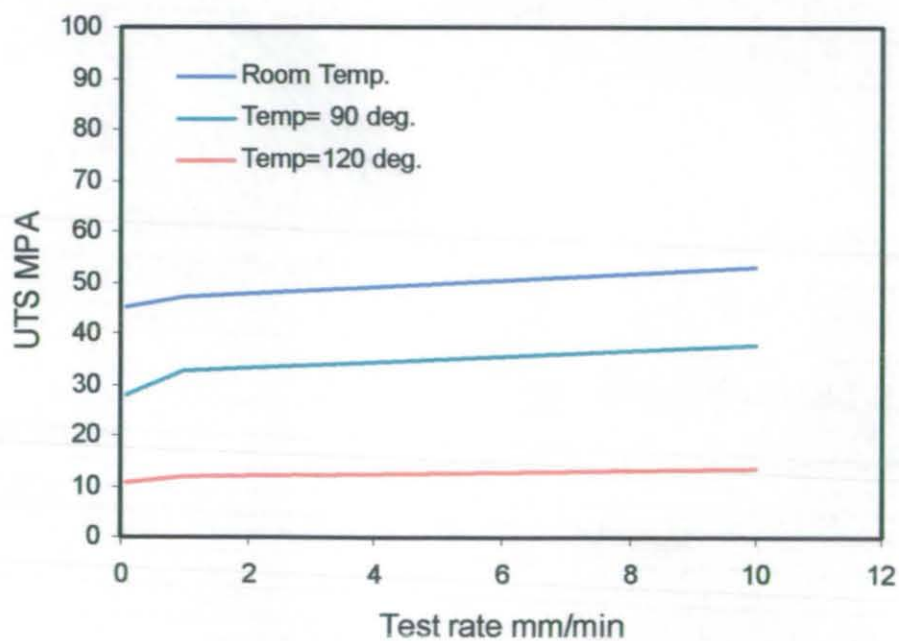
Fig. 7.8 Ultimate tensile stress variation as a function of the loading rate for FM300-2M adhesive.
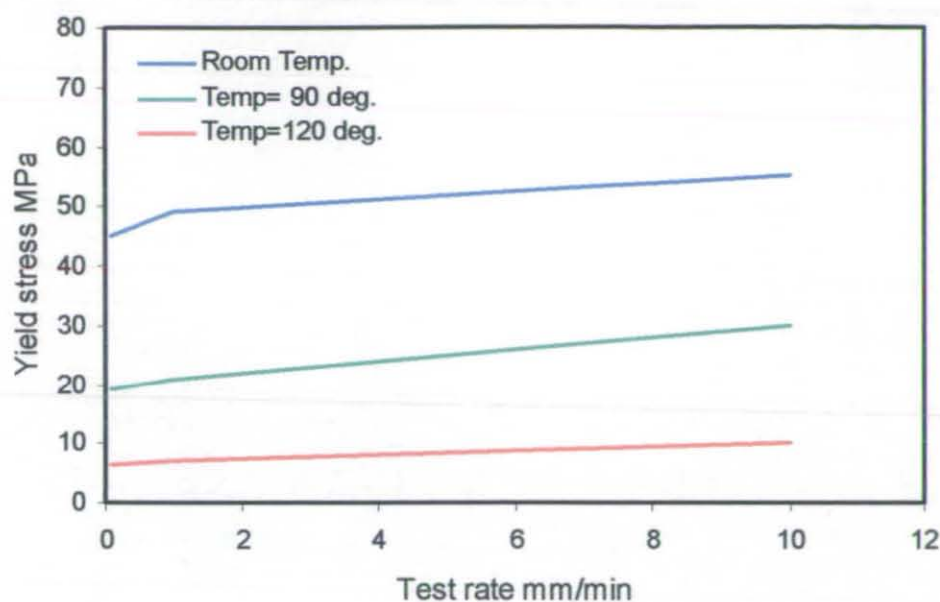
Fig. 7.9 Yield stress variation as a function of the loading rate for FM300-2M adhesive.

7.3.3 Discussion of quasi-static test results

In this investigation efforts have been made to study the effect of the applied rates and temperature on FM300-2M epoxy adhesive. It is seen that, increasing rate and temperature has a significant effect on the mechanical properties of the adhesive. By increasing the loading rate from 0.1 to 10 mm/min, the elastic modulus value increases by 12.4%, 23.1% and 7.3% for samples tested at RT, 90°C and 120°C respectively. Also the UTS value increases by 17.9%, 36.1% and 25.7% and yield stress increases by 22.2%, 57% and 61.1% for samples tested at RT, 90°C and 120°C respectively.

Increasing the test temperature from RT to 90°C and 120°C decreases the elastic modulus value by 53.5% and 83.3% respectively, decreases the UTS value by 32.4 % and 75.4% respectively and decreases the yield stress value by 53% and 84% respectively. This effect can be attributed to the viscoelastic nature of the polymeric

materials used in the adhesive. These arguments are in agreement with previous studies

[7.1-7.2] in obtaining the mechanical properties of epoxy film adhesives.

These results indicate that designers should consider the effect of temperature and

loading rate on the elastic modulus and yield stress during prediction of the failure of

bonded joints. The results also indicate that decreasing the test rate has the same effect

as increasing the temperature in term of the mechanical properties.

7.3.4 Creep tests

The creep rig shown in Figure (7.10) was designed to perform the creep tests at different

temperatures. The specimen is attached by pins to the two grips. The specimen is then

loaded by placing weights on a pan hanging from the other end of the beam. Due to the

lever action the load carried by the specimen is four times that transmitted through the

weight-pan. A linear variable differential transformer (LVDT) is used as a displacement

transducer. The LVDT is attached to the apparatus to measure directly the extension of

the specimen. The reading from the LVDT is fed into a computer and logged on an

Excel spreadsheet. The interval at which the readings are taken can be altered. The use

of the Excel spreadsheet allows easy manipulation of data

A Digital calliper was used to measure the dimensions of each specimen prior to

testing. In order to test the sample at elevated temperatures, a fan oven was used to

house the test rig. The oven was fitted with a controller that enabled the temperature to

be controlled to ±1°C. The control thermocouple was placed close to the test specimens.

The oven had a window that allowed confirmation of the LVDT results via a travelling

microscope.
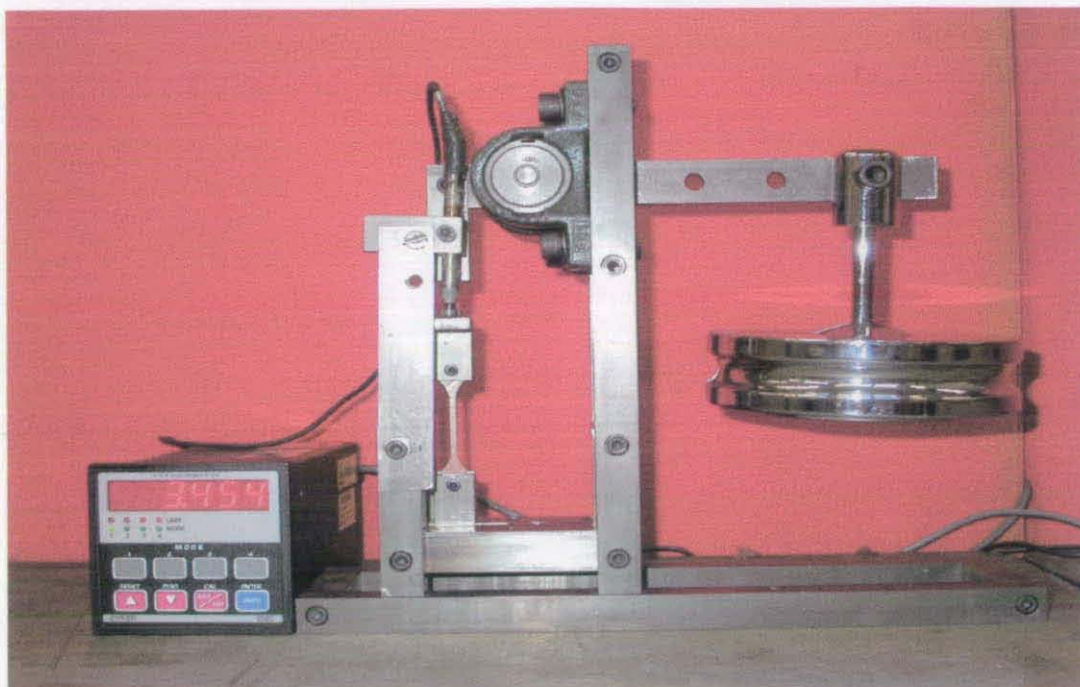
Fig.7.10 Creep rig.

7.3.5 Creep test experimental procedure

1) The width, thickness and effective gauge length (the length of the straight section) of the specimens to be tested were measured.

2) The creep specimen was placed in the testing apparatus using pins. The height of the creep specimen was adjusted so that the beam was approximately horizontal.

3) The LVDT was set up in the testing rig.

4) The applied stress was calculated for each specimen and the corresponding weight added to the weight pan.

5) The LVDT displacement as a function of time was recorded through a computer data acquisition system. Periodically LVDT displacement was checked with the travelling microscope.

6) After testing, the overall length of the tested sample was checked with the LVDT reading.

7) The pin holes were checked for distortion.

8) This procedure was repeated at different levels of stress.

7.3.6 Analysis of creep results

The analysis of creep results was based on standard procedures written for this purpose [7.3-7.5] as follows:

1) The true strain, ε as a function of time, t for each level of stress was plotted. The true strain is given by:

$$\varepsilon(t) = \ln\left(\frac{l_f}{l_o}\right) \qquad (7.1)$$

where

$$l_f = l_o + \Delta l \qquad (7.2)$$

where Δl is the recorded change in length of the specimen and l_o is the measured gauge length. The true stress is given by:

$$\sigma = \frac{P}{A} = \frac{4W}{A} \qquad (7.3)$$

where $W=mg$ and A is the actual or instantaneous area supporting the load.

2) The steady-state creep rate $\dot{\varepsilon}_{ss}$ was calculated from the slope of the best-fit line for each specimen at each stress level.

$$\dot{\varepsilon}_{ss} = \frac{\Delta\varepsilon}{\Delta t} \qquad (7.4)$$

3) Log –log plots of steady-state creep rate against the applied stress were used to find the creep power law constants *A* and *n*.

$$\dot{\varepsilon}_{ss} = A\sigma^n \qquad (7.5)$$

4) The power law constants *A* and *n* were used in the FEA to calculate the creep parameter *C**.

7.3.7 Creep results

Figures (7.11), (7.12) and (7.13) show the displacement-time curves for creep tests at room temperature, 90°C and 120°C respectively.
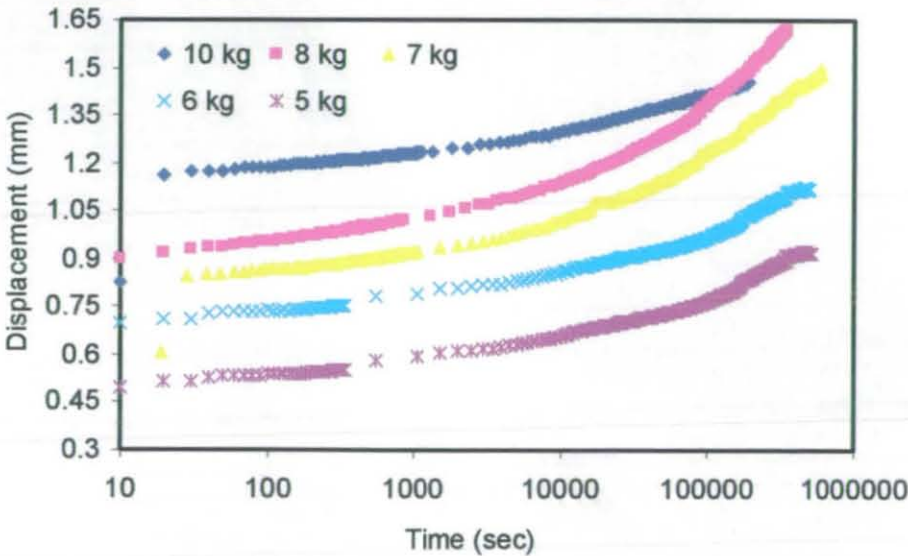
Fig.7.11 Displacement-time curves for creep at RT.
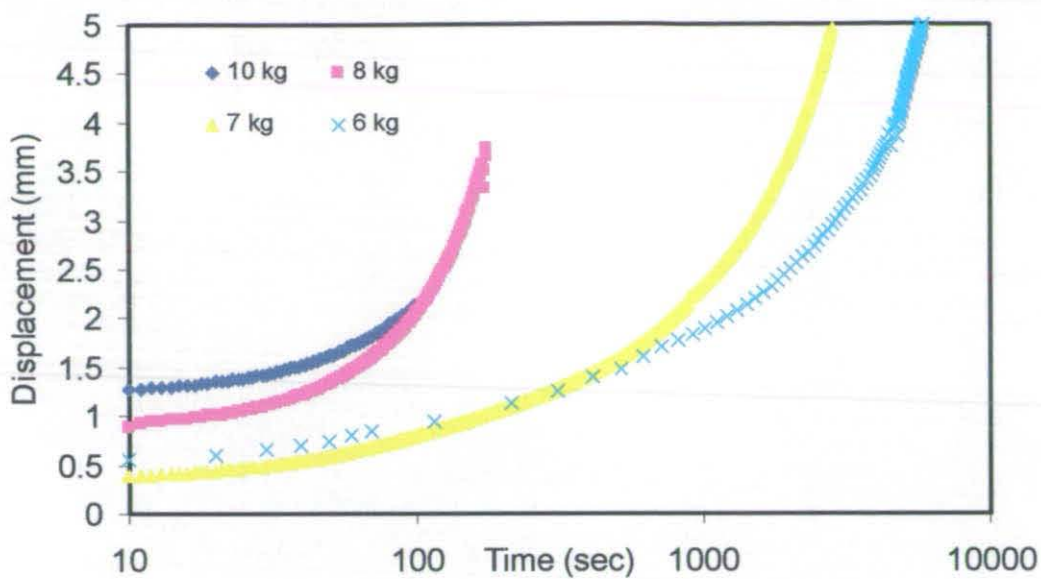
Fig.7.12 Displacement-time curves for creep at 90°C.
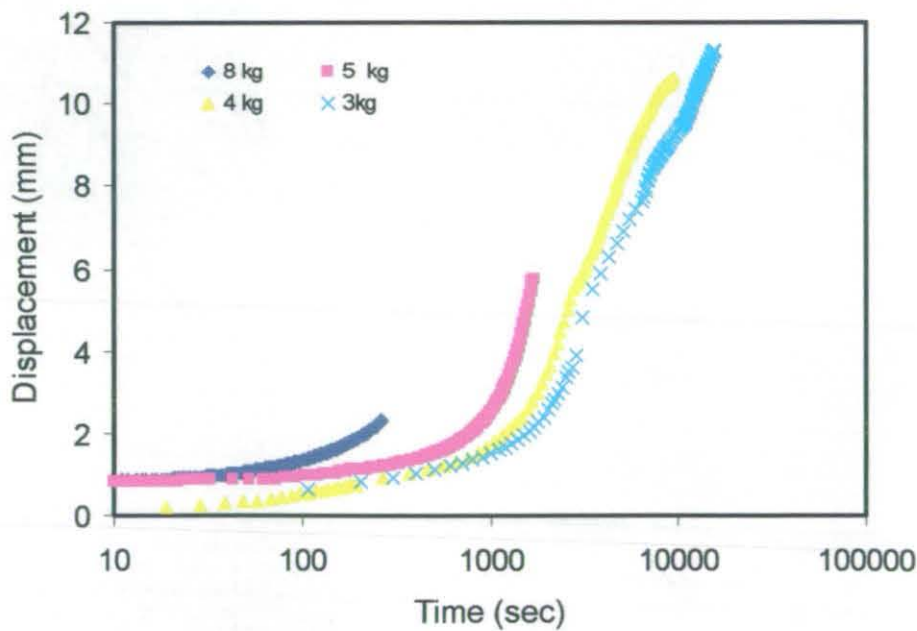
Fig.7.13 Displacement-time curves for creep at 120°C.

Figures (7.14), (7.15) and (7.16) show the strain-time curves for the creep tests at room temperature, 90°C and 120°C respectively.
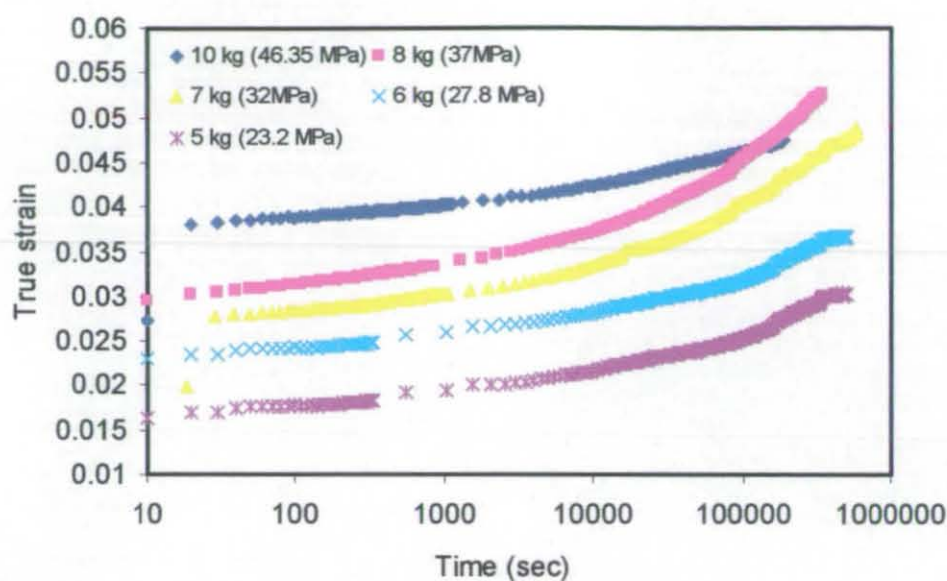
Fig. 7.14 Strain-time curves for creep at RT.
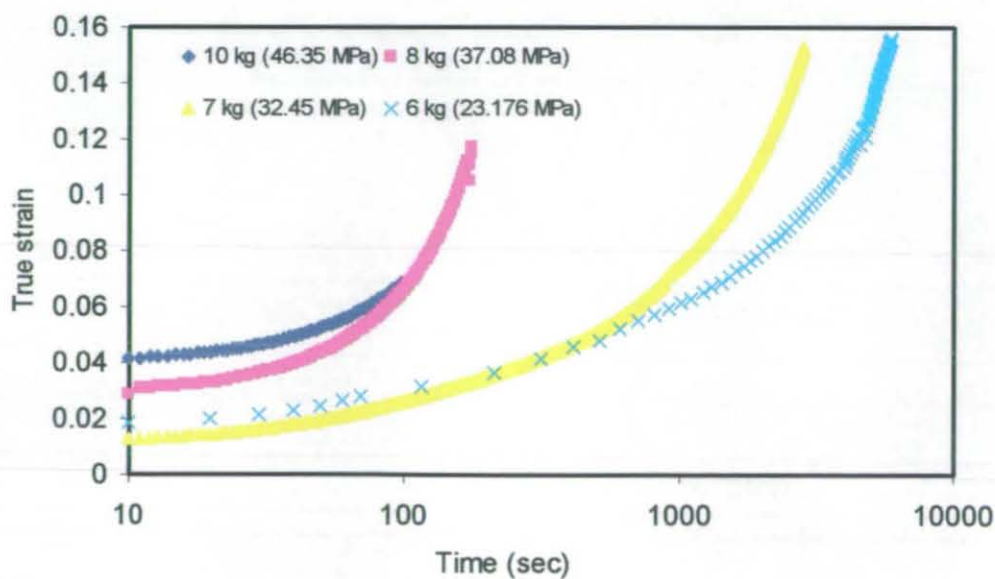
Fig. 7.15 Strain-time curves for creep at 90°C.
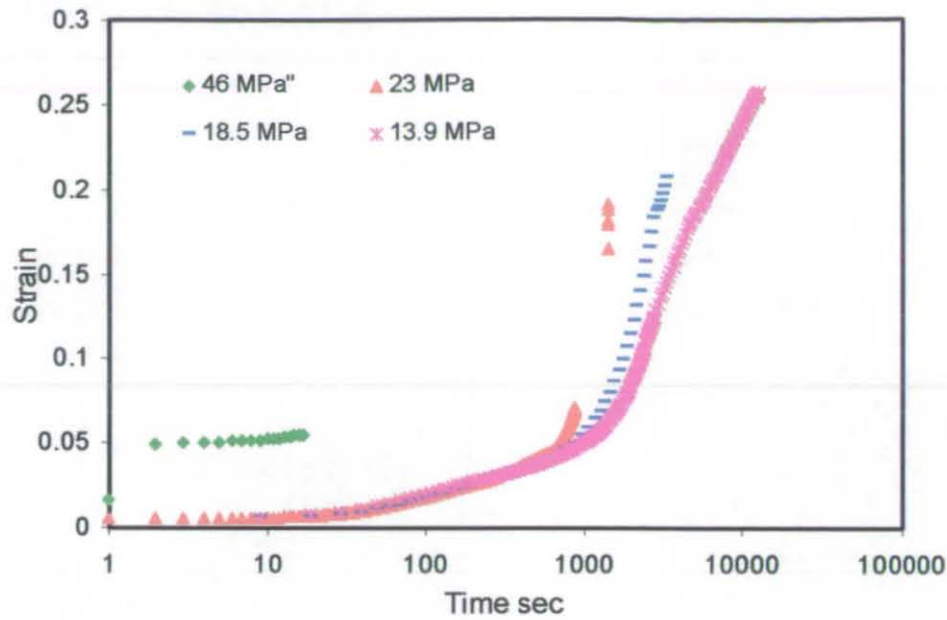
Fig.7.16 Strain-time curves for creep at 120°C.

Log –log plots of steady state creep strain rate against the applied stress at RT, 90 and 120 are shown in figure (7.17), (7.18) and (7.19) respectively.
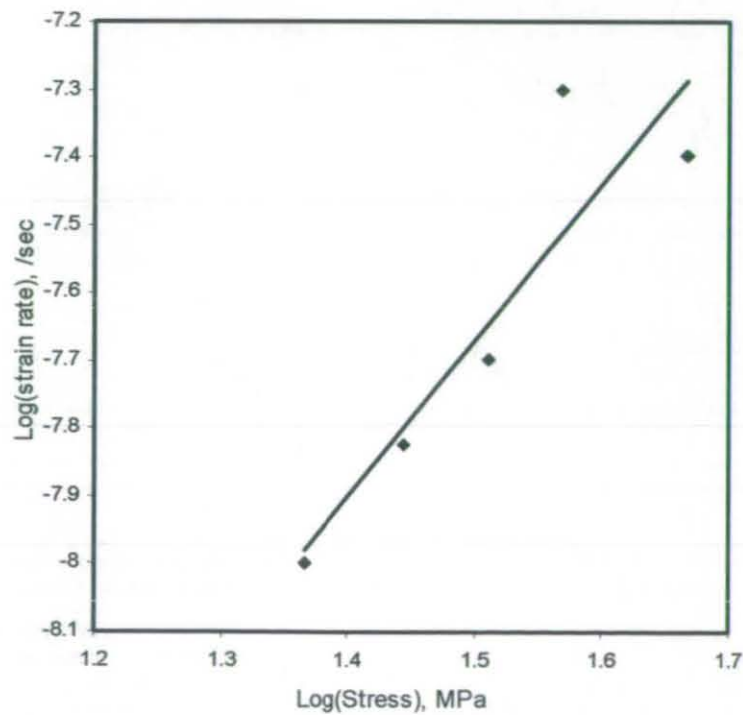
Fig. 7.17 Experimental determination of power-law exponent for creep at RT.
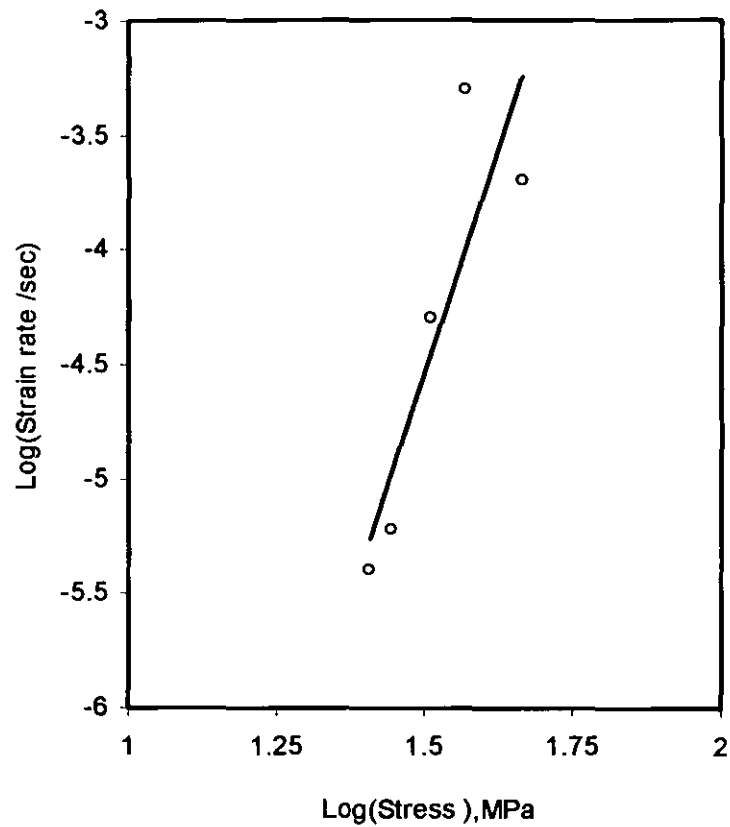
Fig. 7.18 Experimental determination of power-law exponent for creep at 90°C.
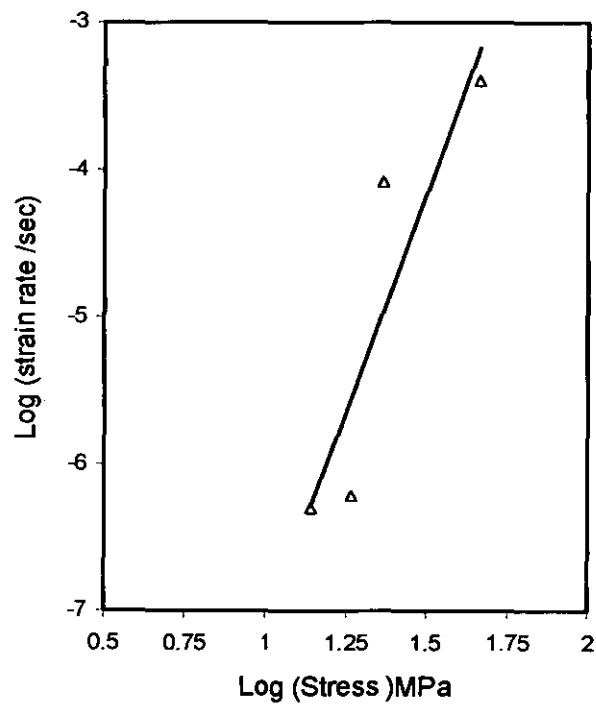
Fig. 7.19 Experimental determination of power-law exponent for creep at 120°C.

Based on the analysis illustrated above, the creep constants in Equation (7.4) at different temperature were determined, and are shown in Table (7.2). These constant are useful in calculating the creep parameters analytically and numerically.

Table (7.2) Power law creep constants for FM300-2M adhesive (Stress (MPa), Strain rate /sec)).

Case	Creep constant (A)	Creep exponent (n)
Room Temp.	7.71×10^{-12}	2.3
90°C	6.00×10^{-17}	7.79
120°C	8.00×10^{-14}	5.96

7.3.7 Discussion of creep test results

In this work efforts have been made to study the effect of creep on FM300-2M epoxy adhesive. It is seen that, increasing temperature has a significant effect on the creep properties of the adhesive. As temperature increased from room temperature the creep rupture time reduced by 89% and 98% for samples tested at 90°C and 120°C respectively. While the creep strain at failure increased by 2.75% and 4.75% for samples tested at 90°C and 120°C respectively. This effect is attributable to the viscoelastic nature of the polymeric materials used in adhesives, which make them susceptible to creep. The creep exponents shown in Table (7.2) are in reasonable agreement with the values seen in previous work [7.6] for similar adhesives, namely FM73 and E27 adhesive. These creep constants are essential in any analytical or numerical investigation of creep or creep fatigue loading.

7.4 Conclusions

The effects of quasi-static and creep loading at different temperatures on the mechanical properties of FM300-2M adhesive have been investigated. The following conclusions were reached.

1) The material properties obtained under tensile and creep loading at different loading rates and temperatures are essential for designers using FM300-2M adhesive or any similar epoxy adhesive.

2) Results show clearly the effect of test rate on the mechanical properties of FM300-2M adhesive. The elastic modulus (E), ultimate tensile stress (UTS) and yield stress (σ_y) increase with the test rate.

3) As the temperature increases, the elastic modulus, UTS and σ_y are significantly reduced, especially at 120°C. This is expected, because of the viscoelastic nature of the adhesive at elevated temperature.

4) Decreasing the test rate has a similar effect to increasing the temperature.

5) Tests show clearly the effect of temperature on the creep process. Increasing temperature from RT to 120°C decreases the creep rupture time by 98% and increases the failure strain by 4.75%. Also the results show the possibility of FM300-2M creeping even at room temperature.

6) It is possible to describe the behaviour of FM300-2M at low temperature as a linear elastic solid; however, plasticity and creep become significant as the temperature increase to 90°C and beyond.

7.5 References

[7.1]   Nelson, L.J., "The Effect of Environment and Loading Rate on the Mechanical Properties of an Epoxy Film Adhesive" University of Bath, July, 1999.

[7.2]   Cheng, Y., Wing, Y. and Sum, "Effect of Substrate Material on Fracture Toughness Measurement in Adhesive Joints", Int. J. of Mechanical Sciences, 43, 2001, pp.2091-2098.

[7.3]   ASTM, Standard D2990, "Test Method for Tensile, Compressive, and Flexural Creep and Creep-Rupture of Plastic", Vol.8, ASTM, Philadelphia, 1999.

[7.4]   Avallone, E.A., and Baumeister T., "Standard Handbook for Mechanical Engineers" 9th ed., New York: McGraw-Hill, 1987, Section 5.1.

[7.5]   Dorn, J.E., "Some Fundamental Experiments on High Temperature Creep", Journal of the Mechanics and Physics of Solids, Vol.3, 1954, pp.85-116.

[7.6]   Yu, X.X., Crocombe, A.D. and Richardson, "Material Modelling for Rate-Dependent Adhesives", Int. J. of adhesion and adhesives, Vo.21, 2001, pp.197-210.

CHAPTER 8

DCB TESTS - EXPERIMENTAL DETAILS

8.1 Introduction

The following chapter introduces the materials used in the DCB tests and the main experimental techniques. A full description of any specialised technique used is given, however, many 'standard' techniques were used and in-depth discussion of these has not been included. However, were relevant references are made to the appropriate standard.

8.2 Experimental Materials

The CFRP used in this study was IM7/8552 supplied by Hexcel Composites (Duxford, UK), and consists of intermediate modulus graphite fibres (IM7) in an epoxy matrix (8552). The other adherend material used was mild steel. The mechanical properties of unidirectional panels of the CFRP and the mild steel are given in Table (8.1). The adhesive used was Cytec's FM300-2M (Cytec, West Patterson, NJ, USA). This is a single part toughened epoxy film that has a variable mat carrier and nominal thickness of 0.2mm. The Young's modulus and Poisson's ratio of the adhesive (FM300-2M) are presented in section (7.3.2).

Table (8.1) The materials properties of IM7-8552 and mild steel

Material	E_x (GPa)	E_y (GPa)	G_{xy} (GPA)	v_{xy}	v_{yx}
IM7-8552	164.41	11.72	5.516	0.36	0.02
Mild steel	209	-	-	0.3	0.3

8.3 Sample manufacture

8.3.1CFRP joint manufacture

Unidirectional CFRP pre-preg was laid up with uncured adhesive film, FM300-2M to manufacture the CFRP DCB samples. A thin film (nominally $10\mu m$) of PTFE was placed at the bond line at one end of the panels to act as a starter crack. This assembly was autoclave cured at 180°C for 2.5 hours with a pressure of 0.6 MPa, as dictated by the advised curing schedule for the CFRP pre-preg. This process, in which both adhesive and CFRP are cured in the same treatment is termed co-bonding and can be compared with secondary bonding, in which the CFRP is cured before being bonded, and co-curing, in which composite parts are joined without an adhesive layer. The adhesive chosen for this study is a dual cure adhesive that is recommended for co-bonding CFRP and also for secondary bonding metals and can be cured in the temperature range 120°C - 180°C. After curing the co-bonded panels, a diamond saw was used to cut the samples to the dimensions shown in Fig. (8.1). Brass hinges were bonded to the joint with a high peel strength adhesive that was cured overnight at 55°C. The width of the test specimen was 25 mm and other dimensions were as shown in Figure (8.1).
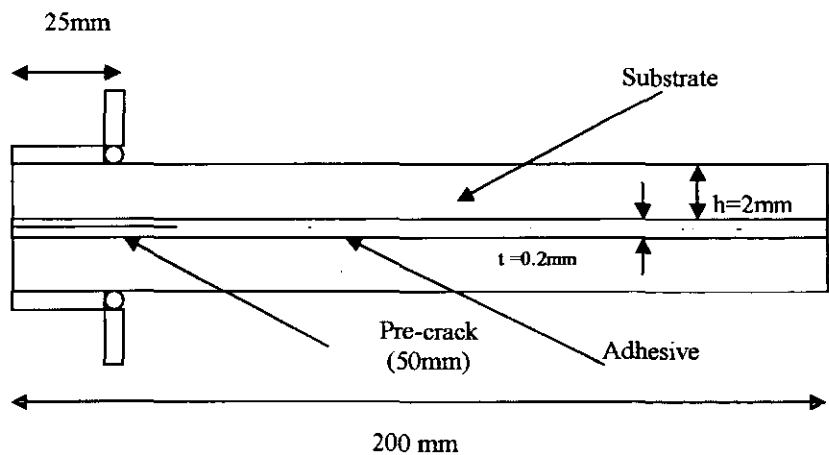
Fig.8.1 Double cantilever beam specimen with CFRP substrates.

8.3.2 Mild steel joint manufacture

The standard procedure for preparation of the mild steel substrates was grit blasting and degreasing. The cleaned and dried substrates were then coated with BR-127 primer, which was applied to the substrates by brush and air dried for 30 minutes prior to an oven cure for 30 minutes at 120 °C. As with the CFRP samples, a thin film of PTFE was placed at the bond line at one end of the panels to act as a starter crack. This assembly was cured for 2.5 hours at 120°C with a pressure of 0.28 MPa. Note that without the need to cure the CFRP pre-preg, the adhesive could be cured at a lower temperature than in the case of the co-bonded CFRP samples. Curing FM300-2M at higher temperature has no significant effect in the mechanical properties of the adhesive or the state of residual stress in the joints [8.1]. After curing, an electrical saw and milling machine were used to cut the samples to the dimensions shown in Figure (8.2). The width of the test specimen was 25 mm and other dimensions were as shown in Figure (8.2).
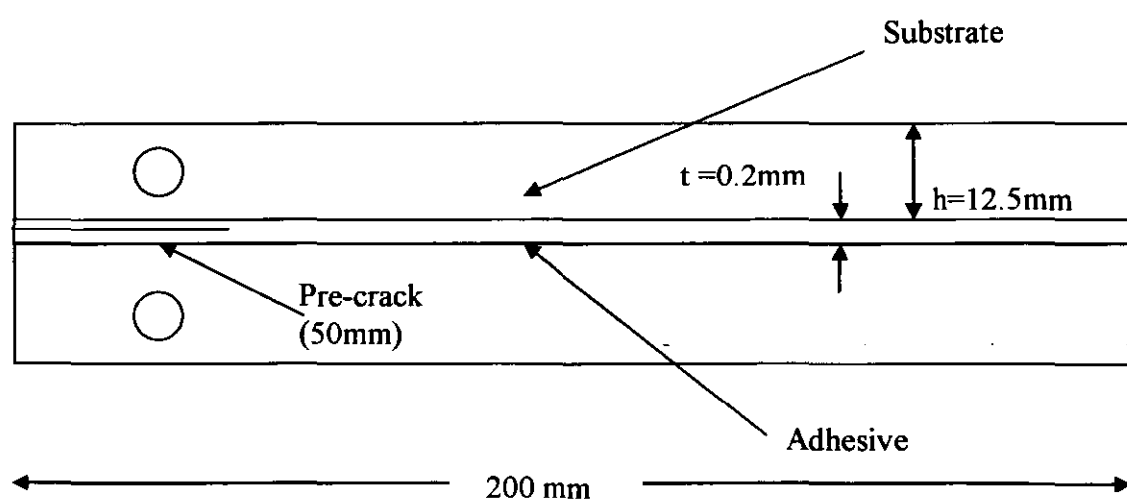
Fig.8.2 Double cantilever beam specimen with steel substrates

8.4 Test set-up

The experimental arrangement is shown in Figure (8.3). Testing was carried out using a servo-hydraulic test machine fitted with computer control and data acquisition. The crack length during the tests was determined using the commercial "Krak-Gage" and "Fractomat" system supplied by RUMUL. The "Krak-Gage" consists of a thin (~ 5 µm) constantan metal-foil which is adhesively-bonded to the side of a test specimen. During the test the "Krak-Gage" is designed to tear coincidentally with the crack in the actual test specimen. This is measured by the Fractomat and converted to a crack length. The output from the Fractomat was input to the computer data acquisition system via a strain channel on the test machine. Direct observations using a travelling microscope as shown in figure (8.4), represent the simplest method of monitoring cracks in bonded joints and therefore it is the method most frequently used. It basically consists of viewing the side of the specimen through an optical microscope which is fixed to a rigid base. The side of the specimen is painted with white correction fluid "Tippex" to highlight the crack. This technique was used during this work to check the reading of the "Krak Gage".

Fig. 8.4 Traveling optical microscope used in this study
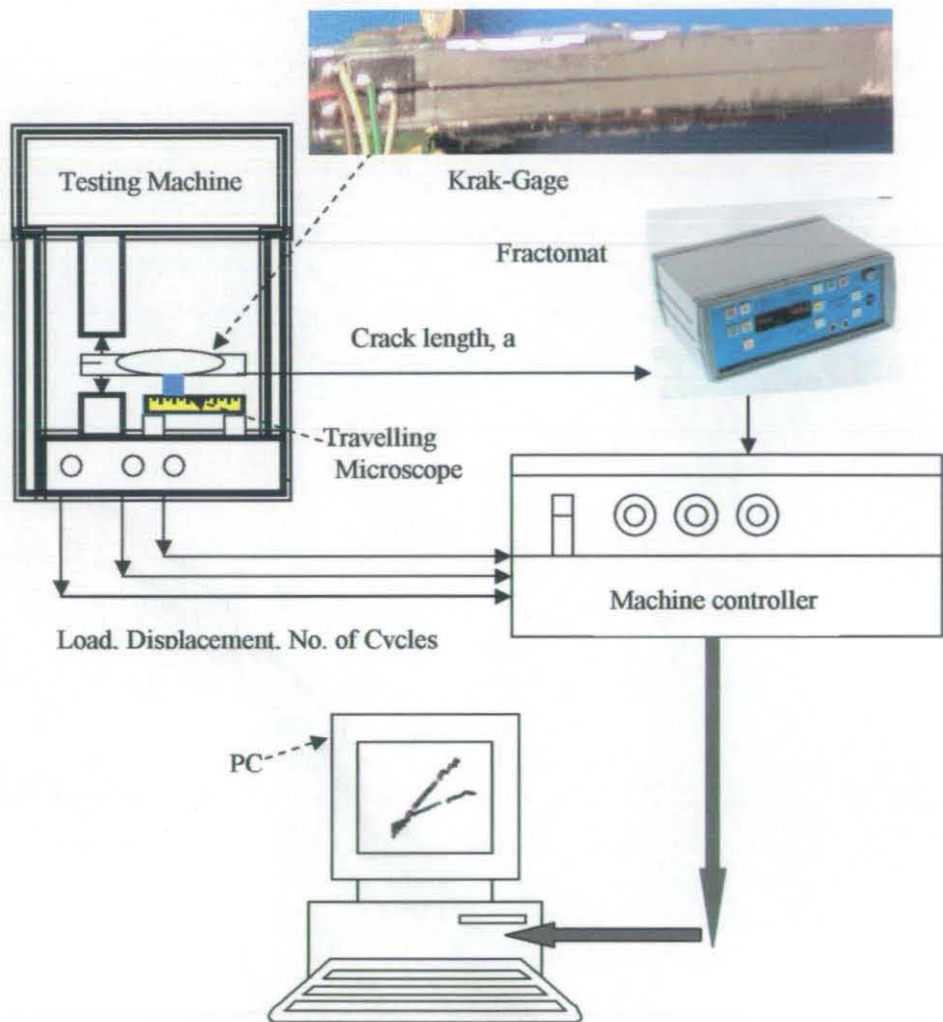
Fig. 8.3 Mechanical test configuration

Silicone rubber heating elements from *WATLOW Ltd* were used to heat the specimen to the desired temperature. The specification of this product is shown in Table (8.2).

Table (8.2) Silicon rubber heating element specification

Width mm	Length mm	Volts	Watts	Code Number
25	125	120	25	K010050C3

The heating elements were attached to the DCB joints as shown in Figure (8.5). Thermocouples (J-types) were used to measure the temperature at the bond line of the tested specimen. A temperature controller (*WATLOW-93* type) was used to control the temperature during testing. An external thermometer was used to check the temperature at different positions on the specimens, the variation in temperature through the bond line was ±1 °C. This method is more accurate and easier to apply to the specimen compared with heating with an oven. Furthermore, it also reduces heating of machine parts.
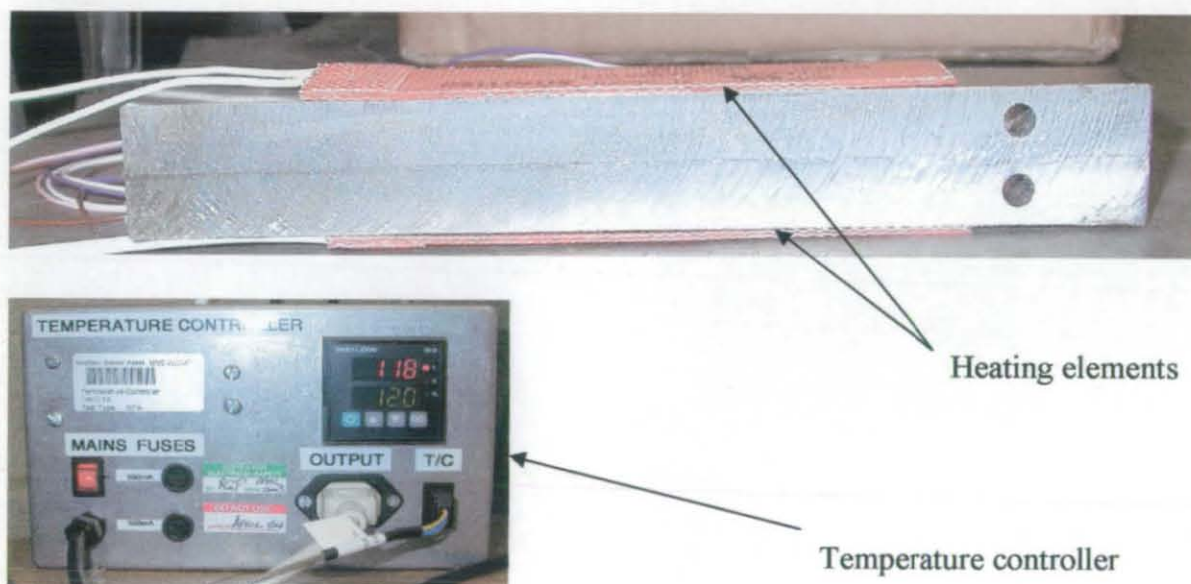
Fig. 8.5 Heating element and controller unit used on testing DCB joints.

The above testing set up was used to perform the different types of tests presented in the next section.

8.5 Testing procedures

8.5.1 Quasi-static tests and the effect of loading rate

Mode I constant displacement rate (or quasi-static) tests were conducted on CFRP and mild steel joints bonded with FM300-2M adhesive. The quasi-static tests were carried out for both joints at 0.1mm/min in order to calculate the critical strain energy release rate, G_c. The rate effects investigation was carried out for mild steel joints using displacement rates of 0.1, 1, 10 mm/min and three different temperatures, namely RT (22±1), 90°C and 120°C. The main reasons for conducting this type of tests were:

a) To determine the critical strain energy release rate, G_c of the adhesive FM300-2M.

b) To use the acquired load versus displacement data to determine the maximum displacement values to employ in the fatigue tests.

c) To study the effect of test rate on the critical strain energy release rate, G_c.

d) To study the effect of temperature on the critical strain energy release rate, G_c.

e) To compare the effect of rate with the effect of temperature.

f) To observe the locus of failure, in order to compare with the fatigue tests.

Determination of the strain energy release rate, G_c, is based on the energy approach. This approach states that crack extension (i.e. fracture) occurs when the energy available for crack growth is sufficient to overcome the resistance of the material. The material resistance may include the surface energy, plastic work, or other type of energy dissipation associated with a propagating crack. From LEFM the value of the adhesive fracture energy, G_c, may be calculated from a test conducted at a constant rate of displacement using Equation (3.20), described early in section (3.3.1). An Excel macro was written using visual basic for applications (VBA) to aid analysis. This required the input of test variables such as specimen dimensions and pre-crack length, before the strain energy

release rates were calculated from the data file. The results were placed into an Excel spreadsheet and the strain energy release rate was calculated automatically.

8.5.2 Fatigue testing

8.5.2.1 Frequency tests

Testing was carried out under displacement control with constant amplitude sinusoidal waveforms, displacement ratios (i.e. min. disp. /max. disp.) of R=0.1 and a range of frequencies (10 Hz, 1 Hz, 0.1 Hz). The adhesive used was a toughened epoxy and the substrates used were carbon fibre reinforced polymer (CFRP) and mild steel. Two to three samples were tested for each case and the average value considered. This type of tests was carried out to investigate the following:

1) The effect of frequency and substrate type on the fatigue crack propagation rate (FCPR).

2) The effect of frequency and substrate type on the fatigue threshold.

3) The effect of frequency and substrate type on the locus of failure.

Experimentally, the principal measurements are crack length, load and displacement as a function of cycles. The next step in the characterisation of FCP in the sample is to calculate the fracture parameters and the FCPR as a function of cycles from the experimental data. The values of (G_{max}) , J_{max} and $(C_t)_{avg}$ were determined as described in chapter (6), while the FCPR was calculated based on the seven- point incremental polynomial method described in section (4.5). An Excel macro was written using VBA to aid analysis using the approaches described above (Appendix-A).

In some polymers, cyclic loading can result in significant hysteretic heating. In order to check if the adhesive used in this testing programme was susceptible to this, the temperature of one of the joints was monitored using thermocouples attached to the specimen during fatigue testing. The thermocouples were attached to the adhesive near the PTFE. This experimental set-up used is shown in Figure 8.6. No increase in temperature was observed during fatigue cycling. This argument was in agreement with previous studies that showed that constant displacement testing does not lead to thermal failure [8.2-8.5]

Fig. 8.6 Set-up used for monitoring hysteretic heating.

8.5.2.2 Temperature tests

Adhesively bonded double-cantilever beam (DCB) samples were tested in fatigue at various frequencies and temperatures. The frequencies used were 0.1 Hz, 1 Hz and 10 Hz

and the temperatures were RT, 90°C and 120°C. The adhesive used was toughened epoxy *FM300-2M* and the substrate used was mild steel. Testing was carried out under displacement control with constant amplitude sinusoidal waveforms and displacement ratios (i.e. min. disp. /max. disp.) of R=0.1. Two to three samples were tested for each case and the average values calculated. This type of tests was carried out to investigate the following:

1)   The effect of temperature and frequency on the crack propagation rate (FCPR)

2)   The effect of temperature on the threshold value.

3)   The effect of temperature on the locus of failure.

Methods of performing the calculations of fracture parameters and the FCPR were described in section (8.5.2.1).

8.5.2.3 Hold time tests

Testing was carried out under displacement control with the constant amplitude trapezoidal waveforms shown in Figure (8.7). The time parameters used to characterize the trapezoidal waveform were t_r =0.1 sec, t_h=30 sec and t_d=0.1 sec. The testing temperatures were 90°C and 120°C. The adhesive used was a toughened epoxy and the substrate used was mild steel. Two samples were tested for each case and the average value calculated. This type of test was carried out to investigate the effect of hold time on fatigue crack growth rate and to validate the creep-fatigue crack growth predictive methods.
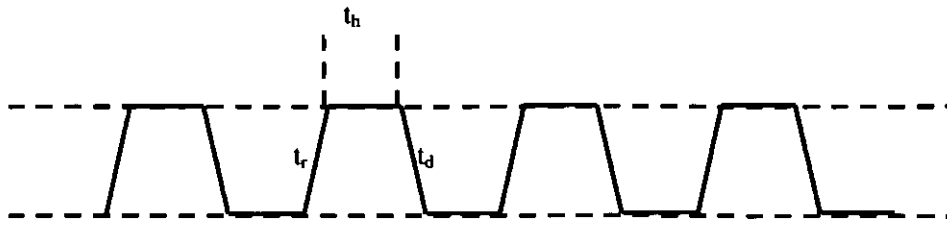
Fig. 8.7 Trapezoidal waveform.

8.5.2.3 Variable frequency tests

The majority of fatigue characterization of bonded joints is undertaken under constant amplitude at a constant applied frequency. Composite or steel structures are rarely subjected to a uniform constant amplitude level in service. The applied frequency could also fluctuate variable, creating a frequency spectrum, or the frequency could vary in sequential steps, i.e. block frequency loading. In this work three types of loading were used to study variable frequency effects, two to three samples were tested for each case and the average value considered. Each type is described below:

1. A three-stage equal cycles block loading spectrum was applied to both CFRP and mild steel joints. This is shown in Figure (8.8). Constant displacement amplitude was applied in all the stages. This resulted in decreasing load amplitude with crack length. The applied frequencies for stages 1, 2 and 3 were 10 Hz, 1 Hz and 0.1 Hz respectively. The number of cycles for each stage was 1000. DCB joints with CFRP and mild steel substrate were tested at room temperature. DCB joints with mild steel substrates were tested at 90°C and 120°C.

178
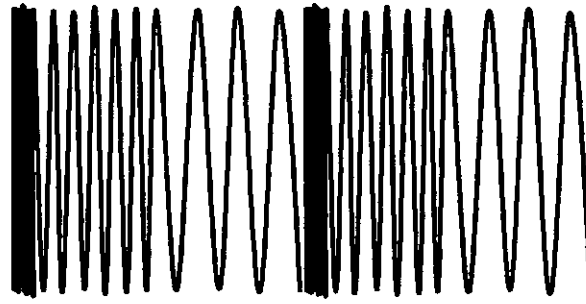
Fig. 8.8   Three-Stage block loading spectrum with equal cycles in each stage.

2.   A three-stage equal time block loading spectrum was used to test mild steel joints at room temperature. This is shown in Figure (8.9). Constant displacement amplitude was applied in the stages. The applied frequencies for stages 1, 2 and 3 were 10 Hz, 1Hz and 0.1 Hz respectively. The number of cycles for stages 1, 2 and 3 was 100, 10 and 1 cycle respectively, i.e. equal time in each stage.
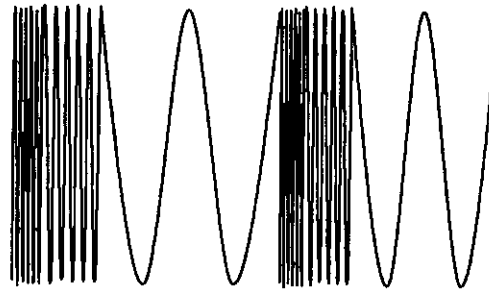
Fig. 8.9   Three-Stage block-loading-spectrum-with-equal-time in each stage.

3.   A Six-stage variable frequency block loading spectrum was used to test mild steel joints at room temperature. This is shown in Figure (8.10). Constant displacement amplitude was applied in the stages. The applied frequencies for stages 1, 2, 3, 4, 5

and 6 were 0.1 Hz, 0.5Hz, 1 Hz, 5Hz and 10 Hz. The numbers of cycles for each

stage varied between 10-15 cycles.
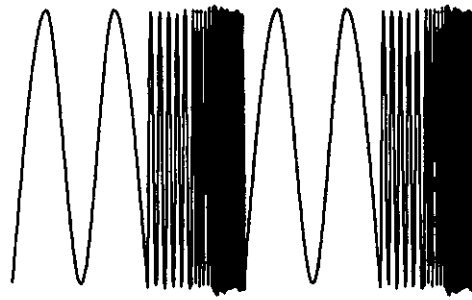
Fig. 8.10 Variable block loading spectrum.

8.5.2.4 Surface treatment tests

A second surface treatment procedure was applied to the mild steel substrates in order to

study the effect of treatment on the locus of failure and fatigue threshold behaviour. This

second was a sodium dichromate/ sulphuric acid etch process as described in section (2.7).

Testing was carried out under displacement control with constant amplitude sinusoidal

waveforms, displacement ratios (i.e. min. disp. /max. disp.) of R=0.1 and a range of

frequencies (10 Hz, 1 Hz, 0.1 Hz). The adhesive used was FM300-2M and the substrate

used was mild steel. Two to three samples were tested for each case and the average value

considered.

8.5.3 Creep testing

Double-cantilever beam (*DCB*) samples were used to provide the creep data using fracture

mechanics principles. Mild Steel was used for the substrates and *FM300-2M* was used for

the adhesive. Creep testing was carried out using an *INSTRON* testing machine under load

control. Tests were carried out at a constant load of *1200N* for joints tested at *90°C* and at

600N for joints tested at *120°C*. Two to three specimens were tested at each temperature.

Specimens were subjected to pre-fatigue loading to sharpen the crack.

The strain energy release rate, G was calculated based on the relationship between G and

the crack length, a, this can be calculated based on the beam on elastic foundation model

described in (6.2.2). The results are tabulated in Table (8.2).

Table (8.2) the strain energy release rate as function of the crack length at assigned load.

Load (*N*)	Case	$G=f(a)$ J/m^2 , a in *mm*
1200	Tests at 90°C	$G(a) = 0.0676\,a^2 + 1.853\,a + 4.569$
600	Tests at 120°C	$G(a) = 0.0169\,a^2 + 0.2965\,a + 1.118$

Experimentally, the crack length and displacement as a function of time are measured. The

next step was the calculation of the creep parameters C^* and C_t. Methods of calculating

these parameters are presented in section (6.4).

8.6 Surface topography

SEM is a very powerful tool for obtaining surface topographical information. An electron

beam is focused to a fine probe (typically 5nm-1μm) and scanned over the sample.

Samples for SEM analyses, 10 mm in length and 25 mm wide were carefully cut from

DCB specimens using a band saw. These were mounted on aluminium stubs. The samples

were coated with gold to ensure electrical conductivity.

A Digital camera was used to obtain the images of the fracture surfaces. Optical

microscopy and scanning electron microscopy (SEM) were used to characterise the nature

of the fracture surface and to investigate the locus of failure.

8.7 References

[8.1]   Atkinson, S., "Investigation of Residual Stresses Bi-Material Laminates", 03MMC500 Individual Project Final Report, Loughborough University, 2004.

[8.2]   Schmidt, A. X. and Marlies, C. A., "Principles of High-Polymer Theory and Practice", McGraw-Hill, New York, 1948, p.578.

[8.3]   Hertzberg, R. W. and Manson, J. A., "Fatigue of Engineering Plastics", Academic Press, INC. (London) LTD., 1980, pp.52-54.

[8.4]   Jethwa, J. K., "The Fatigue Performance of Adhesively-Bonded Metal Joints", PhD dissertation, Imperial College, 1995, pp.40-43.

[8.5]   Erpolat, S., Ashcroft, I.A., Crocombe, A.D. and Abdel-Wahab, M.M., "A study of adhesively bonded joints subjected to constant and variable amplitude fatigue" Int. J. Fatigue, Vol. 26, 2004, pp.1189-1196.

CHAPTER 9

DCB TESTS - EXPERIMENTAL RESULTS

9.1 Introduction

In this chapter the results from the experimental tests on the bonded DCB samples will be presented. This will include the following:

- Quasi-static tests, conducted at room temperature for CFRP and mild steel joints.

- The effect of loading rate on the critical strain energy release rate, G_c at different temperatures for mild steel joints.

- · The effect of fatigue frequency on crack growth rate in CFRP and mild steel joints tested at room temperature.

- The influence of temperature and frequency on crack growth rate in mild steel joints.

- The influence of hold time on the crack growth rate in mild steel joints.

- The influence of variable frequency fatigue on crack growth for mild steel joints at different temperatures.

- The influence of surface treatment on the crack growth rate and fatigue threshold, G_{th}, for mild steel joints tested at room temperature.

- The effect of creep loading on crack growth rate for mild steel joints tested at different temperatures.

- The influence of different types of loading on the locus of failure.

9.2 Quasi-static test results

Figure (9.1) and Figure (9.2) show plots of the experimentally-determined compliance, $C=\delta/P$, against the crack length for CFRP (IM7/8552) and mild steel DCB joints bonded with FM300-2M adhesive respectively.
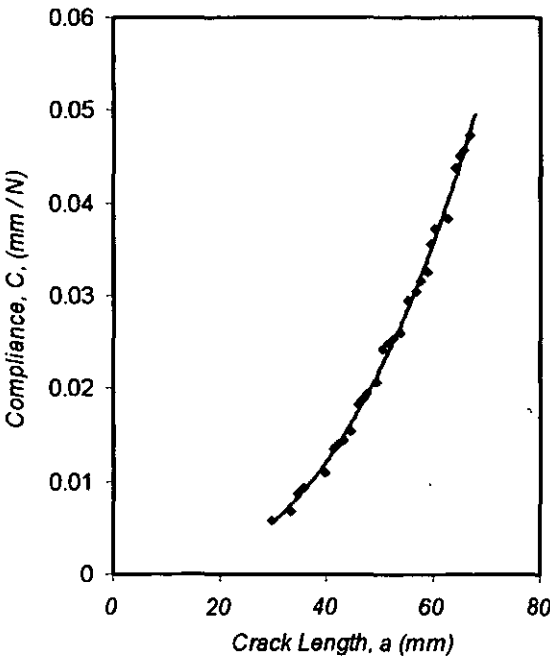
Fig. (9.1) Compliance against crack length for CFRP DCB joint.
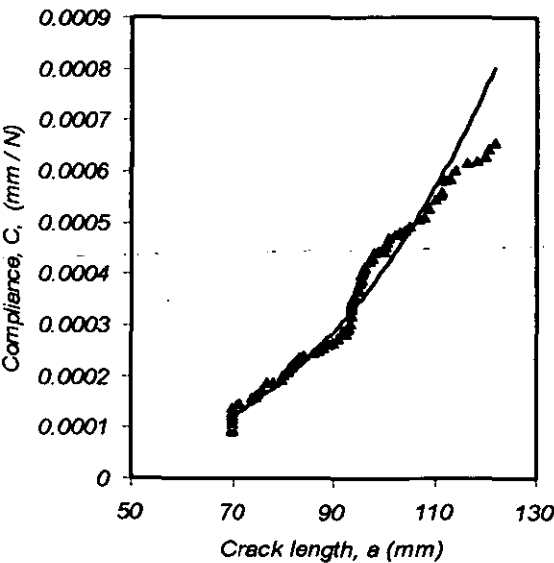
Fig.(9.2) Compliance against crack length for mild steel DCB joint.

Figure (9.3) and Figure (9.4) show plots of load against the crack length for the test specimens. These show clearly a reduction in load value as the crack length increases. This is due to the increase of dC/da with crack length as seen in Figures (9.1) and (9.2).
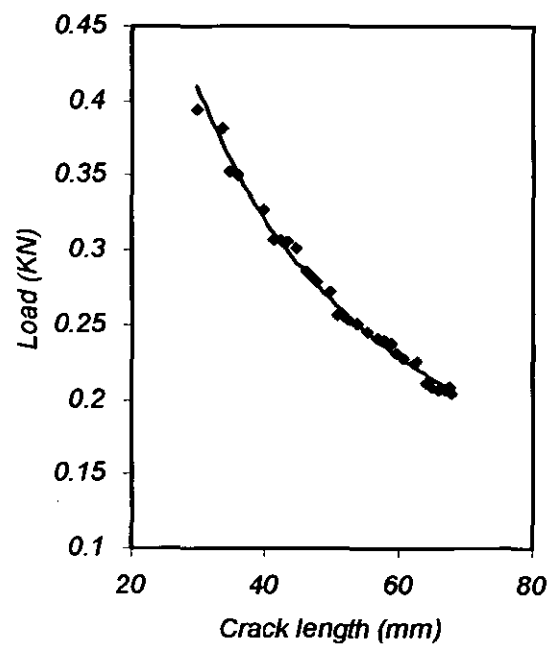
Fig. (9.3) Load against crack length for CFRP DCB joint.
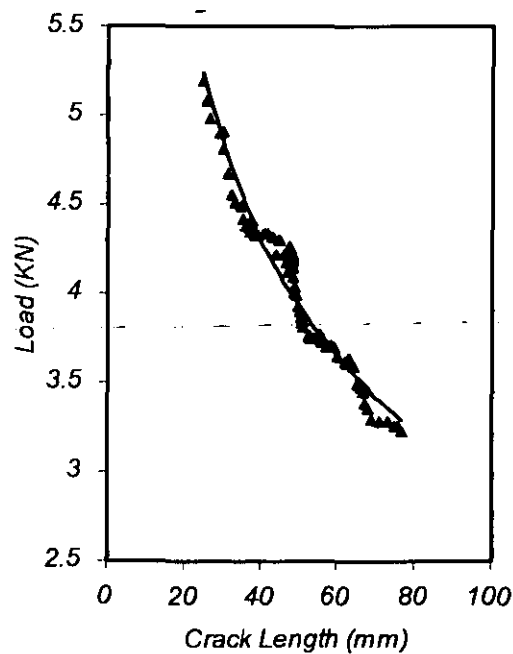
Fig. (9.4) Load against crack length for mild steel joint.

G_c was determined using the experimental dC/da data by applying Equation (3.20). Figure (9.5) shows plots of G_c against crack length for CFRP and mild steel DCB joints bonded with FM300-2M. Three samples were tested for each joint, the repeatability of tests was generally good, and the calculated mean values for each joint are tabulated in Table (9.1). The G_c value of mild steel joints is higher than that of the CFRP joints by a factor of 1.2. This is in agreement with previous studies [11.1]. This will be discussed further in section (11.2). The locus of failure from an optical examination of the fracture surfaces was found to be cohesive fracture of the adhesive for both joints.
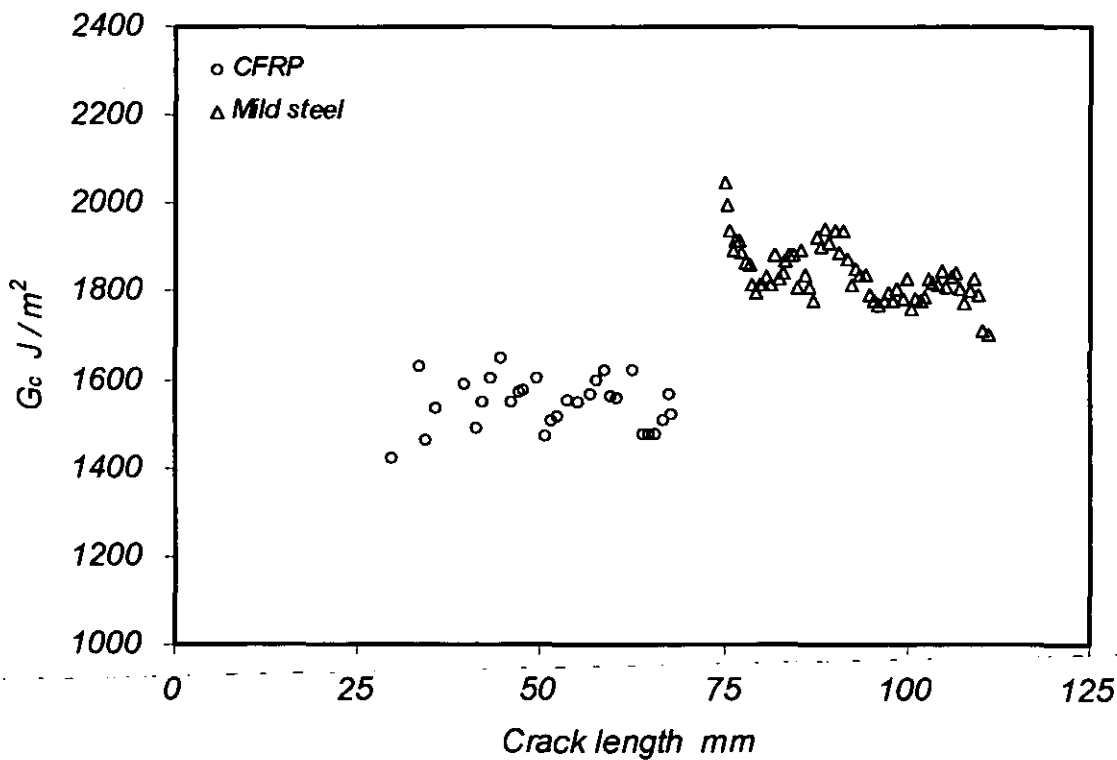
Fig. (9.5) G_c against crack length for CFRP and mild steel DCB joints.

Table 9.1 Results of quasi-static test.

Joints	Specimen type	G_c (average)	Failure type
FM300-2M CFRP	DCB	1546 (J/m^2)	Cohesive in the adhesive
FM300-2M Mild steel	DCB	1893 (J/m^2)	Cohesive in the adhesive

9.3 Effect of loading rate

The effect of loading rate has been investigated for mild steel joints bonded with FM300-2M. The tests were carried out with loading rates of 0.1, 1 and 10 mm/min at RT, 90°C and 120°C, following the procedure in section 9.2. The G_c values calculated from these tests are shown in Table (9.2).

Table 9.2 The critical strain energy, Gc at different rate and temperature.

	RT	Temp. = 90 deg	Temp.= 120 deg.
Rate mm/min	G_c J/m^2	G_c J/m^2	G_c J/m^2
0.1	1500	1224	642.32
1	1893	1215	810.29
10	1832	1567	936.78

Figure (9.6) shows the loading rate vs. the G_c value. It shows clearly that as the rate increases from 0.1 to 10 mm/min the G_c value also increases. It also shows that as temperature increases the G_c value decreases, i.e. decreasing the loading rate has a similar effect to increasing temperature on G_c.
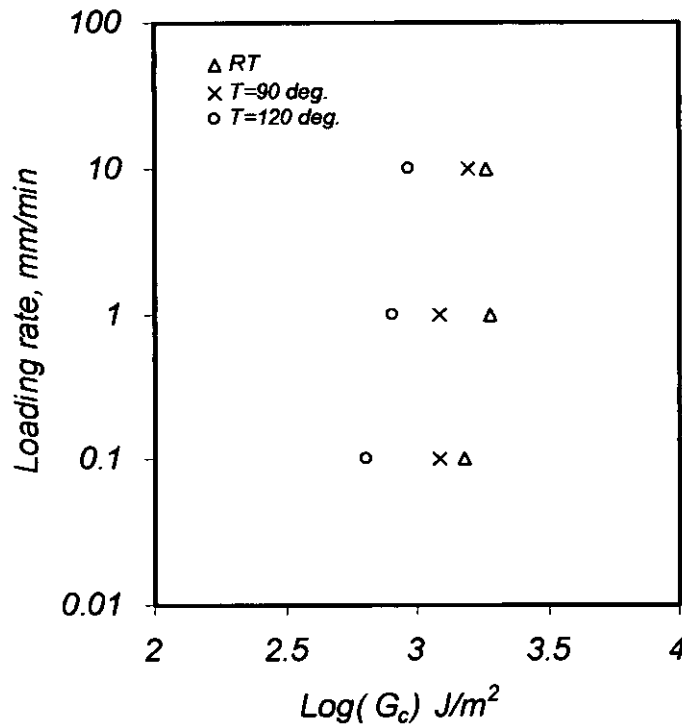
Fig.(9.6) Effect of loading rate on G_c at different temperature for mild steel joints.

9.4 Fatigue test results

DCB test specimens were used to obtain the value of da/dN or da/dt as a function of G_{max}, J_{max} and $(C_i)_{avg}$. Evaluation of results in term of these parameters is used to find the most appropriate parameter to characterise the crack growth rate in adhesively bonded joints subjected to different loading conditions. The best parameter for different types of loading and environmental condition will be discussed in chapter (10). A sine-wave form of

loading was employed at frequencies of 10, 1 Hz and 0.1 Hz. The displacement ratio was maintained at 0.1 in all tests. The method used to obtain the fatigue crack growth rate, da/dN, was the "incremental polynomial method" described in section (4.5). The values of the various fracture parameters were determined as described in chapter (8). The curves exhibit an approximately sigmoidal shape (although not all curves encompassed three regions). Region I is defined by the fatigue threshold, below which measurable crack growth does not occur. Region II shows a linear relationship between log (G_{max}, J_{max} or $(C_i)_{avg}$) and log da/dN. Region III shows fast crack growth as the fracture parameter approaches the critical value, namely G_c, J_c or $((C_i)_{avg})_c$. Three samples were tested for each load case. Repeatability of the tests was generally good as illustrated in Figure (9.7), which shows the FCP curves for three CFRP specimens tested at 10 Hz.
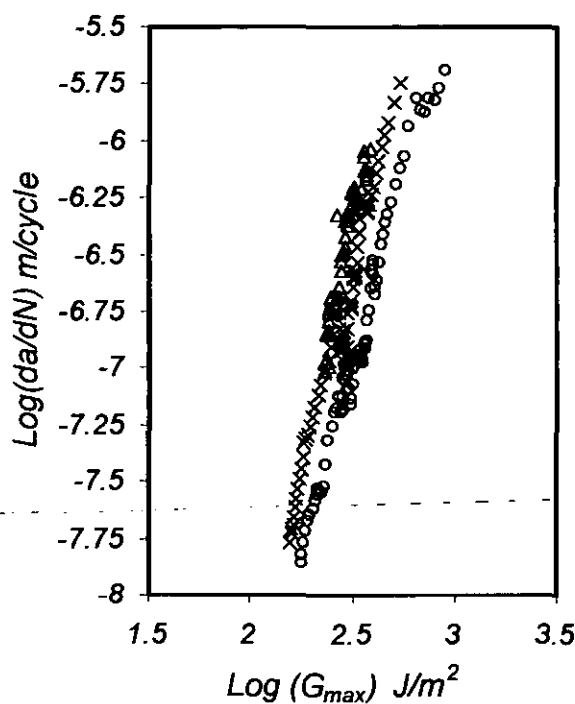
Figure (9.7) FCP curves of three CFRP samples tested at 10 Hz.

9.4.1 Effect of frequency

Example log-log plots of FCPR against G_{max} for the CFRP and mild steel DCB's are shown in Figures (9.8) and (9.9) respectively. Both figures show clearly the effect of fatigue frequency. The fatigue threshold (G_{th}), i.e. the value of G_{max} below which fatigue crack growth is negligible, can be seen to decrease as the test frequency decreases. At $G_{max} > G_{th}$, it can be seen that crack growth is faster for a given value of G_{max} at low frequencies for both types of joints. Comparison of Figures (9.8) and (9.9) also shows that the FCPR is much faster in the mild steel joints than in the CFRP joints. The frequency sensitivity factor (FSF), defined as the multiple by which the FCPR changes per decade change in test frequency, is approximately 1.1 for the CFRP DCB's and 1.2 for the mild steel joints.
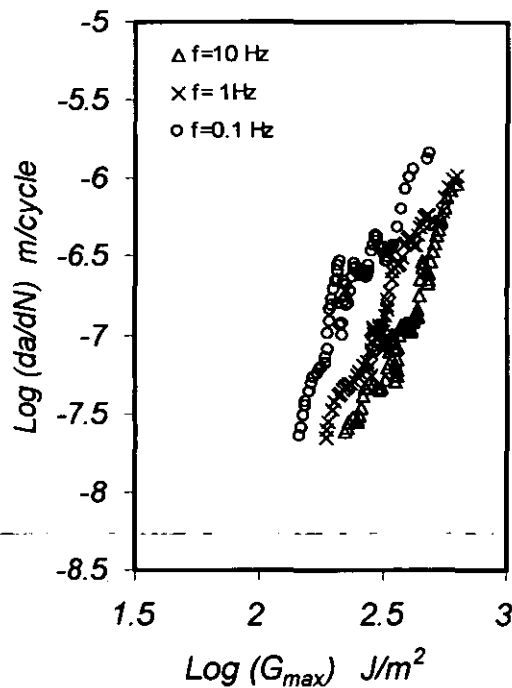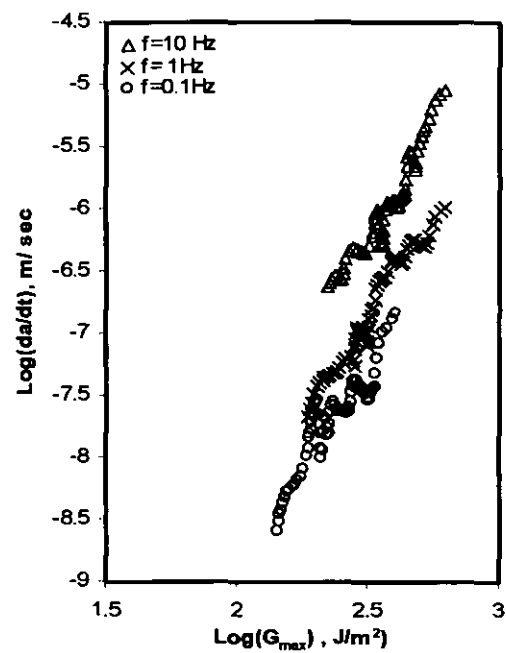

Fig. (9.8) FCP curves for CFRP joints in terms of da/dN tested at RT.
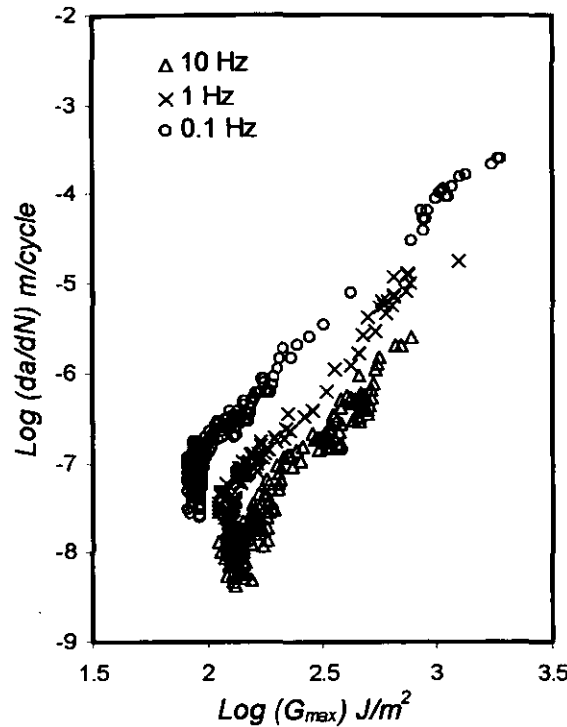
Fig. (9.9) FCP curves for Mild steel joints in terms of da/dN tested at RT.

Fatigue crack growth rates were reprocessed in terms of da/dt and the log-log plot of da/dt versus G_{max} have been plotted in Figures (9.10) and (9.11) for the CFRP and mild steel samples respectively. This has been carried out to investigate the dependency of the crack growth rate, wether it is cyclic dependent or time dependent. It is seen that FCP curves are much closer to each other when plotted in terms of *da/dt* for the mild steel joints but that there is still a significant difference between curves for the CFRP joints. It can also be seen that when plotting crack growth as a function of time, the crack growth rate for a given value of G_{max} is greater at higher frequencies, which is in contrast to the trend seen when crack growth is plotted as a function of cycles (i.e. FCGR). It can be said, therefore, that, for both substrates, fatigue crack growth is dependent on both time and number of cycles but that in the case of apparent interfacial failure crack growth is time dominated. This means that as a first approximation fatigue crack growth for apparent interfacial failure at any frequency can be estimated from a single curve fit through the data points in Figure

(9.11). Table (9.3) summarises the results of the fatigue tests for the CFRP and mild steel

DCB samples.

Fig. (9.10) FCP curves for CFRP joints in terms of da/dt.
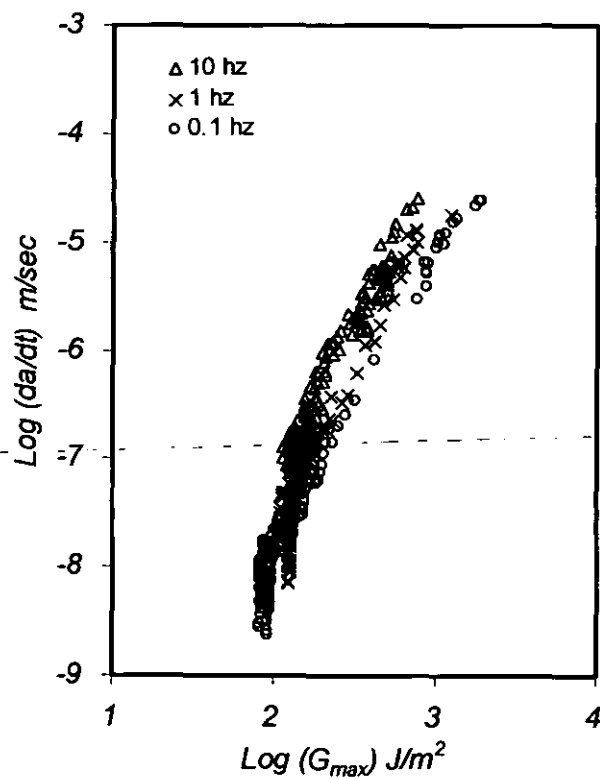
Fig. (9.11) FCP curves for mild steel joints in terms of da/dt tested at RT.

Table (9.3) Results of fatigue /frequency effect tests.

Joint type	Frequency (Hz)	G_{th} (J/m^2)	Failure type	Paris constant $da/dN=D(G_{max})^n$ a in (m), and G in (J/m^2)	
				n	D
CFRP FM300-2M	10	220±9.2	Cohesive	3.35±0.04	2.59E-16 ±1.73E-17
CFRP FM300-2M	5	181.7±4.5	Cohesive	3.016±0.11	1.62E-15±1.2E-16
CFRP FM300-2M	1	187±5.68	Cohesive	3.25±0.03	1.002E-15±2.3E-16
CFRP FM300-2M	0.1	140±10.4	Cohesive	2.992±0.14	1.577E-14±3.1E-15
Mild steel FM300-2M	10	133±5.85	Apparent interfacial	3.117±0.16	2.11E-15±3.5E-16
Mild steel FM300-2M	5	115±6.55	Apparent interfacial	2.85±0.05	1.196E-15±4.7E-16
Mild steel FM300-2M	1	110.7±8.2	Apparent interfacial	2.95±0.14	2.71E-14±2.9E-15
Mild steel FM300-2M	0.1	81.7±5.3	Apparent interfacial	2.59±0.21	4.52E-13±5.7E-14

Figure (9.12) shows clearly the effect of frequency on the fatigue threshold values for the CFRP and mild steel joints. G_{th} decreases as the applied frequency decreases. The G_{th} values for the CFRP joints are significantly higher than those seen with the mild steel joints at all frequencies. This is not surprising as the DCB's with mild steel substrates failed interfacially whilst those with the CFRP substrates failed cohesively in the adhesive. It can also be seen that there is a linear relationship between frequency and log G_{th} for both

cohesive and interfacial crack growth, meaning that prediction of fatigue thresholds at other frequencies should be reasonably reliable.
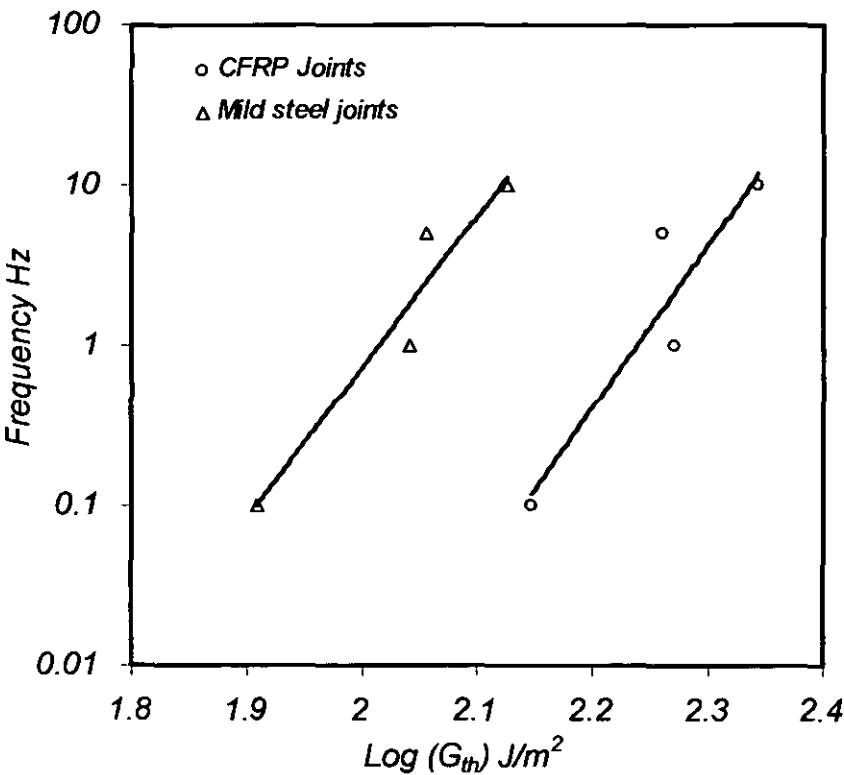
Fig. (9.12) The effect of substrates on threshold value at different applied frequency.

Figure (9.13) and (9.14) shows the relationship between frequency and Paris constants n and D respectively for both joints. The trend in 'n' is increasing with frequency for both joints while 'D' tends to decrease as frequency increases.
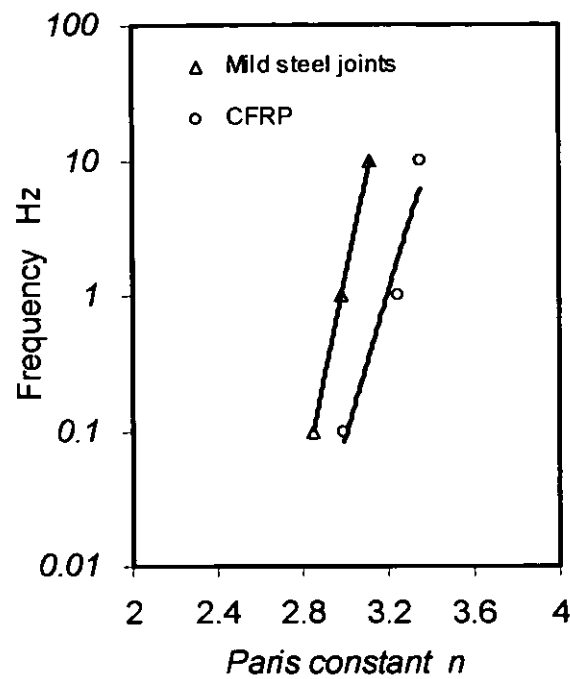
Fig. (9.13) Frequency versus Paris constant, n for mild steel and CFRP joints.
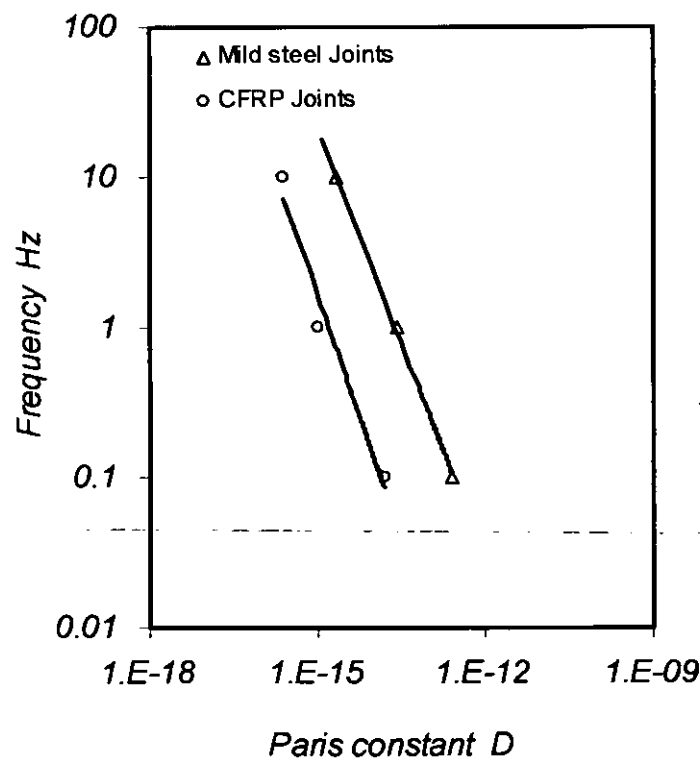
Fig. (9.14) Frequency versus Paris constant, D for mild steel and CFRP joints.

9.4.2 Effect of temperature

Figure (9.15) and Figure (9.16) show the fatigue crack propagation (FCP) of mild steel joints bonded with FM300-2M tested at 90°C and 120°C respectively. It is clearly seen that, the threshold value and the crack growth rate are affected by varying the frequency for both temperatures. At 90°C the threshold values are mostly similar to the threshold values at room temperature. Increasing the temperature to 120°C, however, has a drastic effect on the threshold value. The frequency sensitivity factors, FSF, were approximately 0.9 and 1.28 for 90°C and 120°C respectively.
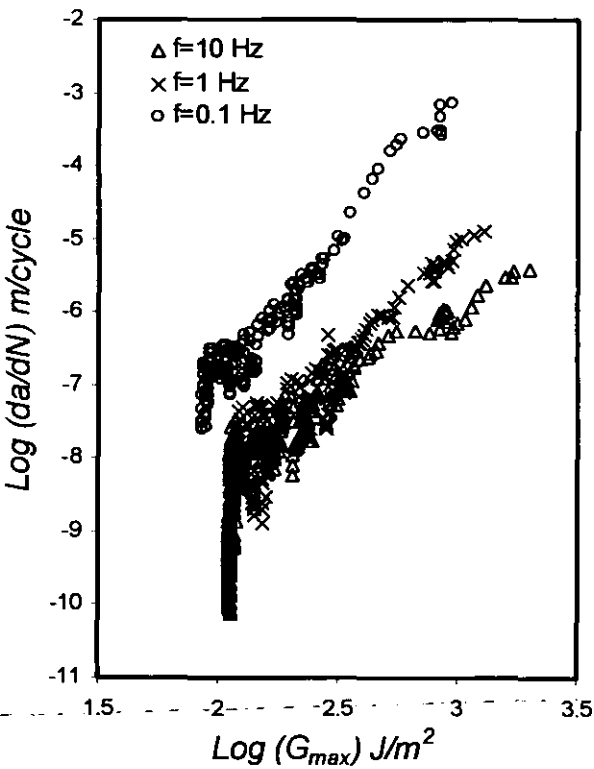
Fig. (9.15) FCP curves for mild steel joints tested at 90°C in terms of da/dN.
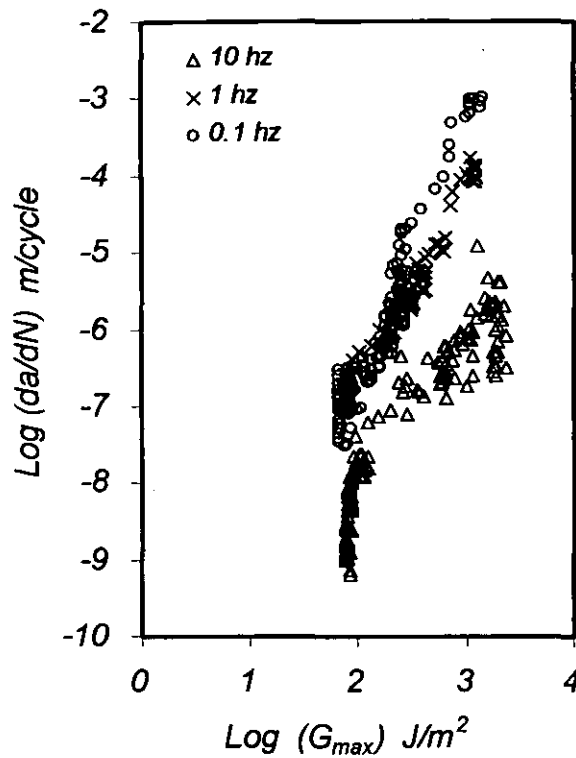
Fig. (9.16) FCP curves for mild steel joints tested at 120°C in terms of da/dN.

FCPR's were reprocessed in terms of da/dt and log-log plots of da/dt versus G_{max} have been plotted in Figure (9.17) and Figure (9.18). These show the same phenomena observed in the RT tests described above. At elevated temperatures, the locus of failure, from an optical examination of the fracture surfaces, appears to change to mostly cohesive failure of the adhesive, with occasional islands of interfacial failure. These islands of interfacial failure appear smaller at lower frequencies and higher temperatures. Tables (9.4) - (9.6) summarise the results of fatigue tests for mild steel DCB samples at 10 Hz, 1Hz and 0.1 Hz respectively.
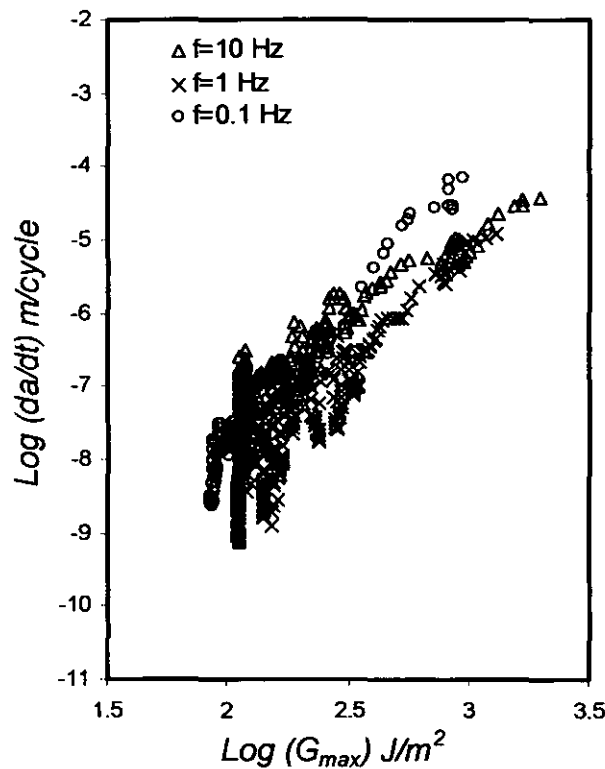
Fig. (9.17) FCP curves for mild steel joints tested at 90°C in terms of da/dt.
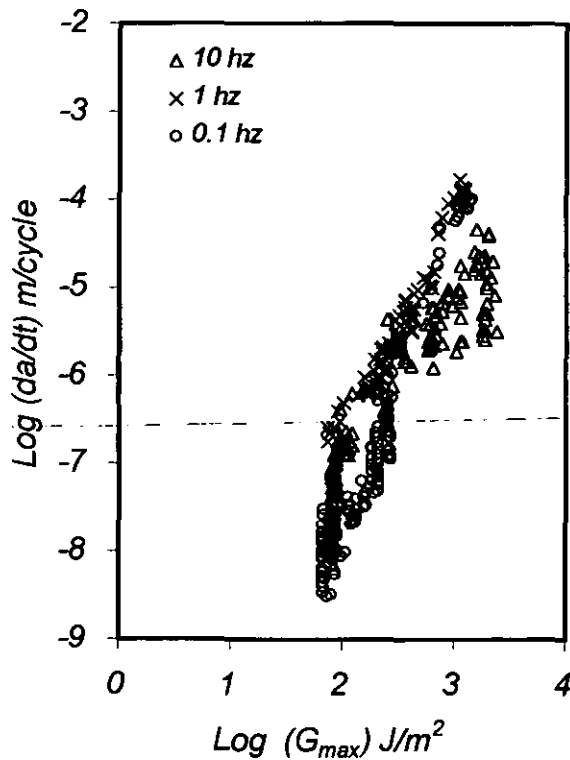
Fig. (9.18) FCP curves for mild steel joints tested at 120°C in terms of da/dt.

Table (9.4) Results of cyclic fatigue tests at 10 Hz.

Joint type	Temperature °C	G_{th} (J/m^2)	Paris constant a in m and G_{max} in J/m^2	
			n	D
Mild steel FM300-2M	RT	133±5.85	3.117±0.16	2.11E-15 ±3.5E-16
Mild steel FM300-2M	90	124±4.6	2.91±0.11	4.65E-15±8.5E-16
Mild steel FM300-2M	120	77.2±3.7	2.49±0.16	3.25E-12±9.65E-13

Table (9.5) Results of cyclic fatigue tests at 1 Hz.

Joint type	Temperature °C	G_{th} (J/m^2)	Paris constant a in m and G_{max} in J/m^2	
			n	D
Mild steel FM300-2M	RT	110.7±8.2	2.95±0.14	2.71E-14±2.9E-15
Mild steel FM300-2M	90	120.3±5.6	2.89±0.12	7.413E-15±2.65E-15
Mild steel FM300-2M	120	73.8±3.2	2.44±0.23	2.168E-12±5.3E-13

Table (9.6) Results of cyclic fatigue tests at 0.1 Hz.

Joint type	Temperature °C	G_{th} (J/m^2)	Paris constant a in m and G_{max} in J/m^2	
			n	D
Mild steel FM300-2M	RT	81.7±5.3	2.59±0.21	4.52E-13±5.7E-14
Mild steel FM300-2M	90	85.8±3.1	3.2±0.105	4.6E-14±9.2E-15
Mild steel FM300-2M	120	68.6±3.6	2.25±0.05	4.61E-14±7.3E-15

Figure (9.19) shows clearly that, the threshold values are affected by varying the frequency and the temperatures. At 90°C the threshold values are similar to the threshold values at room temperatures, while at 120°C the threshold value is drastically affected and reduced by almost 32% compared with the threshold values obtained at room temperature.
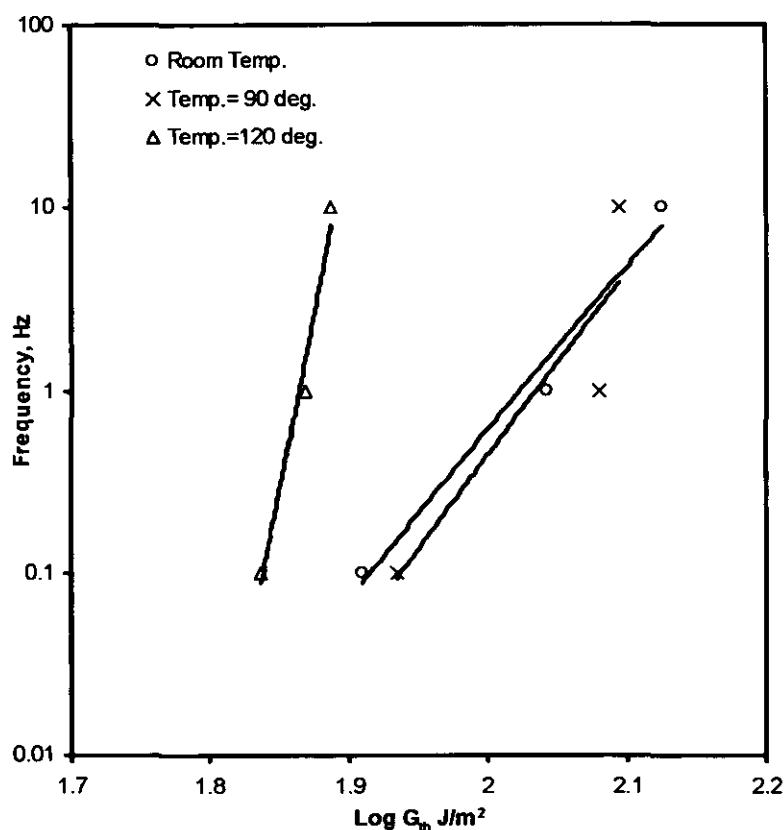

Fig. (9.19) The effect of temperature on threshold value at different applied frequency.

To illustrate the effect of temperature on fatigue crack growth of adhesively bonded joints. FCP curves at 10 Hz, 1Hz and 0.1 are plotted in Figures (9.20), (9.21) and (9.22) respectively. These curves show that, the crack growth rate increases with increasing temperature. This effect is most obvious at 0.1 Hz. The temperature sensitivity factor, TSF, is 1.2. The TSF is defined similarly to FSF i.e. the multiple by which the FCPR changes per decade change in test temperature.
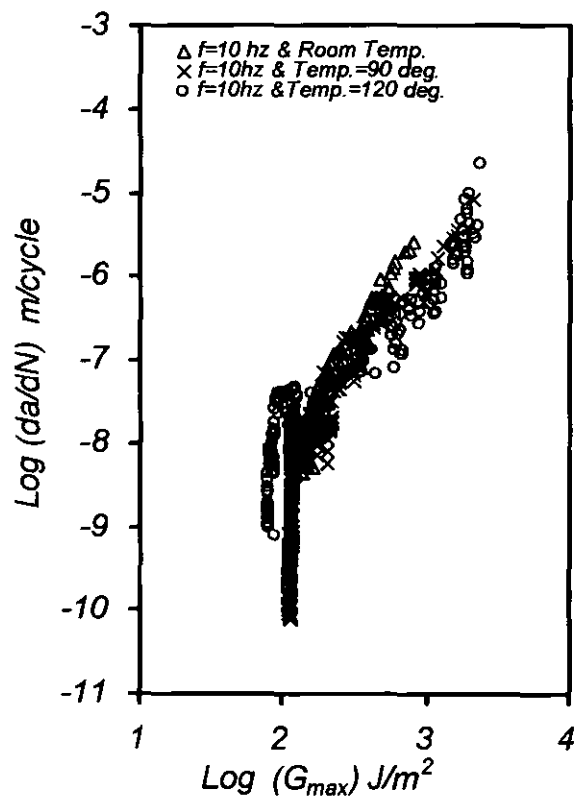
Fig. (9.20) FCP curves for mild steel joints tested at 10Hz.
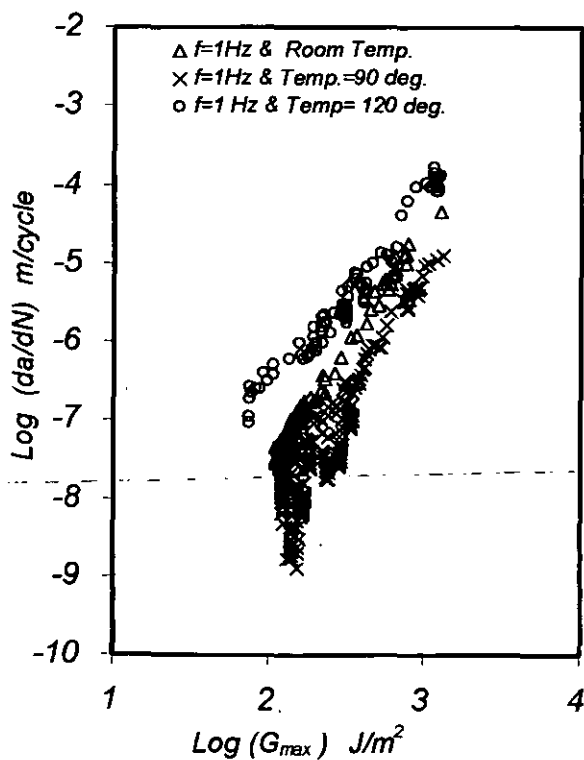
Fig. (9.21) FCP curves for mild steel joints tested at 1Hz.
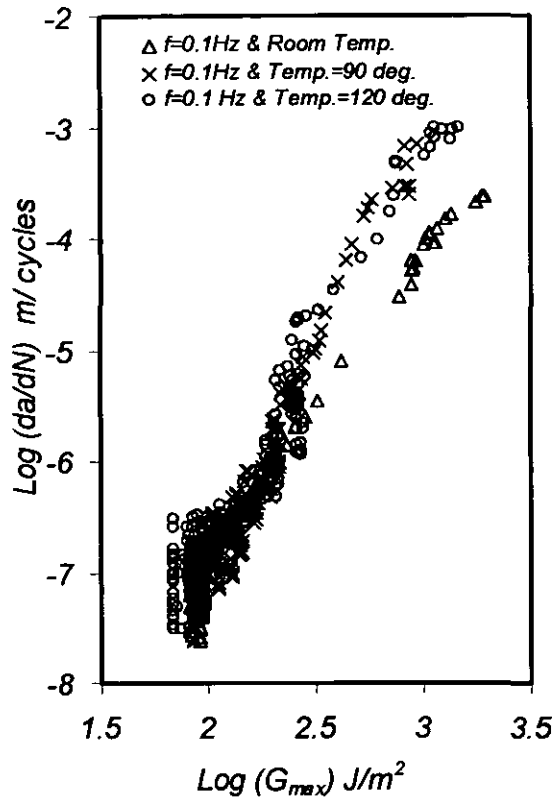
Fig. (9.22) FCP curves for mild steel joints tested at 0.1Hz.

Figures (9.23) and (9.24) show the relationship between frequency and Paris constants n and D respectively at different temperatures. The Paris constant, n, increases with increasing frequency at all temperatures, while the Paris constant, D decreases with increasing frequency at all temperatures. It is also clear that as the temperature increases the Paris constant, n decreases, while the Paris constant, D increases.

Based on theses two figures, it is possible to find the value of Paris constants for a range of frequency and temperature, thus the crack growth rate of adhesively bonded joints in the range of frequency (0.1-10Hz) and the range of temperature (RT-120) can be predicted by interpolation.
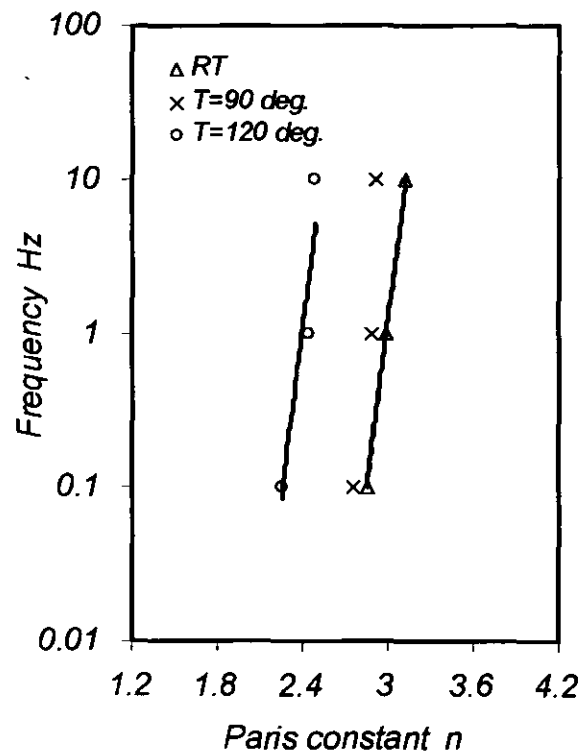
Fig. (9.23) Frequency versus Paris constant, n for mild steel joints.
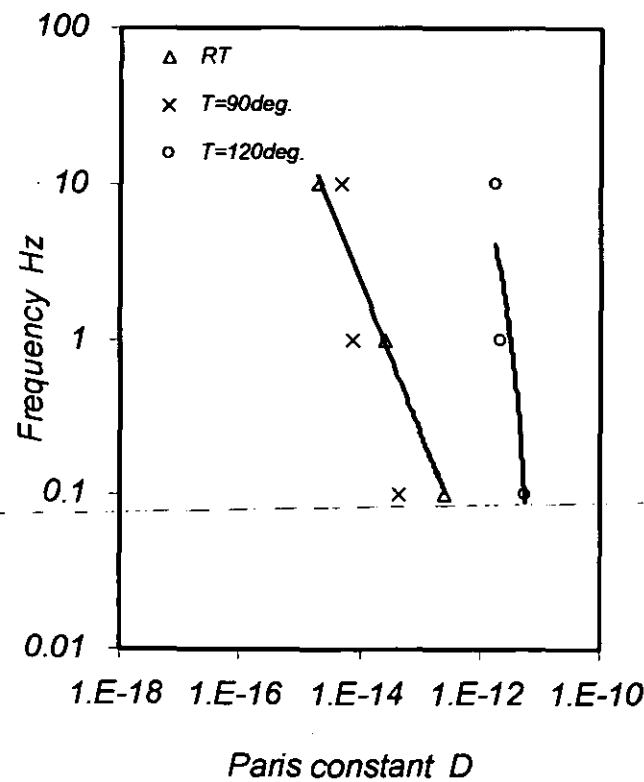
Fig.(9.24) Frequency versus Paris constant, D for mild steel joints.

9.4.3 Results in terms of different parameters of fracture

In the previous section, FCP curves were plotted in term of da/dN vs. G_{max}. In this section other parameters such as J-integral and the creep parameter, $(C_t)_{avg}$, will be considered. This is due to the possibility of extensive plasticity and creep, especially at elevated temperature.

9.4.3.1 Results in terms of J_{max}

Figures (9.25), (9.26) and (9.27) show the fatigue crack propagation (FCP) in terms of J_{max} for mild steel joints bonded with FM300-2M tested at RT, 90°C and 120°C respectively. The trends of the FCP curves in terms of the J-integral are similar to the FCP curves obtained in terms of G_{max}. The thresholds values and the slope of region II of the curves are almost the same, while in the fast region (region III) of the curves higher values of J_{max} were obtained. This indicates the presence of plasticity in the high load region of the curve. Table (9.7), (9.8) and (9.9) summarises the results of the fatigue tests for mild steel DCB samples reprocessed in term of J_{max} at 10 Hz, 1Hz and 0.1 Hz respectively.
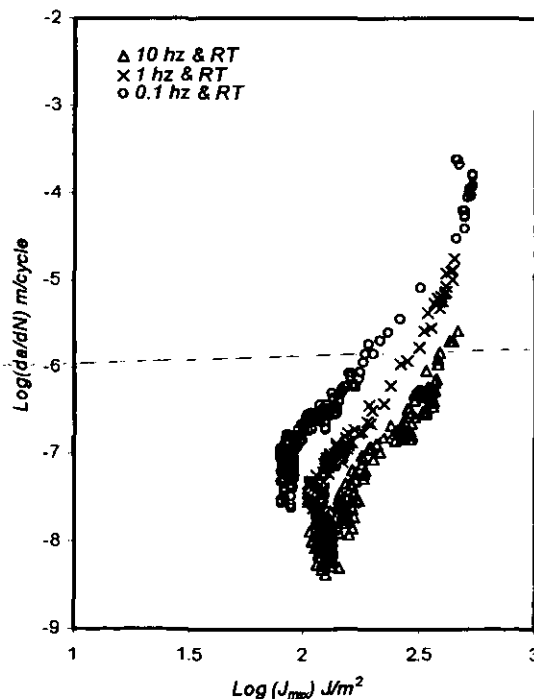

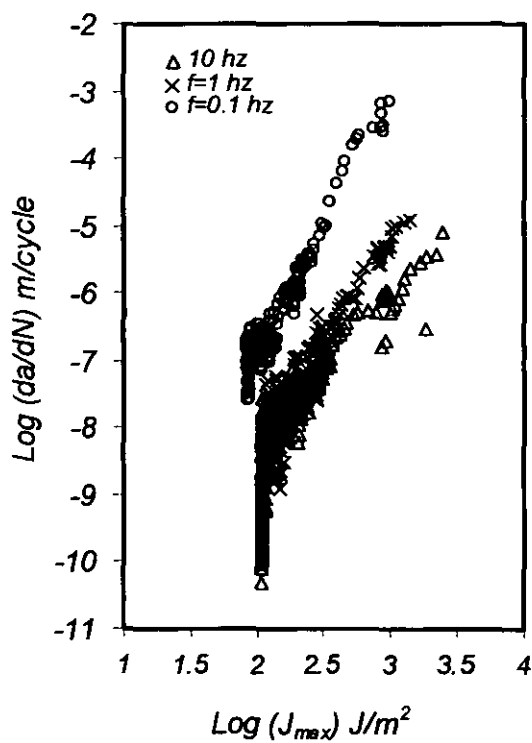Fig.(9.25) FCP curves for mild steel joints tested at RT.

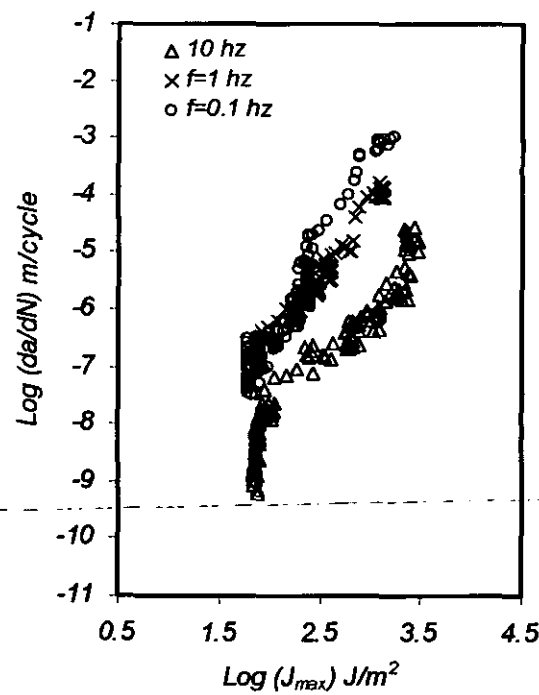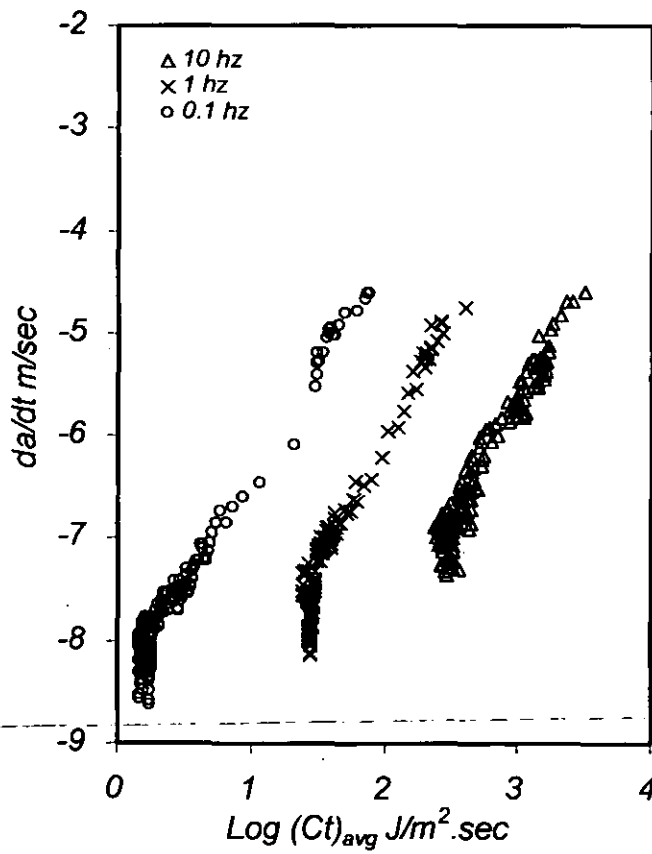Fig.(9.26) FCP curves for mild steel joints tested at 90°C.

Fig.(9.27) FCP curves for mild steel joints tested at 120°C.

Table (9.7) Results of cyclic fatigue tests in term of J_{max} at 10 Hz.

Joint type	Temperature °C	J_{th} (J/m^2)	Paris constant *a in m and J_{max} in J/m^2*	
			n	D
Mild steel FM300-2M	RT	133±5.85	3.433±.18	9.35E-16±1.67E-17
Mild steel FM300-2M	90	124±4.6	3.1196±0.21	3.16E-15±6.5E-16
Mild steel FM300-2M	120	77.2±3.7	2.631±0.69	4.28E-14±5.11E-15

Table (9.8) Results of cyclic fatigue tests in term of J_{max} at 1 Hz.

Joint type	Temperature °C	J_{th} (J/m^2)	Paris constant *a in m and J_{max} in J/m^2*	
			n	D
Mild steel FM300-2M	RT	110.7±8.2	3.743±0.21	8.55E-16±2.23E-17
Mild steel FM300-2M	90	120.3±5.6	3.110±0.13	1.58E-17±0.02E-17
Mild steel FM300-2M	120	73.8±3.2	3.119±.19	1.25E-12±9.5E-13

Table (9.9) Results of cyclic fatigue tests in term of J_{max} at 0.1 Hz.

Joint type	Temperature °C	J_{th} (J/m^2)	Paris constant *a in m and J_{max} in J/m^2*	
			n	D
Mild steel FM300-2M	RT	81.7±5.3	3.0226±0.23	1.496E-13±1.34E-14
Mild steel FM300-2M	90	85.8±3.1	3.126±0.53	3.16E-15±2.64E-16
Mild steel FM300-2M	120	68.6±3.6	2.428±0.43	3.00E-12±3.45E-13

9.4.3.2 Results in terms of $(C_t)_{avg}$

Figures (9.28), (9.29) and (9.30) show the fatigue crack propagation (FCP) in term of the creep parameter $(C_t)_{avg}$ for mild steel joints bonded with FM300-2M tested at RT, 90°C and 120°C respectively. The FCP curves with this parameter show less scatter than those seen with other parameters and more distinctive threshold regions are seen. The effect of test frequency also appears more clearly. Tables (9.10), (9.11) and (9.12) summarise the results of the fatigue tests for mild steel DCB samples reprocessed in term of $(C_t)_{avg}$ at 10 Hz, 1Hz and 0.1 Hz respectively.

Fig. (9.28) FCP curves for mild steel joints in term of $(C_t)_{avg}$ tested at RT.
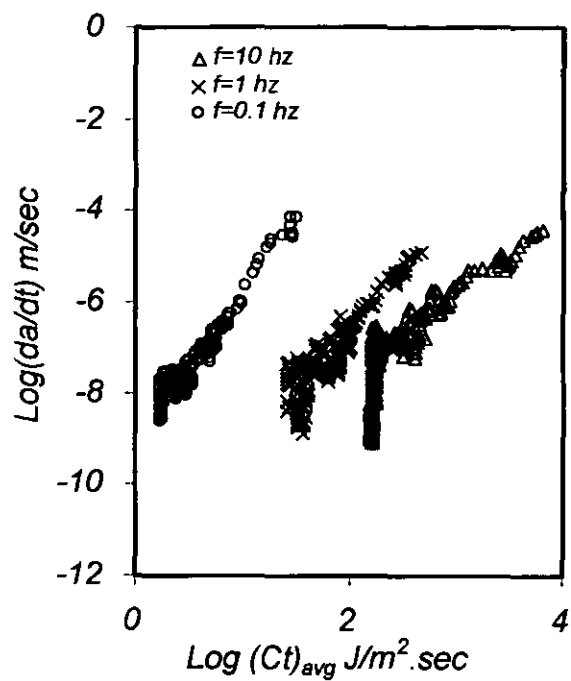
Fig. (9.29) FCP curves for mild steel joints in term of $(C_t)_{avg}$ tested at 90°C.
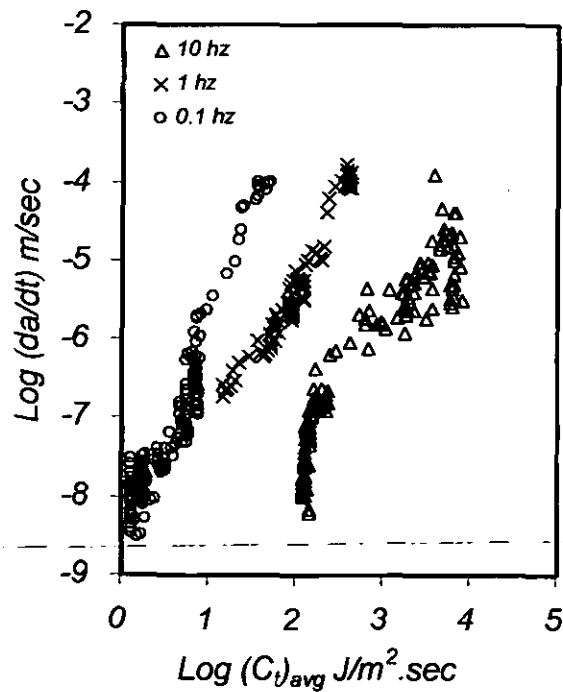

Fig. (9.30) FCP curves for mild steel joints tested at 120°C.

Table (9.10) Results of cyclic fatigue tests in term of $(C_t)_{avg}$ at 10 Hz.

Joint type	Temperature °C	$((C_t)_{avg})_{th}$ (J/m^2-sec)	Paris constant a in m and $(C_t)avg$ in J/m^2.sec	
			n	D
Mild steel FM300-2M	RT	227.3±10.9	2.4093±0.21	1.26E-13±1.29E-14
Mild steel FM300-2M	90	163.7±15.6	2.8547±0.16	1.076E-15±4.6E-16
Mild steel FM300-2M	120	135.4±18.6	1.7969±0.32	5.61E-13±5.9E-14

Table (9.11) Results of cyclic fatigue tests in term of $(C_t)_{avg}$ at 1 Hz.

Joint type	Temperature °C	$((C_t)_{avg})_{th}$ (J/m^2-sec)	Paris constant a in m and $(C_t)avg$ in J/m^2.sec	
			n	D
Mild steel FM300-2M	RT	24.4±2.5	2.3801±0.12	1.74E-11±5.5E-12
Mild steel FM300-2M	90	27.33±3.9	2.7502±0.24	5.12E-13±6.9E-14
Mild steel FM300-2M	120	16.1±2.88	1.7531±0.18	8.97E-10±7.7E-11

Table (9.12) Results of cyclic fatigue tests in term of $(C_t)_{avg}$ at 0.1 Hz.

Joint type	Temperature °C	$((C_t)_{avg})_{th}$ (J/m^2-sec)	Paris constant a in m and $(C_t)avg$ in J/m^2.sec	
			n	D
Mild steel FM300-2M	RT	1.77±0.21	2.1713±0.2	2.69E-9±1.23E-10
Mild steel FM300-2M	90	1.61±0.15	2.5918±0.15	15.59E-9±1.43E-10
Mild steel FM300-2M	120	1.45±0.08	1.702±0.22	3.99E-8±2.4E-9

9.4.4 Hold time effects

Figures (9.31) and (9.32) show the fatigue crack propagation (FCP) in term of $(C_t)_{avg}$ for mild steel joints bonded with FM300-2M tested at 90°C and 120°C respectively. Testing was carried out under displacement control with the constant amplitude trapezoidal waveforms described in section (8.5.2.3). Both plots are for tests at 0.1 Hz. Table (9.13) summarises the results of the hold time fatigue tests.

Table (9.13) Results of cyclic fatigue tests at t_h=30 sec.

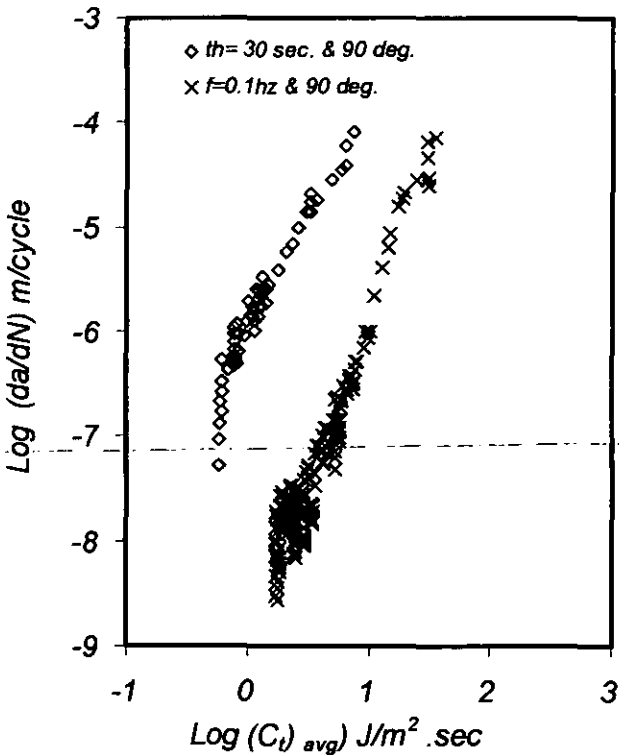| Joint type	Temperature °C	$((C_t)_{avg})_{th}$ $(J/m^2 .sec)$	Paris constant a in m and $(C_t)avg$ in $J/m^2.sec$	
			n	D
Mild steel FM300-2M	90	0.68±0.16	2.025±0.12	1.81E-6±2.2E-7
Mild steel FM300-2M	120	0.52±0.12	2.60±0.2	3.126E-6±3.5E-7

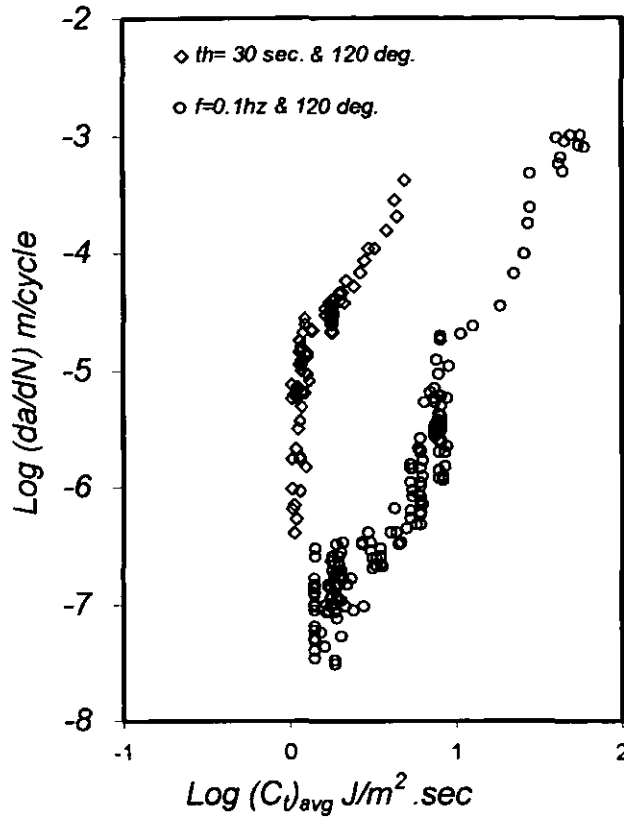Fig. (9.31)FCP curve for mild steel joints tested at 90°C.

Fig. (9.32) FCP curve for mild steel joints tested at 120°C.

It is seen clearly that, the hold time during fatigue loading decreases the threshold values and accelerates the crack growth rate. This type of test will be used in the prediction of crack growth under fatigue/creep loading conditions.

9.4.5 Variable frequency results

9.4.5.1 Equal cycle loading stages

Variable frequency testing was carried out using the three-stage block-loading spectrum shown in Figure (8.5). The applied frequency for stages 1, 2 and 3 were 10 Hz, 1Hz and 0.1Hz respectively. The number of cycles in each stage was 1000. Figures (9.33) and (9.34) show the experimental crack growth under variable frequency loading for CFRP and mild steel joints tested at room temperature respectively.
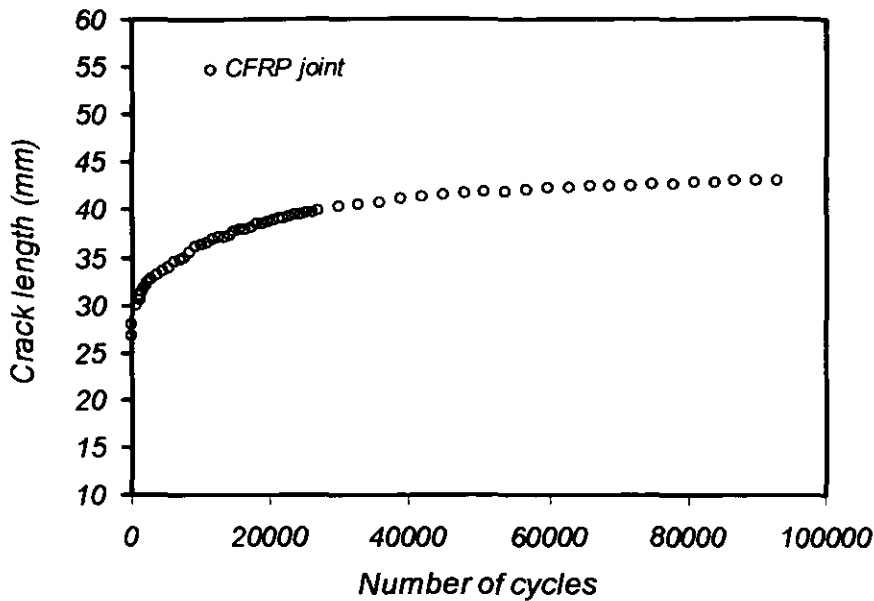
Fig. (9.33) Crack growth under variable frequency-loading for CFRP tested at RT.
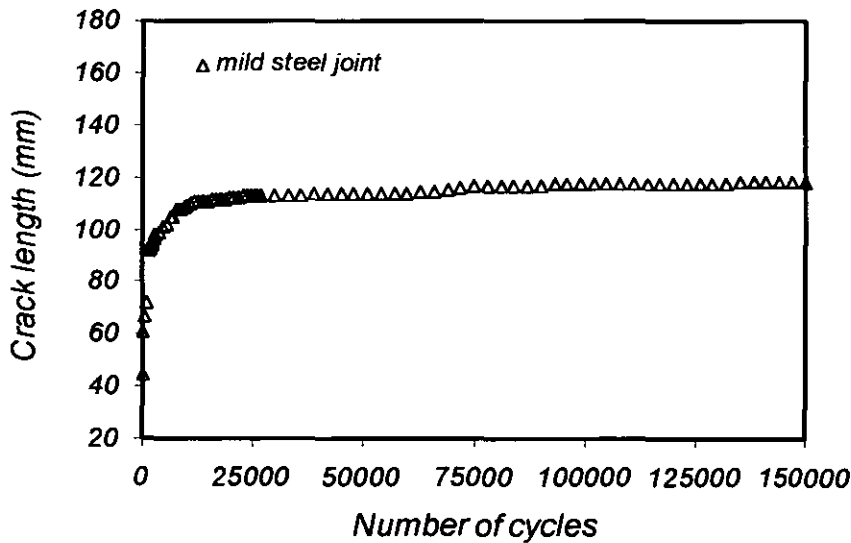

Fig. (9.34) Crack growth under variable frequency-loading for mild steel tested at RT.

Figures (9.35) and (9.36) show the experimental crack growth under variable frequency loading for mild steel joints at 90°C and 120°C respectively.
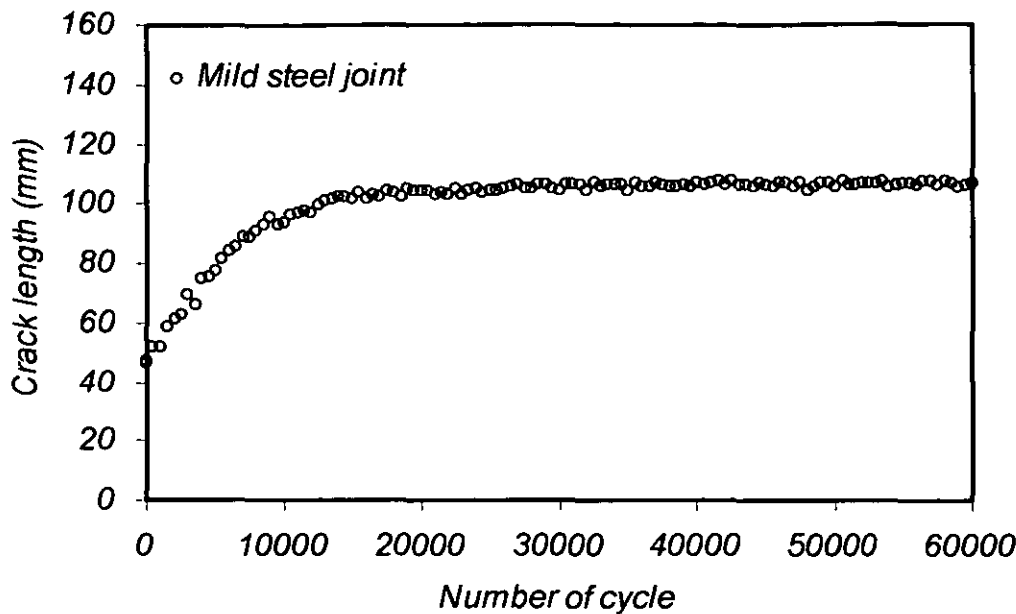
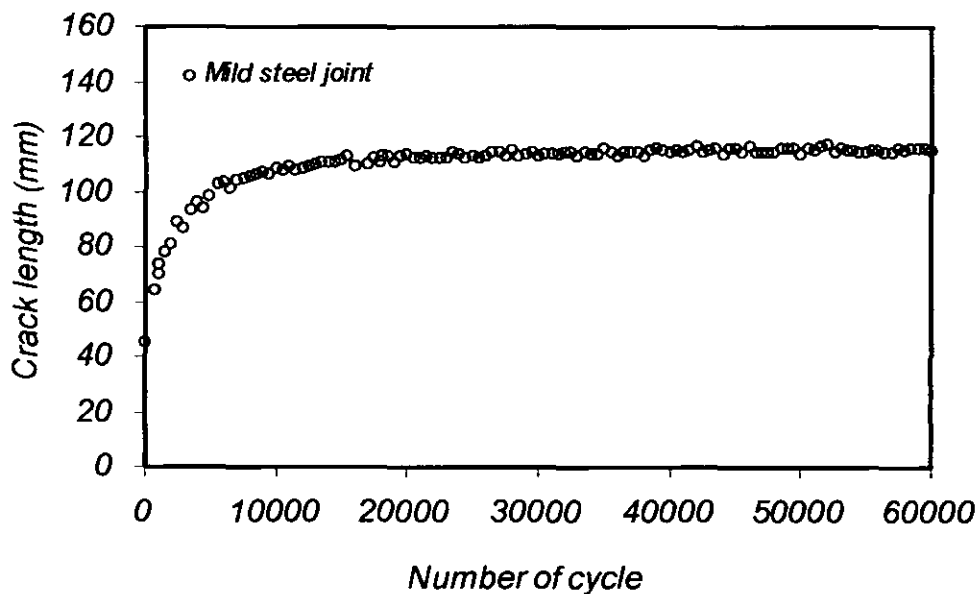Fig. (9.35) Crack growth under variable frequency-loading for Mild steel tested at 90°C.

Fig. (9.36) Crack growth under variable frequency-loading for Mild steel tested at 120°C.

9.4.5.2 Equal time and variable loading stages

Figure (9.37) shows the experimental crack growth under variable frequency loading for mild steel joints tested at room temperature. It shows the three types of loading form,

namely equal number of cycle stages, equal time stages and variable stages. Results indicate that the equal cycle stage is slightly faster than the equal time stage. This is seen more clearly in Figure (9.38) which gives an expanded view of the early stage of the crack growth. The variable stage is similar to the equal time stage.
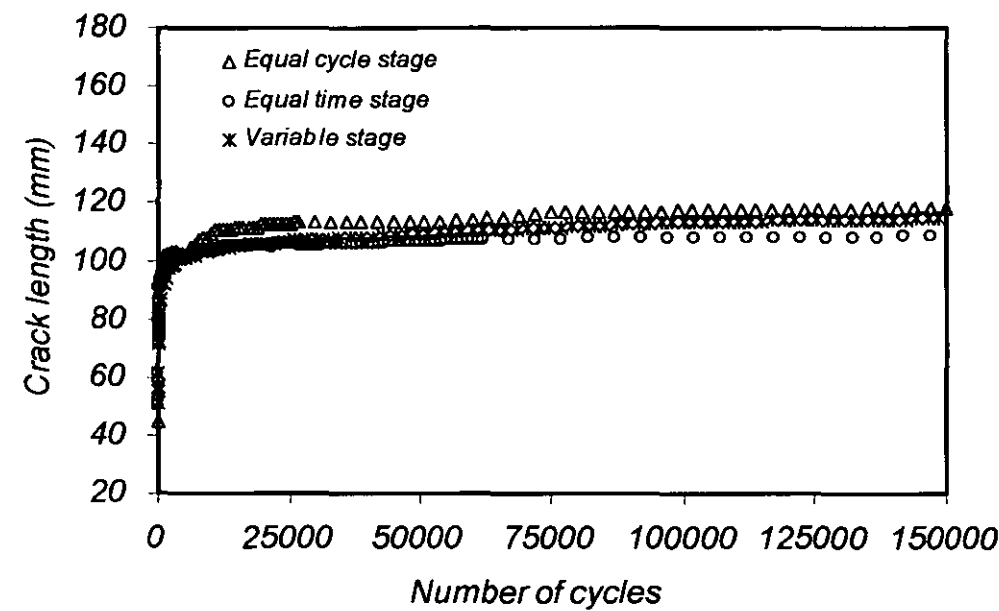
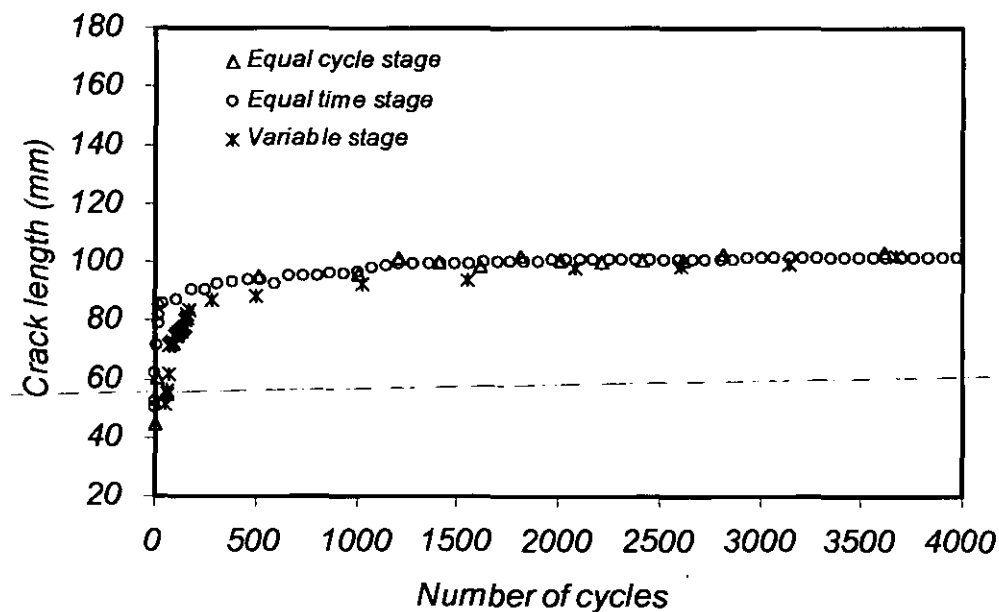Fig. (9. 37) Crack growth under variable frequency-loading for Mild steel tested at RT.

Fig. (9.38) Crack growth under variable frequency-loading for Mild steel tested at RT, early stage.

9.4.6 Effect of surface treatment on locus of failure

The second surface treatment procedure, a sulphuric-acid etch (SAE), described in section (2.7) was applied to the mild steel joints to investigate the effect of surface treatment on the locus of failure and fatigue threshold values. This is compared with the standard grit blast and degreases (GBD) procedure described in section (8.3).

Log-log plots of FCPR against G_{max} for SAE treated mild steel DCB's are shown in Figure (9.39). This shows clearly the effect of fatigue frequency. The fatigue threshold (G_{th}), can be seen to decrease as the test frequency decreases. The locus of failure changed from the apparent interfacial failure seen with GBD treated adherends to completely cohesive failure with the SAE pre-treatment. The threshold value exhibited an increase associated with this change in locus of failure. Table (9.14) summarises the results of the fatigue tests for the mild steel DCB samples with both treatments and the CFRP samples all tested at room temperature.
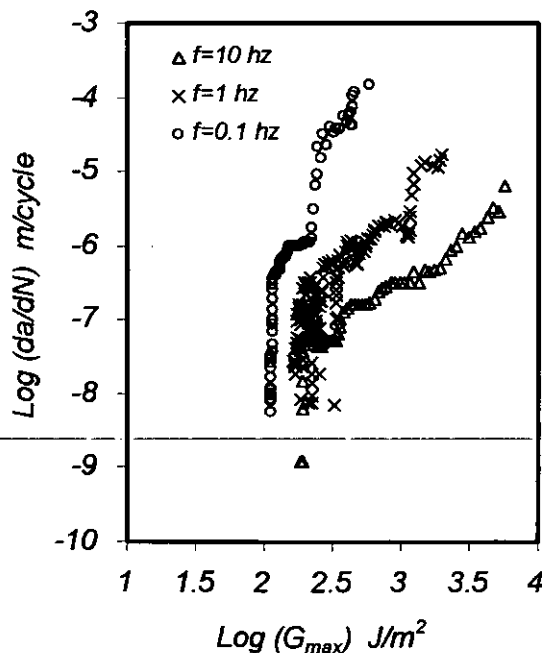

Fig. (9.39) FCP curves for mild steel joints tested at RT: SAE pre-treatment.

Table (9.14) Results of fatigue /treatments effect tests.

Joint type	Treatment procedure	Frequency (Hz)	G_{th} (J/m^2)	Failure type
CFRP FM300-2M	*GBD*	10	220±9.2	Cohesive
CFRP FM300-2M	*GBD*	1	187±5.68	Cohesive
CFRP FM300-2M	*GBD*	0.1	140±10.4	Cohesive
Mild steel FM300-2M	*GBD*	10	133±5.85	Apparent interfacial
Mild steel FM300-2M	*GBD*	1	110.7±8.2	Apparent interfacial
Mild steel FM300-2M	*GBD*	0.1	81.7±5.3	Apparent interfacial
Mild steel FM300-2M	*SAE*	10	188.8±5.2	Cohesive
Mild steel FM300-2M	*SAE*	1	165.2±9.2	Cohesive
Mild steel FM300-2M	*SAE*	0.1	111.6±6.8	Cohesive

It is clear that, treating mild steel joints with the SAE pre-treatment increases their performance. However, this performance still seems to be less than that seen with the CFRP joints.

9.5 Creep test results

Figures (9.40) and (9.41) show crack growth versus time for DCB joints bonded with FM300-2M adhesive tested at 90°C and 120°C respectively. The plots show three stages of creep behaviour at 120°C; while at 90°C only the secondary and tertiary stages are notable.
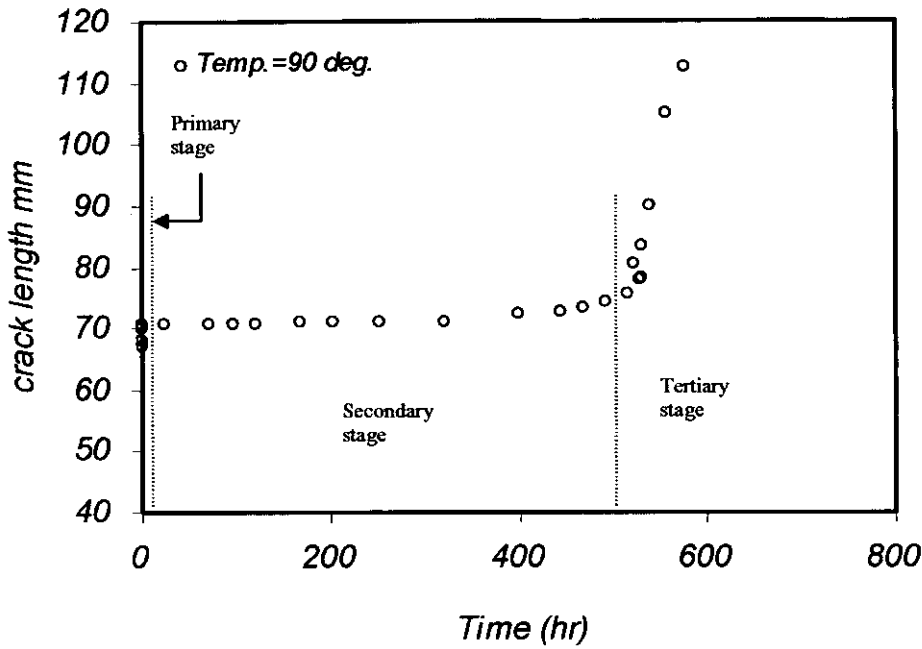
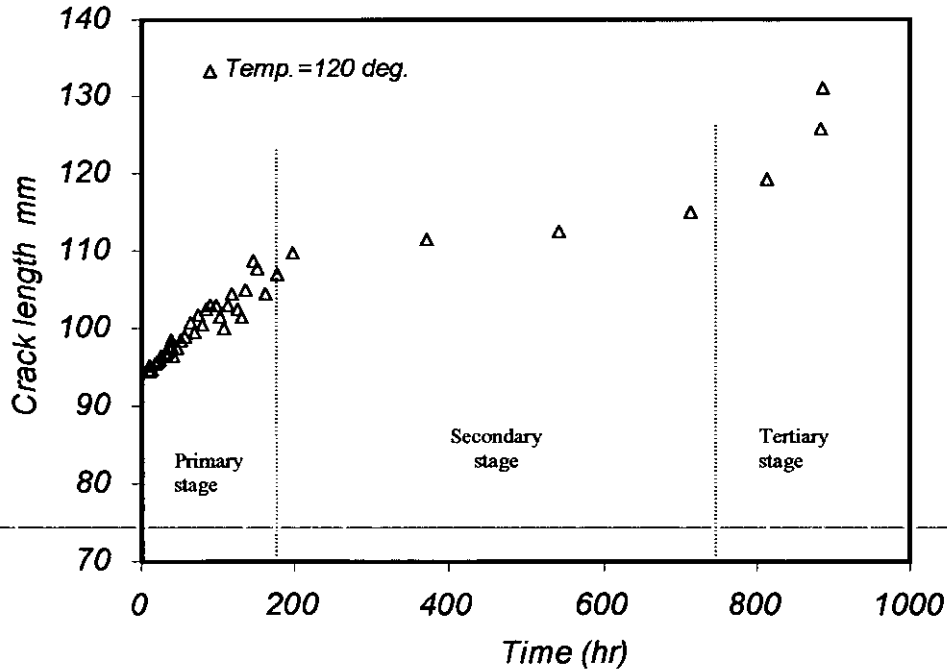Fig. (9.40) Creep crack growth against time for DCB joint tested at 90°C.

Fig. (9.41) Creep crack growth against time for DCB joint tested at 120 °C.

Figure (9.42) and Figure (9.43) show the displacement versus time for joints tested at *90°C*
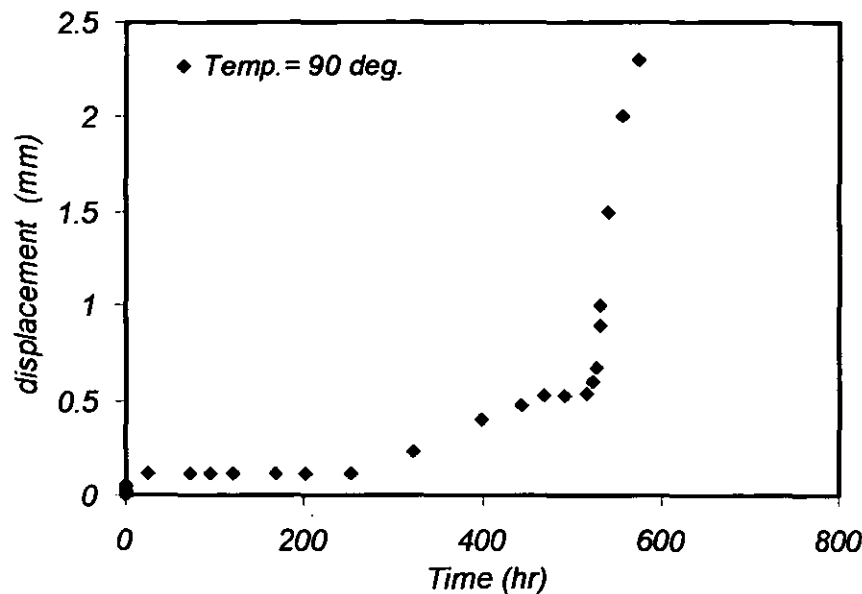
and *120°C* respectively.

Fig. (9.42) Displacement against time for DCB joint tested at 90°C.

At *90°C* the variation of displacement appears to be lower than the variation obtained at

120°C, as expected. Also the three stages of creep can be seen more clearly at *120°C*.

Fig. (9.43) Displacement against time for DCB joint tested at 120°C.

Log – log plots of creep crack propagation rate (CCPR) against the creep parameter, C*, for mild steel joints bonded with FM300-2M are shown in Figure (9.44) and Figure (9.45) for joints tested at 90°C and 120°C respectively. Similar trends have been seen in similar studies in metals [4.18]

Fig. 9.44 CCPR against creep parameter, C* for joint tested at 90°C.
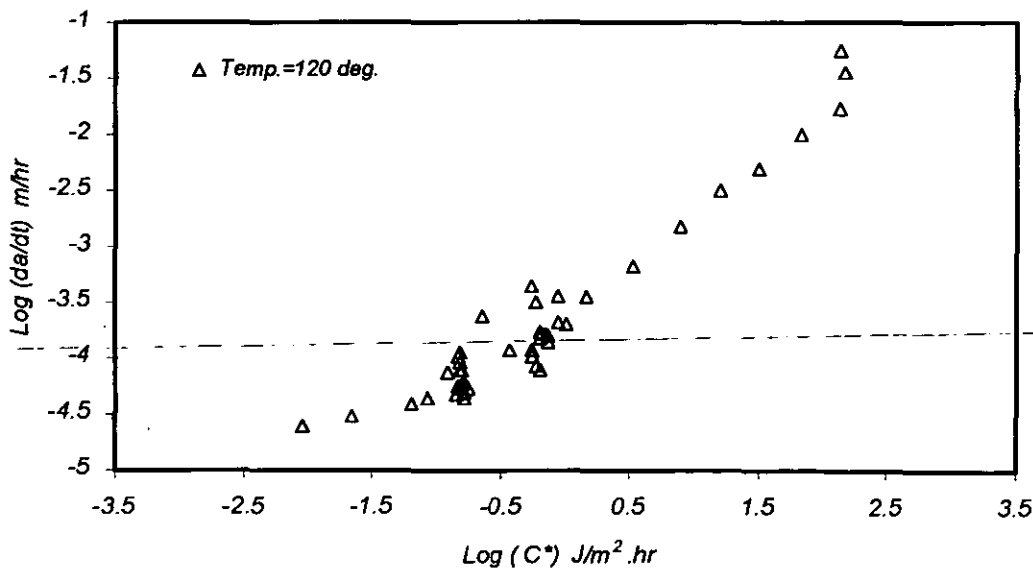
Fig. 9.45 CCPR against creep parameter, C* for joint tested at 120°C.

Log – log plots of displacement rate (du/dt) against creep parameter, C*, for mild steel joints bonded with FM300-2M are shown in Figure (9.46) and Figure (9.47) for joints tested at 90°C and 120°C respectively.

Fig. (9.46) The displacement rate against creep parameter, C* for joint tested at 90°C.
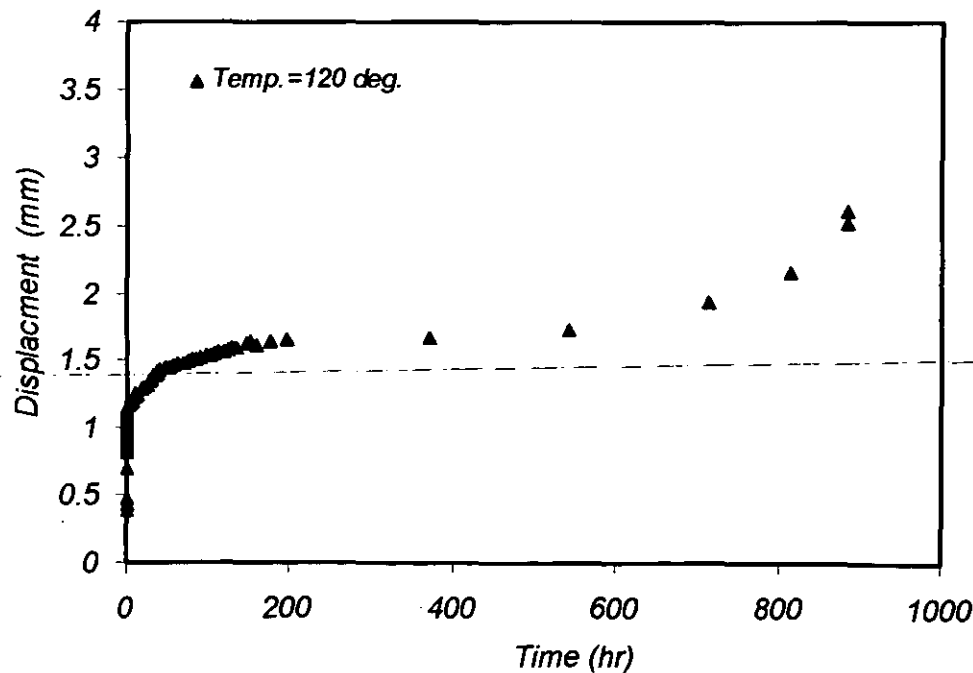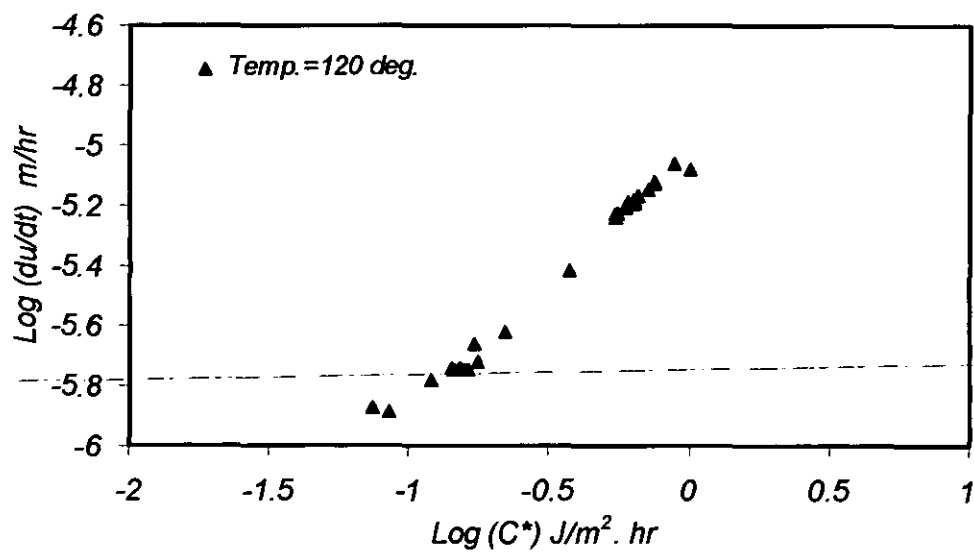

Fig. (9.47) The displacement rate against creep parameter, C* for joint tested at 120°C.

Log – log plots of creep crack propagation rate (CCPR) against the creep parameter, C_t, for mild steel joints bonded with FM300-2M are shown in Figure (9.48) and Figure (9.49) for joints tested at 90°C and 120°C respectively. These show similar trends to C^*. The required material constants are tabulated in Table (9.15) for both joints.
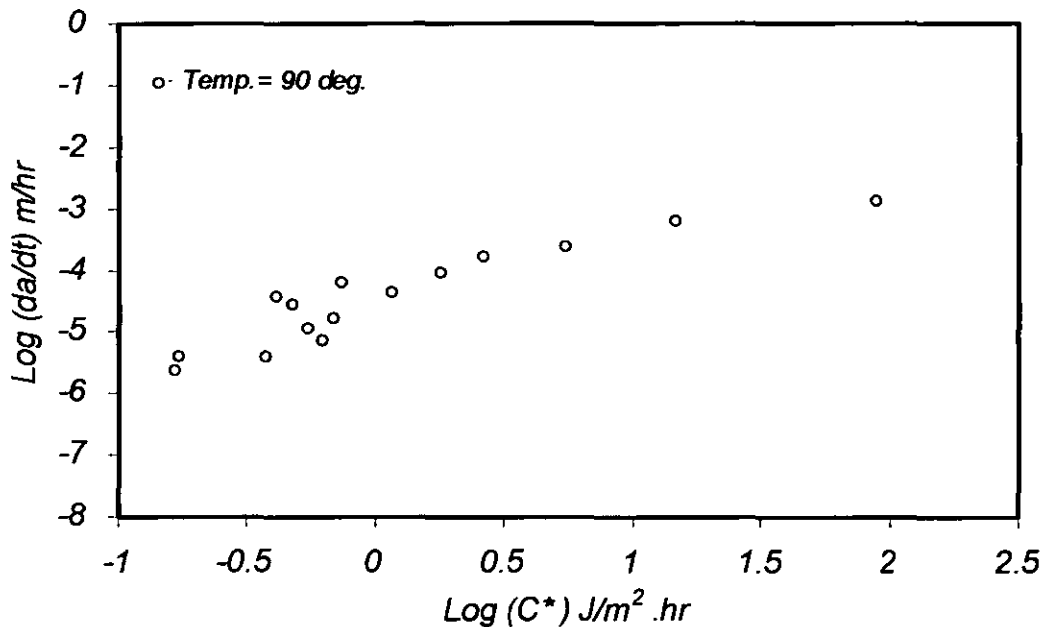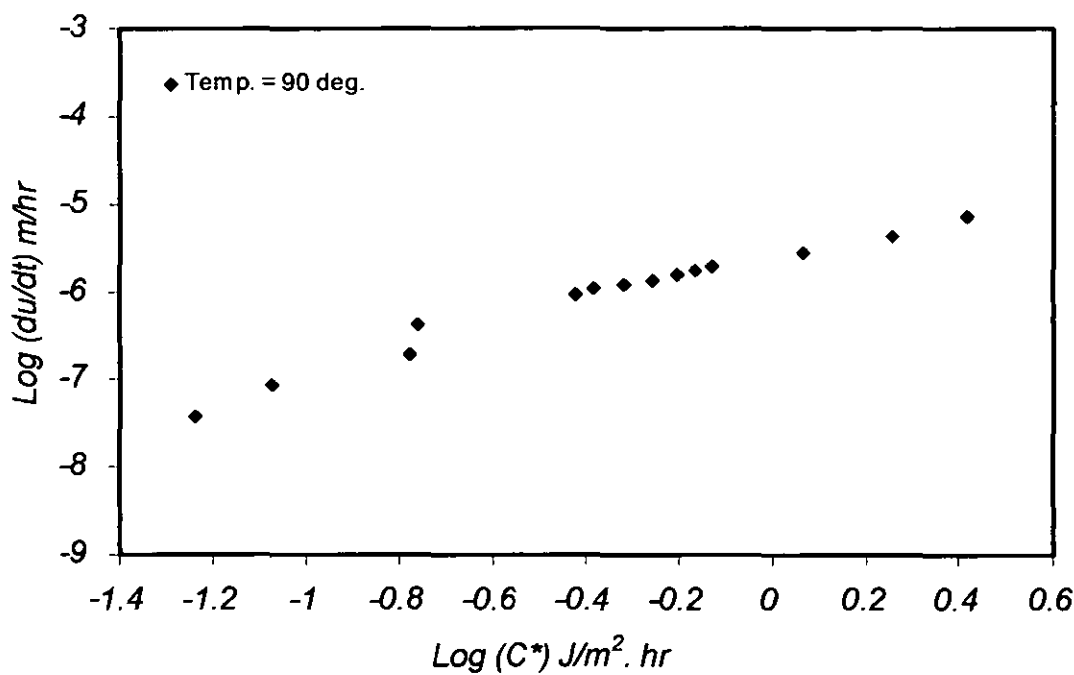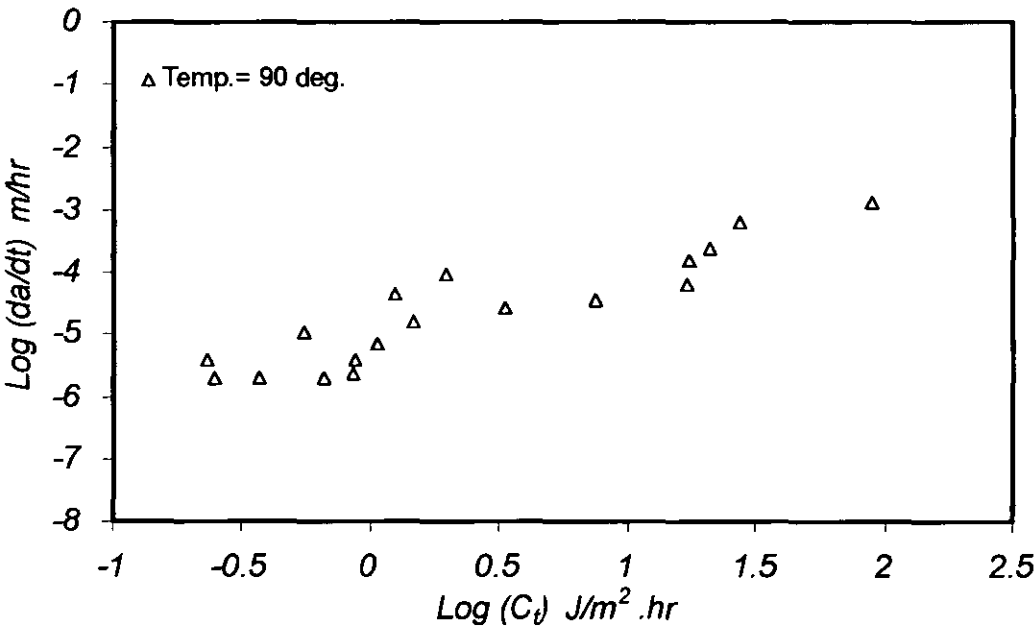

Fig. 9.48 CCPR against creep parameter, Ct for joint tested at 90°C.
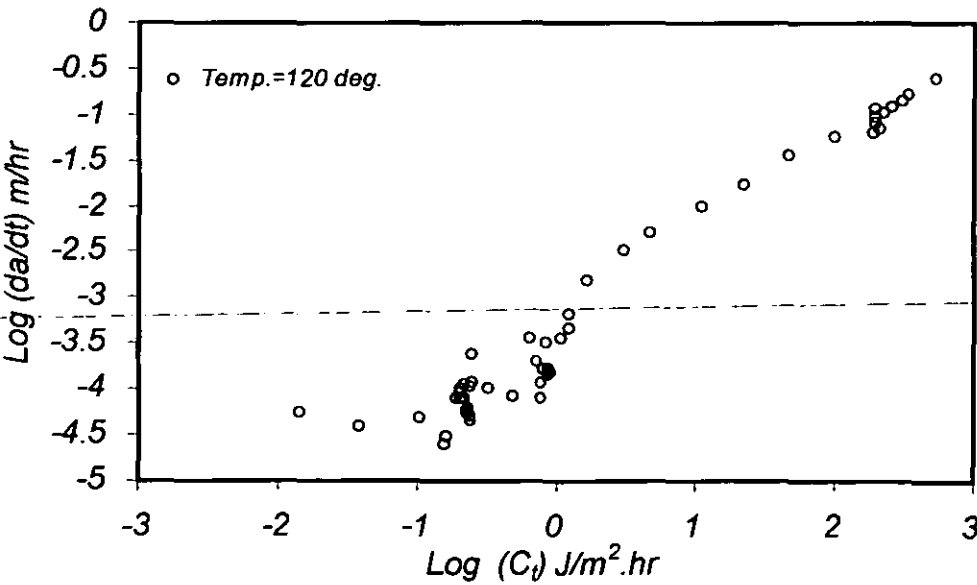
Fig. 9.49 CCPR against creep parameter, Ct for joint tested at 120°C.

Table (9.15) Results of creep tests.

Joint type	Temperature	$da/dt = m \ (c_t)^q$ $t \ in \ hr \ and \ Ct \ in \ J/m^2.hr$	
		q	m
Mild steel Fm300-2M	90°C.	1.0548±0.15	8.892E-6±6.23E-7
Mild steel Fm300-2M	120°C.	0.921±0.12	196.5E-6±3.33E-7

To compare the crack velocity under creep loading with that under fatigue loading, da/dt data obtained from both creep and fatigue tests were plotted against strain energy release rate G, as shown in Figures (9.50) and (9.51) for joints tested at $90°C$ and $120°C$ respectively.
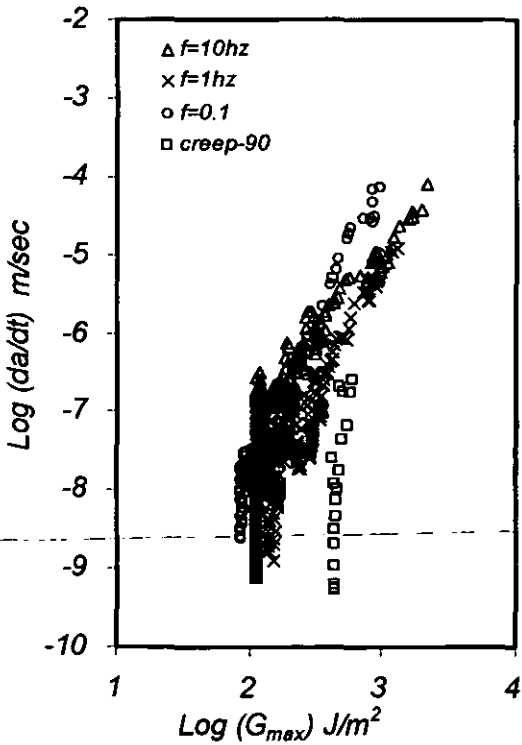
Fig. (9.50) FCP curves (fatigue and creep) for mild steel joints tested at 90°C.
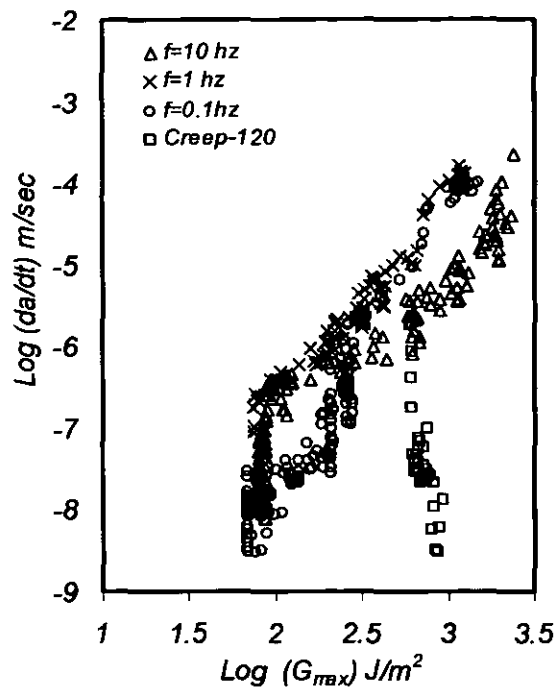
Fig. (9.51) FCP curves (fatigue and creep) for mild steel joints tested at 120°C

The strain energy release rate, G for creep was calculated based on the relationship between G and the crack length, a, shown in Table (8.2). It is seen that da/dt for creep is lower than that for fatigue. The higher da/dt for fatigue is due to the additional cyclic loading component that the joints experience in addition to the sustained load.

9.6 Fractography

In this section the fracture surfaces of failed mild steel test specimens at room temperature, 90°C and 120°C are investigated at different applied frequencies. The images show that the locus of failure for the mild steel joints at room temperature is mostly in the interfacial region whereas at elevated temperature it tends to be mostly cohesive in the adhesive with occasional islands of interfacial failure, these islands of interfacial failure getting smaller at lower applied frequency and as the temperature increases to 120°C.

Figure (9.52) shows failed test specimens at room temperature. The locus of failure is dependent on the frequency. It is completely in the interfacial region at 10 Hz and become increasingly cohesive as frequency decreases.
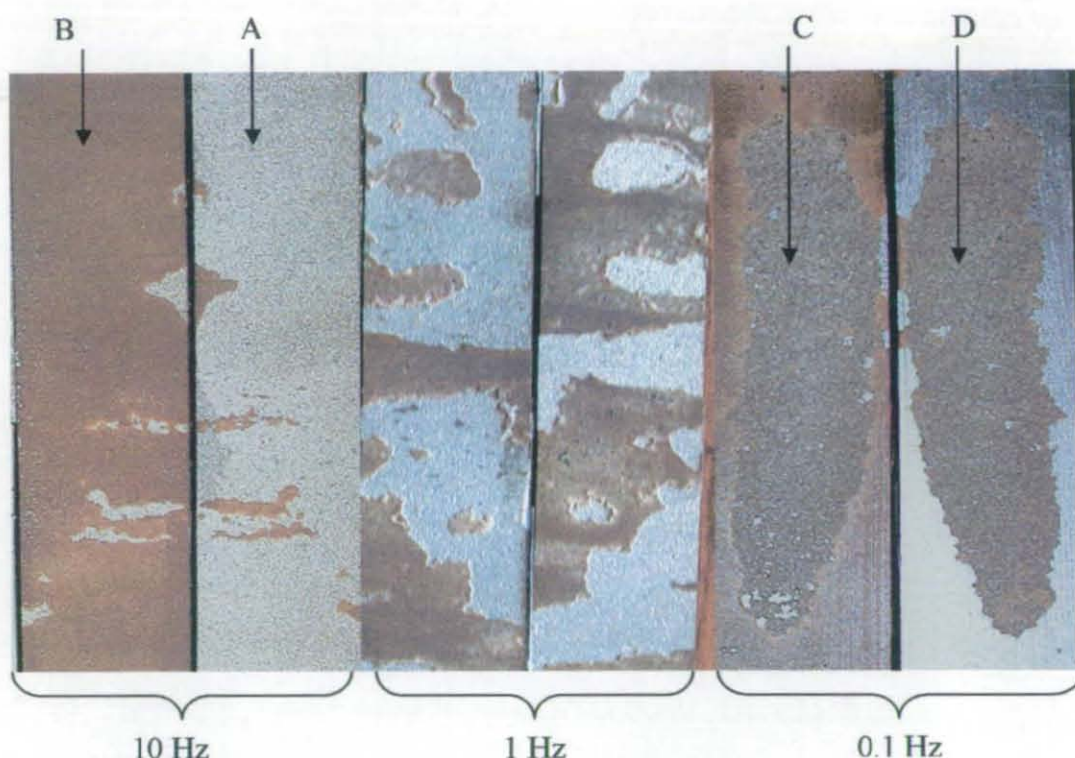
Fig. (9.52) Failed test specimens of, mild steel joints tested at RT.

SEM micrographs are shown in Figure (9.53) and figure (9.54) for the positions A-D shown in Figure (9.52). Figure (9.53) shows apparent interfacial fracture at 10 Hz. Cracks and a plate like structure can be seen on the "metal" side of the "apparent interfacial failure". This is possibly an indication that the apparent interfacial failure is in fact in a thin layer of brittle, modified adhesive resin adjacent to the steel adherend. Although the exact location and nature of this apparent interfacial failure isn't known it can be seen that this is very different to the "cohesive failure" seen at higher temperatures and lower frequencies. It can also be said that this apparent interfacial failure is associated with poorer mechanical performance than the cohesive failure. Although these images indicate that true interfacial

failure has not occurred the term "apparent interfacial failure" will continue to be used in order to differentiate between the two types of fracture observed. However, this term now indicate the apparent interfacial failure somewhere in the interphase region close to the steel substrate. Figure (9.54) shows the change in the fracture surface at 0.1 Hz. This appeared to be approximately 70% cohesive to 30% apparent interfacial failure. Figure (9.54) shows the fracture surface in a cohesive failure region. The carrier fibres can be seen clearly in this fracture surface, however, the cracks seen in the apparent interfacial failure are absent. This change in failure locus may be related to the change in the state of the epoxy from brittle to more ductile at lower frequency as it is believed that a slower strain rate (lower frequency) has the same effect as raising the test temperature.

Crack

Adhesive

Position A (substrate side)   Position B (adhesive side)
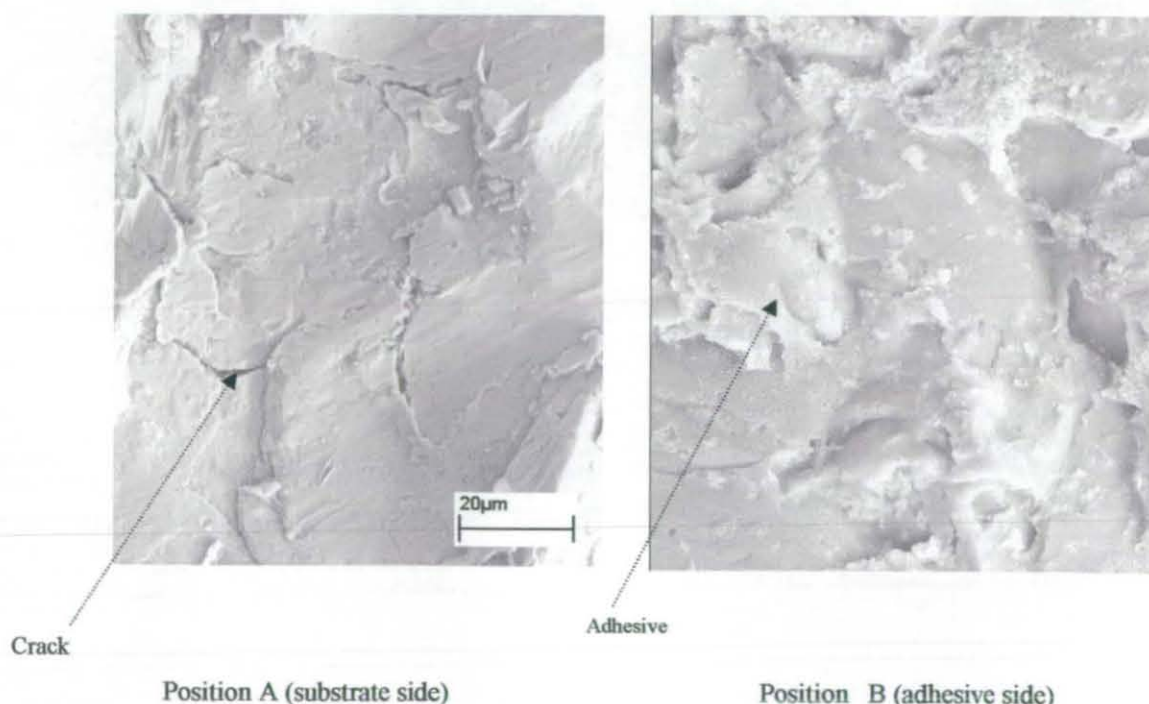
Fig. (9.53) SEM Image of failed surface at (RT & 10 Hz) at selected position.

Position C   Position D
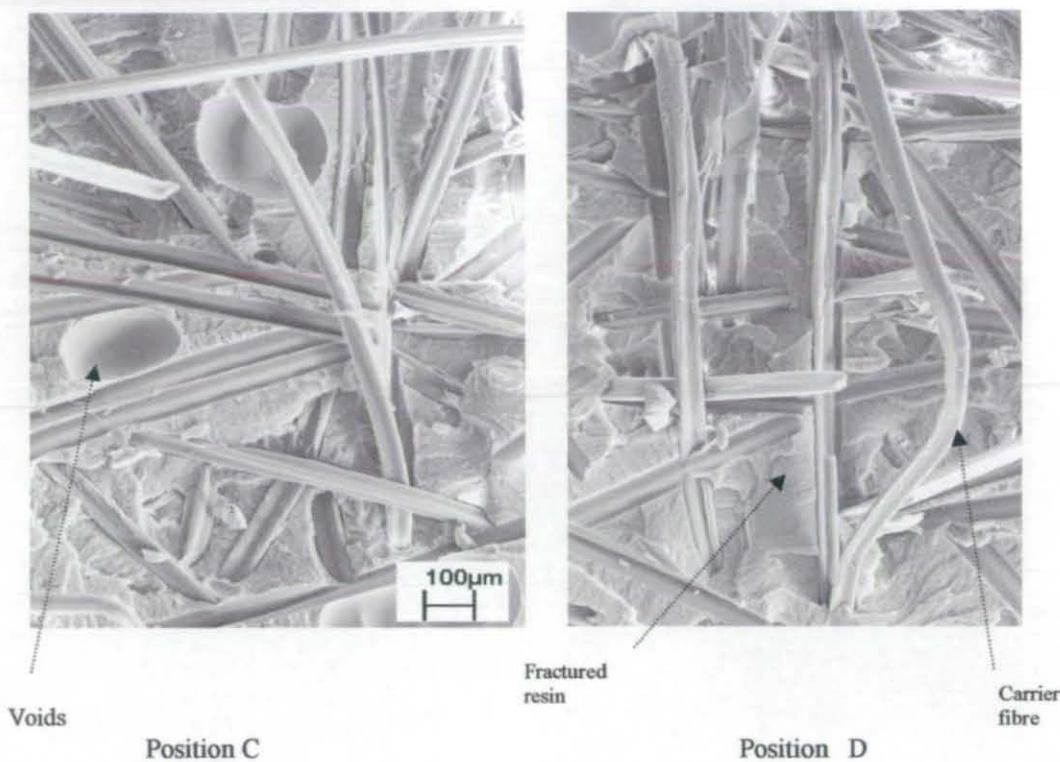
Fig. (9.54) SEM Image of failed surface at (RT & 0.1 Hz) at selected position.

Figure (9.55) shows images of failed test specimens at 90°C. The locus of failure is clearly effected by temperature and applied frequency; the locus of failure at 10 Hz/90°C is in the interfacial region, while at low applied frequency, failure tends to be mostly cohesive.

10 Hz   1 Hz   0.1 Hz
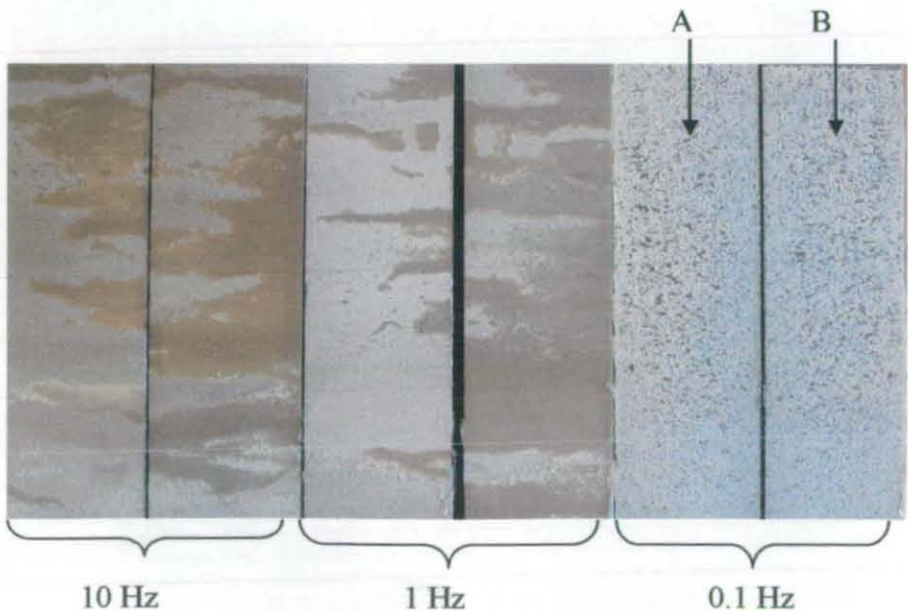
Fig. (9.55) Image of failed test specimen of mild steel joints tested at 90°C.

The SEM micrographs shown in Figure (9.56) are from the selected positions A and B in Figure (9.55). The locus of failure appeared to be 95% cohesive to 5% apparent interfacial failure. Figure (9.56) shows the presence of loose carrier fibres and shows the appearance of more ductile fracture than that seen in Figure (9.54).

Position A   Position B

Fig. (9.56) Image of failed test specimen of mild steel joints tested at 90°C

Figure (9.57) shows failed test specimens at 120°C. In this case the locus of failure appears to be mostly cohesive failure in the adhesive .The change of locus of failure may be due to the increase in viscoelasticity of the adhesive with temperature. A progressive change in the mode of failure can be seen as the temperature and frequency change. The fatigue failure modes are summarised in Table (9.16).
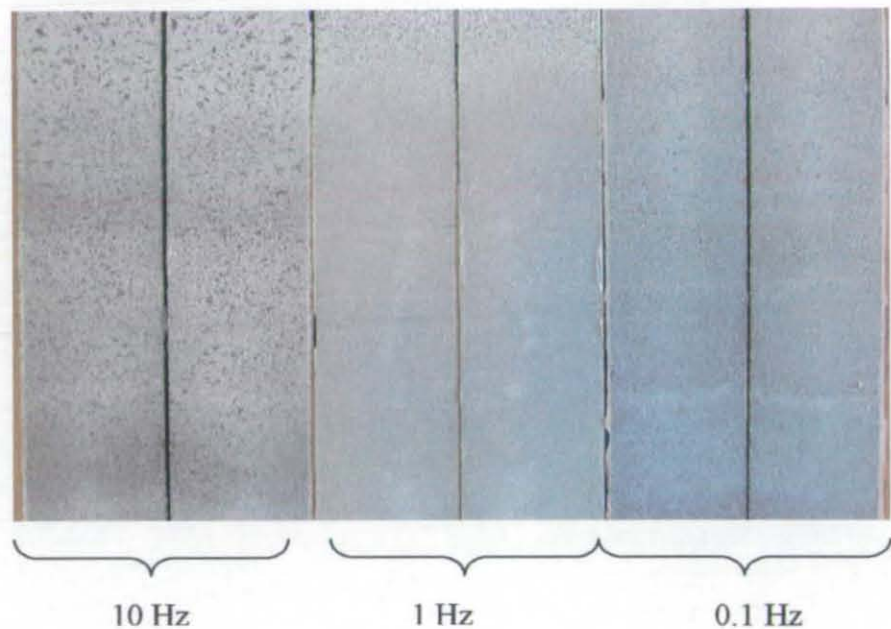
Fig. (9.57) Image of failed test specimen of mild steel joints tested at 120°C.

Table (9.16) Summary of Fatigue failure modes

Temp.	Frequency	Failure path
RT	10	Completely interfacial (one side)
	1	Apparent interfacial + Two side
	0.1	Mostly interfacial + bigger cohesive islands
90°C	10	Completely interfacial (two side)
	1	Apparent interfacial + cohesive
	0.1	Mostly cohesive
120°C	10	Mostly cohesive
	1	Mostly cohesive
	0.1	Mostly cohesive

The fatigue failure mode for other tests described through out this chapter are summarised

and tabulated in Table (9.17).

Table (9.17) Summary of Fatigue failure modes

Test type	Temperature	Failure path
Quasi static tests (with different loading rate)	RT	Cohesive in the adhesive
	90°C	Cohesive in the adhesive
	120°C	Cohesive in the adhesive
Variable frequency tests	RT	Apparent interfacial + Small cohesive island
	90°C	Cohesive in the adhesive
	120°C	Cohesive in the adhesive
Fatigue (Hold time tests)	90°C	Cohesive in the adhesive
	120°C	Cohesive in the adhesive
Fatigue (treatment tests)	RT	Cohesive in the adhesive
Creep tests	90°C	Cohesive in the adhesive
	120°C	Cohesive in the adhesive

9.7 Summary

In this chapter efforts have been made to study the effect of various applied loading conditions on the crack growth in adhesively bonded joints. The effects of loading rate and temperature on the G_c value were investigated. It was seen that, G_c value decreases as temperature is increased. Also it was seen that, decreasing the loading rate had a similar effect to increasing temperature on G_c. Thus it is very important to consider temperature and loading rate during the design of adhesively bonded joints. The effect of fatigue frequency on crack growth in bonded DCB samples with mild steel and CFRP substrates was investigated. It was seen that for both cohesive and interfacial failure, reducing the fatigue frequency had a significant effect in reducing the fatigue threshold and accelerating crack growth. This effect is most probably attributable to the viscoelastic nature of the polymeric materials used in adhesives, which make them rate sensitive and susceptible to creep. It was seen that, plotting the crack growth rate as a function of time rather than number of cycles, i.e. da/dt brought the crack growth curves at different frequency closer together. This makes it possible, in the case of interfacial failure to estimate the crack growth at different frequencies form a master da/dt vs G_{max} plot. Results showed that, the

relationship between frequency and the Paris constants was a log- linear relationship. This is significant as it means that a FCP curve can be easily constructed for any frequency and temperature by interpolation, hence, crack growth at any frequency and temperature can be easily predicted.

In this chapter various parameters of fracture, i.e. G_{max}, J_{max} and $(C_t)_{avg}$ were used to relate the crack growth rate. Results indicate that; $J_{max} > G_{max}$. This is due to plasticity occurring at the crack tip. At elevated temperatures, the creep parameter $(C_t)_{avg}$ is a candidate parameter to characterise the crack growth. Therefore, these different fracture parameters were investigated in order to find which was most suitable in various loading and environmental conditions. This will be discussed further in chapter (10).

It was seen that, the creep behaviour of mild steel joints showed the three stages of creep for joint tested at 120°C while joints tested at 90°C only showed two stages clearly. Relating the crack growth rate *da/dt* to the creep parameter C_t showed a similar trend to that obtained by Saxena [4.18]. With these tests it possible to use the approach described in section (5.8) to characterise the fatigue and creep crack growth independently and to compare this with experimental tests involving both fatigue and creep, such as fatigue testing at low frequency, fatigue testing with hold times and variable frequency fatigue tests.

SEM studies showed that the locus of failure for both CFRP and grit blast degreased (GBD) mild steel joints tested quasi-statically was cohesive failure in the adhesive. However, the locus of failure in fatigue loading for mild steel joints was apparently interfacial failure at low temperatures and test frequencies. However, SEM seemed to indicate that this apparent interfacial failure could in fact be fracture of a thin layer of modified polymer material adjacent to the steel. An improved surface treatment (SAE) for the mild steel substrate changed the locus of failure to cohesive failure even at room

temperature. It was also seen that, the locus of failure for GBD mild steel joints tested at

elevated temperature and low frequency tended to be mostly cohesive failure with some

interfacial failure. The change of locus of failure may be due to viscoelasticity effects of

the adhesive with elevated temperature or the slower rate of loading (low frequency).

CHAPTER 10

PREDICTION OF CREEP AND FATIGUE CRACK GROWTH IN ADHESIVELY BONDED JOINTS

10.1 Introduction

The ultimate aim of any fracture mechanics research must be the ability to predict, with confidence, the useful service life of structures. In previous work by a number of authors [10.1-10.6] attempts have been made to predict the fatigue performance of adhesively bonded joints. In this work four methods are used to predict crack growth under fatigue and fatigue-creep conditions. The first method assumes that crack growth can be described by a suitable crack growth law and that the crack growth law constants can be determined experimentally as functions of frequency and temperature. The second method assumes creep and fatigue crack growth are competing mechanisms and the crack growth rate is determined by whichever is dominant. The third method, assumes that crack growth can be partitioned into cyclic dependent (fatigue) and time dependent (creep) components and that crack growth can be predicted by simply adding the two components. The fourth method is used when crack growth is faster than predicted by adding the individual fatigue and creep components, indicating a fatigue-creep interaction effect. In this case an empirical interaction term is added to the fatigue and creep components. These methods will be compared with the experimental work presented in the previous chapter.

10.2 Empirical crack growth law method

This method assumes that crack growth can be described by a suitable crack growth law and the crack growth law constants can be determined experimentally as a function of frequency and temperature.

10.2.1 Crack growth rate in term of frequency (da/dN = F (f))

Based on the experimental data obtained at different frequencies and temperatures for mild steel joints, the crack growth rate da/dN verses G_{max} (J_{max} or $(C_t)_{avg}$) can be calculated at a range of frequencies.

The procedure for this approach is based on first obtaining constant amplitude fatigue crack propagation (*FCP*) curves (i.e. plotting *da/dN* vs. $G_{max.}$, J_{max} or $(C_t)_{avg}$) within the desired frequency range. The crack growth rate, *da/dN*, can be correlated to a suitable fracture mechanics parameter using a suitable fatigue law, such as the Paris law given by:

$$\frac{da}{dN} = D(G_{max})^n \qquad (10.1)$$

To perform the predictions, the values for the 'Paris law' coefficients D and n need to be derived from the experimental data. These coefficients along with the threshold strain energy release rate (G_{th}) and the critical strain energy release rate (G_c) are all that are required to describe the *FCP* curve and can be considered as material properties. This has been done for mild steel joints. The Paris constants were formulated as a function of frequency, f by interpolating values from the experimental tests carried out over a range of frequencies *(0.1-10Hz)* as shown in Tables (10.1), (10.2) and (10.3) for joints tested at RT, 90°C and 120°C respectively.

Prediction of crack length is based on a simple iterative algorithm in which the fracture parameter, such as G_{max}, is first calculated for the initial crack length, a_0. The Paris law constants for that particular condition are then used to determine the crack growth rate, da/dN, which is multiplied by the number of cycles to give the overall crack growth (Δa). A new crack size ($a_1 = a_0 + \Delta a$) is then calculated and the process repeated. This procedure

is repeated until G_{max} becomes equal to the threshold value G_{th}. The steps used in this prediction method are illustrated in Fig. (10.1).
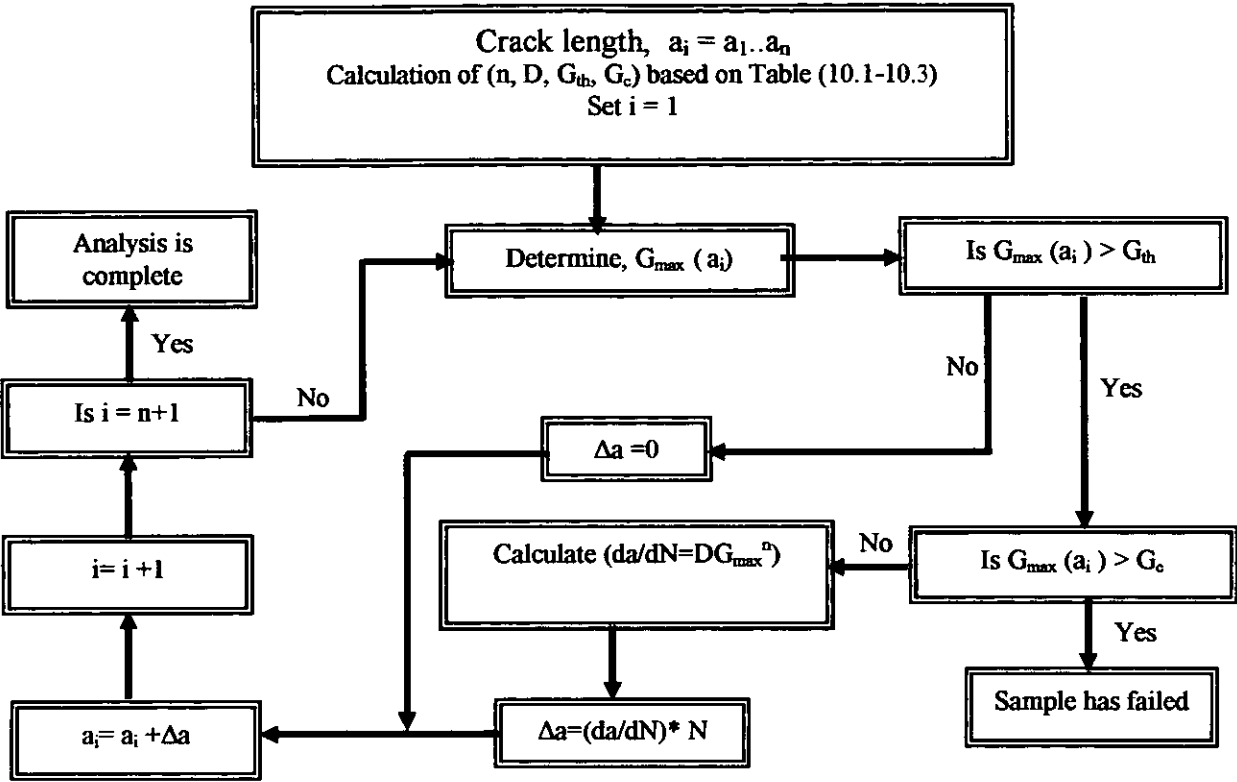
Fig. (10.1)   Fatigue life prediction algorithm

Table (10.1) Crack growth rate as function of frequency for joints tested at RT.

Fracture parameters in form of Paris law	Paris constants		Conditions
	D	n	
$\dfrac{da}{dN} = DG_{max}^n$	$2X10^{-14} f^{-1.0443}$	$2.9803 f^{0.0210}$	$G_{th} > 105.95 f^{0.1085}$
$\dfrac{da}{dN} = DJ_{max}^n$	$5X10^{-15} f^{-1.102}$	$3.3863 f^{0.0277}$	$J_{th} > 105.95 f^{0.1085}$
$\dfrac{da}{dN} = D(Ct)_{avg.}^n$	$2X10^{-11} f^{-2.1655}$	$2.3178 f^{0.0226}$	$((Ct)_{avg})_{th} > 21.285 f^{1.054}$

234

Table (10.2) Crack growth rate as function of frequency for joints tested at 90°C.

Fracture parameters in form of Paris law	Paris constants		Conditions
	D	n	
$\dfrac{da}{dN} = DG_{max}^n$	$1X10^{-14} f^{-0.4981}$	$2.95 f^{0.0123}$	$G_{th} > 108.63 f^{0.0803}$
$\dfrac{da}{dN} = DJ_{max}^n$	$5X10^{-17} f^{-1.5}$	$4.0061 f^{0.0172}$	$J_{th} > 108.63 f^{0.0803}$
$\dfrac{da}{dN} = D(Ct)_{avg}^n$	$2X10^{-12} f^{-3.581}$	$2.7301 f^{0.021}$	$((Ct)_{avg})_{th} > 19.597 f^{0.9896}$

Table (10.3) Crack growth rate as function of frequency for joints tested at 120°C.

Fracture parameters in form of Paris law	Paris constants		Conditions
	D	n	
$\dfrac{da}{dN} = DG_{max}^n$	$3X10^{-12} f^{-0.2514}$	$2.391 f^{0.022}$	$G_{th} > 73.114 f^{0.0256}$
$\dfrac{da}{dN} = DJ_{max}^n$	$5X10^{-13} f^{-0.923}$	$2.5956 f^{0.0225}$	$J_{th} > 73.114 f^{0.0256}$
$\dfrac{da}{dN} = D(Ct)_{avg}^n$	$3X10^{-10} f^{-2.428}$	$1.7502 f^{0.0118}$	$((Ct)_{avg})_{th} > 14.639 f^{0.9847}$

Figures (10.2), (10.3) and (10.4) show the experimental and predicted crack growth rates at room temperature for 10 Hz, 1 Hz and 0.1 Hz respectively. Results indicate that; G_{max} and J_{max} are the best parameters to correlate to the crack growth rate at room temperature. At the beginning of the test J_{max} tended to be the best parameter. This is understandable as plasticity will be most significant at the loads seen at the beginning of the test.

Fig. (10.2) Crack growth under fatigue loading for mild steel joints at RT.

Fig. (10.3) Crack growth under fatigue loading for mild steel joints at RT.

Fig. (10.4) Crack growth under fatigue loading for mild steel joints at RT.

Figures (10.5), (10.6) and (10.7) show the experimental and predicted crack growth at 90°C for 10 Hz, 1Hz and 0.1Hz respectively.

Fig. (10.5) Crack growth under fatigue loading for mild steel joints at 90°C.

Fig. (10.6) Crack growth under fatigue loading for mild steel joints at 90°C.

Fig. (10.7) Crack growth under fatigue loading for mild steel joints at 90°C.

Figures (10.8), (10.9) and (10.10) show the experimental and predicted crack growth at 120°C for 10 Hz, 1Hz and 0.1 Hz respectively.
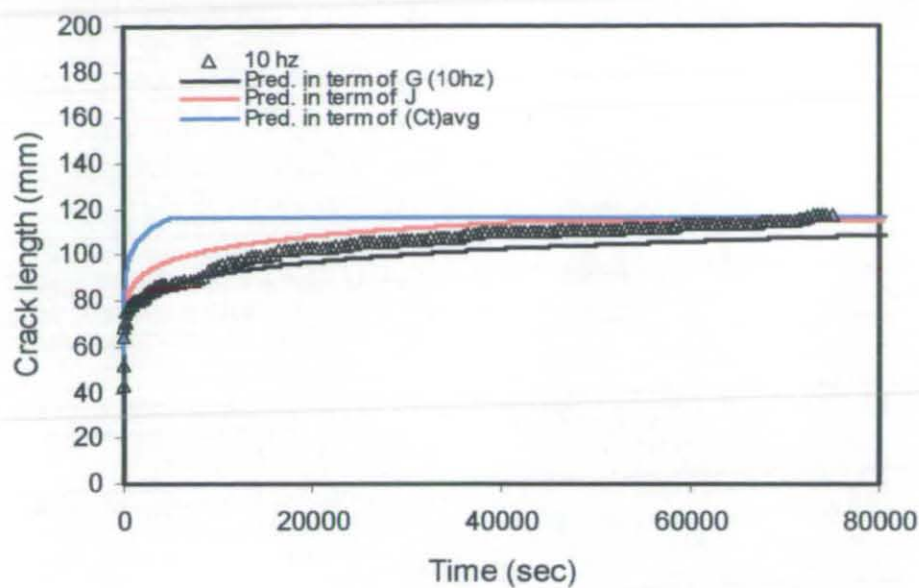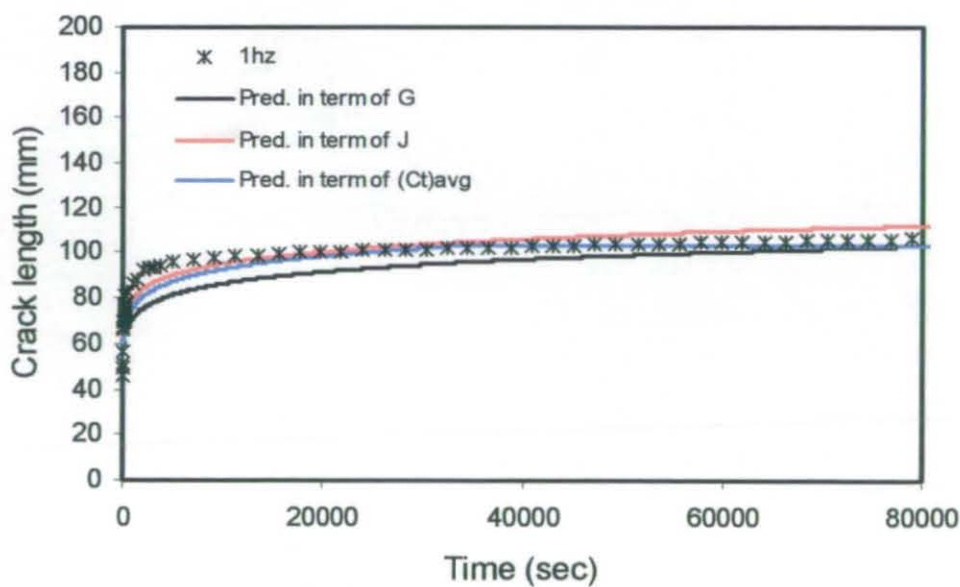
Fig. (10.8) Crack growth under fatigue loading for mild steel joints at 120°C.

Fig. (10.9) Crack growth under fatigue loading for mild steel joints at 120°C.
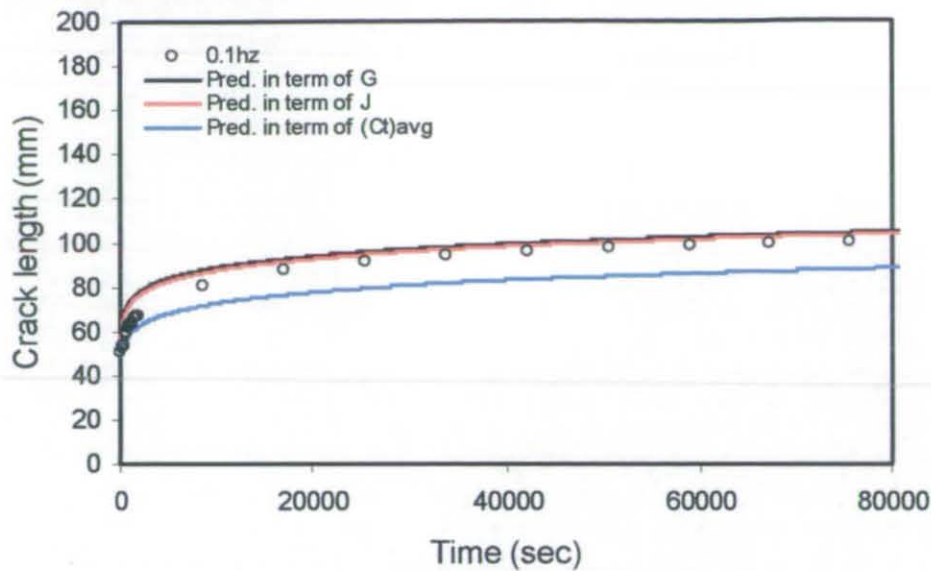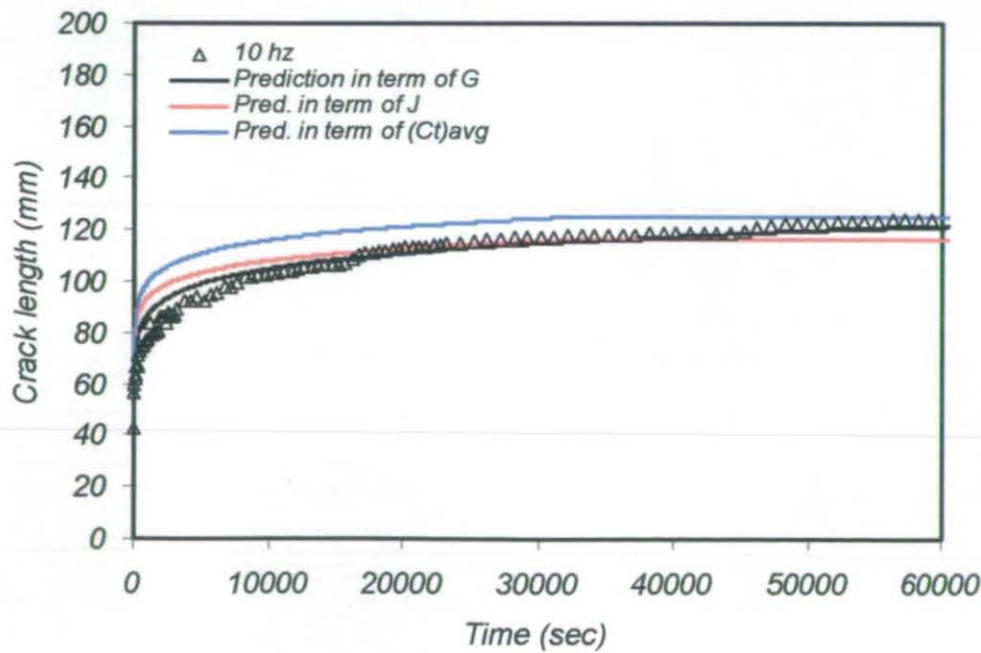
Fig. (10.10) Crack growth under fatigue loading for mild steel joints at 120°C.

Tests results at elevated temperatures indicate that; G_{max} was the most suitable parameter in the range of frequency (1-10 Hz) while J_{max} and $(C_t)_{avg}$ were found to be in good agreement with tests at lower frequency. This can attributed to the increased plasticity and creep at elevated temperatures and low frequencies.

10.2.2 Crack growth rate in terms of frequency and temperature ($(da/dN=F\ (f, T)$))

The empirical formulae described in the previous section have been extended to evaluate the crack growth rate as function of temperature and frequency. Table (10.4) show these correlations for different fracture parameters, namely, G_{max}, J_{max} and $(C_t)_{avg}$.

Table (10.4) da/dt as function frequency and temperature for mild steel joints

$\dfrac{da}{dN} = DG_{max}^{n}$ T: temperature f: frequency	D	$3X10^{-14} f^{-0.2445} T - 7X10^{-13} f^{-0.1337}$
	n	$f^{0.021}(3.2345 - 6.06X10^{-3}T)$
	G_{th}	$112.34 f^{0.1214} - 0.3156 T f^{0.2993}$
$\dfrac{da}{dN} = DJ_{max}^{n}$	D	$5X10^{-15} T f^{-0.9212} - 1X10^{-13} f^{-0.913}$
	n	$3.5686 f^{0.0286} - 0.00817 T f^{0.0447}$
	J_{th}	$112.34 f^{0.1214} - 0.3156 T f^{0.2993}$
$\dfrac{da}{dN} = D(Ct)_{avg}^{n}$	D	$3X10^{-12} T f^{-2.4494} - 5X10^{-11} f^{-2.6053}$
	n	$2.4462 f^{0.0244} - 0.00577 T f^{0.056}$
	$((C_t)_{avg})_{th}$	$22.789 f^{1.0645} - 0.0654 T f^{1.2081}$

This method to predict the crack growth at a range of frequencies and temperatures shows a good agreement with the experimental tests. Examples of these results are shown in Figures (10.11) and (10.12). Figure (10.11) show the predicted and experimental results for mild steel joints tested at 120°C and 1Hz whilst Figure (10.12) shows similar results at room temperature and 5Hz.
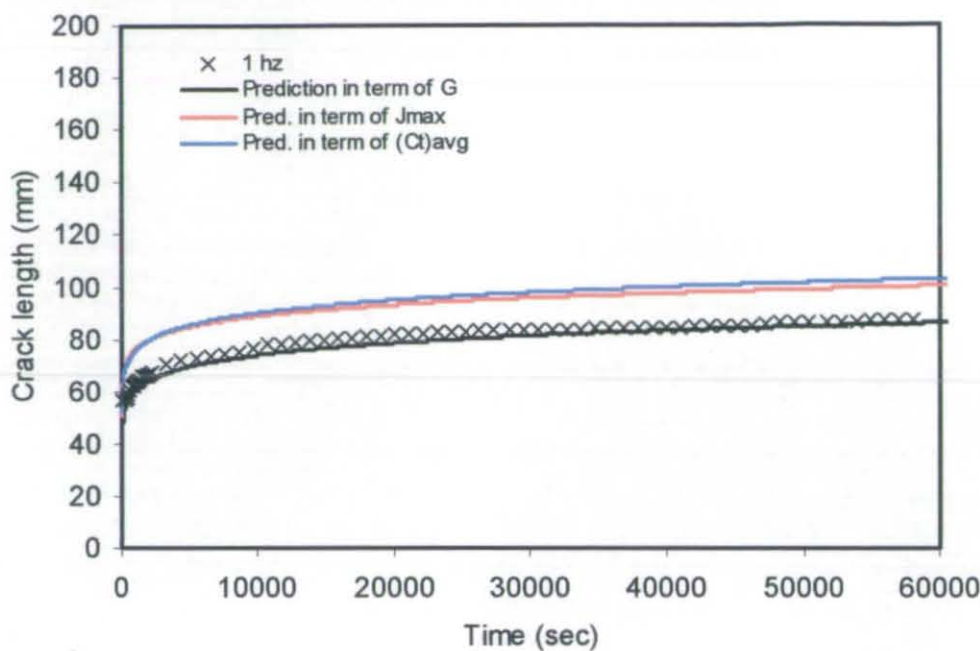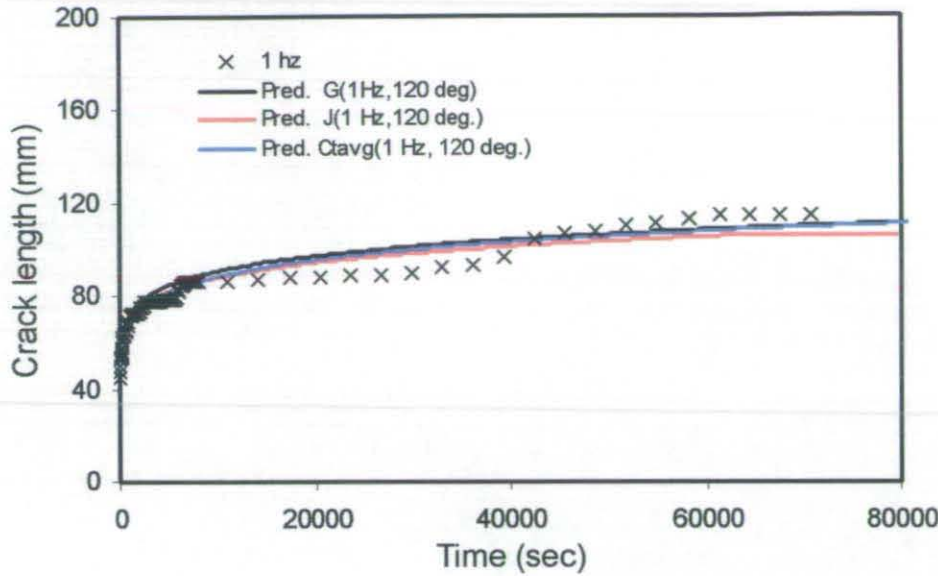
Fig. (10.11) Crack growth under fatigue loading for mild steel joints at 120°C.

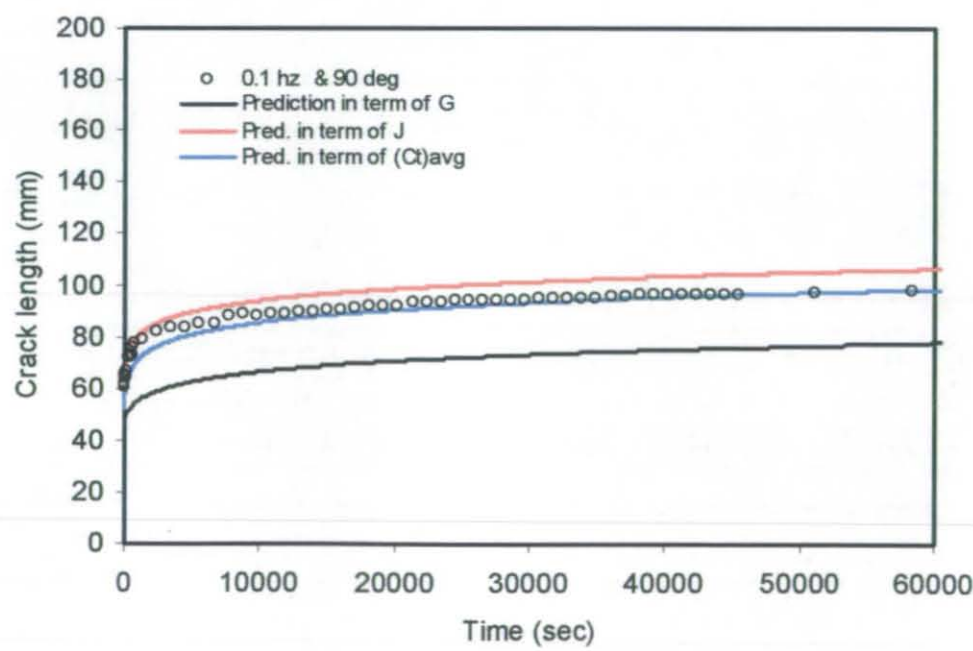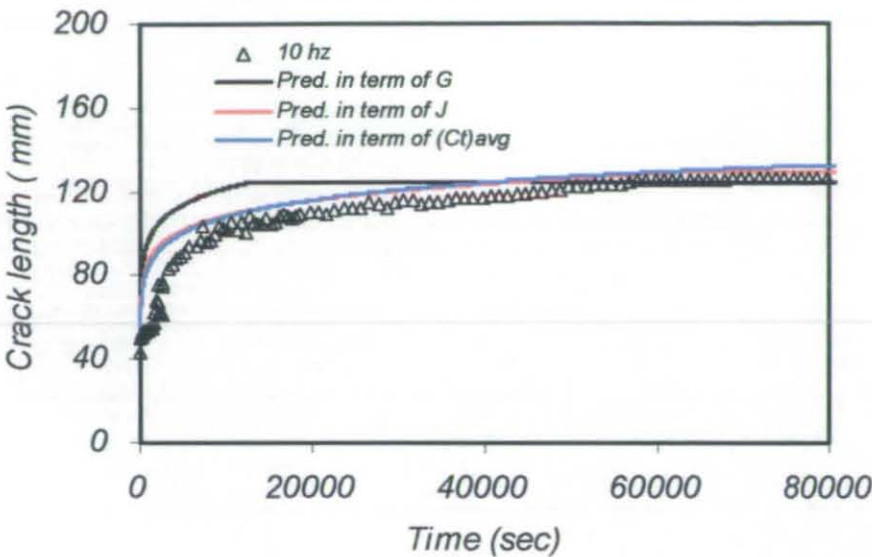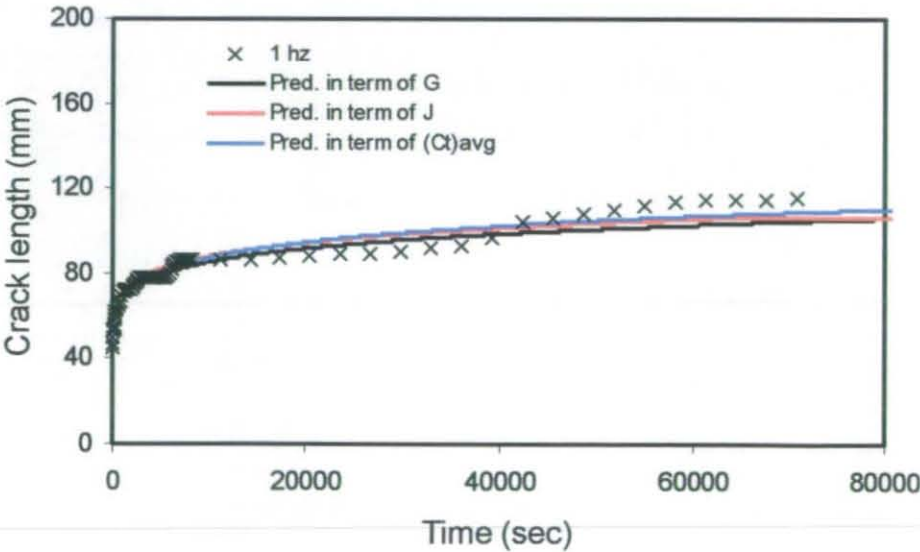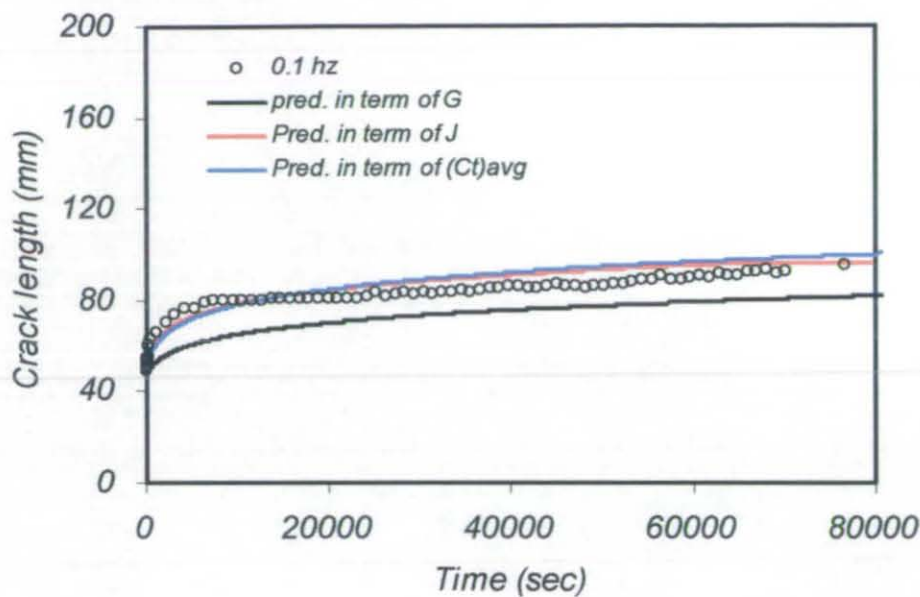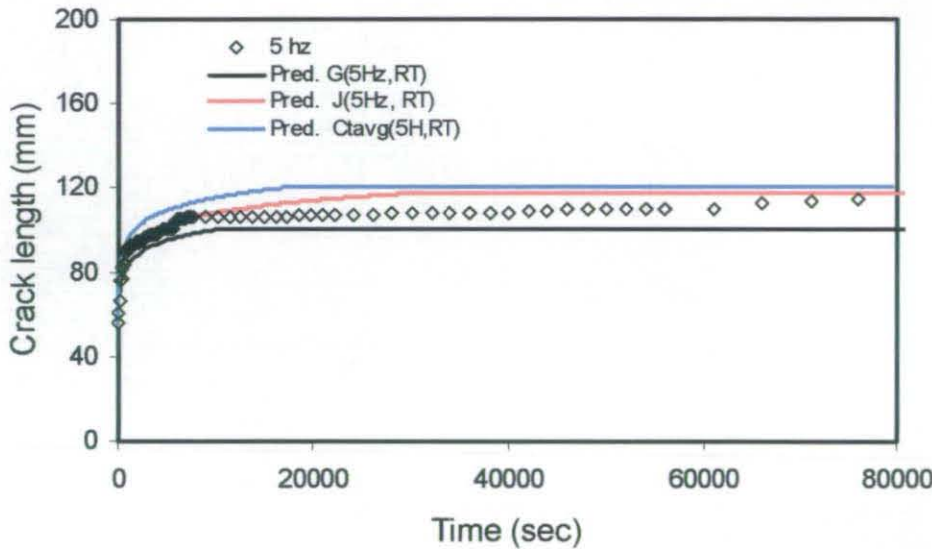Fig. (10.12) Crack growth under fatigue loading for mild steel joints at RT.

10.3 Dominant damage method

This method assumes creep and fatigue crack growth are competing mechanisms and the crack growth rate is determined by whichever is dominant. Experimental results showed that, the fatigue crack growth in term of da/dt verses G_{max} for mild steel joints tested at room temperature brought the fatigue crack growth curves much closer to each other than

when fatigue crack growth was plotted in terms of *da/dN*, as shown in Figure (9.11). This means that as a first approximation fatigue crack growth for interfacial failure at any frequency can be estimated from a single curve fit through all the data points of a plot of G_{max} against *da/dt*.

The procedure of this approach is based on first obtaining constant amplitude fatigue crack propagation (*FCP*) curves (i.e. plotting *da/dt* vs. *G_{max}*) within the desired frequency range. The crack growth rate, *da/dt*, can be correlated to a suitable fracture mechanics parameter using a suitable fatigue law, such as:

$$\frac{da}{dt} = D(G_{max})^n \qquad\qquad (10.2)$$

To perform the predictions, the values for the coefficients D and n need to be derived from the experimental data. These coefficients along with the threshold strain energy release rate (G_{th}) and the critical strain energy release rate (G_c) are all that are required to describe the *FCP* curve and can be considered as material properties. This has been done at room temperature (RT) for mild steel joints. Intermediate values of (n, D, G_{th} and G_c) were calculated and results tabulated in Table (10.5) for joints tested at RT.

Table (10.5) Intermediate values of Paris constants for joints tested at RT.

Paris law	Paris constants		Conditions
	D	n	
$\frac{da}{dt} = DG_{max}^n$ *a in m, t in hr and G in J/m²*	1.432 E-14 ±3.32E-15	3.110±0.22	G_{th} >108.53±14.6

The iterative algorithm used in the previous method was used to predict the crack growth. This method was used to predict the crack growth in term of da/dN at any frequency, f based on the following correlation:

$$\frac{da}{dN} = \frac{da/dt}{f}$$

(10.2)

Figures (10.13), (10.14) and (10.15) show the predicted and experimental crack growth rate, da/dN for mild steel joints at 10 Hz, 1Hz and 0.1Hz respectively. It is clear that there is good agreement between the experimental test and the prediction method.
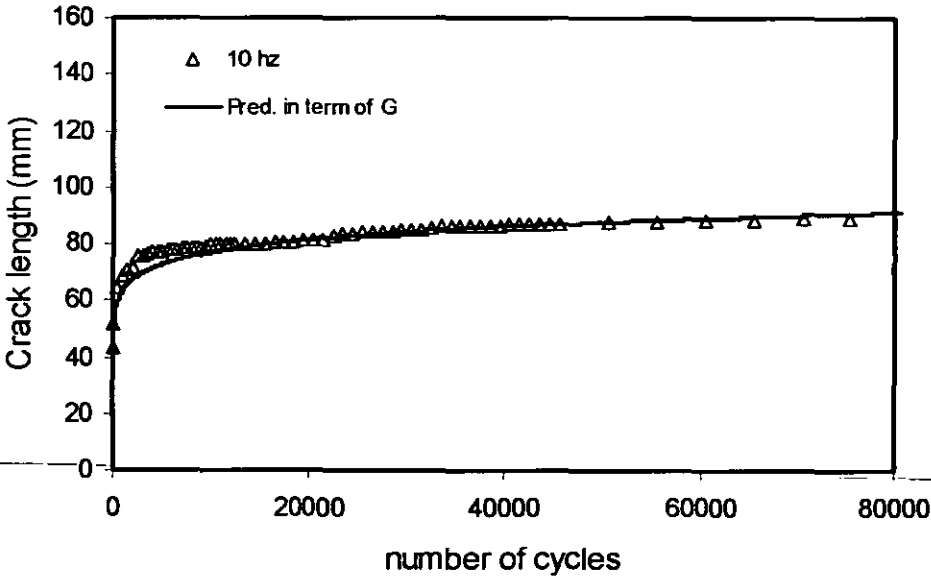
Fig. 10.13 Crack growth under fatigue loading for mild steel joints tested at RT.
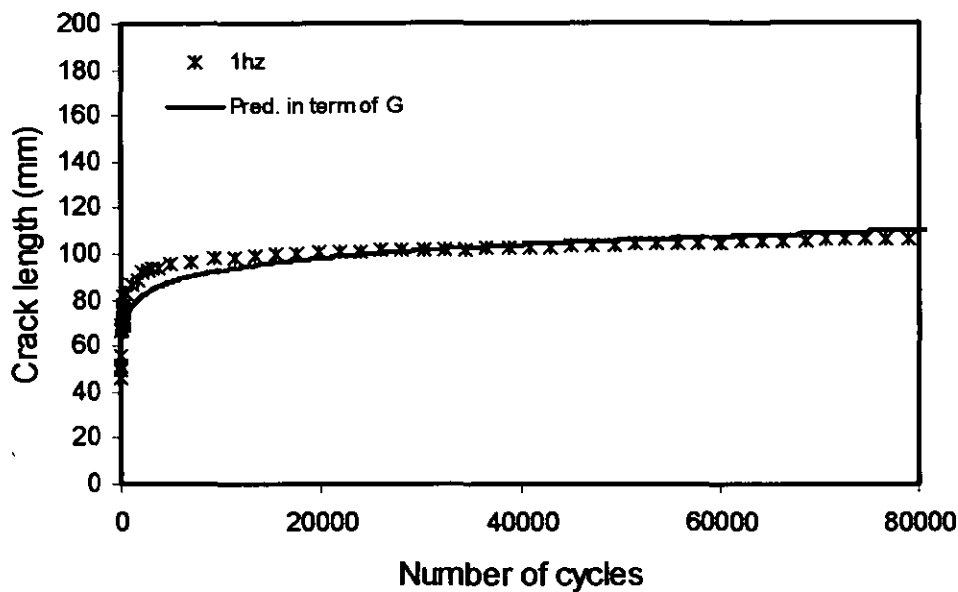
Fig. 10.14 Crack growth under fatigue loading for mild steel joints tested at RT.
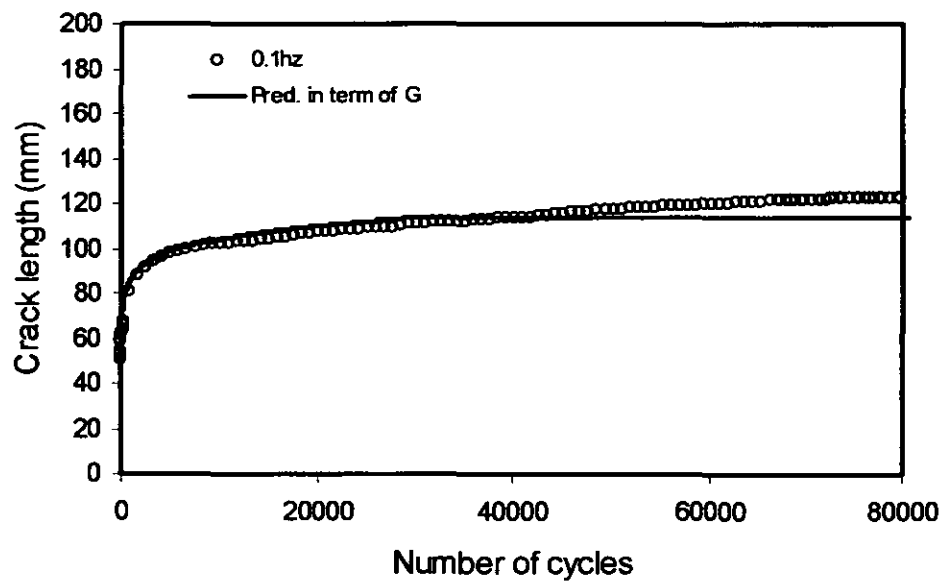
Fig. 10.15 Crack growth under fatigue loading for mild steel joints tested at RT.

Furthermore, it is possible to use the predicted crack growth verses number of cycle to predict the FCP curve at different frequencies. Figures (10.16), (10.17) and (10.18) show the predicted and experimental FCP curves for joints tested at 10Hz, 1Hz and 0.1Hz respectively.
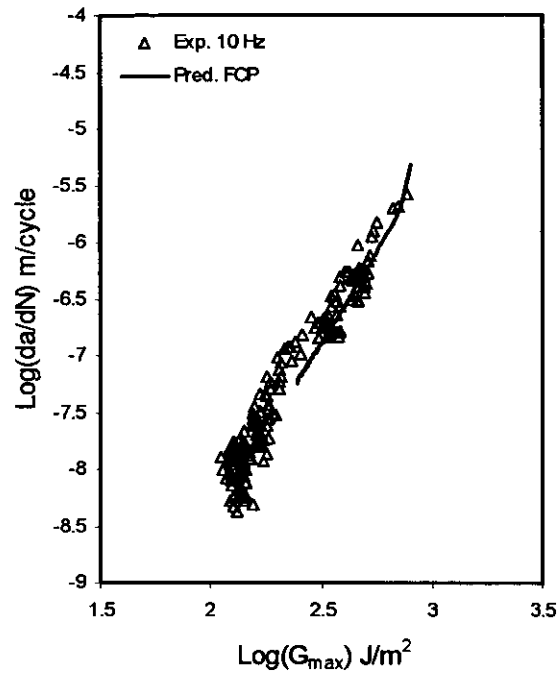
Fig. 10.16 FCP curves for mild steel joints in term of da/dN.
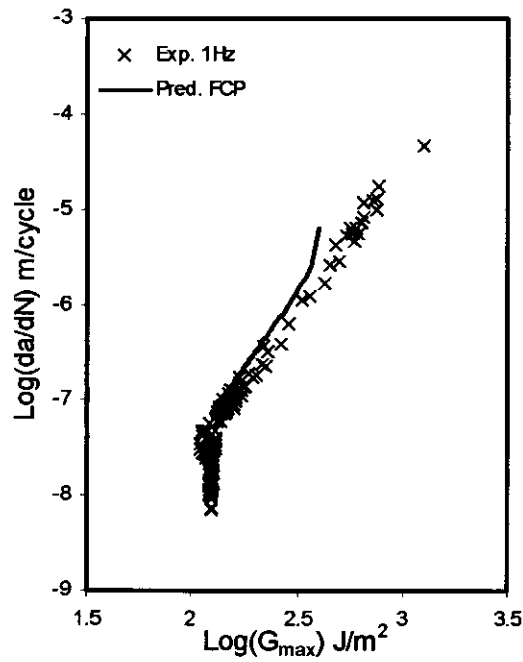
Fig. 10.17 FCP curves for mild steel joints in term of da/dN.
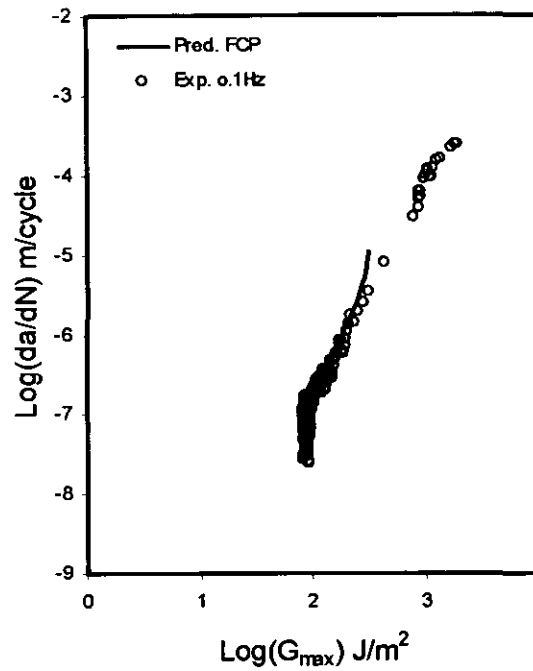
Fig.10.18 FCP curves for mild steel joints in term of da/dN.

10.4 Damage partition method

In this section an attempt is made to extend the prediction method discussed in the previous sections to predict fatigue-creep crack growth from nominally 'pure' fatigue and creep data. In this method the crack is growth is assumed to be partitioned into independent cyclic dependent (fatigue) and time dependent (creep) components.

The following equation is used to represent the creep-fatigue crack growth rate, as discussed in section (5.8).

$$\frac{da}{dN} = \left(\frac{da}{dN}\right)_{fatigue} + \frac{1}{f}\left(\frac{da}{dt}\right)_{creep} \qquad (10.3)$$

or

$$\frac{da}{dt} = \left(\frac{da}{dt}\right)_{creep} + f\left(\frac{da}{dN}\right)_{fatigue} \qquad (10.4)$$

This concept can be extended to suitable crack growth laws for fatigue and creep as:

$$\frac{da}{dN} = D(G_{max})^n + \frac{mC_t^q}{f} \qquad (10.5)$$

The values for the coefficients D, n are derived from experimental fatigue data tested at high frequency (where creep is assumed to be negligible) and the creep coefficient m and q, are derived from the experimental creep data. These coefficients along with the threshold strain energy release rate (G_{th}), critical strain energy release rate (G_c) and the threshold value of the creep parameter C_t are all that are required to predict the crack growth at any frequency and can also be used to predict crack growth in fatigue spectra incorporating hold times at constant load.

Prediction of crack length under fatigue and creep is based on a simple iterative algorithm in which G_{max} and C_t are first calculated for the initial crack length, a_0. The material constants (D, n, m, q) for the high frequency and creep loading are then used to determine the crack growth rate, da/dN, which is multiplied by the number of cycles in the stage to give the overall crack growth during the stage (Δa). A new crack size ($a_1 = a_0 + \Delta a(fatigue) + \Delta a(creep)$) is then calculated and the process repeated. This procedure is repeated until G_{max} and C_t become equal to the threshold values G_{th} and $(C_t)_{th}$. The steps used in this prediction method are illustrated in Figure (10.19).

The experimental *da/dN* due to fatigue and creep can be simulated by tests carried out at elevated temperature combined with low applied frequency, fatigue with hold time or variable frequency fatigue loading conditions.
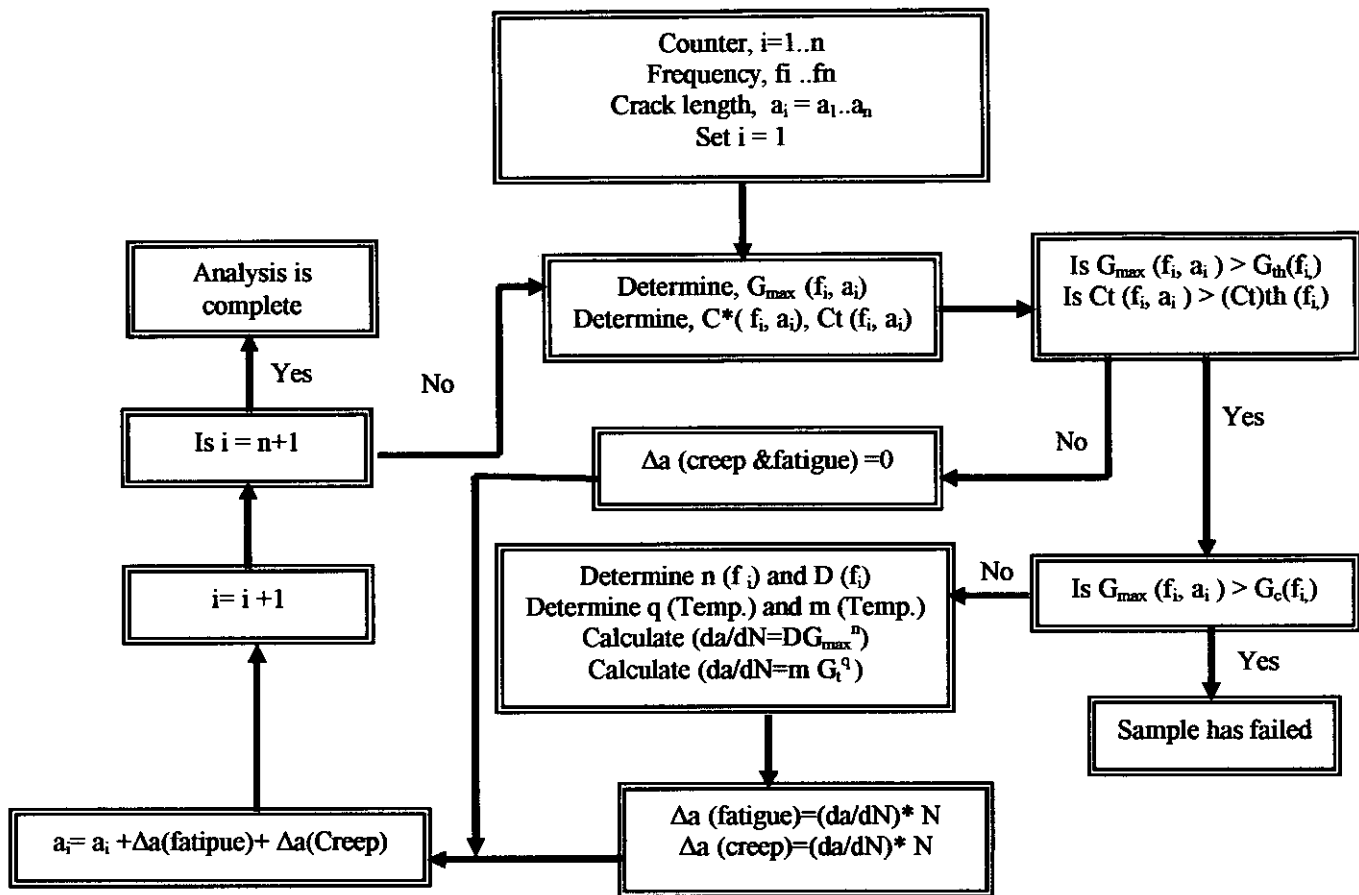
Fig. (10.19)   Fatigue-Creep life prediction algorithm

Figure (10.20) and Figure (10.21) shows the prediction and the experimental crack growth

at 0.1 Hz/90°C and 0.1 Hz/120°C respectively.

Fig. (10.20) Crack growth under fatigue/ creep loading for mild steel joints at 0.1 Hz/ 90°C.

Fig. (10.21) Crack growth under fatigue/ creep loading for mild steel joints at 0.1 Hz/120°C.

Figure (10.22) and Figure (10.23) shows the prediction and the experimental crack growth

at variable frequency/90°C and variable frequency/120°C respectively.

Fig. (10.22) Crack growth under variable frequency fatigue/creep loading for mild steel joints at 90°C.

Fig. (10.23) Crack growth under variable frequency fatigue/creep loading for mild steel joints at 120°C.

Figure (10.23) and Figure (10.24) shows the prediction and the experimental crack growth at t_h=30sec/90°C and t_h=30sec /120°C respectively.

Fig. (10.24) Crack growth under fatigue/creep loading with hold time for mild steel joints at 90°C.

Fig. (10.25) Crack growth under fatigue/creep loading with hold time for mild steel joints at 120°C.

It can be seen from the above figures that both creep and fatigue components are important for the overall crack growth and that there is quite good agreement between the

experimental and predicted crack growth using this method. However, the initial crack growth is underestimated in a number of cases. This is because Equation (10.5) does not account for any interaction between fatigue and creep, which may have an accelerating effect on crack growth. This concept is considered in the next section.

10.5 Damage partition method with interaction term:

In this section an attempt is made to extend the prediction method discussed in the previous sections to include fatigue/creep interaction effects. Equation (10.5) does not account for any interaction between fatigue and creep. In this section, the effect of adding a new term to account for this interaction will be investigated, i.e.

$$\frac{da}{dN} = A(G_{max})^n + \frac{mC_t^q}{f} + CF_{int.}$$ (10.6)

where

$$CF_{int.} = R_f^p R_c^y C_{fc}$$ (10.7)

where R_f and R_c are scalar factors for the cyclic and time dependent components respectively.

$$R_f = \frac{(da/dN)}{(da/dN) + (da/dt)/f}$$ (10.8)

$$R_c = \frac{(da/dt)/f}{(da/dN) + (da/dt)/f}$$ (10.9)

and p, y and C_{fc} are empirical constants in the interaction term from the experimental data. The values of these constants are tabulated in Table (10.6) for joints tested at 90°C and 120°C. It can seen that the form of the interaction term in Equation (10.6) is such that if either fatigue or creep dominates the crack growth process ($R_f=1$, $R_c=0$ or $R_f=0$, $R_c=1$, respectively), no interaction takes place and Equation (10.6) reduced to Equation (10.5).

Obviously, the interaction becomes a maximum when $R_f = R_c = 0.5$, i.e. equal contribution

for fatigue and creep.

Table (10.6) Fatigue/ Creep interaction constants.

Joints	p	y	C_{fc}
90°C	0.1	0.09	0.015
120°C	0.12	0.11	0.008

The iterative algorithm used in the pervious method was used to predict the crack growth

based on Equation (10.6).

Figure (10.26) and Figure (10.27) shows the prediction and the experimental crack growth

at 0.1Hz/90°C and 0.1Hz /120°C respectively.
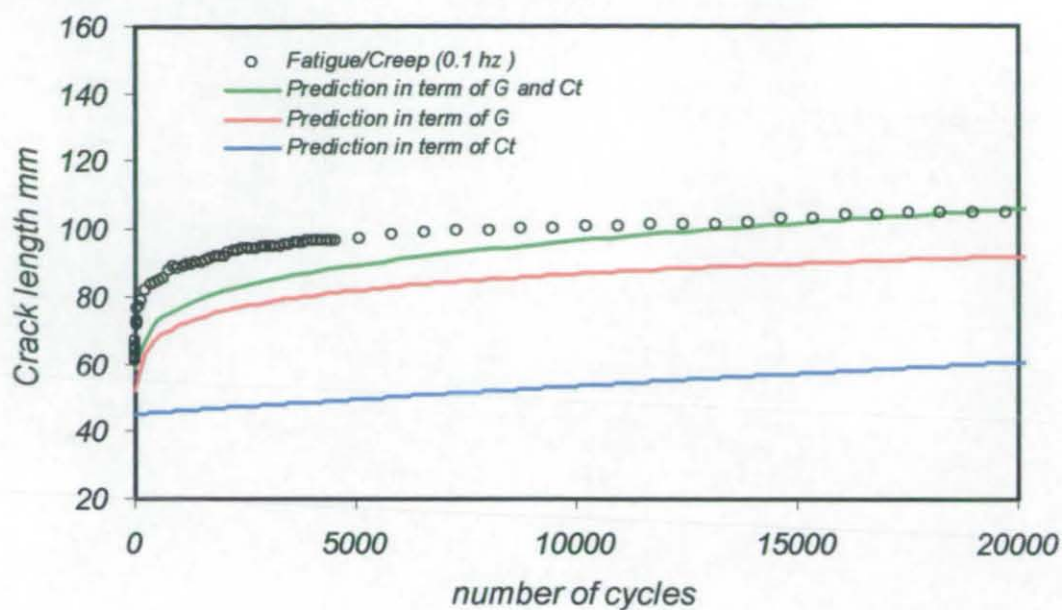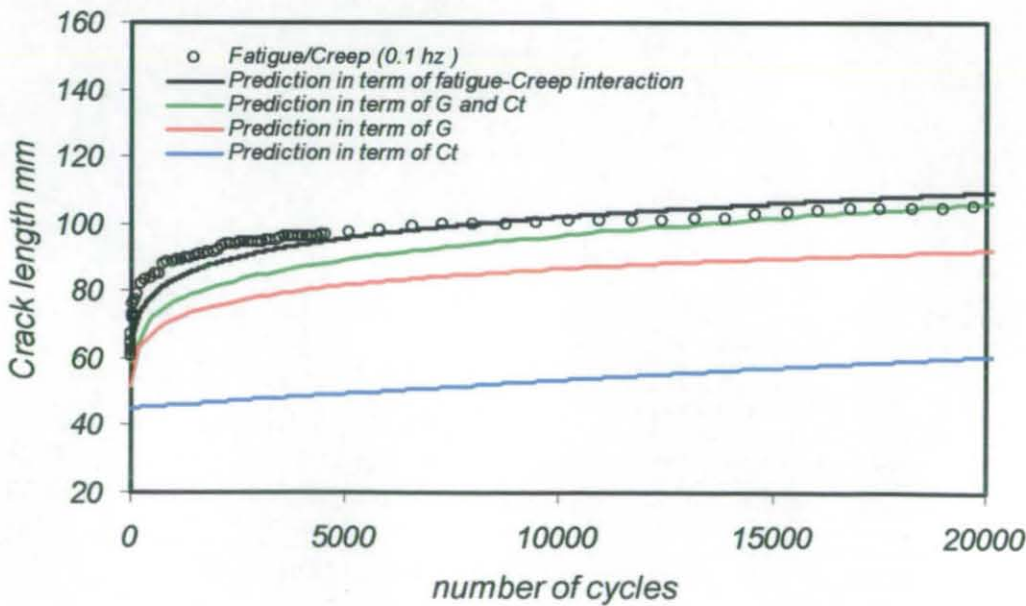

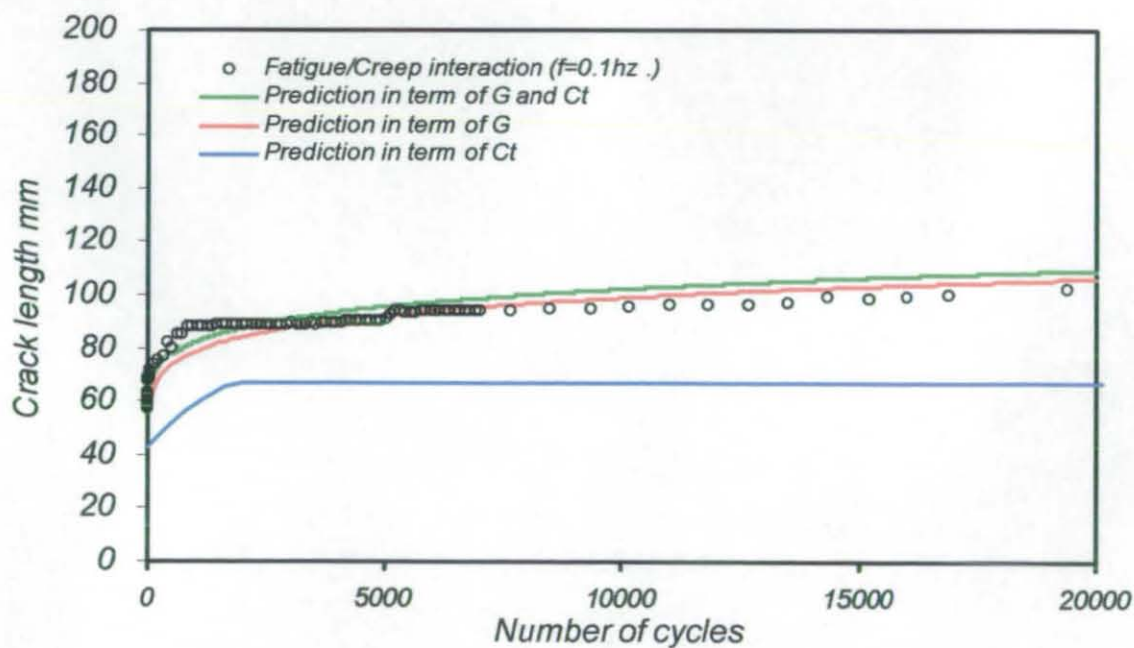Fig. (10.26) Crack growth under fatigue/creep loading for mild steel joints at 90°C.
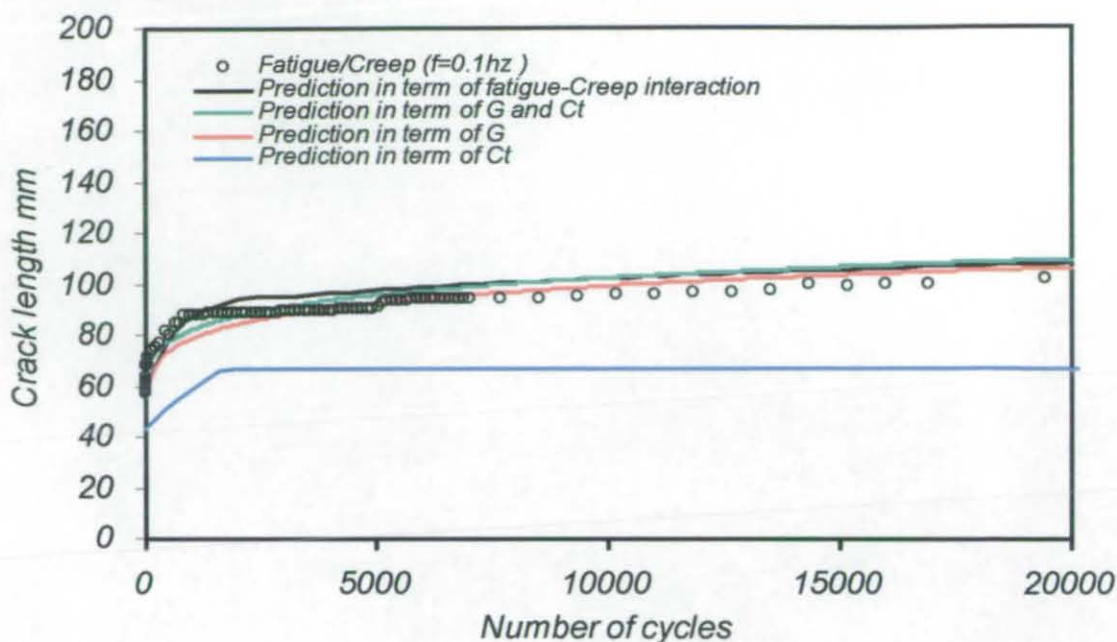
Fig. (10.27) Crack growth under fatigue/creep loading for mild steel joints at 120°C.

Figure (10.28) and Figure (10.29) shows the prediction and the experimental crack growth at variable frequency/90°C and variable frequency /120°C respectively.
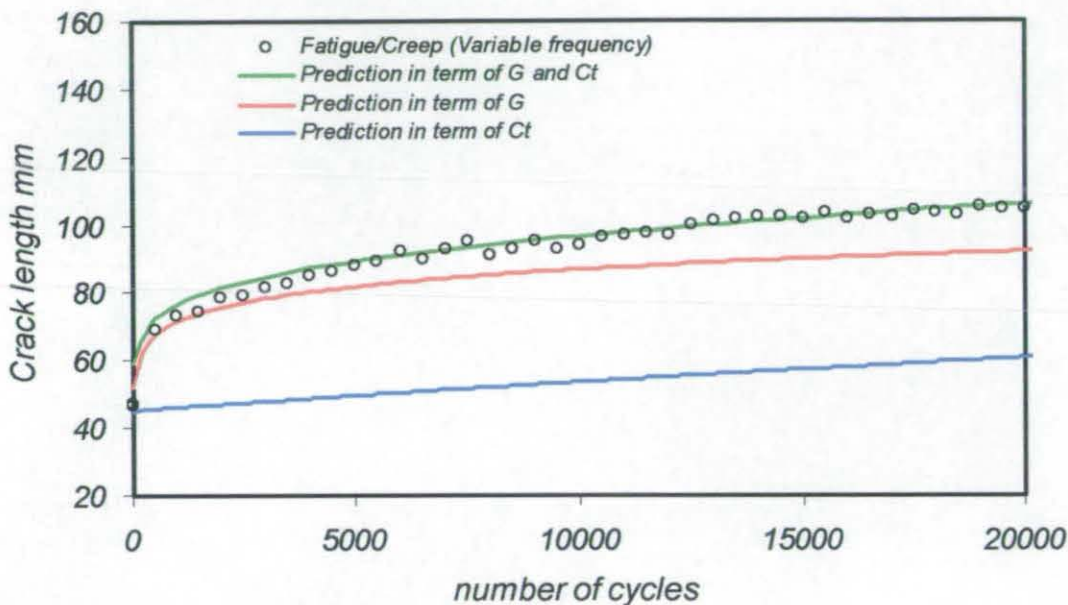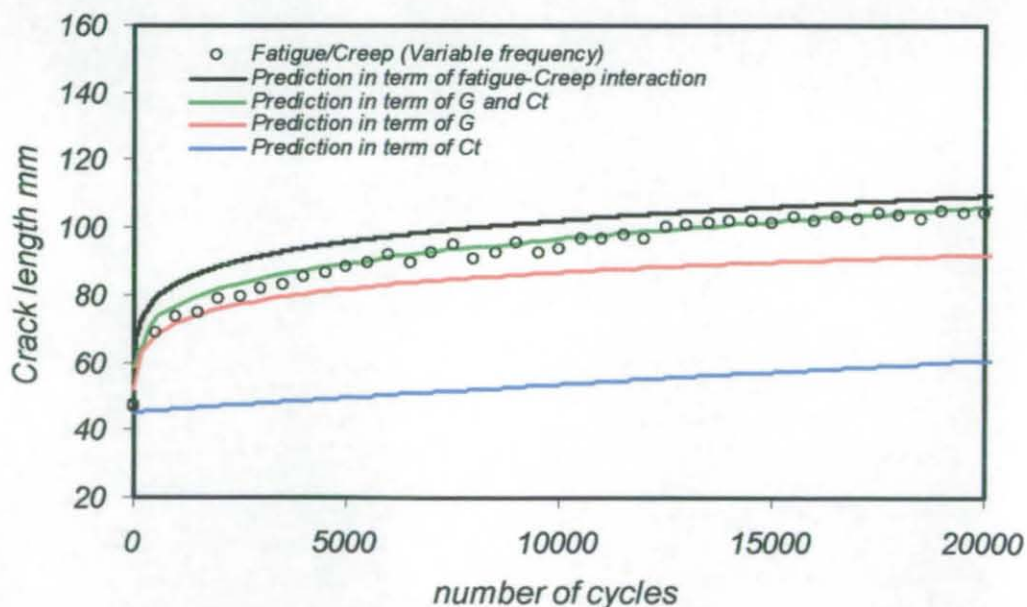

Fig. (10.28) Crack growth under variable frequency fatigue/creep loading for mild steel joints at 90°C.
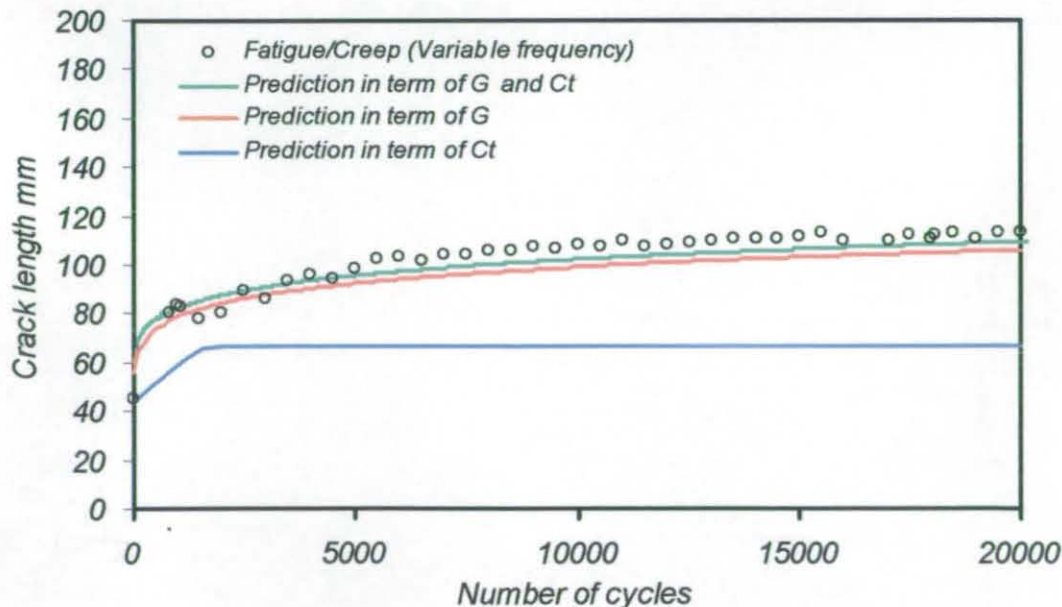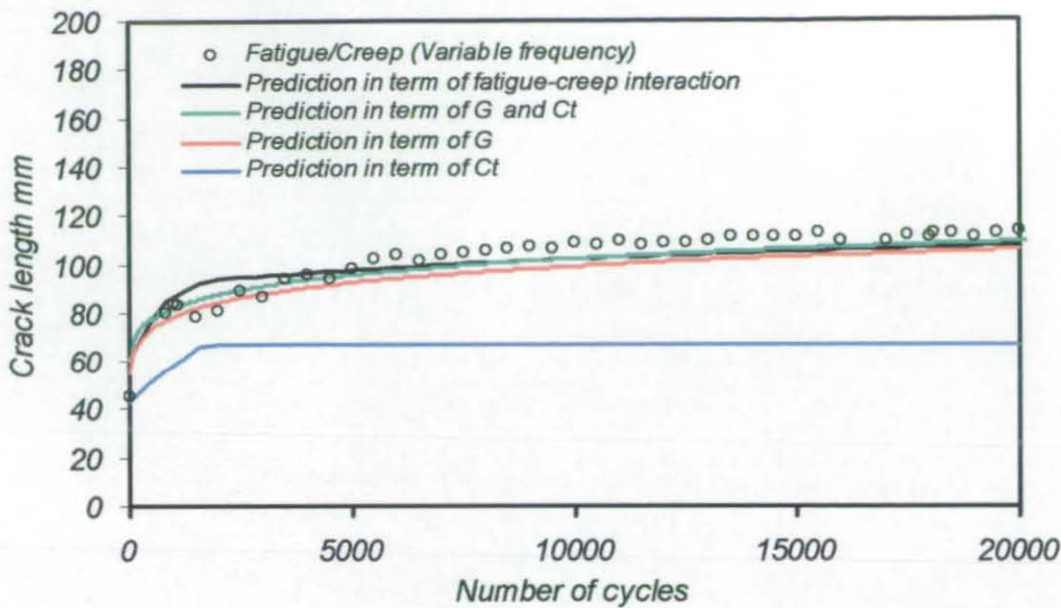
Fig. (10.29) Crack growth under variable frequency fatigue/creep loading for mild steel joints at 120°C.

Figure (10.30) and Figure (10.31) shows the prediction and the experimental crack growth at t_h=30sec/90°C and t_h=30sec /120°C respectively.
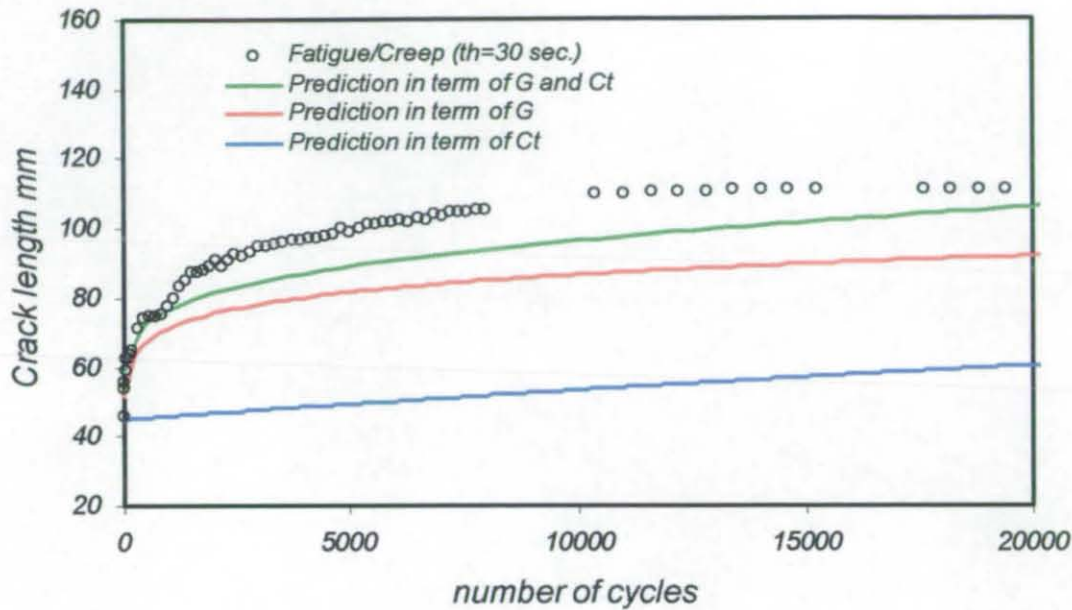

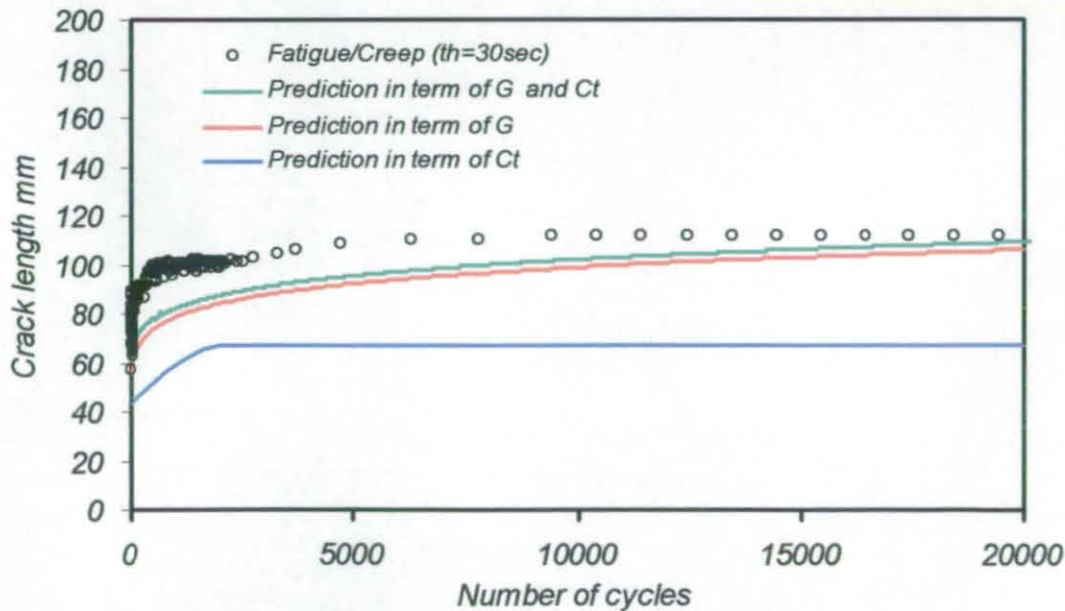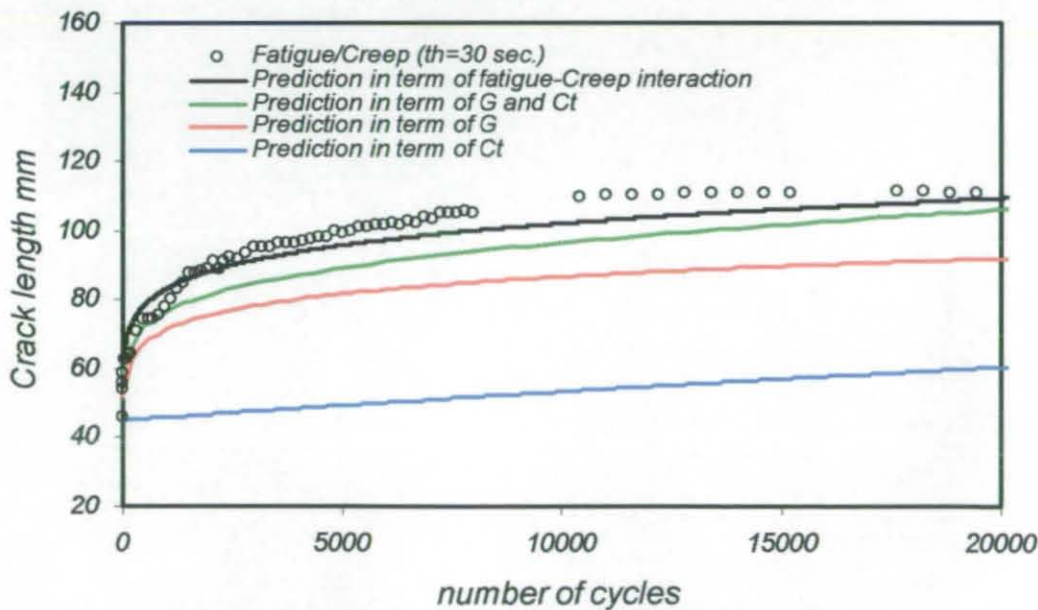Fig. (10.30) Crack growth under fatigue/creep loading with hold time for mild steel joints at 90°C.
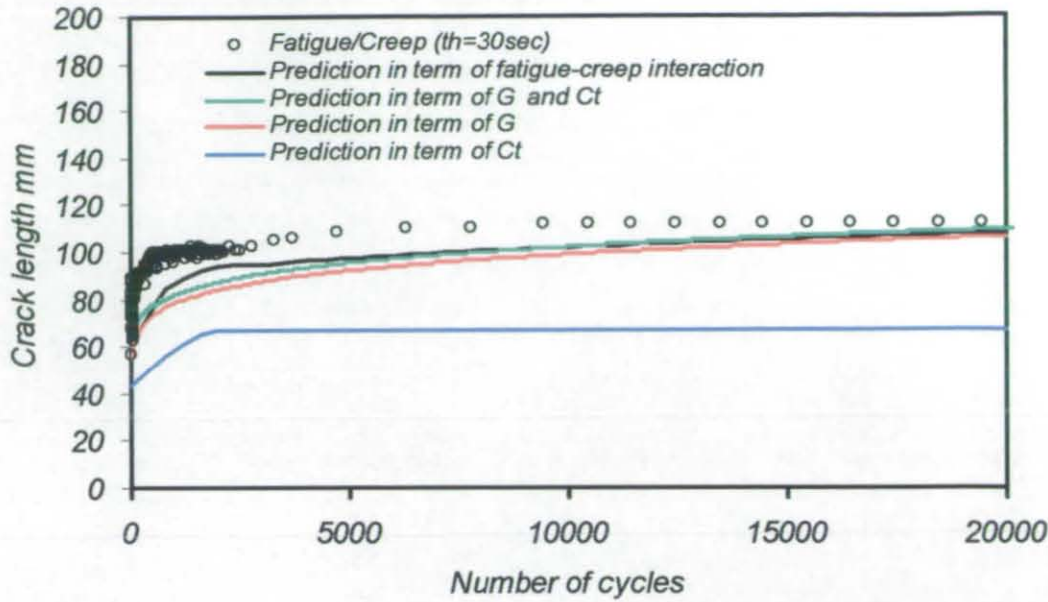
Fig. (10.31) Crack growth under fatigue/creep loading with hold time for mild steel joints at 120°C.

It can be seen from the above figures there is an improved agreement between the experimental and predicted crack growth using this method. The difference between experimental and predicted crack growth seen in the previous method at the initial stage of the crack growth was minimized by including the effect of interaction between fatigue and creep, given by Equation (10.6).

10.5 Summary

In this chapter, the prediction of the crack growth rate in terms of different fracture parameters was discussed in detail. Four methods were developed and validated through the various types of testing presented in the previous chapter. The first method was based on the determination of empirical crack growth laws formula derived from experimental data; this method, can be used accurately to predict crack growth rate at range of frequencies and temperatures, and has been successfully applied to both cohesive and interfacial failure. In this method G_{max} and J_{max} were found to be the best parameters at

room temperature, G_{max} was found to be the most suitable parameter at elevated temperature loaded at high frequency and J_{max} and the creep parameter $(C_t)_{avg}$ were found to be more applicable at elevated temperature accompanied with lower frequency. The second method indicates the ability to predict the crack growth for range of frequencies when crack growth is predominately time dependent, and also demonstrates the possibility of constructing FCP curves at different frequencies when this occurs. The damage partition method deals with the separation of crack growth into creep and fatigue components. This method shows the possibility of predicting the crack growth for loading cases combining both fatigue and creep loading, such as fatigue tests at low applied frequency, fatigue tests combined with hold time and variable frequency fatigue testing. In some cases this method tended to underestimate crack growth, in which an additional interaction term was introduced. This method improved the prediction of crack growth for cases subjected to fatigue creep loading conditions.

10.6 References

[10.1] Ripling, E.J. and Mostovoy, S., "Application of Fracture Mechanics" ASTM STP360, American Society for Testing Materials, (1964).

[10.2] Abdel-Wahab, M.M., Ashcroft, I.A., Crocombe, A.D., Hughes, D.J. and Shaw, S.J., "The Effect of Environment on the Fatigue of Bonded Composite Joints; Part 2: Fatigue Threshold Prediction Composites Part A, Vol. 32, 2001, pp. 59-69.

[10.3] Abdel-Wahab, M.M., Ashcroft, I.A., Crocombe, A.D., Hughes, D.J. and Shaw, S.J "Prediction of Fatigue Threshold in Adhesively Bonded Joints Using Damage Mechanics and Fracture Mechanics", *J. Adhesion Sci. and Tech.*, Vol. 15, (2001), pp.763-868.

[10.4] Curley A.J., Hadavinia H., Kinloch A.J. and Taylor A.C., "Prediction the Service-life of Adhesively-bonded joints", Int. J. Fracture, Vol. 103, 41-69, (2000).

[10.5] Ashcroft, I.A. and Shaw, S.J., "Mode I Fracture of Epoxy Bonded Composite Joints; 2. Fatigue Loading", Int. J. Adhesion and Adhesives, Vol. 22, 2002, pp.151-167.

[10.6] AbdelWahab, M.M., Ashcroft, I.A., Crocombe, A.D. and Smith, P.A., "Numerical Prediction of Fatigue Crack Propagation Lifetime in Adhesively Bonded Structures", *Int. J. Fatigue*, Vol. 24, 2001, pp. 705-714.

CHAPTER 11

DISCUSSION

11.1 Introduction

This chapter presents a discussion of the experimental, analytical and numerical studies throughout this work. This will include the following:

- The quasi-static and rate effect test results. This will include a comparison between the *CFRP* joints and mild steel joints and the effect of temperature and loading rate on the G_c value and locus of failure.

- The effect of fatigue loading on G_{th} and the locus of failure. This will include the effect of frequency on both CFRP and mild steel joints at room temperature, the effect of temperature and frequency on mild steel joints, and the effect of surface treatment on mild steel joints.

- The effect of creep on mild steel joints tested at elevated temperature.

- The influence of loading type and temperature on the topography of failed surfaces.

- The numerical methods used to calculate the various parameters of fracture as a function of crack length.

- The various methods used to predict crack growth in adhesively bonded joints.

11.2 Quasi- static tests

In this work *DCB* samples composed of *CFRP* and mild steel adherends bonded with an epoxy adhesive, *FM300-2M*, were tested at a range of temperatures and loading rates. It was seen that, G_c tends to be higher at the start of the test. This may be because the starter crack formed by the *PTFE* film is relatively blunt and therefore more difficult to

propagate. On loading, a plastic zone will form ahead of the 'blunt' crack, which will also influence initial crack propagation. As the crack sharpens, the value of G_c tends to decrease to an approximately constant level. However, this was not the case for mild steel joints tested at elevated temperature, where G_c tended to continue to decrease along the bond line. This may be explained in relation to the viscoelastic nature of the adhesive at elevated temperature. This observation is in agreement with previous work by Ashcroft et al. [3.57]. They attribute the decrease in G_c to two factors: firstly, the reduced stiffness/increased compliance of the joints and increased toughness of the adhesive at elevated temperature will require increased displacement to propagate failure and hence increased non-linearity. Secondly, they showed a marked increase in plasticity of the adhesive at 90°C and so tests at this temperature may have exceeded the limits of LEFM. Similar arguments can be used in this case as the decreasing G_c with crack length is seen in the sample with the greater fracture toughness, which would result in greater non-linearity in the test. The G_c value of mild steel joints is higher than the G_c value of CFRP joints by a factor of 1.22. This observation is in agreement with previous work by Bell et al. [11.1]. They showed that, the substrate type used has a significant effect upon the plastic zone size and stress levels within the adhesive layer, the substrates with a higher value of transverse modulus produce a larger plastic zone size and greater stresses within the adhesive layer. This in turn gives a greater G_c value. This result is a further indication of the effect of the specimen geometry upon the local stress-field ahead of the crack tip, which in turn controls the energy dissipated in the plastic, or damage, zone ahead of the crack; and so affects the measured value of G_c. The locus of failure from the visual appearance of both the CFRP joints and the mild steel joint was found to be cohesive failure of the adhesive.

The effect of loading rate at different temperatures on mode I crack growth for mild steel DCB samples bonded with an epoxy adhesive was investigated. The G_c values increased

by 81 %, 78 % and 68 % as the rate increased from 0.1 mm/min to 10 mm/min for joints tested at room temperature, 90°C and 120°C respectively. As indicted in Figure (9.6) the G_c value are sensitive to temperature, increasing the temperature from RT to 120°C decreases G_c by 45%. It is noted that decreasing the rate of loading has a similar effect to increasing temperature on the critical strain energy release rate. This argument is in agreement with Richardson [11.2]. Thus it can be seen that, it is very important to consider the environmental conditions, such as temperature and the operating conditions, such as loading rate during the design of adhesively bonded joints.

11.3 Fatigue tests

11.3.1 Frequency effect

In this investigation efforts were made to study the effect of fatigue frequency on crack growth in bonded DCB samples with mild steel and CFRP substrates. It was seen that for both cohesive and interfacial failure, reducing the fatigue frequency has a significant effect in reducing the fatigue threshold and accelerating crack growth for adhesively bonded joints. By reducing the fatigue frequency from 10 to 0.1 Hz, the threshold value of G_{max} decreased by 64 % and 61 % for DCB's with CFRP and mild steel substrates respectively. This effect is most probably attributable to the viscoelastic nature of the polymeric materials used in adhesives, which make them rate sensitive and susceptible to creep. As the loading in this case is always in tension there may be a significant creep accumulation effect, which will increase as the frequency decreases, as the time under load per cycle will increase. This argument is in agreement with many studies [1.1-1.6] that have shown that modern adhesives may exhibit significant creep behaviour within their prescribed service range. This result indicates that designers should not use high frequency test data to predict the time to failure of bonded joints subjected to low frequency loading. There is a

temptation to do this as the shorter time required to complete a series of high frequency tests means that this data is more commonly available. However, whereas this may be an acceptable practice for some materials it is unadvisable with polymeric materials as this will result in non-conservative predictions. It should also be noted that this effect would be expected to worsen as temperature increases or moisture is absorbed by the adhesive. This time dependency is further explored by plotting the crack growth rate as a function of time rather than number of cycles, i.e. da/dt. In the case of interfacial failure this brought the crack growth curves at different frequencies much closer together. This demonstrates that crack growth in this case is more dependent on time under load than number of cycles and as a first approximation crack growth at any frequency can be estimated from a master da/dt vs G_{max} plot.

The threshold strain energy release rate is a potentially useful design criterion as this can be used to determine the load, below which fatigue crack growth is negligible. It is clear from Figure (9.12) that the fatigue threshold values for the CFRP joints are significantly higher (approx. 60%) than those seen with the mild steel joints at all frequencies. This is not surprising as the DCB's with mild steel substrates failed interfacially whilst those with the CFRP substrates failed cohesively in the adhesive. It can also be seen that there is a linear relationship between frequency and log G_{th} for both cohesive and interfacial crack growth, meaning that the prediction of fatigue thresholds at other frequencies should be reasonably reliable. This indicates that the fatigue resistance is influenced by the nature of the adhesive in both cases. The results in Table (9.3) show, as indicated by the Paris law exponents, n and D, that, crack growth is faster for a given load with the mild steel substrates than with the CFRP substrates.

11.3.2 Temperature effect

Work has been conducted to assess the extent to which temperature and frequency affect the fatigue characteristics of mild steel joints bonded with FM300-2M adhesive. DCB joints were tested at RT, 90°C and 120°C under cyclic fatigue loading with different applied frequencies, namely 10 Hz, 1Hz and 0.1Hz.

Results indicated clearly the effect of temperature on the threshold values of adhesively bonded joints. Increasing temperature from RT to 120°C reduced the threshold value by almost 32 %. Results also showed the effect of temperature on crack growth rate; this can be seen clearly in Figures (9.20-9.22). These show that the crack growth rate increased with increasing temperature, this effect being most apparent at 0.1 Hz. The increase in crack growth rate with temperature may be due to a general reduction in structured resistance of the adhesive at elevated temperature due to its viscoelastic nature.

Most fatigue testing at elevated temperatures of bonded joints has been undertaken at relatively high frequency, typically 10 Hz. However, the visco-elastic nature of polymeric adhesives means that rate and frequency dependence might be expected and that this would increase at elevated temperatures or when the adhesive has absorbed moisture. There is, therefore, a requirement to understand the effect of frequency on the fatigue life of bonded joints and how parameters such as temperature and moisture effect this behaviour.

Results indicated, as shown in Figure (9.9), that a reduced frequency during fatigue at room temperature has a significant effect in reducing the fatigue threshold and accelerating crack growth for adhesively bonded joints. At the lowest applied frequency, namely 0.1 Hz, the threshold value decreases by 61% compared to joints tested at high frequency, namely 10 Hz.

Figures (9.15) and (9.16) show the fatigue crack propagation (FCP) of mild steel joints bonded with FM300-2M tested at 90°C and 120°C respectively. These figures clearly show

that the threshold value and the crack growth rate are affected by varying the frequency for both temperatures, but this effect is lower than the effect observed at room temperature, as shown in Figure (9.9). At 90°C the threshold values are mostly similar to the threshold values at room temperature, while at 120°C the threshold value is reduced by almost 32% compared to joints tested at room temperature. This is expected, as the structure integrity of the adhesive decreases significantly at temperatures close to T_g. This argument is in agreement with many studies [3.56-3.58] that show that creep plays a significant role in the fatigue life of adhesively bonded joints at elevated temperatures. It is proposed, therefore, that creep/fatigue interaction in adhesively bonded joints can considerably shorten the fatigue life of a joint, particularly at elevated temperatures. This needs to be taken into account in designing a joint and indicates caution must be taken when using data taken from one type of joint and using it to predict the behaviour of a different type of joint. Figure (9.9) shows that the effect of frequency at room temperature is more pronounced than that at elevated temperature. This may be related to the change in locus of failure from interfacial in the case of RT to mostly cohesive failure at elevated temperature. Similarly the CFRP joints, that failed cohesively, exhibited higher threshold values compared to the mild steel joints that failed interfacially at RT.

As illustrated above, creep has a significant effect on the fatigue life at elevated temperature. Therefore, it is logical that the crack growth rate should be reprocessed in terms of a creep fracture parameter that accounts for creep in its formulation. This argument is in agreement with many studies in metallic components [5.12-5.16]. Therefore the fatigue data for the DCB joints was reprocessed in terms of the creep parameter $(C_t)_{avg}$ as shown in Figures (9.28), (9.29) and (9.30) for joints tested at RT, 90°C and 120°C respectively. With this representation the effect of frequency is seen clearly and the noise in the data is reduced.

An alternative mild steel surface treatment (SAE), based on an etching process, was found to change the locus of failure from interfacial failure to cohesive failure for joints tested at room temperature. The threshold values were still affected by decreasing frequency as shown in Figure (9.39), however, the fatigue threshold was almost 65 % greater than that seen during interfacial failure with the mild steel joints.

11.4 Creep investigation

The creep behaviour of mild steel joints bonded with *FM300-2M* has been characterised, as shown in Figure (9.40) and Figure (9.41) for joints tested at 90°C and 120°C respectively. The plots show all three stages of creep behaviour at 120°C, whilst at 90°C only two stages are clearly visible.

The creep crack growth data were correlated with the creep parameter, C_t, as shown in Figure (9.46) and Figure (9.47) for joints tested at 90°C and 120°C respectively. Relating the crack growth rate *da/dt* to the creep parameter C_t showed a similar trend to that obtained by Saxena [4.18] in previous studies on metals. This relationship allows creep fracture to be predicted in a similar way that the Paris law allows fatigue failure to be predicted.

Figures (9.50) and (9.51) indicate that the creep crack growth rate, *da/dt*, for pure creep is lower than that for creep-fatigue. The higher *da/dt* for fatigue is must be due to the cyclic loading component that the joints experience in addition to the sustained load. It is seen that in most cases crack growth under cyclic loading of bonded joints has both a cyclic and a time dependence, indicating both fatigue and creep mechanisms are operating.

11.5 Locus of failure

The locus of failure from optical and SEM examination of the fracture surfaces was found to be predominantly cohesive fracture of the adhesive for the CFRP joints tested under

fatigue and quasi static loading. Similar results were obtained for mild steel joints tested quasi-statically.

In the case of the mild steel DCB joints tested under fatigue loading; failure was found to be predominantly in the interfacial region between the adhesive and adherend. However, the locus of failure was seen to be dependent on frequency. Fracture was completely in the interfacial region at RT for samples tested at 10 Hz, however, frequency decreases, small islands of cohesive failure appeared. Evidence of toughening spheres on the surfaces of these islands indicates they are localized areas of cohesive failure of the adhesive. By comparison, the fracture surfaces at 120°C show that the locus of failure is clearly effected by temperature and has become mostly cohesive failure of the adhesive with small areas of apparent interfacial failure. The change of locus of failure may be attributed to the viscoelasticity of the adhesive with, the slower rate of loading (low frequency) having a similar effect to rising temperature [11.2].

SEM analysis of the fracture surfaces indicated that the type of failure termed "apparent interfacial failure" could in fact be fracture in a thin layer of brittle polymeric resin adjacent to the steel (oxide) surface. Further investigation of this, although outside the scope of the present study, would be of interest. However, whilst the "interfacial failure" may not be truly interfacial, it is clearly different to the "cohesive failure" observed and is clear to the interface; hence the term "interfacial" and "cohesive" failure are retained to maintain this distinction.

The use of an alternative surface treatment for the mild steel joints tested at room temperature resulted in a change in the locus of failure from interfacial to completely cohesive failure in the adhesive. This also increased the fatigue threshold value by 75%, this value now being close to the value obtained from CFRP joints tested under similar conditions.

In summary then, it can be seen that the locus of failure is dependent on the substrate used, the pre-treatment of the substrate, the test temperature and the test frequency and this in turn effects the mechanical performance of the joint.

11.6 Finite element studies

A finite element model was used to calculate the strain energy release rate, G at different crack lengths for CFRP and mild steel joints as shown in Figures (6.8) and (6.9) respectively. Result showed that the BEF model agreed more closely with the FE results than the SBT model, therefore, the BEF model has been used during this work to analyse the experimental data in terms of the strain energy release rate , G.

The J- integral has also been calculated using FEA, as shown in Figures (6.13) and (6.14) for CFRP and mild steel joints respectively. Results indicate that the BEPF model agreed well with the FE model, therefore, the BEPF model has been used during this work to analyse the experimental data in terms of the J-integral. Figures (6.15-6.17) show a comparison between the fracture parameters G and J. These show higher values of J at the beginning of the tests due to plasticity at the crack tip. However, as the crack length increases the value of the G and J-integral become almost equal. This argument agreed with the theory of these parameters discussed in section (3.5.4).

The finite element method was also used to calculate the creep parameter C* at different crack lengths for mild steel joints tested at 90°C and 120°C, as shown in Figure (6.19) and Figure (6.20) respectively. Again, this showed good agreement with the experimental results and the FEA method has the advantage that it can be adapted to calculate C* automatically at different locations ahead of the crack in joints of different geometry.

Thus the FEA work has been used to assess and validate the analytical methods used to determine the various fracture parameters used in this work. It should also be noted that for

more complex sample geometries accurate analytical methods may not be available and in these cases the FE methods described in this work may be used.

11.7 Prediction methods

In this research project efforts have been made to predict fatigue and creep-fatigue crack growth using a range of different prediction methods, utilizing various fracture parameters. To find the best use of these methods, a number of factors should be considered in order to select the optimum method to predict the crack growth. Some of the more important factors are listed below:

- o   Failure mode (Interfacial failure or cohesive failure)
- o   Temperature (room temperature or elevated temperature)
- o   Frequency (high or low frequency)
- o   Complex loading (variable frequency)
- o   Hold time during fatigue

Throughout this research, effect was focused on the above factors in order to find the best method to predict the crack growth behaviour in various conditions.

The first method investigated was based on empirical crack growth laws derived from experimental data, where the material constants were determined as a function of temperature and frequency. With this method, it was possible to accurately predict crack growth over a wide range of frequencies and temperatures. In this method G_{max} and J_{max} were found to be the most suitable fracture mechanics parameters for crack growth prediction at room temperature and also at elevated temperatures for specimens tested at high frequency, as shown in Figures (10.2-10.4). However, the creep-fatigue parameter

$(C_t)_{avg}$ appeared to be more applicable at elevated temperature accompanied by low applied frequency, as shown in Figures (10.7) and (10.10). This trend is in agreement with the logic of using the creep parameters as discussed in section (5.4), as creep would be more significant at high temperatures and low frequencies. This method is good for a wide range of loading and environmental conditions; however care must be taken to use a suitable fracture parameter as described above. Also, as the crack growth laws are empirical a significant amount of testing must be carried out to determine the equations describing the crack growth law constants as functions of frequency and temperature.

The second method was used to predict crack growth in cases where failure was time dominant, but could equally be used when cyclic dominant behaviour was observed. This method was found to be applicable for specimens that failed with interfacial failure when tested at room temperature. In this case the crack growth curves in term of *da/dt* at different frequencies were almost coincident, as shown in Figure (9.11). This demonstrates that in this case crack growth is more dependent on time under load than number of cycles. Thus the crack growth at any frequency can be predicted from master *da/dt* verses G_{max} plots. With this method it is possible to predict crack growth accurately at different frequencies as shown in Figures (10.13-10.15). This method was valid only for the case of interfacial failure and testing at room temperature, thus it can be seen that whereas this method is simple, it has only limited applicability and this must be determined by testing.

The third method that was investigated was based on the partitioning approach, which assumes that crack growth can be partitioned into cyclic dependent (fatigue) and time dependent (creep) components and that the total crack growth can be determined by simply

summing these components. This method was applied to cases in which both creep and fatigue contributed to the crack growth, as shown in Figures (10.20-10.25). These figures show the capability of this method to predict fatigue-creep crack growth. However in some cases (90°C/0.1Hz and 120°C/t_h=30sec) this method tended to underestimate the crack growth, as is seen clearly in Figures (10.20) and (10.25). However, this was only significant at the beginning of the crack growth, and related to fatigue-creep interaction effects. This method required less testing than the empirical method and is more powerful and flexible as it can be applied to a wide variety of loading forms, including those combining both fatigue and creep such as fatigue tests at low frequency, fatigue tests combined with hold time and variable frequency fatigue testing.

The fourth method investigated was used to account for the interaction effects noted in the previous method. This was carried out using the procedure described in section (10.5) and the results are shown in Figures (10.26-10.31). This method improved the prediction of crack growth for cases subjected to fatigue-creep loading conditions. This is probably the most flexible of the predictive methods. An accurate prediction of crack growth can be determined over a wide range of loading conditions including, high and low frequency fatigue and complex fatigue spectra incorporating ramps and plateaus. It is also a relatively safe method as crack growth tends to be overestimated, leading to slightly conservative designs when the method is implemented. The drawback of the method is the additional testing that is required to determine the constants in the empirical interaction term.

Among these four methods, the designer can select the most suitable method to predict crack growth based on loading and environmental conditions. A summary of the recommended usage of these methods are tabulated in Table (11.1)

Table (11.1) Recommend methods to predict the crack growth for various loading and environmental conditions.

Prediction method	Conditions	Failure mode C: cohesive I: interfacial	Recommended parameters
Empirical method	RT	C or I	G_{max} or J_{max}
F(Temp., f)	Elevated Temp + High f	C or I	G_{max} or J_{max}
Table (10.4)	Elevated Temp + Low f	C or I	$(C_t)_{avg}$
Dominant damage method Table (10.5)	RT	I	G_{max}
Damage partition method Table (9.4) Table(9.15)	120°C + Low f	C or I	G_{max} and C_t Value of G_{max} at high f Eq.(10.5)
	Elevated Temp + variable f		
Damage partition method with interaction term Table (9.4) Table(9.15)	Elevated Temp + Low f	C or I	G_{max}, C_t and int .term Value of G_{max} at high f Eq.(10.6)
	Elevated Temp + variable f		
	Elevated Temp + hold time		

11.8 References

[11.1] Bell, A.J., Kinlock, A.J. and Wang, Y., "Effect of Adherend Type Upon the Adhesive Mode-I Fracture Energy of DCB Joints", 18th Annual Meeting of the Adhesion Society, USA, 1995, pp.167-170.

[11.2] Richardson G., PhD. Thesis, University of Surrey, 1993.

CHAPTER 12

CONCLUSIONS AND FUTURE WORK

12.1 Conclusions

12.1.1 Quasi static and creep studies of FM300-2M

- As the test rate increases, the elastic modulus (E), the ultimate tensile stress (UTS) and yield stress (σ_y) increase. Decreasing the test rate has the same effect as increasing the temperature.

- Increasing the temperature from RT to 120°C decreases the creep rupture time by 98% and increases the failure strain by 4.75%.

- It is possible to describe the behaviour of FM300-2M at low temperature as a linear elastic solid, however, plasticity and creep become significant as the temperature increases towards the glass transition temperature T_g.

12.1.2 Quasi -static and loading rate studies of DCB joints

- The G_c value of mild steel joints is higher than the G_c value of CFRP joints by a factor 1.22.

- G_c increases as the rate of loading increases from 0.1 mm/min to 10 mm/min by almost 70%. As temperature increases G_c decreases. This is expected due to the viscoelasticity of the adhesive at elevated temperature.

12.1.3 Fatigue loading studies

- The fatigue threshold decreases and the fatigue crack propagation rate increases as the fatigue frequency is reduced from 10 to 0.1 Hz. This indicates that designers should not use high frequency test data to predict the time to failure of bonded joints subjected to low frequency loading.

- Linear relationships were seen between log frequency and log Gth, D and n. These relationships can be used to construct a FCP curve and hence, predict crack growth at any frequency.

- The fatigue threshold values for the CFRP joints (cohesive failure) were higher than those for the mild steel joints (interfacial failure) for all frequencies. Crack growth between G_{th} and G_c was greater in the mild steel joints for a given value of G_{max}.

- A sulphuric etching process (SAE) changed the locus of failure with the mild steel adherends to cohesive failure of the adhesive. G_{th} increased by almost 65% compared with the interfacial failure.

- The fatigue threshold is reduced by 32% as temperature is increased from RT to 120°C.

- The locus of failure was affected by both frequency and temperature. As the frequency decreased, the locus of failure tended to become more cohesive.

Increasing temperature tended to change the locus of failure from interfacial to cohesive in the adhesive.

12.1.4 Creep loading studies

- The logarithmic creep crack growth velocity *Log (da/dt)* appears to have a linear relationship with the logarithmic creep parameters. This relationship allows creep fracture to be predicted in a similar way that Paris law allows fatigue failure to be predicted.

12.1.5 Predictive studies

12.1.5.1 Empirical crack growth law method

- The prediction of crack growth rate in term of *da/dt* or *da/dN* can be predicted at any frequency and temperature and for both types of failure mode, namely cohesive failure or interfacial failure. Empirical formulas can be used to correlate the crack growth rate with various parameters of fracture, namely, G_{max}, J_{max} and $(C_t)_{avg}$.

  a) G_{max} or J_{max} can be used to predict the crack growth at room temperature. However, at the beginning of the test J_{max} is more accurate. This may refer to increased plasticity in this region.

  b) At elevated temperature, G_{max} was found to be the most suitable parameter at high frequency, while $(C_t)_{avg}$ was found to be the more suitable at low applied frequencies.

12.1.5.2 Dominant damage method

- The prediction of crack growth rate at room temperature in terms of cycles interfacial failure at any frequency could be estimated from a master *da/dt* versus G_{max}. From the master *da/dt* for interfacial failure, it was also possible to predict a FCP curve in term of *da/dN* at any frequency.

12.1.5.3 Dominant partitioning method

- The damage partition method was able to predict crack growth under a range of creep and fatigue loading conditions. The disadvantage of this method was underestimating the crack growth for some cases at the beginning of the crack growth.

12.1.5.4 Dominant partitioning method with interaction term

- The damage partition method with an empirical interaction term was the most suitable method for a wide range of loading conditions including high and low frequency fatigue and complex fatigue spectra incorporating ramps and plateaus.

12.1.6 Finite element studies

- FEA calculations of the fracture parameters, G, J-integral and C* showed good agreement with the analytical results.

12.2 Future work

- ➤ The use of DCB specimens provides fracture and fatigue data under mode I loading. However, it is realised that the values for the adhesive fracture energy, G_c and G_{th} for mode II loading may be different. Thus it is proposed that a similar

program of testing be undertaken, as used in the present study, to obtain data for mode II and mixed mode loading conditions.

➤ This study was only concerned with crack propagation. In some cases fatigue initiation may be important and in these cases uncracked joints, such as lap joints, should be tested under similar creep-fatigue conditions.

➤ The locus of failure in the mild steel joints was only determined superficially in this work. It would be an interest project to apply advanced surface analysis technique to the fractured joints in order to build a more complete understanding of the nature of failure in these joints.

➤ Measuring the strain near the crack tip to investigate the presence of creep strain under various loading conditions would be of interest. This is now possible due to the development of techniques such as high resolution moiré interferometry.

➤ The prediction methods investigated in this work could be developed into a form suitable for implementing in a finite element analysis or single structural analysis program.

➤ The prediction methods developed through out this work need further investigation and validation. The aim should be to provide clear and confident guidelines for designers of adhesively bonded joints subjected to complex loading.

➤ More investigation, based on finite element and analytical methods, of the creep zone size and the transition time from small scale creep to extensive creep is needed. This will contribute to a sound basis for the selection of suitable fracture parameters for the prediction of crack growth under different combinations of material, geometry, temperature and loading.

APPENDIX A

DETERMINATION OF CRACK GROWTH RATE

A hard copy of the computer program written in visual basic for determining the fatigue crack growth rate, da/dN as recommended in E-647-88- 'Standard Test Method for Measurement of Fatigue Crack Growth Rate'.

List of the program:

```
Sub PolydadN()
' PolydadN Macro
' Selects increments of 7-points
' Calculates slope by fitting 2nd order polynomial curve
' As outlined in ASTM E-647-88


    Dim i, l, m As Integer
    Dim a, y1, y2, y3, y4, y5, y6, y7, sy, sxy, sx2y, y_, dadN As Double
    Dim n, x1, x2, x3, x4, x5, x6, x7, sx, sx2, sx3 As Double
    Dim sx4, t2, t3, t4 As Double
    Dim b0, b1, b2, C1, C2, den As Double
    Cells(1, 12).Value = "a_"
    Cells(1, 13).Value = "dadN poly"
    Cells(1, 14).Value = "log dadN"
    CellCount = Cells(2, 5).Value
    m = 3    '2m + 1 datapoints
    i = 5
    Do Until i = (CellCount - 1)
        a = 9
        n = 1
'Sets up the 7-point data sub-sets
        y1 = Cells(i - 3, a).Value
        y2 = Cells(i - 2, a).Value
        y3 = Cells(i - 1, a).Value
        y4 = Cells(i, a).Value
```

y5 = Cells(i + 1, a).Value

y6 = Cells(i + 2, a).Value

y7 = Cells(i + 3, a).Value

x1 = Cells(i - 3, n).Value

x2 = Cells(i - 2, n).Value

x3 = Cells(i - 1, n).Value

x4 = Cells(i, n).Value

x5 = Cells(i + 1, n).Value

x6 = Cells(i + 2, n).Value

x7 = Cells(i + 3, n).Value

'Calculates the summations of the different terms needed

sy = (y1 + y2 + y3 + y4 + y5 + y6 + y7)

sx = (x1 + x2 + x3 + x4 + x5 + x6 + x7)

sx2 = ((x1 ^ 2) + (x2 ^ 2) + (x3 ^ 2) + (x4 ^ 2) + (x5 ^ 2) + (x6 ^ 2) + (x7 ^ 2))

sx3 = ((x1 ^ 3) + (x2 ^ 3) + (x3 ^ 3) + (x4 ^ 3) + (x5 ^ 3) + (x6 ^ 3) + (x7 ^ 3))

sx4 = ((x1 ^ 4) + (x2 ^ 4) + (x3 ^ 4) + (x4 ^ 4) + (x5 ^ 4) + (x6 ^ 4) + (x7 ^ 4))

sxy = ((x1 * y1) + (x2 * y2) + (x3 * y3) + (x4 * y4) + (x5 * y5) + (x6 * y6) + (x7 * y7))

sx2y = ((x1 ^ 2 * y1) + (x2 ^ 2 * y2) + (x3 ^ 2 * y3) + (x4 ^ 2 * y4) + (x5 ^ 2 * y5) + (x6 ^ 2 * y6) + (x7 ^ 2 * y7))

'Calculates the curve fitting constants (where y = ax2 + bx + c)

t2 = (sy * ((sx2 * sx4) - (sx3 * sx3))) - (sxy * ((sx * sx4) - (sx2 * sx3))) + (sx2y * ((sx * sx3) - (sx2 * sx2)))

t3 = ((2 * m + 1) * ((sxy * sx4) - (sx2y * sx3))) - (sx * ((sy * sx4) - (sx2y * sx2))) + (sx2 * ((sy * sx3) - (sxy * sx2)))

t4 = ((2 * m + 1) * ((sx2 * sx2y) - (sx3 * sxy))) - (sx * ((sx * sx2y) - (sx3 * sy))) + (sx2 * ((sx * sxy) - (sx2 * sy)))

den = ((2 * m + 1) * ((sx2 * sx4) - (sx3 * sx3))) - (sx * ((sx * sx4) - (sx2 * sx3))) + (sx2 * ((sx * sx3) - (sx2 * sx2)))

b0 = (t2 / den) 'c

b1 = (t3 / den) 'b

b2 = (t4 / den) 'a

'Calculates the input scaling parameters C1 & C2

C1 = (0.5 * (x1 + x7))

C2 = (0.5 * (x7 - x1))

'Checks that the data sub-sets satisfy the condition (-1 <= x <= +1) where x = (Ni - C1)/C2

'NB THIS DOES NOT USE THE SCALING FACTORS IN THE ACTUAL CALCULATIONS

If C2 <> 0 Then

If -1 <= ((x4 - C1) / C2) <= 1 Then

y_ = (b2 * (x4 ^ 2)) + (b1 * x4) + b0   'y = a.x2 + b.x + c

279

```
            Cells(i, 12).Value = y_

            dadN = (2 * b2 * x4) + b1    ' dy/dx = 2.a.x + b

            Cells(i, 13).Value = dadN

        End If

    End If


'Calculates log dadN to the base 10

    If Cells(i, 13).Value > 0 Then

        dadN = Cells(i, 13).Value

        logdadN = Log(dadN) / Log(10#)

        Cells(i, 14).Value = logdadN

    End If

    i = i + 1

Loop

End Sub
```

APPENDIX B

DETERMINATION OF STRAIN ENERGY RELEASE RATE

A hard copy of the computer program written in visual basic for determining the Strain

energy release rate, G based on beam on elastic foundation methods, BEF.

List of the program:

```
Sub GBEF()

   Range("W1").Select

   ActiveCell.FormulaR1C1 = "E="

   Range("X1").Select

   ActiveCell.FormulaR1C1 = "20.9E+10"

   Range("W2").Select

   ActiveCell.FormulaR1C1 = "Es="

    Range("X2").Select

   ActiveCell.FormulaR1C1 = "2.45E+09"

   Range("W3").Select

   ActiveCell.FormulaR1C1 = "t="

   Range("X3").Select

   ActiveCell.FormulaR1C1 = "0.1e-3"

   Range("W4").Select

   ActiveCell.FormulaR1C1 = "2h="

   Range("X4").Select

   ActiveCell.FormulaR1C1 = "2.4E-02"

   Range("W5").Select

   ActiveCell.FormulaR1C1 = "d="

   Range("X5").Select

   ActiveCell.FormulaR1C1 = "1.5E-01"

   Range("W6").Select

   ActiveCell.FormulaR1C1 = "b="

   Range("X6").Select

   ActiveCell.FormulaR1C1 = "2.50E-02"
```

```
Range("W8").Select

ActiveCell.FormulaR1C1 = "h="

Range("X8").Select

ActiveCell.FormulaR1C1 = "=R[-4]C/2-R[-5]C"

Range("W9").Select

ActiveCell.FormulaR1C1 = "EI="

Range("X9").Select

ActiveCell.FormulaR1C1 = "=R[-8]C*R[-3]C*R[-1]C^3/12"

Range("W10").Select

ActiveCell.FormulaR1C1 = "q="

Range("X10").Select

ActiveCell.FormulaR1C1 = "=(R[-8]C*R[-4]C/(4*R[-1]C*R[-7]C))^0.25"

Range("Y1").Select

ActiveCell.FormulaR1C1 = "D1"

Range("Y2").Select

ActiveCell.FormulaR1C1 = "=1+2*R[1]C[-16]*R10C24"

Range("Y2").Select

Selection.AutoFill Destination:=Range("Y2:Y252"), Type:=xlFillDefault

Range("Y2:Y252").Select

Range("Z1").Select

ActiveCell.FormulaR1C1 = "D2"

Range("Z2").Select

ActiveCell.FormulaR1C1 = "=1+RC[-17]*R10C24"

Range("Z2").Select

Selection.AutoFill Destination:=Range("Z2:Z252"), Type:=xlFillDefault

Range("Z2:Z252").Select

Range("AA1").Select

ActiveCell.FormulaR1C1 = "P"

Range("AA2").Select

ActiveCell.FormulaR1C1 = _

    "=RC[-21]*R9C24/(2*(RC[-18]^3/3+RC[-2]*RC[-18]/(2*R10C24^2)+RC[-1]/(2*R10C24^3)))"

Range("AA2").Select

Selection.AutoFill Destination:=Range("AA2:AA252"), Type:=xlFillDefault

Range("AA2:AA252").Select
```

282

```
Range("AB1").Select

ActiveCell.FormulaR1C1 = "GBEF"

Range("AB2").Select

ActiveCell.FormulaR1C1 = _

    "=12*RC[-1]^2*RC[-2]^2/(R6C24^2*R8C24^3*R1C24*R10C24^2)"

Range("AB2").Select

Selection.AutoFill Destination:=Range("AB2:AB252"), Type:=xlFillDefault

Range("AB2:AB252").Select

Columns("AB:AB").Select

With Selection

    .HorizontalAlignment = xlCenter

    .VerticalAlignment = xlBottom

    .WrapText = False

    .Orientation = 0

    .AddIndent = False

    .IndentLevel = 0

    .ShrinkToFit = False

    .ReadingOrder = xlContext

    .MergeCells = False

End With

Selection.NumberFormat = "0.0"

With Selection.Font

    .Name = "Arial"

    .FontStyle = "Italic"

    .Size = 10

    .Strikethrough = False

    .Superscript = False

    .Subscript = False

    .OutlineFont = False

    .Shadow = False

    .Underline = xlUnderlineStyleNone

    .ColorIndex = xlAutomatic

End With

End Sub
```

APPENDIX C

Calculation of G based on FE analysis (crack closer method)

A hard copy of the command file written in LUSAS format to calculate the displacements

and forces needed to calculate the strain energy release rate, G

! Version 13.1-2 Date 29-04-99 Time 11:50

SET RESULTS DISPLACEMENT

RESULTS HISTORY NODE NODE=276949 COLUMN=DX

RESULTS HISTORY NODE NODE=276949 COLUMN=DY

RESULTS HISTORY NODE NODE=65387 COLUMN=DX

RESULTS HISTORY NODE NODE=65387 COLUMN=DY

SELECT ELEMENT TYPE LNAME=jnt3

SET RESULTS STRESS

RESULTS HISTORY NODE NODE=65390 COLUMN=FX

RESULTS HISTORY NODE NODE=276954 COLUMN=FY

PRINT DATASET SPREADSHEET IDAT=ALL FILENAME=C:\Lusas13\Gcrackl45

CONFRM=YES

APPENDIX D

Calculation of J-integral based on FE analysis

A hard copy of the command file written in LUSAS format to calculate the displacements,

stresses and strains needed to calculate the J-integral.

```
! Version 13.1-2 Date 29-04-99 Time 11:50
SET RESULTS STRESSES
SECTION LINE POINTS COLUMN ="Sx"  P1=119.6;2   P2=119.6;0.5
SECTION LINE POINTS COLUMN ="Sxy" P1=119.6;2   P2=119.6;0.5
SECTION LINE POINTS COLUMN ="Sy"  P1=119.6;2   P2=119.6;0.5

SET RESULTS STRAINS
SECTION LINE POINTS COLUMN ="Ex"  P1=119.6;2   P2=119.6;0.5
SECTION LINE POINTS COLUMN ="EXY" P1=119.6;2   P2=119.6;0.5
SECTION LINE POINTS COLUMN ="EY"  P1=119.6;2   P2=119.6;0.5

SET RESULTS DISPLACEMENTS
SECTION LINE POINTS COLUMN ="DX"  P1=119.6;2    P2=119.6;0.5
SECTION LINE POINTS COLUMN ="DY"  P1=119.6;2    P2=119.6;0.5
SECTION LINE POINTS COLUMN ="DX"  P1=119.725;2  P2=119.725;0.5
SECTION LINE POINTS COLUMN ="DY"  P1=119.725;2  P2=119.725;0.5

SET RESULTS STRESSES
SECTION LINE POINTS COLUMN ="Sx"  P1=120.6;0.5  P2=120.6;2
SECTION LINE POINTS COLUMN ="Sxy" P1=120.6;0.5  P2=120.6;2
SECTION LINE POINTS COLUMN ="Sy"  P1=120.6;0.5  P2=120.6;2

SET RESULTS STRAINS
SECTION LINE POINTS COLUMN ="Ex"  P1=120.6;0.5  P2=120.6;2
SECTION LINE POINTS COLUMN ="EXY" P1=120.6;0.5  P2=120.6;2
SECTION LINE POINTS COLUMN ="EY"  P1=120.6;0.5  P2=120.6;2

SET RESULTS DISPLACEMENTS
SECTION LINE POINTS COLUMN ="DX"  P1=120.6;0.5   P2=120.6;2
SECTION LINE POINTS COLUMN ="DY"  P1=120.6;0.5   P2=120.6;2
SECTION LINE POINTS COLUMN ="DX"  P1=120.725;0.5 P2=120.725;2
SECTION LINE POINTS COLUMN ="DY"  P1=120.725;0.5 P2=120.725;2

SET RESULTS STRESSES
SECTION LINE POINTS COLUMN ="Sxy" P1=119.6;0.5   P2=120.6;0.5
SECTION LINE POINTS COLUMN ="Syy" P1=119.6;0.5   P2=120.6;0.5

SET RESULTS DISPLACEMENTS
SECTION LINE POINTS COLUMN ="DX" P1=119.6;0.5    P2=120.6;0.5
SECTION LINE POINTS COLUMN ="DY" P1=119.6;0.5    P2=120.6;0.5
SECTION LINE POINTS COLUMN ="DX" P1=119.725;0.5  P2=120.725;0.5
SECTION LINE POINTS COLUMN ="DY" P1=119.725;0.5  P2=120.725;0.5


PRINT OPEN C:\Lusas13\STJ(a120).CSV
PRINT DATASET=1T12
PRINT DATASET=13T20
PRINT DATASET=21T32
PRINT DATASET=33T40
PRINT DATASET=41T44
PRINT DATASET=45T52
PRINT CLOSE
```

APPENDIX E

Calculation of C*-integral based on FE analysis

A hard copy of the command file written in LUSAS format to calculate the displacements,

stresses and creep strains needed to calculate the C*-integral.

```
! Version 13.1-2 Date 29-04-99 Time 11:50
SET RESULTS STRESSES
SECTION LINE POINTS COLUMN ="Sx"  P1=89.6;2  P2=89.6;1
SECTION LINE POINTS COLUMN ="Sxy" P1=89.6;2  P2=89.6;1
SECTION LINE POINTS COLUMN ="Sy"  P1=89.6;2  P2=89.6;1

SET RESULTS CREEP STRAINS
SECTION LINE POINTS COLUMN ="ECx"  P1=89.6;2  P2=89.6;1
SECTION LINE POINTS COLUMN ="ECXY" P1=89.6;2  P2=89.6;1
SECTION LINE POINTS COLUMN ="ECY"  P1=89.6;2  P2=89.6;1

SET RESULTS DISPLACEMENTS
SECTION LINE POINTS COLUMN ="DX"  P1=89.6;2    P2=89.6;1
SECTION LINE POINTS COLUMN ="DY"  P1=89.6;2    P2=89.6;1
SECTION LINE POINTS COLUMN ="DX"  P1=89.725;2  P2=89.725;1
SECTION LINE POINTS COLUMN ="DY"  P1=89.725;2  P2=89.725;1

SET RESULTS STRESSES
SECTION LINE POINTS COLUMN ="Sx"  P1=90.5;1  P2=90.5;2
SECTION LINE POINTS COLUMN ="Sxy" P1=90.5;1  P2=90.5;2
SECTION LINE POINTS COLUMN ="Sy"  P1=90.5;1  P2=90.5;2

SET RESULTS CREEP STRAINS
SECTION LINE POINTS COLUMN ="ECx"  P1=90.5;1  P2=90.5;2
SECTION LINE POINTS COLUMN ="ECXY" P1=90.5;1  P2=90.5;2
SECTION LINE POINTS COLUMN ="ECY"  P1=90.5;1  P2=90.5;2

SET RESULTS DISPLACEMENTS
SECTION LINE POINTS COLUMN ="DX"  P1=90.5;1     P2=90.5;2
SECTION LINE POINTS COLUMN ="DY"  P1=90.5;1     P2=90.5;2
SECTION LINE POINTS COLUMN ="DX"  P1=90.625;1   P2=90.625;2
SECTION LINE POINTS COLUMN ="DY"  P1=90.625;1   P2=90.625;2

SET RESULTS STRESSES
SECTION LINE POINTS COLUMN ="Sxy" P1=89.6;1     P2=90.5;1
SECTION LINE POINTS COLUMN ="Syy" P1=89.6;1     P2=90.5;1

SET RESULTS DISPLACEMENTS
SECTION LINE POINTS COLUMN ="DX" P1=89.6;1      P2=90.5;1
SECTION LINE POINTS COLUMN ="DY" P1=89.6;1      P2=90.5;1
SECTION LINE POINTS COLUMN ="DX" P1=89.725;1    P2=90.625;1
SECTION LINE POINTS COLUMN ="DY" P1=89.725;1    P2=90.625;1


PRINT OPEN C:\Lusas13\CR(a90)c.CSV
PRINT DATASET=1T12
PRINT DATASET=13T20
PRINT DATASET=21T32
PRINT DATASET=33T40
PRINT DATASET=41T44
PRINT DATASET=45T52
PRINT CLOSE
```

APPENDIX F

PREDICTION OF FATIGUE LIFE UNDER FATIGUE AND CREEP LOADING

A hard copy of the computer program written in visual basic to predict the crack growth

under fatigue / creep loading condition.

List of program:

```
Sub fatiguecreep()
Dim a, ai, v1, v2, v3, N1, N2, N3, b, h, t, E, Ea As Single
Dim i, j As Single
ai = 40 / 1000       'initial crack length'
v1 = 0.65 / 1000
N1 = 100
b = 25 / 1000
h = 12.5 / 1000
t = 0.1 / 1000
E = 209000000000#
Ea = 2450000000#
k = Ea * b / t
EI = E * b * h ^ 3 / 12
q = (Ea * b / (4 * EI * t)) ^ 0.25
P = 1200
W = 150 / 1000
z = 0.83
dvt = 0.0000009
j = 1
a = ai
For i = 1 To 200000       'i: No. of Blocks'
D11 = 1 + 2 * a * q
D12 = 1 + a * q
P1 = (v1 * EI / 2) / (a ^ 3 / 3 + D11 * a / (2 * q ^ 2) + D12 / (2 * q ^ 3))
F1 = 1.6971 + 174.49 * (a / W) + 13.366 * (a / W) ^ 2 - 12.047 * (a / W) ^ 3 + 4.1151 * (a / W) ^ 4
F2 = 174.49 + 26.732 * (a / W) - 36.141 * (a / W) ^ 2 + 16.46 * (a / W) ^ 3
X = F2 / F1
G1 = 0.75 * (12 * P1 ^ 2 * (q ^ 3 * a ^ 2 + 2 * q ^ 2 * a + q) / (b ^ 2 * h ^ 3 * E * q ^ 3))
If G1 > 77.2 Then
dadN1 = (0.00000000000325) * G1 ^ 2.49 'as a function of G'
Daf = dadN1 * N1       'incremental a'
Else
Daf = 0
```

287

```
End If
CC = P * dvt / (b * (W - a)) * (1 - a / W) * z * (1 - a / W) / (a / W)
CtSSC = P * dvt / (b * W) * X
Ct = CtSSC + CC
If Ct > 0.35 Then
dadn2 = 0.000008892 * Ct ^ 1.0548
dac = dadn2 / 10 * N1
Else
dac = 0
End If
a = a + Daf + dac
Cells(j, 1) = i * (N1)    'for printing'
Cells(j, 2).Value = a
Cells(j, 3) = Da
Cells(j, 23) = dadN1
Cells(j, 24) = dadn2
Cells(j, 26) = (dadN1 + dadn2)
Cells(j, 27) = Cells(j, 26) + a
Cells(j, 28) = Cells(j, 26) + ai
j = j + 1
Next i
End Sub
```

APPENDIX G

LIST OF PUBLICATIONS

List of publications by the author:

1. Al-Ghamdi, A.H., Ashcroft, I.A., Crocombe, A. C., Abdel-wahab, M.M., "Crack Growth in Adhesively Bonded Carbon Fibre Composite Joints Subjected To Fatigue and Creep", EURADH 2002, 6th European Adhesion Conference, University of Strathclyde, Glasgow, 2002, pp. 190-193.

2. Al-Ghamdi, A.H., Ashcroft, I.A., Crocombe, A. C., Abdel-wahab, M.M., "Crack Growth in Adhesively Bonded Joints Subjected to Variable Frequency Loading", Journal of Adhesion, Vol.79, no. 12, 2003. pp.1135-1160.

3. Al-Ghamdi, A.H., Ashcroft, I.A., Crocombe, A. C., Abdel-wahab, M.M., "Creep and Fatigue Crack growth in DCB joints" , SAE VII, 7th International Conference on Structural Adhesives in Engineering, Bristol, 2004.

4. Al-Ghamdi, A.H., Ashcroft, I.A., Crocombe, A. C., Abdel-wahab, M.M., "The Effect of Temperature and Frequency on the Fatigue Performance of Adhesively Bonded Joints" In process, Int. Journal of Fatigue.

5. Al-Ghamdi, A.H., Ashcroft, I.A., Crocombe, A. C., Abdel-wahab, M.M., "Prediction of crack growth in Adhesively Bonded Joints under Fatigue Creep Loading" In process, Journal of Adhesion and Adhesive.

6. Al-Ghamdi, A.H., Ashcroft, I.A., Crocombe, A. C., Abdel-wahab, M.M., "The Effect of Rate and Creep Loading on the Performance of FM300-2M epoxy adhesive" In process, Journal of Adhesion.